Université de Montréal

Recherche et caractérisation des étoiles jeunes de faible masse dans le voisinage solaire

par
Lison Malo

Département physique
Faculté des arts et des sciences

Thèse présentée à la Faculté des études supérieures
en vue de l'obtention du grade de Philosophiæ Doctor (Ph.D.)
en physique

Juin, 2014

Université de Montréal
Faculté des études supérieures

Cette thèse intitulée:

**Recherche et caractérisation des étoiles jeunes de faible masse dans le voisinage
solaire**

présentée par:

Lison Malo

a été évaluée par un jury composé des personnes suivantes:

Gilles Fontaine,	président-rapporteur
René Doyon,	directeur de recherche
Paul Charbonneau,	membre du jury
Caroline Soubiran,	examinateur externe
Gilles Fontaine,	représentant du doyen de la FES

Thèse acceptée le: 30 mai 2014

RÉSUMÉ

Près de 70% des étoiles de la Galaxie ont une masse inférieure à $\sim$0.8 $M_\odot$. Cependant, étant donné que ces étoiles sont plus difficilement observables en raison de leur plus faible luminosité, cette statistique ne reflète pas le recensement actuel de la population d'étoiles de faible masse dans le voisinage solaire, ni dans les groupes cinématiques d'étoiles jeunes. Cette population a une grande importance pour contraindre la forme de la fonction de masse Galactique, et aussi pour contraindre les modèles évolutifs. Les étoiles de faible masse sont aussi d'excellentes cibles pour la recherche d'exoplanètes avec des techniques variées (imagerie directe, vitesse radiale, transit). La caractérisation des exoplanètes autour de ces étoiles est tributaire des connaissances fondamentales sur celles-ci, c'est-à-dire de leur luminosité bolométrique, température effective, rayon et âge.

Dans la présente thèse, dont le but est d'identifier et caractériser les étoiles de faible masse, une méthode statistique a été développée afin d'établir quantitativement l'appartenance d'une étoile à un groupe en dérivant une probabilité d'association. Cette méthode combine l'inférence Bayesienne et des modèles empiriques de plusieurs observables, dont la luminosité, vitesse spatiale et position galactique, de membres confirmés de 7 groupes d'étoiles jeunes (8-120 Mans) ainsi que d'étoiles vieilles du champ. Les étoiles ayant une probabilité d'association minimale de 90% sont considérées comme des candidates. L'analyse développée prédit aussi la vitesse radiale et la distance trigonométrique qu'une étoile aurait dans une association donnée. L'analyse a montré, pour les 177 membres confirmés, un excellent accord entre les paramètres prédits et observés, soit de 1.9 km s^{-1} et 10% respectivement, pour la vitesse radiale et la parallaxe. La mesure de ces paramètres pour les candidats est donc une bonne manière de confirmer leur appartenance à l'association.

Cette méthode robuste a été appliquée sur un échantillon de 758 étoiles montrant des signes de jeunesse (émission Hα et rayons X). L'analyse a permis d'identifier 214 candidates hautement probables, et le suivi spectroscopique de ces étoiles a permis, jusqu'à présent, de confirmer la justesse de la prédiction en vitesse radiale pour 130 étoiles. Ces

iv

observations spectroscopiques ont aussi permis de mesurer leur vitesse de rotation, qui s'est avérée élevée comparativement aux étoiles vieilles du champs. La mesure de la distance trigonométrique était aussi en accord avec la prédiction pour 18 candidates jeunes. Grâce aux membres dont l'appartenance à un groupe jeune a été confirmée, un modèle empirique de la luminosité en rayon X des étoiles a pu être établi. Cette luminosité s'est avérée significativement plus élevée (environ 4 fois plus) pour les étoiles des groupes les plus jeunes ($\sim$8-12 Mans) que pour celles des groupes plus vieux ($\sim$120 Mans). Cet observable constitue donc un bon indicateur d'âge.

La comparaison des spectres de 59 candidates à des modèles d'atmosphère a permis de déterminer trois paramètres fondamentaux : la luminosité bolométrique, la température effective et le rayon. Globalement, les candidates jeunes ont une luminosité plus élevée et un rayon plus grand que les étoiles vieilles. De récents modèles évolutifs incluant le traitement d'une dynamo de type rotationnel et générant un champ magnétique de surface de 1 à 2.5 kGauss ont été utilisés pour déterminer l'âge isochronal de ces étoiles. Les âges ainsi déterminés pour les étoiles de l'association βPictoris en utilisant des étoiles de types spectraux différents sont davantage cohérents (types K5V-M0V : 24 Mans, types M1V-M4V : 14 Mans) et sont aussi cohérents avec l'âge déterminé indépendamment pour le groupe en utilisant l'abondance du lithium des membres de faible masse (26 Mans).

Mots clés: Étoiles de faible masse, associations jeunes.

ABSTRACT

About 70% of the stars in the Galaxy have a mass inferior than $\sim$0.8 $M_\odot$. However, this statistic does not reflect the current census population of low mass in the solar neighborhood and in young kinematic groups, since their low luminosity make their observation more difficult. This population is of great interest to check the validity of the Galactic mass function, and also to constraint evolutionary models. The low-mass stars are also excellent targets for the search for exoplanets using various techniques (direct imaging, radial velocity, transit). The characterization of the exoplanets orbiting these stars depends mostly on our basic knowledge of the host star, that is their bolometric luminosity, effective temperature, radius and age.

The present thesis aim to identify and characterize low-mass stars. Toward that end, a statistical method has been developed to determine quantitatively the membership probability of a star to a young kinematic group. This method combines the Bayesian inference and empirical models of several observables such as the brightness, Galactic space velocity and position of *bona fide* members of 7 young stars groups (8-120 Mans), as well as old field stars. Stars with a membership probability greater than 90% are considered candidate members. The analysis also predicts the radial velocity and distance that a star would have if it was an actual member. For the 177 previously-known members, an excellent agreement was found between the predicted and observed parameters (1.9 km s^{-1} and 10% for the radial velocity and parallax, respectively). Measuring these observables for the candidates stars is thus a good way to confirm their membership.

This robust method was applied to a sample of 758 stars which showed signs of youth (Hα and X-ray emission). It allowed to identify 214 highly probable candidates. The spectroscopic follow-up yields a radial velocity in agreement with predictions for 130 stars. These spectroscopic observations also allowed to measure their projected rotational velocity, which turned out to be higher than that of the old population of stars. Trigonometric distance measurements were also obtained and were coherent with predictions for 18 young candidates. Using the confirmed members, a new empirical model of the X-ray luminosity was developed. The X-ray luminosity was found to be about 4

times higher for stars around ∼8-12Myr than for older, ∼120Myr stars, thus, this observable is a good age indicator in this range.

Comparing the spectra of 59 young candidate members to atmosphere models allowed to determine three basic parameters: the bolometric luminosity, the effective temperature and the radius. Overall, these candidates are more luminous and have a greater radius than old stars. Recent evolutionary models that include the rotational dynamo-type treatment and produce magnetic field strength of 1 to 2.5 kGauss were used to derive an isochronal age for each star. The ages determined for β Pictoris moving group members using stars of different spectral types are coherent with one another (types K5V-M0V: 24 Mans, types M1V-M4V: 14 Mans) and are also coherent with age determined independently using lithium abundance of the low-mass members (26 Mans).

Keywords: low-mass stars, moving groups, M dwarfs.

TABLE DES MATIÈRES

LISTE DES TABLEAUX

LISTE DES FIGURES

LISTE DES ANNEXES

LISTE DES SIGLES

2MASS	Two Microns All Sky Survey
Å	Angstrom
DENIS	Deep Near Infrared Survey of the Southern Sky
FMI	Fonction de Masse Initiale
Gaia	Global Astrometric Interferometer for Astrophysics
HIPPARCOS	High Precision Parallax Collecting Satellite
IRAS	InfraRed Astronomical Satellite
EW	Largeur Équilavente
$M_\odot$	Masse du soleil
μm	Micron
Mans	Millions d'années
PSP	Pré-Séquence Principale
RECONS	Reseach COnsortium on Nearby Stars
ROSAT	RontgenSAtelliT
SP	Séquence Principale
SDSS	Sloan Digital Sky Survey
WISE	Wide-field Infrared Survey Explorer

Cette thèse est dédiée à ma mère Francine, à mon beau-père Gilles Demers, et à toutes ces personnes passionnées qui m'inspirent depuis près de 30 ans.

REMERCIEMENTS

CHAPITRE 1

INTRODUCTION

Suivant l'effondrement gravitationnel d'un nuage moléculaire, les objets émergents de masse variable sont caractérisés par une luminosité élevée. Durant la première centaine de millions d'années (dépendamment de la masse), la décroissance de la luminosité des objets suit une séquence appelée Hayashi (Hayashi et al., 1962) où la température demeure presque constante dans le temps. La contraction lente provoque une décroissance du volume de l'étoile jusqu'au moment où le gradient de pression égale la force de gravité, c'est-à-dire l'atteinte de l'équilibre hydrostatique.

La jeunesse de l'étoile, tel que décrite dans cette thèse, définit une période d'environ 120 millions d'années (Mans) après la formation de l'étoile, où les étoiles plutôt massives atteignent rapidement l'équilibre hydrostatique, mais où les étoiles de faible masse sont toujours en contraction. La durée de cette période est étroitement liée à la masse initiale de l'objet et à l'évolution de sa structure stellaire. Les étoiles de type spectral B et A, caractérisées par une température effective de plus de 10000 K, nécessiteront une période de 1-3 Mans, tandis que les étoiles similaires à notre Soleil, de type spectral F et G ($T_{\text{eff}} \sim 6000$ K) auront besoin de 20-30 Mans. Puis les étoiles caractérisées par leur faible masse et leur température effective sous les 4500 K, soit les étoiles de type K et M, auront besoin de plus de 100 Mans. La facilité avec laquelle la caractérisation de ces astres est réalisée dépend de leur âge, de leur masse et de leur brillance.

Il existe trois motivations principales à l'étude des étoiles jeunes du voisinage solaire. La première motivation est la plus grande facilité d'observation et de caractérisation de ces objets à proximité du Soleil. Étant plus près du Soleil, la brillance apparente d'un objet est grande ce qui permet une mesure plus précise de plusieurs caractéristiques, et ce par des observations de relatives courtes durées. La détection et caractérisation des systèmes binaires sont facilitées par la proximité des objets, permettant un plus faible biais sur la détermination des fonctions de luminosité et de masse.

Dans le voisinage solaire, la majorité des étoiles jeunes se trouvent dans les associa-

tions cinématiques, c'est-à-dire un regroupement d'étoiles formées vraisemblablement suite au passage d'une onde de choc dans le bras de la Galaxie (Fernández et al., 2008). Les laboratoires que sont les groupes d'étoiles jeunes et proches permettent une étude approfondie de la Fonction de Masse Initiale (FMI) du disque galactique. La FMI définit la distribution des étoiles formées dans un intervalle de masse lors de l'effondrement du nuage moléculaire. L'étude pionnière de Salpeter (1955) a montré que la FMI s'exprime par une loi de puissance de la forme $\psi(M) \propto M^{\alpha}$, avec $\alpha \sim -2.35$ pour $0.4 < M < 10\,M_{\odot}$. Puis l'étude de Kroupa (2002) a montré un comportement similaire de la FMI entre $0.25 < M < 0.9\,M_{\odot}$. Les études successives ont montré quelques différences, allant même jusqu'à poser l'hypothèse que la FMI serait dépendante du lieu de formation des étoiles. La distribution exacte n'est pas bien contrainte et une partie de la solution provient de la mesure de la fonction de masse (FM) des amas très jeunes qui, en première approximation, est une FMI (Bastian et al., 2010).

Finalement, la recherche d'étoiles jeunes et proches dans le voisinage solaire permet une meilleure compréhension de la formation et de l'évolution des systèmes protoplanétaires. Pour comprendre la séquence des évènements menant à la formation et à l'évolution des disques protoplanétaires, il est nécessaire de connaître des étoiles âgées précisément de 10 à 100 Mans. La découverte de systèmes extraplanétaires ces dernières années nécessite de connaître précisément l'âge de l'étoile hôte, afin de déterminer la masse des exoplanètes. De plus, l'étude approfondie des étoiles très jeunes permet d'obtenir un meilleur contraste de luminosité entre l'étoile hôte et la planète, facilitant sa détection et sa caractérisation (e.g., Lafrenière et al., 2007).

Pour toutes ces raisons, la communauté scientifique se mobilise pour accroître les connaissances sur les étoiles jeunes, et déjà on observe que le nombre d'étoiles jeunes connues a presque triplé depuis 2008. Les prochaines sections décrivent les associations du voisinage solaire et les indicateurs fréquemment utilisés pour déterminer l'âge de ses membres.

1.1 L'environnement solaire et ses membres

L'étude et l'identification des étoiles jeunes dans l'environnement local ont pris leur envol avec l'arrivée des premières mesures du rayonnement X. Ce faible rayonnement est anti-corrélé avec la densité d'hydrogène neutre (HI), montrant la présence d'une cavité du milieu interstellaire rempli par un plasma chauffé à 10^6 K, portant le nom de « Bulle Locale » (Fernández et al., 2008). Les analyses approfondies de l'environnement local ont montré l'existence d'épisodes de formation stellaire récents formant les associations d'étoiles OB. Ces regroupements d'étoiles massives forment la ceinture de Gould (Gould, 1874), un anneau de 600 pc de diamètre dont l'épaisseur est de 60 pc. La partie gauche de la figure 1.1 montre une représentation de la ceinture de Gould et des groupes d'étoiles situés à l'intérieur de 200 pc du Soleil, et la partie droite de la figure montre la position galactique des groupes d'étoiles.
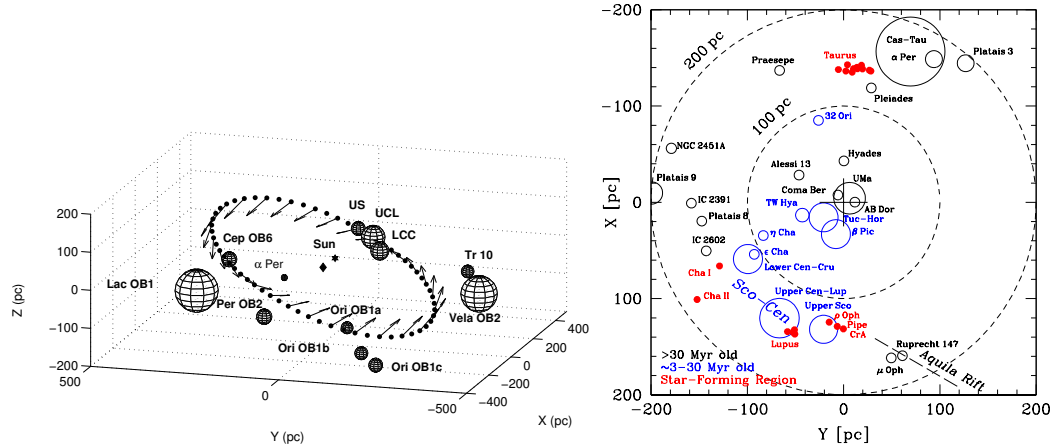
Figure 1.1 **Figure de gauche :** Représentation de la ceinture de Gould tirée de Perrot & Grenier (2003). **Figure de droite :** Schéma de la position galactique, dans le plan de la galaxie, des groupes d'étoiles du voisinage solaire dans un rayon de 200 pc. Le Soleil est situé au centre de la figure (X=0, Y=0). Figure tirée de Rice et al. (2011).

L'arrivée du télescope spatial ROSAT (Voges, 1994) a permis de faire l'étude approfondie de 125 000 étoiles ($V < 17$) du voisinage solaire en mesurant leur émission dans le domaine des rayons X. Quelques années plus tard, le télescope spatial Hipparcos (Perryman et al., 1997) a révolutionné nos connaissances dans le domaine optique en offrant une astrométrie et une photométrie précises d'environ 120 000 étoiles ($V <12$). Les ob-

servations obtenues par ce télescope ont permis de mesurer les positions galactiques de ces objets. La corrélation des catalogues dans le domaine optique et de ROSAT a mis en évidence les étoiles jeunes, plutôt massives (1-3$M_\odot$) du voisinage solaire qui n'avaient pas été découvertes jusqu'à présent (Fernández et al., 2008). Cependant, les étoiles de faible masse, de par leur faible luminosité, n'ont pas été détectées. Pour avoir un meilleur portrait des membres de faible masse du voisinage solaire, il a fallu attendre le recensement mené par le groupe "Reseach COnsortium on Nearby Stars" (RECONS) au début des années 2000, pour découvrir une centaine de nouvelles étoiles de faible masse dans le voisinage solaire. Pour les objets de plus faible luminosité, l'utilisation récente d'une combinaison entre plusieurs relevés grands champs en infrarouge, tel que les sondages 2MASS, DENIS, WISE a permis d'identifier plusieurs naines brunes et objets de masse planétaire dans le voisinage solaire.

Grâce à ces relevés, le portrait du voisinage solaire dénombre plusieurs groupes d'étoiles jeunes entremêlées avec les étoiles vieilles du champ. L'environnement solaire compte une vingtaine d'associations, dont l'âge et les caractéristiques principales sont résumées au Tableau 1.I (crédit Jonathan Gagné). Les étoiles formant ces groupes peuvent être caractérisées selon trois grandes classes représentant les trois phases marquantes de l'évolution de la jeunesse d'une étoile, soit la phase T Tauri, la phase post-T Tauri ou pré-séquence principale (PSP) et finalement la phase séquence principale (SP). Les trois prochaines sections décrivent les principales caractéristiques des étoiles peuplant ces groupes.

1.1.1 Amas d'étoiles très jeunes (1-10 Mans)

Les amas d'étoiles très jeunes ont été découverts grâce à leur proximité des régions de formation d'étoiles et des nuages moléculaires, tels que Chamaeleon, Ophiuchus et Scorpius-Centaurus (Fernández et al., 2008). Ces groupes sont composés principalement d'étoiles de type Herbig Ae/Be ($1.5 < M < 15\,M_\odot$) et celles de type T Tauri ($M < 1.5\,M_\odot$). Il existe deux types d'étoiles T Tauri : les étoiles « Classical T Tauri star »(CTTS) et « Weak-line T Tauri star » (WTTS). Les étoiles les plus actives de type CTTS montrent une forte émission des raies d'hydrogène (EW H$\alpha > 10$ Å) et de plusieurs raies alcalines.

Table 1.I. Tableau résumé des associations de l'environnement solaire

Nom du groupe	Age (Mans)	Distance (pc)	Nbre de membres[a]	Références
Hyades	625-650	32-62	150	1,2,3
Ursa Major	300-600	9-123	55	2,4,5
Orion	1-12	414	3500[b]	9
Scorpius-Centaurus complex	5-15	117-144	522	6
TWA	8-20	28-92	10	1,2,7
η Cha	2-18	93-120	18	2,7
ε Cha	2-18	93-123	23	2,7
β Pictoris	12-22	9-73	44	2,7
Tucana-Horologium	20-40	36-71	44	2,7
ABDMG	70-120	7-77	47	2,7
Columba, Carina	20-40	35-88	30	7
Octan, Argus	3-50	8-175	26	7
IC 2391	35-75	143-148	11	3,4,7
IC 2602	68	147-149	15	3
α Persei	35	169-176	50	3,8
Pleiades	100-120	118-122	33	2,3,4

[a]Membres dont la distance trigonométrique est connue.

[b]Membres dont la distance trigonométrique n'est pas connue.

Note. — (1) Zuckerman et al. (2011) ; (2) Zuckerman et al. (2004) ; (3) van Leeuwen (2009) ; (4) Shkolnik et al. (2012) ; (5) King et al. (2003) ; (6) Fernandez et al. (2008) ; (7) Torres et al. (2008) ; (8) Jilinski et al. (2009) ; (9) Menten et al. (2008).

Un excès de luminosité dans les domaines de l'infrarouge thermique trahit la présence de disques de poussières gravitant autour de ces étoiles jusqu'à un âge d'environ 10 Mans. Le second type d'étoiles, les WTTS, présentent un très faible excès de luminosité dans l'infrarouge thermique puisque la partie interne du disque circumstellaire est dissipée. Cette population d'étoiles joue un rôle important pour contraindre la durée de la formation et de l'évolution stellaire (Basri et al., 1996), en plus de l'étude de l'évolution des disques circumstellaires. La connaissance de plusieurs amas, dont les étoiles proviennent de différents milieux, permet de mieux contraindre les modèles évolutifs. Plus précisément, ils permettent de contraindre le taux d'accrétion durant les premiers Mans suivant la formation.

1.1.2 Groupes cinématiques et amas d'étoiles adolescentes (1-150 Mans)

Les étoiles adolescentes sont regroupées à l'intérieur de plusieurs associations, dont les plus étudiées se trouvent dans un rayon de 100 pc du Soleil et sont âgées d'au plus 150 Mans. Cette classe d'étoiles est caractérisée par la phase évolutive précédant l'atteinte de l'équilibre hydrostatique, soit moins de 3 Mans pour une étoile de type B et

jusqu'à environ 150 Mans pour une étoile de type M.

Jusqu'au début des années 2000, la majorité de la population connue de ces groupes était composée d'étoiles plutôt massives (F, G) et de quelques étoiles de faible masse. La distribution de la masse des membres est en fait un biais observationnel puisque la découverte initiale de ces groupes a été réalisée dans les domaines optique et rayon X (Zuckerman & Song, 2004). Le scénario de formation de ces étoiles dans les groupes cinématiques demeure incertain, puisque ces dernières sont éloignées d'un nuage moléculaire ou d'une région de formation. Cependant, l'existence de ponts de matière liant les nuages aux groupes permet de réconcilier les modèles et lieux de formation stellaire. L'étude de Feigelson (1996) a montré que la formation stellaire peut avoir eu lieu à l'extérieur d'un nuage moléculaire. Cette situation explique, partiellement, pourquoi ces groupes n'ont été découverts que récemment (Neuhauser & Brandner, 1998). La deuxième raison est le fait que les associations cinématiques couvrent une grande étendue du ciel, une conséquence de leur proximité. Cette population d'étoiles représente une période évolutive peu étudiée dans la littérature, en raison du faible nombre d'étoiles connues. De plus, cette population constitue le chaînon manquant pour comprendre le stade évolutif entre la naissance de l'étoile et le moment où l'équilibre hydrostatique est atteint. Une description détaillée de ces groupes est présentée au Chapitre 2. Les groupes les plus étudiés sont TW Hydrae (TWA), β Pictoris, Tucana-Horologium et AB Doradus.

1.1.3   Amas d'étoiles plus âgées (3-600 Mans)

Les étoiles ayant atteints l'équilibre hydrostatique forment plusieurs amas ouverts, dont l'étude pionnière de Proctor (1869) a mis en évidence deux groupes à moins de 50 pc du Soleil, soit les Hyades et Ursa Major. L'étude de ces amas permet une meilleure compréhension de la durée des processus d'évolution dynamique (« disk heating »). L'évolution dynamique des membres des amas (Makarov, 2006) a pour effet de disperser les objets les moins massifs plus facilement du centre vers l'extérieur de l'amas en raison des forces induites par la galaxie et celles provenant du mouvement interne des membres entre eux (Soderblom, 2010). Pour mieux comprendre ce processus, il est nécessaire de connaître le recensement complet de la population formant l'amas.

1.1.4 Fonction de luminosité et fonction de masse

Deux informations essentielles à notre compréhension du processus de formation des étoiles ainsi qu'à la structure de la Galaxie résident en la détermination de la fonction de luminosité (FL) et la fonction de masse (FM). Les fonctions quantifient la distribution des étoiles par unité de magnitude absolue ou de masse en fonction d'une unité de volume. La précision avec laquelle la détermination de ces deux quantités est réalisée dépend de la proximité des étoiles et du type d'étoiles sondées. Cette relation requiert un recensement complet des objets stellaires à sous-stellaires en utilisant une photométrie précise et une mesure trigonométrique de la distance. Dans le voisinage solaire, la figure 1.2 montre les différentes FL obtenues en utilisant plusieurs échantillons limités en distance. La FL a été mesurée à l'intérieur de 20 pc et à l'intérieur de 25 pc du Soleil d'après les études de (Reid et al., 2004) et (Reid & Cruz, 2002), respectivement. Le maximum de ces distributions se situe à $M_J = 7.25$. Ces études montrent l'importante de déterminer adéquatement la distribution de luminosité dans un rayon de 8, 20 et 25 pc du Soleil, afin de déterminer la contribution de chaque type d'étoiles à la luminosité globale de la galaxie, du voisinage solaire ou des amas d'étoiles.

Plusieurs facteurs limitent l'évaluation de la FL dont la forte concentration d'étoiles près du plan galactique et la multiplicité des systèmes non-résolus. Près de 40% des étoiles de la séquence principale se trouvent en système multiple et 32% pour les étoiles jeunes membres des amas (Bergfors et al., 2010). L'avantage de sonder les groupes d'étoiles pour déterminer la FL est de s'assurer que toutes les étoiles sont issues d'une formation et d'une évolution presque simultanée. En utilisant la FL et la relation masse-luminosité appropriée, on peut calculer la fonction de masse associée. Pour définir la relation masse-luminosité, il serait adéquat d'utiliser des systèmes d'étoiles éclipsantes jeunes.

Les travaux de Chabrier (2003) montrent que la fonction de masse décrite par les étoiles vieilles est maximale autour de $0.25\,M_\odot$ d'après une mesure de la fonction de luminosité des étoiles du disque galactique. La FM est un paramètre important pour les amas d'étoiles afin de connaître la masse stellaire totale composant l'amas. Les amas
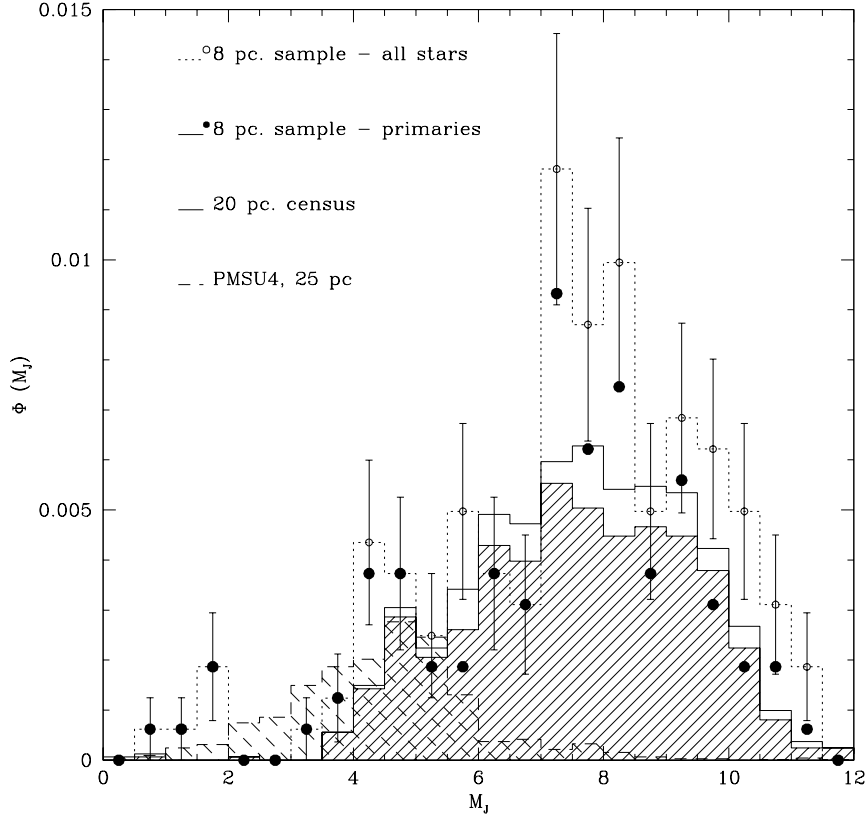
Figure 1.2 Fonction de luminosité (M$_J$) des étoiles situées à l'intérieur de 20 pc (histogramme ligne pleine). Les résultats de Reid & Gizis (1997) sont représentés par les lignes pointillées et pleines (échantillon à 8 pc). La fonction de luminosité des résultats de Reid et al. (2002a) est représentée par l'histogramme hachurée avec une ligne en tirets (échantillon à moins de 25 pc), figure tirée de Reid et al. (2004).

d'étoiles plus âgés tels que les Hyades, Pléiades et quelques amas ouverts montrent une distribution de masse similaire à celle des étoiles du disque. Lodieu et al. (2011) a fait l'étude de la FM pour l'amas d'étoiles très jeunes Upper Scorpius montrant qu'il existerait un premier maximum autour de $0.16\,M_\odot$ et un second dans le régime sous-stellaire autour de $0.02\,M_\odot$.

L'intérêt principal de mesurer la FL des amas d'étoiles est de pouvoir déterminer la FM correspondante. Lorsque la FM d'un amas est connue, il est possible de connaître la masse totale des étoiles de l'amas engendrée lors de l'effondrement du nuage moléculaire initial. Combiné à la FMI, une estimation de la masse du nuage moléculaire

nécessaire pour engendrer les étoiles est obtenue, ce qui permet de préciser l'efficacité des processus de formation.

1.2 Indicateurs d'âge des étoiles jeunes dans le voisinage solaire

Quel est l'âge de cette étoile ? L'âge d'une étoile est un paramètre plus difficile à déterminer comparativement à la mesure de la distance d'une étoile. En effet, il n'existe pas de relation simple pour tous les types d'étoiles entre l'âge et le comportement d'un indicateur (Soderblom, 2010, Soderblom et al. 2013). Pour estimer l'âge des étoiles, il est nécessaire d'utiliser des méthodes indirectes, des indicateurs variés ou de tirer avantage de leur position galactique. Les techniques d'estimation de l'âge des étoiles peuvent être divisées en deux catégories : les méthodes empiriques et celles théoriques. La première englobe les outils cinématiques (mouvement propre, vitesse radiale, parallaxe), la vitesse de rotation, les mesures de l'activité chromosphérique et coronale et la présence du lithium. La seconde classe englobe les dérivées des modèles évolutifs et d'atmosphère stellaire : les spectres théoriques, les isochrones de luminosité, les prédictions de l'abondance de lithium et les modèles évolutifs de la perte du moment cinétique des étoiles jeunes. Pour confronter les différentes classes d'indicateurs et obtenir la meilleure précision sur l'âge d'une étoile, il est avantageux d'observer une population de masses variées ayant été contrainte aux mêmes conditions de formation et d'évolution, c'est-à-dire les amas d'étoiles. Malgré cela, la dispersion de l'âge des étoiles peut dévier de quelques millions d'années (Baraffe et al., 2009), d'où l'importance de sonder les groupes d'étoiles jeunes afin d'évaluer précisément la sensibilité d'un indicateur pour un intervalle d'âge donné. Cependant, plusieurs facteurs peuvent influencer la détermination de l'âge d'une étoile : l'évolution rapide des étoiles d'une certaine masse, la présence des disques stellaires, la présence résiduelle de champs magnétiques, et l'évolution de la structure stellaire.

Le tableau synthèse 1.II résume l'intervalle d'âge pouvant être inféré selon la classe spectrale et le type d'indicateurs.

Tableau 1.II Tableau résumé des indicateurs d'âge

Indicateur d'âge	B-F précoce (Mans)	F tardive-K précoce (Mans)	K tardive-M (Mans)
Diagramme C-M	1-(3-20)	1-(20-100)	1-150
Âge cinématique	1-600+	1-600+	1-600+
Hα chromosphérique	-	(20-100)-600+	150-600+
Hα accrétion	1-10	1-10	1-10
Ca II HK et IRT	-	5-600+	pas de conclusions
Émission X	-	1-100	1-100
Émission UV	-	1-50	1-100
Lithium	pas de conclusions	1-300	1-(50-70)
Gravité de surface	1-(3-20)	1-(20-100)	1-150
Gyrochronologie	-	300+	600+

1.2.1 Diagrammes Hertzsprung-Russell, couleur-magnitude et modèles évolutifs

L'outil le plus utilisé pour déterminer l'âge absolu d'une étoile demeure le diagramme Hertzsprung-Russell (H-R) et sa contrepartie observationnelle : le diagramme couleur-magnitude (C-M). La position de l'étoile sur le diagramme H-R dépend à la fois de la luminosité bolométrique (L_{bol}) et de la température effective (T_{eff}) de celle-ci, et ces deux quantités sont également fonction de l'âge de l'étoile. Selon un portrait global, les étoiles jeunes sont caractérisées par une surluminosité à une température donnée.

La détermination des paramètres fondamentaux, L_{bol} et T_{eff}, nécessite la mesure de la distance, du rayon et du type spectral (la distribution spectrale d'énergie). Les principaux facteurs limitatifs sont la connaissance de la distance de l'étoile et la mesure de son rayon, soit deux observations très coûteuses en temps d'observation et de précision limitée. Plus communément, la température sera estimée en utilisant une relation liant le type spectral à la largeur équivalente (EW) de certaines raies atomiques et moléculaires, ou en comparant le spectre et la distribution spectrale d'énergie observationnelle aux modèles théoriques d'atmosphère. Une estimation de la luminosité bolométrique requiert la brillance de l'étoile dans un certain intervalle de longueur d'onde et d'appliquer la correction bolométrique correspondante (selon le type spectral). L'estimation obtenue

sera limité par la précision de la correction.

Pour se défaire de toutes ces contraintes observationnelles, une méthode analogue et plus répandue est l'utilisation du diagramme C-M, nécessitant les connaissances des magnitudes relatives ou absolues de l'étoile selon différentes couleurs. Dépendamment de la masse ou du type spectral de l'objet, les étoiles jeunes montreront entre 0.5 et 2 magnitudes de différence comparativement aux étoiles de la SP. Le diagramme C-M permet d'inférer un âge qualitatif à une étoile. Ce type d'outil est plus sensible à la métallicité, à l'indice de couleur utilisé et à la précision photométrique, tel que montré par Boyajian et al. (2012). La sur-métallicité d'un astre est interprétée comme une surluminosité par rapport à une étoile de la SP et donc un signe de jeunesse.

Pour estimer l'âge absolu d'une étoile, il est requis d'utiliser les modèles évolutifs qui décrivent les paramètres physiques de l'objet, tel L_{bol}, T_{eff}, et le rayon, en fonction de la masse et de l'âge (e.g., Baraffe et al., 2003, Burrows et al., 2001). Il existe présentement quelques modèles d'évolution ayant des différences notables entre le traitement des types d'atmosphère, des paramètres de mélange, des abondances solaires et du traitement de la convection. Toutes ces petites différences ont des implications significatives sur les propriétés prédites à un âge donné, tel que présenté par Yee et al. (2010). La figure 1.3 montre l'utilisation du diagramme C-M pour inférer un âge à un groupe d'étoile, en utilisant les modèles théoriques pour un âge de 10 et 100 Mans. Pour un âge donné, la figure illustre quatre modèles évolutifs différents, soit ceux de Baraffe et al. 1998, D'Antona & Mazzitelli 1997, Palla & Stahler 1993 et Siess et al. 2000. La comparaison des membres de différentes masses d'un amas aux modèles évolutifs permet également de mettre en relief la différence d'âge inféré entre la population plutôt massive de l'association et la population de faible masse. De façon générale, les modèles évolutifs des étoiles PSP montrent qu'une étoile de 3 $M_\odot$ requiert environ 3 Mans pour atteindre la SP tandis qu'une étoile de masse solaire nécessite 50 Mans. De plus, une étoile de 0.5 $M_\odot$ (∼M1) requiert 100 Mans pour atteindre l'équilibre hydrostatique, tandis qu'une étoile de 0.1 $M_\odot$ (∼M8.5) nécessite 10 fois plus de temps (D'Antona & Mazzitelli, 1994).

Plusieurs facteurs ayant des implications sur l'évolution d'une étoile ne sont pas pris en compte présentement dans les modèles évolutifs typiques, dont la vitesse de rotation

des étoiles ou un épisode d'accrétion spontanée. Plus particulièrement pour les étoiles de faible masse, le traitement du champ magnétique n'est pas un élément pris en compte dans son intégralité. Les modèles évolutifs de Chabrier et al. (2003) ont traité le champ magnétique comme une réduction de la convection. Récemment, les modèles évolutifs de type Dartmouth ont inclus le traitement de la dynamo de type rotationnelle et celle de type turbulente dans leurs modèles évolutifs. Cet ajout change considérablement l'interprétation des observations actuelles (Feiden & Chaboyer 2013b). Nous reviendrons sur les implications de cet aspect au Chapitre 4.
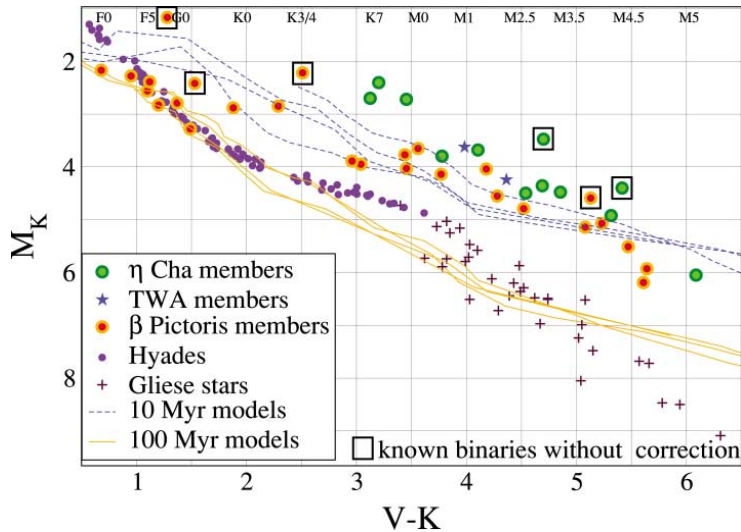
Figure 1.3 Diagramme couleur-magnitude (M_K vs $V - K$) représentant les membres d'associations jeunes. La séquence principale est illustrée par les étoiles de l'amas des Hyades et celles du catalogue Gliese. Les isochrones théoriques de 10 et 100 Mans pour une métallicité solaire, sont représentés par un trait pointillé et plein, respectivement. Pour chaque modèle théorique à un âge donné, quatre traits sont illustrés représentant les modèles théoriques des études de Baraffe et al. 1998, D'Antona & Mazzitelli 1997, Palla & Stahler 1993 et Siess et al. 2000 (Song et al., 2003). Cette figure est tirée de Zuckerman & Song (2004).

1.2.2 Âge cinématique

Historiquement, la cinématique d'une étoile a été utilisée pour différencier la population du disque galactique épais à celle du disque mince ou bien du halo offrant une estimation grossière de l'âge d'une étoile. L'approche utilisée dans le voisinage solaire est similaire à plus petite échelle, et ce en utilisant des groupes restreints en taille.

L'identification des étoiles situées dans le voisinage solaire a débuté dans les années 1950 avec les travaux de Eggen (1958) développant une méthode cinématique, dite du point convergent, pour identifier les étoiles membres du groupe des Hyades.

L'âge cinématique d'une étoile est déterminé par la comparaison du mouvement spatial galactique et de la position galactique de celle-ci à ceux d'un groupe. Les étoiles membres d'un groupe cinématique comportent caractéristiques communes découlant de leur naissance simultanée : le mouvement dans l'espace, la position galactique et l'âge.

Le mouvement dans l'espace est décrit par la combinaison d'un mouvement tangentiel au plan du ciel et d'un mouvement radial. Le déplacement tangentiel est mesuré par son mouvement propre en ascension droite et en déclinaison, tandis que le mouvement radial est mesuré par la vitesse radiale de l'étoile. Finalement, il faut connaître la distance à l'étoile en mesurant la parallaxe de celle-ci. En utilisant toutes ces informations, le mouvement global est quantifié dans l'espace selon les coordonnées de vitesses galactiques U, V, W (Johnson & Soderblom, 1987). Ces dernières décrivent le mouvement de l'étoile vers le centre galactique, dans le sens de la rotation galactique, et vers le pôle Nord galactique. De plus, la formation simultanée des étoiles place le groupe à une position galactique (XYZ) qui lui est propre et dont la paramétrisation nécessite la position sur le ciel (α, δ) et de la distance à celle-ci.

Cependant, l'utilisation de cette méthode afin de déterminer l'âge d'une étoile nécessite l'hypothèse de la formation simultanée de tous les membres de l'amas, où l'âge de l'amas est pré-établit en utilisant une autre technique (par exemple le diagramme H-R). L'hypothèse peut s'avérer erronée dans une situation où le passage d'une onde de choc aurait provoqué la formation des étoiles. Par conséquent, il existerait une dispersion réelle de l'âge des étoiles dans un même amas, et il est important de bien quantifier cette dispersion pour connaître l'histoire complète du processus de formation des étoiles du groupe et donc connaître la durée totale de ce processus (Hillenbrand, 2009, Mamajek et al., 2008).

Plusieurs études récentes (Kiss et al., 2010, Lépine & Simon, 2009, Montes et al., 2001, Schlieder et al., 2010, Torres et al., 2006, 2008) ont estimé l'appartenance et donc, l'âge cinématique de plus de 200 étoiles, en modélisant les vitesses et positions galac-

tiques des membres d'un groupe et en recherchant les propriétés similaires de ceux-ci. Un âge cinématique peut aussi être dérivé en utilisant la méthode du « Trace back », où les vitesses spatiales et les positions galactiques actuelles des étoiles d'un groupe sont combinées à une hypothèse du potentiel galactique pour prédire le moment où la distance entre les membres de l'amas est minimale (Asiain et al. 1999b). Cette estimation de temps correspond à la formation de l'amas et donc l'âge de celui-ci. Cette méthode est limitée par nos connaissances du potentiel galactique en place il y a près de 100 millions d'années.

En résumé, l'âge cinématique dépend de l'âge attribué préalablement aux membres d'un groupe par une autre technique. L'appartenance de l'étoile à un groupe est une condition nécessaire pour lui inférer l'âge de l'amas, mais il faut utiliser d'autres indicateurs afin de s'assurer de l'âge de l'étoile (Zuckerman & Song, 2004).

1.2.3   Le champ magnétique : activité chromosphérique

Suivant la formation de l'étoile, le champ magnétique d'origine fossile provoque l'accélération des gaz accrétés vers la surface de l'étoile et aussi l'éjection de matière par les vents stellaires de celle-ci (Dudorov, 1995, Lamm et al., 2005). L'évolution de l'intensité du champ magnétique, au cours de la vie d'une étoile, a une forte dépendance sur sa structure stellaire.

Les étoiles de type spectral B à F précoce (3 à 1.5 $M_\odot$) sont constituées d'un coeur convectif entouré par une enveloppe radiative, dont l'amplitude du champ généré est de quelques dizaines de Gauss. Les étoiles un peu moins massives transforment leur coeur convectif en coeur radiatif, provoquant une augmentation des champs magnétiques mesurés (Pizzolato et al., 1998). La structure stellaire des étoiles semblables à notre Soleil (F tardive à G tardive) est composée d'un coeur radiatif entouré d'une enveloppe convective. L'interaction entre la rotation différentielle longitudinale et la convection force la matière de la zone convective à être conductrice, ce qui crée une dynamo de type α-Ω (Browning et al., 2010), où le terme Ω est obtenu en présence de la rotation différentielle tandis que le terme α provient des mouvements de convection. Pour les étoiles de type spectral plus tardif, la profondeur de la couche convective augmente en

taille, jusqu'au moment où l'étoile est formée exclusivement par la zone convective. Dans le cas précis des étoiles ayant une masse sous les 0.4 $M_\odot$, l'âge de l'étoile a une forte dépendance sur la structure stellaire. Par exemple, une étoile de 0.4 $M_\odot$ âgée de 30 Mans sera complètement convective, tandis que la même étoile âgée de 400 Mans aura construit son coeur radiatif. L'amplitude des champs magnétiques mesurée est de l'ordre de 2-3 kGauss (Reiners 2012).

Il a été montré en 2006 par l'étude de binaires de type M éclipsantes (Stassun et al. 2006), que le principal impact de la présence du champ magnétique sur l'observation d'une étoile, est une diminution de la température effective et une inflation du rayon. L'énergie générée par le champ magnétique se répercute en activité chromosphérique et coronale, en chauffant les gaz de ces structures à des températures extrêmes. C'est donc par l'observation des manifestations chromosphériques (raies d'émission alcaline) et coronales (rayons X, UV, radio), que le champ magnétique sert d'indicateur de jeunesse.

L'étude pionnière de Skumanich (1972) a montré que l'activité chromosphérique décroît avec le temps selon une relation de la forme $\tau^{-1/2}$ pour les étoiles de la séquence principale. Cette décroissance est le résultat du transport de matière par les vents stellaires magnétisés dans l'environnement solaire ce qui implique une perte de moment cinétique et une diminution de la vitesse de rotation de l'étoile. Ce changement de la vitesse de rotation de l'étoile provoque une diminution de l'amplitude de la dynamo et donc des manifestations chromosphériques et coronales.

1.2.3.1   Émission Hα

La manifestation chromosphérique la plus couramment mesurée est celle qui provient de l'émission de la raie d'hydrogène (Hα) à 6562.8 Å. L'émission Hα est un traceur de l'activité chromosphérique causé par deux processus sur des échelles de temps différentes. Le premier processus causant cette émission provient de la force de la dynamo, en chauffant les gaz de la chromosphère provoquant l'émission de raies d'hydrogène. Cependant, pour les étoiles de type F précoce, en l'absence de zone convective l'émission de la raie Hα est directement fonction de l'âge de l'étoile et s'observe durant quelques Mans. Les étoiles de faible masse, dont la couche convective est importante,

montrent l'émission d'une raie Hα durant une longue période. Plus précisément, l'âge inféré à une étoile de type M0V montrant une émission Hα est de moins de 1 millard d'années, tandis que cet âge augmente à 4 milliard d'années pour une étoile de type M4V (West et al. 2008).

Une limitation de l'utilisation du flux Hα provient de l'émission instantanée d'hydrogène faisant augmenter et diminuer rapidement la luminosité en Hα (« flares »). Cette manifestation a pour effet de créer une dispersion du flux Hα pour un même type d'étoile, n'ayant pas de lien avec la jeunesse de cette dernière.

Le second processus d'émission Hα prend naissance lors de l'accrétion de matière du disque de poussières à la surface de l'étoile jeune produisant l'émission Hα par les gaz chauffés et accélérés. Le profil de la raie d'une telle émission est légèrement différent de l'émission chromosphérique. En effet, la raie est élargie (par l'effet Doppler) et la largeur de la raie (« 10% width » ; $W_{H\alpha}$) est supérieure à 10 Å ou entre 200 et 300 km s^{-1}(Shkolnik et al., 2009, White & Basri, 2003). Ce type d'émission disparaît à l'intérieur des premiers 10 Mans de l'étoile, lorsque l'évaporation du disque interne de poussière est terminée (Barrado y Navascués & Martín, 2003).

1.2.3.2　Émission CaII H-K et IRT

Depuis l'étude pionnière de Wilson (1963), la mesure de l'intensité des raies de calcium (Ca II) constitue la façon la plus fréquente de mesurer une manifestation chromosphérique du champ magnétique pour les étoiles de type solaire. Le projet HK au Mont Wilson a fait la mesure des raies de Ca II H (3968.3 Å) et K (3933.3 Å) pour plusieurs étoiles sur une longue période de temps. La mesure des raies de calcium permet de relier l'intensité de celles-ci avec l'âge de l'étoile selon la relation Ca $\propto \tau^{-1/2}$ (Skumanich, 1972). L'évaluation comparative de l'activité pour tous les types d'étoiles est réalisée en faisant le rapport entre le flux des raies HK et le flux bolométrique, ce qui définit l'indice R'_{HK} (Noyes et al., 1984). La figure 1.4 montre le comportement de l'indice R'_{HK} en fonction de l'âge de l'étoile provenant de différentes études. Plus précisément, en utilisant les relations de Mamajek & Hillenbrand (2008) pour les étoiles de type spectral entre F7V et K2V, il est possible d'estimer l'âge d'une étoile entre 40 Mans et quelques milliards

d'années.
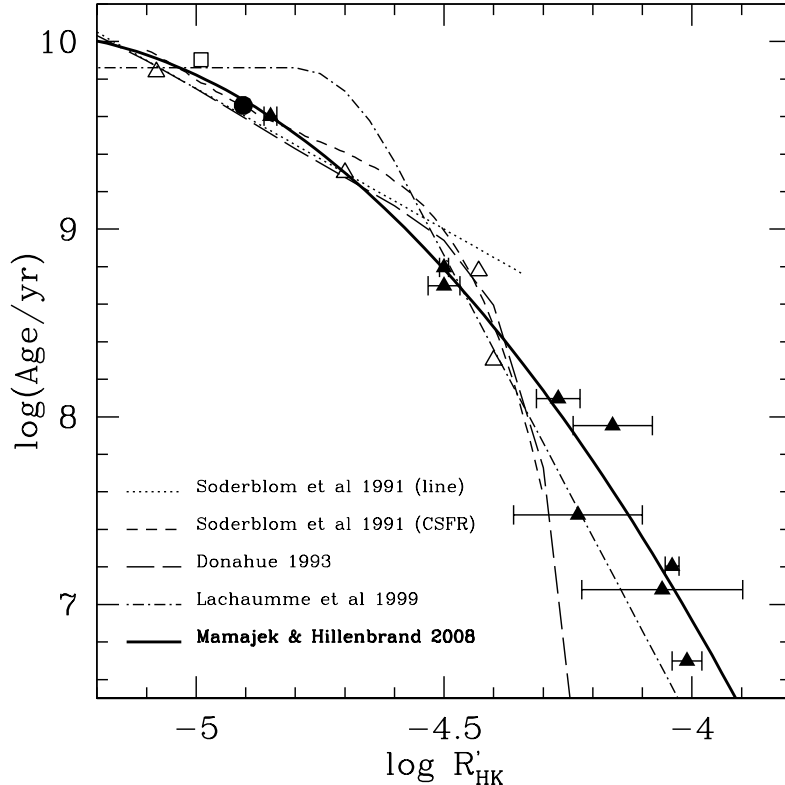
Figure 1.4 L'âge d'une étoile de type spectral entre F7V et K2V en fonction de la moyenne du rapport d'activité chromosphérique des raies de calcium HK. Les valeurs moyennes de R'_{HK} provenant de Mamajek & Hillenbrand (2008) sont représentées par des triangles pleins et les valeurs moyennes provenant d'études précédentes par des triangles vides. Le cercle noir plein représente le Soleil. Cette figure est tirée de Mamajek & Hillenbrand (2008).

Le désavantage principal de cet indicateur provient de l'inefficacité d'utilisation pour les étoiles de faible masse puisque la distribution d'énergie est maximale dans l'infrarouge proche, laissant très peu d'énergie entre 3500 et 4500 Å. Une alternative serait d'utiliser le triplet du calcium infrarouge (Ca II IRT) à 8498, 8542, 8662 Å pour ce type d'étoile (López-Santiago et al., 2010, Martínez-Arnáiz et al., 2011).

En résumé, le log R'_{HK} est un bon indicateur pour les étoiles de type F à K précoce afin d'estimer l'âge de celles-ci entre 5 Mans et quelques milliards d'années. Pour les étoiles de type K tardifs à M, il est possible de quantifier l'intensité des raies de calcium sans toutefois pouvoir inférer précisément l'âge de celles-ci.

1.2.4   Le champ magnétique : activité coronale

L'activité coronale est produite lorsque les gaz de la couronne de l'étoile sont chauffés par la dynamo stellaire. Le rayonnement X et UV de l'étoile sont deux manifestations montrant l'activité coronale pour les étoiles de type F tardives à M tardives. La relation entre l'activité coronale et l'âge de l'étoile provient principalement des observations en rayons X. Depuis quelques années, les observations en UV ont permis le développement des connaissances sur l'activité coronale pour les étoiles de plus faible luminosité s'inscrivant sous la limite de détection des précédents télescopes spatiaux à rayons X.

1.2.4.1   Émission de rayons X

Les gaz de la couronne d'une étoile sont chauffés par la dynamo et ils émettent des rayons X. Pour mesurer le flux X, il faut combiner les mesures des rayons X *doux* entre 0.1 et 2.4 keV (6-100 Å) et *durs* entre 0.06 et 0.2 keV (60-300 Å) à ceux du nombre d'évènements par seconde (Kastner et al., 2003, Mamajek & Hillenbrand, 2008).

L'étude de Preibisch & Feigelson (2005) a montré que $L_X \propto \tau^{-0.75}$ d'après l'observation d'étoiles dont la masse varie entre 0.1 et 1.5 $M_\odot$ et l'âge entre 1 et 625 Mans. Cette étude a également montré qu'il existe une relation entre la luminosité X, l'âge de l'étoile et la masse de celle-ci, cette relation est présentée à la figure 1.5. La partie gauche de la figure 1.5 illustre la valeur moyenne du $\log L_X$ pour trois classes d'étoiles et cinq groupes d'âge. Les étoiles âgées entre 1 et 10 Mans montrent un $\log L_X$ entre 29.5 et 30.5 ergs^{-1}, tandis que les étoiles membres des Hyades ($\sim$ 650 Mans) montrent un $\log L_X$ entre 28 et 29 ergs^{-1}. Cette relation liant la luminosité X à l'âge nécessite donc la connaissance de la distance trigonométrique de l'objet, une information inaccessible pour la vaste majorité des étoiles. Il a donc été proposé d'utiliser le rapport entre la luminosité X et la luminosité bolométrique ($R_x = \log L_x/L_{bol}$) comme indicateur d'âge. Ce rapport montre une saturation à la valeur de -3 pour les étoiles de type M (Berger et al., 2010, Pizzolato et al., 2003), limitant ainsi son utilisation pour estimer l'âge d'une étoile à l'intérieur d'un intervalle de 10-100 Mans. La majorité des mesures du champ magnétique provient de l'utilisation de la spectro-polarimétrie. Il est aussi possible de

mesurer l'effet Zeeman sur les raies de Fer dans la partie rouge du spectre d'une étoile.
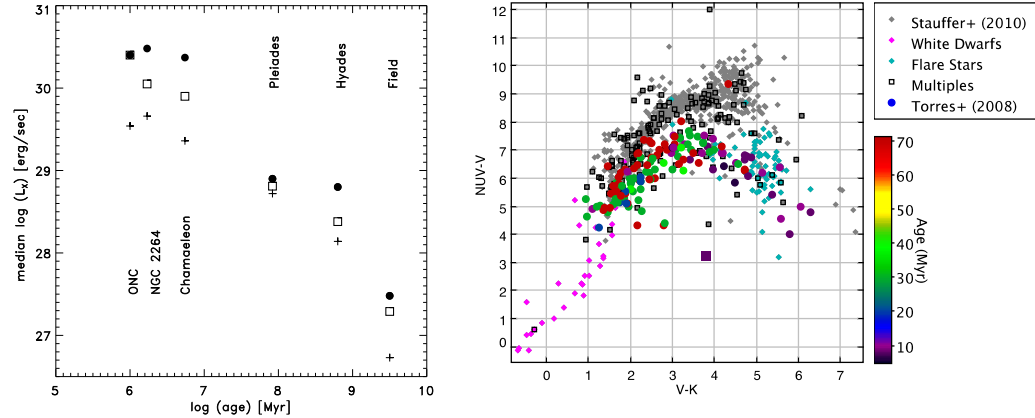
Figure 1.5 **Figure de gauche :** Luminosité en rayons X en fonction de l'âge (ONC = 1 Man, NGC2264 = 1.7 Mans, Chamaeleon = 5.5 Mans, Pléiades = 80 Mans, Hyades = 650 Mans) pour les étoiles de type G (0.9-1.2 $M_\odot$; cercles noirs), les naines K (0.5-0.9 $M_\odot$; carrés) et les naines M (0.1-0.5 $M_\odot$; croix). Cette figure est tirée de Preibisch & Feigelson (2005). **Figure de droite :** Rayonnement $NUV - V$ en fonction l'indice de couleur $V - K$ pour un échantillon d'étoiles jeunes du voisinage solaire (cercles de différentes couleurs). L'échantillon d'étoiles vieilles est représenté par les losanges gris. Cette figure est tirée de Rodriguez et al. (2011).

En résumé, l'émission de rayons X permet de mesurer une manifestation de l'intensité du champ magnétique et de relier cette dernière à l'âge de l'étoile. Pour les étoiles dont la masse varie entre 0.9 et 1.5 $M_\odot$, la luminosité X semble montrer une diminution avec l'augmentation de l'âge de l'étoile. Il faut noter que la binarité d'un objet peut être interprétée similairement au comportement d'une étoile jeune montrant une forte activité coronale.

1.2.4.2 Rayonnement ultraviolet

Le champ magnétique des étoiles est responsable du chauffage des gaz de la chromosphère ($T \sim 10^4$) à la région de transition ($T \sim 10^5$) puis à la couronne ($T \sim 10^6$), produisant une émission dans le domaine ultraviolet. Cet indicateur est utilisé depuis peu, puisque l'émergence de cette technique provient, principalement, des résultats du télescope spatial *Galaxy Evolution Explorer* (GALEX; Martin et al., 2005). Le télescope observe simultanément en ultraviolet proche (*NUV*) entre 1750 et 2750 Å et dans

l'ultraviolet lointain (FUV) entre 1350 et 1750 Å. De façon générale, les étoiles jeunes montrent un indice $NUV - V$ inférieur aux étoiles vieilles pour un type spectral donné (partie droite de la figure 1.5). Les étoiles de faible masse (K7-M : $V - K$ = 3.2-6.1) présentent un indice $NUV - V$ environ 2 magnitudes plus faibles que les étoiles vieilles (voir la partie droite de la figure 1.5). Tandis que les étoiles jeunes de type F et G ($V - K$ = 1.0-2.0) ont sensiblement la même brillance que les étoiles vieilles du champ. Par conséquent, l'utilisation du rayonnement ultraviolet permet d'identifier plus facilement les étoiles de faible masse montrant une forte activité coronale (Findeisen & Hillenbrand, 2010).

1.2.5   La gyrochronologie

La gyrochronologie est une méthode utilisant la vitesse de rotation d'un objet pour lui inférer un âge, et cet indicateur est étroitement lié à la force du champ magnétique. Lors de l'effondrement d'un nuage moléculaire, la conservation du moment cinétique a pour effet de créer un disque circumstellaire autour de l'étoile naissante en rotation (Shu et al., 1987). Par la suite, l'évolution du moment cinétique d'une étoile jeune est régie par plusieurs étapes. Premièrement, la présence du disque de poussière permet le transfert du moment cinétique de l'étoile vers le disque provoquant le freinage de la rotation pendant les premiers millions d'années. Deuxièmement, lorsque la phase évolutive d'accrétion et de couplage du disque pour les étoiles PSP est terminée, les étoiles toujours en contraction, voient leur vitesse de rotation augmenter (Weise et al., 2010). L'augmentation de la vitesse de rotation provoque un accroissement du champ magnétique et de l'interaction entre les éjections de masse et les vents stellaires. Durant cette période, la contraction gravitationnelle est plus forte que la perte de moment cinétique par les interactions avec le millieu, donc la vitesse de rotation continue de croître. Enfin, après l'atteinte de l'équilibre hydrostatique, les interactions entre l'étoile et son environnement sont toujours importantes, par conséquent il y a ralentissement de la vitesse de rotation de l'étoile (Weise et al., 2010).

Deux méthodes sont utilisées pour mesurer la rotation stellaire. La première mesure la vitesse projetée de l'étoile par le $v \sin i$, soit l'élargissement des raies dans le spectre

de l'étoile. On peut transformer le *v* sin *i* en une période de rotation en utilisant l'hypo-
thèse que la rotation de l'étoile est décrite par la rotation d'un corps rigide (Bailer-Jones,
2004), et utiliser les estimations de rayon provenant des modèles évolutifs (Valenti &
Fischer, 2005, Weise et al., 2010).
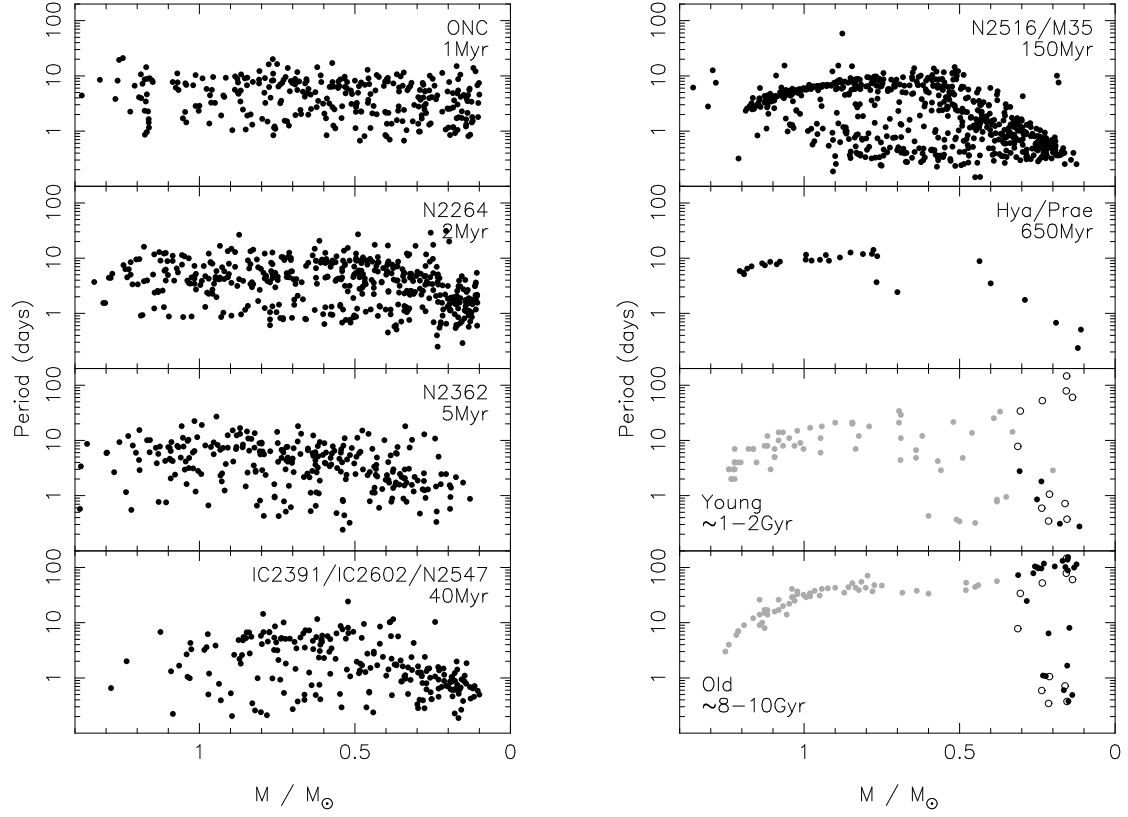
Figure 1.6 Diagramme masse-période des membres de 6 amas âgés entre 1 et 600 Mans, comparé à la
distribution des étoiles jeunes et vieilles du disque Galactique. Cette figure est tirée de Irwin et al. (2011).

La deuxième méthode utilise la période de rotation quantifiée par la variabilité pho-
tométrique de l'étoile, la période varie entre 1 et 10 jours pour les étoiles très jeunes
(1-10 Mans). La figure 1.6 présente les diagrammes masse-période pour une population
d'étoiles (F5V-M5V) âgées entre 30 et 600 Mans, où on peut constater le comportement
de type Skumanich, c'est-à-dire une augmentation de la période en fonction du temps.
De plus, il est possible d'utiliser les modèles d'évolution du moment cinétique pour
obtenir une prédiction sur la vitesse de rotation d'une étoile.

Les modèles évolutifs de la rotation des étoiles montrent un comportement similaire

à celui qui est observé dans les amas d'étoiles. La figure 1.7 présente les résultats des modèles évolutifs pour des étoiles dont la masse varie entre $0.1 < M < 1.0\,M_{\odot}$.
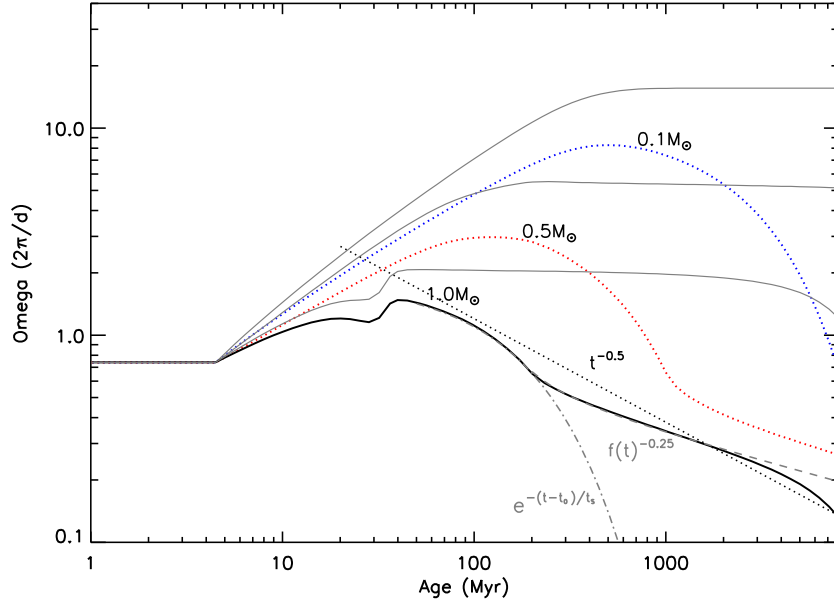
Figure 1.7 Évolution de la vitesse angulaire (proxi du moment cinétique) en fonction de l'âge et de la masse de l'étoile. Les traits continus noirs représentent l'évolution du moment angulaire en l'absence de facteurs pouvant ralentir la vitesse de rotation. Cette figure est tirée de Reiners & Mohanty (2012).

Selon ces modèles, le comportement rotationnel d'une étoile à 10 Mans est similaire à celui d'une étoile de 100 Mans pour une masse donnée. Dans cette situation, il faut donc combiner la gyrochronologie à d'autres indicateurs de jeunesse pour inférer plus précisément l'âge d'une étoile.

1.2.6 La présence de lithium

Le lithium (Li) est un élément primordial qui compose la photosphère des étoiles naissantes. Normalement détruit dans le coeur radiatif de l'étoile où la température est supérieure à 2.5 x 10^6 K, celle-ci s'exprime par la réaction $Li^7 + p \rightarrow He^4 + He^4$ (Reid & Cruz, 2002, Rebolo et al., 1992). Le taux auquel le lithium est détruit dépend de la structure stellaire de l'étoile. Plus la zone convective d'une étoile est profonde, plus facile est le transport du lithium vers le coeur de l'étoile par les processus de convection et de

mélange. La destruction est donc plus efficace, et l'abondance de lithium diminue sur une période de temps plus courte. Cependant, les dernières années ont montré l'influence de plusieurs facteurs sur le taux de destruction, dont le champ magnétique. La spectroscopie à moyenne résolution d'une étoile permet de mesurer la EW_{Li} à 6707.8 Å. Pour les étoiles riches en lithium, il est possible d'observer une seconde raie à 6103 Å.

Il est important d'étudier la présence de lithium dans les atmosphères des étoiles membres de plusieurs groupes afin d'étudier l'efficacité des processus de mélange en fonction de l'âge. De plus, la présence de lithium est souvent utilisée pour estimer l'âge relatif d'un groupe. La partie gauche de la figure 1.8 présente le comportement de la EW_{Li} en fonction du type spectral (F à M) pour 5 groupes d'étoiles dont les membres sont âgés entre 5 et 70 Mans. Pour les étoiles de faible masse, la principale conclusion est l'absence de relation simple entre la présence de Li et l'âge de l'étoile. Cependant, selon ce recensement il n'existe pas de Li dans l'atmosphère des étoiles de faible masse âgées de plus de 70 Mans.
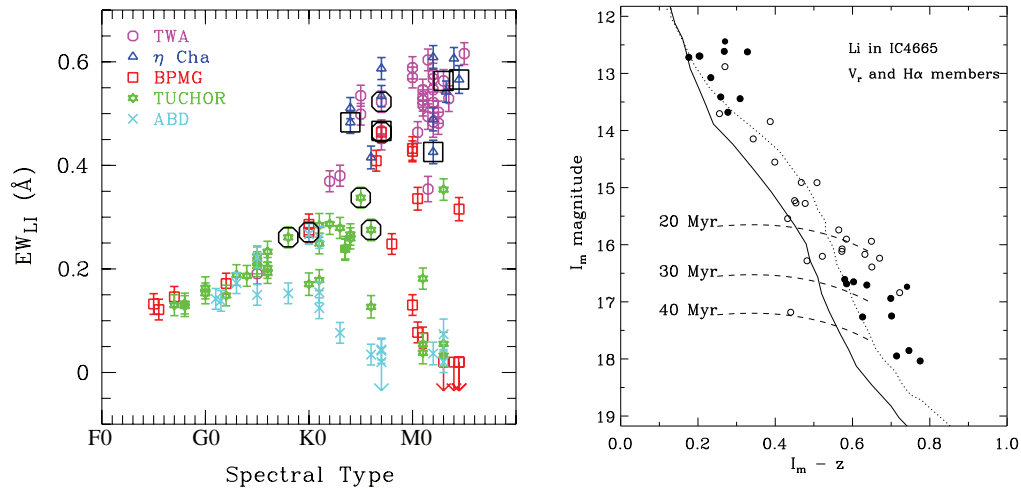
Figure 1.8 **Figure de gauche :** Largeurs équivalentes du lithium en fonction du type spectral pour un échantillon d'étoiles jeunes membres des groupes cinématiques (8-70 Mans). Les étoiles ayant de grandes vitesses de rotation et celles montrant des signes d'accrétion sont représentées, respectivement, par des octogones et des carrés. Cette figure est tirée de Mentuch et al. (2008). **La figure de droite :** Séquence du lithium (I vs $I - z$) pour les membres de l'amas IC 4665 âgés de 30 Mans. Les cercles noirs pleins et vides représentent, respectivement, les étoiles avec détection de lithium et sans détection. Cette figure est tirée de Mamajek et al. (2008).

La comparaison de plusieurs amas ayant des âges similaires montre une dispersion

de la EW_{Li}. De plus, il demeure difficile d'interpréter ces dispersions, puisque la masse de l'objet, la période de rotation et le champ magnétique peuvent influencer les processus de convection et le taux de destruction du Li.

Pour estimer l'âge absolu de l'amas et celui d'une étoile isolée, il faut comparer l'abondance du Li à celle prédite selon les modèles théoriques. La conversion de la EW_{Li} en abondance est dépendante des modèles théoriques et donc des processus physiques pris en compte (théorie mélange, rotation, taux de perte du moment cinétique). De plus, le potentiel d'ionisation du lithium est faible ce qui implique une forte dépendance sur la stratification en température de l'étoile. Pour faire cette conversion, il faut connaître préalablement la T_{eff} et utiliser des spectres synthétiques provenant des modèles théoriques (Mentuch et al., 2008).

Pour un amas d'étoiles, la présence ou l'absence de lithium permet de décrire une séquence empirique appelée « Lithium Depletion Boundary »(LDB) dépendamment de l'âge du groupe (Jeffries, 2000). La partie droite de la figure 1.8 montre la séquence LBD pour l'amas d'étoiles IC 4665. Cette méthode a été proposée pour la première fois par Rebolo et al. (1992) afin de discriminer les naines brunes du champ et les étoiles de très faible masse. La séquence empirique est déterminée sur un diagramme couleur-magnitude, et l'âge de l'amas est estimé selon la magnitude à laquelle on perçoit une coupure entre les étoiles de faible masse et les étoiles de très faible masse. La magnitude de l'étoile à laquelle se produit cette coupure est comparée avec celle prédite par les modèles évolutifs, en appliquant la correction bolométrique appropriée (Mamajek et al., 2008).

L'utilisation de la destruction du lithium pour inférer un âge aux étoiles se heurte à plusieurs problèmes lorsqu'on compare les observations aux modèles. Le champ magnétique des étoiles PSP pourrait interrompre le processus de destruction du lithium (Soderblom, 2010). La binarité des systèmes pourrait faire augmenter la vitesse de rotation et donc diminuer l'efficacité des processus de destruction (López-Santiago et al., 2010). Un autre facteur pouvant expliquer la dispersion en lithium proviendrait de la formation de planètes autour des étoiles. Pour le moment, peu d'études observationnelles montrent de relation entre le faible taux de Li et la présence de planètes (Baraffe & Cha-

brier, 2010). Finalement, les épisodes d'accrétion de matière ont pour effet d'augmenter la température centrale de l'étoile et de causer la destruction plus rapide du Li (Baraffe & Chabrier, 2010).

1.2.7 La gravité de surface

L'étoile jeune de la PSP n'a pas atteint l'équilibre hydrostatique, par conséquent le volume de l'étoile est plus grand que celui d'une étoile de la séquence principale, impliquant une gravité de surface plus faible (Shkolnik et al., 2009). Les étoiles jeunes ont des gravités de surface ($\log g$) entre 3.5-4.5 par rapport à 4.5-5.5 pour les étoiles plus âgées (dépendamment de la masse). Ainsi, la gravité de surface est un indicateur clé traçant la naissance récente de l'étoile.

Une mesure quantitative de la gravité de surface d'une étoile provient de l'ajustement des spectres théoriques aux données observationnelles (Mentuch et al., 2008, Mohanty et al., 2004a). Pour ce faire, il faut sélectionner préalablement les raies spectrales (NaI, KI, CaH, VO, CN, TiO) sensibles à la température et/ou à la gravité de surface de l'étoile. La partie gauche de la figure 1.9 montre le comportement de la gravité de surface en fonction de la T_{eff} en utilisant plusieurs raies différentes pour déterminer la gravité. On constate que le comportement de la gravité de surface varie peu en fonction de l'âge pour les étoiles dont la T_{eff} est supérieure à 5000 K. La partie droite de la figure 1.9 montre la variation de l'indice spectral du NaI en fonction de l'âge et du type spectral de l'objet. L'utilisation de cet indice permet de contraindre plus facilement l'âge des étoiles plus tardives que M4V, comparativement aux étoiles de type M0V.

Le désavantage de la molécule du CaH est sa sensibilité à la métallicité de l'objet. Une forte métallicité peut influencer le comportement de la bande moléculaire et dans cette situation imiter un objet de faible gravité de surface. De plus, les doublets de potassium (K I) et sodium (Na I) sont affectés par l'activité stellaire de l'étoile. Pour les étoiles de type M, l'activité chromosphérique tend à faire gonfler les étoiles, ce qui s'observe en une diminution de la largeur équivalente des raies et donc, on mesure un indicateur similaire à celui d'une étoile ayant une faible gravité de surface (Shkolnik et al., 2009).

En résumé, l'estimation de l'âge d'une étoile jeune en utilisant la gravité de surface
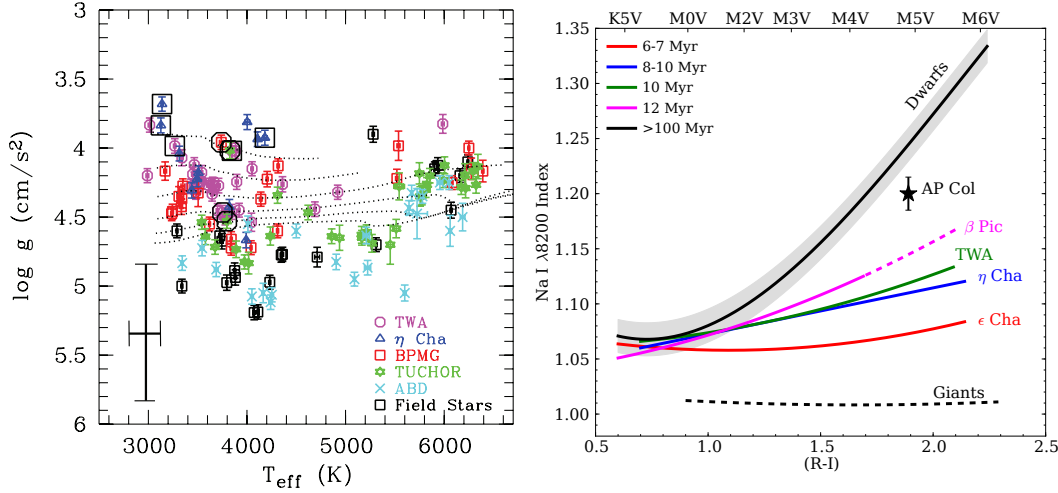
Figure 1.9 **Gauche** : Gravité de surface en fonction de la température effective pour des étoiles jeunes membres des groupes cinématiques (8-70 Mans). Les lignes pointillées représentent résultats des modèles évolutifs pour un âge de 4, 8, 15, 25, 35, 45 et 150 Mans. Les étoiles ayant de grandes vitesses de rotation et celles montrant des signes d'accrétion sont représentées, respectivement, par des octogones et des carrés. Cette figure est tirée de Mentuch et al. (2008). **Droite** : L'indice de NaI à 8200Å en fonction de l'indice de couleur $R - I$. Figure tirée de Riedel et al. (2011)

est une méthode efficace, mais plus précise pour les étoiles ayant une T_{eff} inférieure à 5000 K.

1.3 Intérêt porté aux étoiles jeunes de faible masse

Représentant près de 70% du contenu stellaire de notre Galaxie, les étoiles de faible masse permettent une étude statistique de leurs propriétés fondamentales. Favorisée par la position galactique des associations jeunes du voisinage solaire, l'identification des étoiles jeunes de faible masse permet de contraindre les fonctions de masse et de luminosité pour finalement dériver une FMI. Tel que présenté dans les sections précédentes, les connaissances actuelles des paramètres fondamentaux des étoiles jeunes de faible masse se butent à de nombreux obstacles. Cependant, l'intérêt marqué pour ces étoiles depuis quelques années provoque aussi la tombée des barrières de façon rapide et efficace.

Cet intérêt s'est accru par la récente évolution des capacités technologiques (vitesse radiale) provoquant la découverte de nombreux objets de masse planétaire, orbitant au-

tour des étoiles de faible masse. Il est donc essentiel de caractériser précisément les paramètres des étoiles hôtes. Un second avantage est l'importance de la présélection des étoiles montrant certains indicateurs de jeunesse, favorisant ainsi la détection de planètes de quelques fois la masse de Jupiter, en utilisant la technique de l'imagerie directe. De plus, notre quête de connaissances des exoplanètes situées dans la zone habitable dirige nos recherches vers les étoiles de faible masse. Ces petites étoiles cachent un fort champ magnétique entretenu par leur dynamo et par l'évolution de leur structure stellaire. Il y a donc une motivation supplémentaire à vouloir contraindre observationnellement l'amplitude du champ magnétique pour un âge donné. Ces contraintes sont importantes pour vérifier la validité des modèles évolutifs et d'atmosphère, et permettre de quantifier l'impact d'un facteur spécifique (l'accrétion et la rotation) sur le résultat obtenu.

1.4 Objectifs de cette étude

Le but premier de cette thèse est la recherche d'étoiles jeunes de faible masse, afin de complémenter nos connaissances sur les objets du voisinage solaire. Pour augmenter l'efficacité de ce travail, une méthode statistique a été développée, fondée sur les propriétés connues des étoiles jeunes par rapport aux étoiles vieilles. Découlant de cette première étape, un programme de caractérisation des objets supposés jeunes a été mis sur pied. L'objectif de ce programme est la caractérisation des systèmes permettant de contraindre plus précisément (10-50 Mans) l'âge d'une étoile.

Le Chapitre 2 présente une nouvelle méthode d'identification des systèmes jeunes faisant partie des associations cinématiques du voisinage solaire. La méthode statistique est basée sur l'inférence bayésienne, ce qui permet d'obtenir une probabilité d'appartenance étant donné certaines connaissances et hypothèses. Des modèles empiriques représentants les caractéristiques des étoiles jeunes connues jusqu'au début de l'année 2012 ont été développés pour ensuite être appliqués à un échantillon d'étoiles de faible masse montrant *a priori* des signes de jeunesse.

Le Chapitre 3 présente une étude de caractérisation cinématique des 219 systèmes identifiés au Chapitre 2. Trois paramètres ont été caractérisés, soit la vitesse radiale, la

vitesse de rotation et la luminosité X par rapport aux étoiles vieilles du champ. Ceci a mené à la paramétrisation de la luminosité X pour les étoiles jeunes de faible masse en fonction du groupe cinématique associé.

Le Chapitre 4 présente la détermination des paramètres fondamentaux de 59 étoiles de faible masse, obtenus en combinant des observations spectroscopiques et photométriques. Ces paramètres fondamentaux ont permis une comparaison avec de nouveaux modèles d'évolution stellaire spécifiques aux étoiles de faible masse, lesquels comportent le traitement du champ magnétique (dynamo rotationnelle).

1.5 Déclaration de l'étudiant

Les articles présentés aux chapitres 2, 3 et 4 sont le résultat de mes travaux réalisés dans le cadre de ce doctorat. Pour le chapitre 2, le formalisme de l'analyse statistique a été développé en collaboration avec René Doyon, David Lafrenière et Étienne Artigau. J'ai bâti l'échantillon de référence pour développer les modèles empiriques utilisés par l'analyse. Par la suite, j'ai bâti un échantillon d'étoiles (en me référant à la littérature connue) pour y appliquer l'analyse. Les résultats obtenus et les simulations Monte-Carlo sont le fruit de mon travail. La discussion des résultats a été améliorée par la lecture des coauteurs. De plus, plusieurs suggestions d'analyses par les coauteurs ont grandement amélioré la qualité de cet article.

Pour le chapitre 3, l'article est constitué d'une immense quantité d'observations réalisées sur trois grands télescopes internationaux et dont les demandes de temps nécessaires à ce projet ont été rédigées par l'ensemble des auteurs. Par la suite, j'ai préparé les observations et analysé les données scientifiques en étroite collaboration avec Étienne Artigau. La présentation et la discussion des résultats ont été faites en collaboration avec René Doyon. La révision du manuscrit a été réalisée par tous les coauteurs, ce qui a grandement amélioré la qualité de l'article.

Pour le chapitre 4, j'ai planifié les observations utilisées dans cet article, en plus d'utiliser des données d'archive du télescope Canada-France-Hawaii. Le dépouillement des données a été réalisé en collaboration avec Loic Albert et Étienne Artigau ; l'analyse

et la discussion ont été faites principalement en collaboration avec René Doyon. Les plus récents modèles théoriques proviennent d'une collaboration avec Gregory Feiden. Les résultats observationnels ont été comparés à ces nouveaux modèles magnétiques et l'interprétation des résultats a été réalisée en étroite collaboration avec René Doyon et Gregory Feiden.

L'annexe I présente une brève description des articles publiés en tant qu'auteur secondaire. Les articles présentés à la section I.1 découlent directement des collaborations scientifiques entamées grâce aux développements des travaux présentés dans cette thèse.

BIBLIOGRAPHIE

Allard, F., Hauschildt, P. H., Alexander, D. R., & Starrfield, S. 1997, ARA&A, 35, 137

Bailer-Jones, C. A. L. 2004, A&A, 419, 703

Baraffe, I., & Chabrier, G. 2010, A&A, 521, A44+

Baraffe, I., Chabrier, G., Allard, F., & Hauschildt, P. 2003, in IAU Symposium, Vol. 211, Brown Dwarfs, ed. E. Martín, 41–+

Barnes, S. A. 2003, ApJ, 586, 464

—. 2007, ApJ, 669, 1167

Barrado y Navascués, D., & Martín, E. L. 2003, AJ, 126, 2997

Barrado y Navascués, D., Stauffer, J. R., & Jayawardhana, R. 2004, ApJ, 614, 386

Basri, G., Marcy, G., Oppenheimer, B., Kulkari, S. R., & Nakajima, T. 1996, in Astronomical Society of the Pacific Conference Series, Vol. 109, Cool Stars, Stellar Systems, and the Sun, ed. R. Pallavicini & A. K. Dupree, 587–+

Bastian, N., Covey, K. R., & Meyer, M. R. 2010, ARA&A, 48, 339

Berger, E., et al. 2010, ApJ, 709, 332

Bergfors, C., et al. 2010, A&A, 520, A54+

Beristain, G., Edwards, S., & Kwan, J. 2001, ApJ, 551, 1037

Blaauw, A. 1946, Publications of the Kapteyn Astronomical Laboratory Groningen, 52, 1

—. 1964, ARA&A, 2, 213

Bochanski, Jr., J. J. 2008, PhD thesis, University of Washington

Browning, M. K., Basri, G., Marcy, G. W., West, A. A., & Zhang, J. 2010, AJ, 139, 504

Burrows, A., Hubbard, W. B., Lunine, J. I., & Liebert, J. 2001, Reviews of Modern Physics, 73, 719

Chabrier, G. 2003, PASP, 115, 763

Cox, D. P. 1998, in Lecture Notes in Physics, Berlin Springer Verlag, Vol. 506, IAU Colloq. 166 : The Local Bubble and Beyond, ed. D. Breitschwerdt, M. J. Freyberg, & J. Truemper, 121–131

D'Antona, F., & Mazzitelli, I. 1994, ApJS, 90, 467

de Zeeuw, P. T., Hoogerwerf, R., de Bruijne, J. H. J., Brown, A. G. A., & Blaauw, A. 1999, AJ, 117, 354

Dobbie, P. D., Lodieu, N., & Sharp, R. G. 2010, MNRAS, 409, 1002

Donati, J., et al. 2003, MNRAS, 345, 1145

Dudorov, A. E. 1995, AZh, 72, 884

Eggen, O. J. 1958, MNRAS, 118, 65

Epchtein, N., et al. 1997, The Messenger, 87, 27

Feigelson, E. D. 1996, ApJ, 468, 306

Fernández, D., Figueras, F., & Torra, J. 2008, A&A, 480, 735

Findeisen, K., & Hillenbrand, L. 2010, AJ, 139, 1338

Frink, S., Roeser, S., Alcala, J. M., Covino, E., & Brandner, W. 1998, A&A, 338, 442

Genzel, R., & Stutzki, J. 1989, ARA&A, 27, 41

Gould, B. A. 1874, Proceedings of the American Association for Advanced Science

Gray, R. O., Corbally, C. J., Garrison, R. F., McFadden, M. T., Bubar, E. J., McGahee, C. E., O'Donoghue, A. A., & Knox, E. R. 2006, AJ, 132, 161

Guedel, M., Guinan, E. F., & Skinner, S. L. 1997, ApJ, 483, 947

Hauschildt, P. H., Allard, F., & Baron, E. 1999, ApJ, 512, 377

Hayashi, C., Hōshi, R., & Sugimoto, D. 1962, Progress of Theoretical Physics Supplement, 22, 1

Herbig, G. H. 1985, ApJ, 289, 269

Herbig, G. H., & Kameswara Rao, N. 1972, ApJ, 174, 401

Hillenbrand, L. A. 1997, AJ, 113, 1733

Hillenbrand, L. A. 2009, in IAU Symposium, Vol. 258, IAU Symposium, ed. E. E. Mamajek, D. R. Soderblom, & R. F. G. Wyse, 81–94

Irwin, J., & Bouvier, J. 2009, in IAU Symposium, Vol. 258, IAU Symposium, ed. E. E. Mamajek, D. R. Soderblom, & R. F. G. Wyse, 363–374

James, D. J., Jardine, M. M., Jeffries, R. D., Randich, S., Collier Cameron, A., & Ferreira, M. 2000, MNRAS, 318, 1217

Jeffries, R. D. 2000, in Astronomical Society of the Pacific Conference Series, Vol. 198, Stellar Clusters and Associations : Convection, Rotation, and Dynamos, ed. R. Pallavicini, G. Micela, & S. Sciortino, 245–+

Johnson, D. R. H., & Soderblom, D. R. 1987, AJ, 93, 864

Kastner, J. H., Crigger, L., Rich, M., & Weintraub, D. A. 2003, ApJ, 585, 878

Kiss, L. L., et al. 2010, ArXiv e-prints

Kroupa, P. 2002, in Astronomical Society of the Pacific Conference Series, Vol. 285, Modes of Star Formation and the Origin of Field Populations, ed. E. K. Grebel & W. Brandner, 86–+

Lafrenière, D., et al. 2007, ApJ, 670, 1367

Lamm, M. H., Mundt, R., Bailer-Jones, C. A. L., & Herbst, W. 2005, A&A, 430, 1005

Lépine, S., & Simon, M. 2009, AJ, 137, 3632

Lodieu, N., Dobbie, P. D., & Hambly, N. C. 2011, A&A, 527, A24+

López-Santiago, J., Micela, G., & Montes, D. 2009, A&A, 499, 129

López-Santiago, J., Montes, D., Gálvez-Ortiz, M. C., Crespo-Chacón, I., Martínez-Arnáiz, R. M., Fernández-Figueroa, M. J., de Castro, E., & Cornide, M. 2010, A&A, 514, A97+

Luhman, K. L. 2001, ApJ, 560, 287

Luhman, K. L., Briceño, C., Stauffer, J. R., Hartmann, L., Barrado y Navascués, D., & Caldwell, N. 2003, ApJ, 590, 348

Makarov, V. V. 2006, AJ, 131, 2967

Mamajek, E. E., Barrado y Navascués, D., Randich, S., Jensen, E. L. N., Young, P. A., Miglio, A., & Barnes, S. A. 2008, in Astronomical Society of the Pacific Conference Series, Vol. 384, 14th Cambridge Workshop on Cool Stars, Stellar Systems, and the Sun, ed. G. van Belle, 374–+

Mamajek, E. E., & Hillenbrand, L. A. 2008, ApJ, 687, 1264

Mamajek, E. E., Lawson, W. A., & Feigelson, E. D. 1999, ApJ, 516, L77

—. 2000, ApJ, 544, 356

Marsden, S. C., Carter, B. D., & Donati, J. 2009, MNRAS, 399, 888

Martin, D. C., et al. 2005, ApJ, 619, L1

Martínez-Arnáiz, R. M., López-Santiago, J., Crespo-Chacón, I., & Montes, D. 2011, ArXiv e-prints

Mentuch, E., Brandeker, A., van Kerkwijk, M. H., Jayawardhana, R., & Hauschildt, P. H. 2008, ApJ, 689, 1127

Messina, S., Desidera, S., Lanzafame, A. C., Turatto, M., & Guinan, E. F. 2011, ArXiv e-prints

Mihalas, D., & Binney, J. 1981, Galactic astronomy : Structure and kinematics /2nd edition/, ed. Mihalas, D. & Binney, J.

Mohanty, S., Basri, G., Jayawardhana, R., Allard, F., Hauschildt, P., & Ardila, D. 2004, ApJ, 609, 854

Montes, D., López-Santiago, J., Gálvez, M. C., Fernández-Figueroa, M. J., De Castro, E., & Cornide, M. 2001, MNRAS, 328, 45

Neugebauer, G., et al. 1984, ApJ, 278, L1

Neuhauser, R., & Brandner, W. 1998, A&A, 330, L29

Noyes, R. W., Hartmann, L. W., Baliunas, S. L., Duncan, D. K., & Vaughan, A. H. 1984, ApJ, 279, 763

Perrot, C. A., & Grenier, I. A. 2003, A&A, 404, 519

Perryman, M. A. C., et al. 1997, A&A, 323, L49

Pizzolato, N., Maggio, A., Micela, G., Sciortino, S., & Ventura, P. 2003, A&A, 397, 147

Pizzolato, N., Maggio, A., & Sciortino, S. 1998, in Astronomical Society of the Pacific Conference Series, Vol. 154, Cool Stars, Stellar Systems, and the Sun, ed. R. A. Donahue & J. A. Bookbinder, 1146–+

Preibisch, T., & Feigelson, E. D. 2005, ApJS, 160, 390

Preibisch, T., & Mamajek, E. 2008, The Nearest OB Association : Scorpius-Centaurus (Sco OB2), 235–+

Proctor, R. A. 1869, Royal Society of London Proceedings Series I, 18, 169

Rebolo, R., Martin, E. L., & Magazzu, A. 1992, ApJ, 389, L83

Rebolo, R., Zapatero Osorio, M. R., & Martín, E. L. 1995, Nature, 377, 129

Reid, I. N., et al. 2004, AJ, 128, 463

Reid, I. N., Cruz, K. L., & Allen, P. R. 2007, AJ, 133, 2825

Reid, I. N., Gizis, J. E., & Hawley, S. L. 2002, AJ, 124, 2721

Reid, I. N., Hawley, S. L., & Gizis, J. E. 1995, AJ, 110, 1838

Reid, N., & Hawley, S. L., eds. 2000, New light on dark stars : red dwarfs, low mass
    stars, brown dwarfs

Rice, E. L., et al. 2011, ArXiv e-prints

Rodriguez, D. R., Bessell, M. S., Zuckerman, B., & Kastner, J. H. 2011, ApJ, 727, 62

Salpeter, E. E. 1955, ApJ, 121, 161

Schlieder, J. E., Lépine, S., & Simon, M. 2010, AJ, 140, 119

Shkolnik, E., Liu, M. C., & Reid, I. N. 2009, ApJ, 699, 649

Shkolnik, E. L., Liu, M. C., Reid, I. N., Dupuy, T., & Weinberger, A. J. 2011, ApJ, 727,
    6

Shu, F. H., Adams, F. C., & Lizano, S. 1987, ARA&A, 25, 23

Skrutskie, M. F., et al. 2006, AJ, 131, 1163

Skumanich, A. 1972, ApJ, 171, 565

Soderblom, D. R. 2010, ARA&A, 48, 581

Soderblom, D. R., Duncan, D. K., & Johnson, D. R. H. 1991, ApJ, 375, 722

Soderblom, D. R., Jones, B. F., Balachandran, S., Stauffer, J. R., Duncan, D. K., Fedele, S. B., & Hudon, J. D. 1993, AJ, 106, 1059

Song, I., Zuckerman, B., & Bessell, M. S. 2003, ApJ, 599, 342

Stauffer, J. R., Hartmann, L. W., Prosser, C. F., Randich, S., Balachandran, S., Patten, B. M., Simon, T., & Giampapa, M. 1997, ApJ, 479, 776

Stauffer, J. R., Jones, B. F., Backman, D., Hartmann, L. W., Barrado y Navascués, D., Pinsonneault, M. H., Terndrup, D. M., & Muench, A. A. 2003, AJ, 126, 833

Sterzik, M. F., & Durisen, R. H. 1995, A&A, 304, L9+

Sterzik, M. F., Durisen, R. H., & Pickett, B. K. 2001, in Astronomical Society of the Pacific Conference Series, Vol. 244, Young Stars Near Earth : Progress and Prospects, ed. R. Jayawardhana & T. Greene, 116–+

Takami, M., Chrysostomou, A., Bailey, J., Gledhill, T. M., Tamura, M., & Terada, H. 2003, Ap&SS, 287, 143

Torres, C. A. O., Quast, G. R., da Silva, L., de La Reza, R., Melo, C. H. F., & Sterzik, M. 2006, A&A, 460, 695

Torres, C. A. O., Quast, G. R., Melo, C. H. F., & Sterzik, M. F. 2008, Young Nearby Loose Associations, 757–+

Valenti, J. A., & Fischer, D. A. 2005, ApJS, 159, 141

van Leeuwen, F. 2009, A&A, 497, 209

Voges, W. 1994, in New Horizon of X-Ray Astronomy. First Results from ASCA, ed. F. Makino & T. Ohashi, 197–+

Walkowicz, L. M., Hawley, S. L., & West, A. A. 2004, PASP, 116, 1105

Walter, F. M. 1986, ApJ, 306, 573

Weise, P., Launhardt, R., Setiawan, J., & Henning, T. 2010, A&A, 517, A88+

West, A. A., Hawley, S. L., Bochanski, J. J., Covey, K. R., Reid, I. N., Dhital, S., Hilton, E. J., & Masuda, M. 2008, AJ, 135, 785

West, A. A., et al. 2011, AJ, 141, 97

White, R. J., & Basri, G. 2003, ApJ, 582, 1109

Wilson, O. C. 1963, ApJ, 138, 832

Yee, J. C., & Jensen, E. L. N. 2010, ApJ, 711, 303

York, D. G., et al. 2000, AJ, 120, 1579

Zuckerman, B., & Song, I. 2004, ARA&A, 42, 685

Zuckerman, B., Song, I., & Webb, R. A. 2001, ApJ, 559, 388

RECHERCHE DE NOUVELLES ÉTOILES MEMBRES DES ASSOCIATIONS CINÉMATIQUE PROCHE EN UTILISANT UNE ANALYSE BAYESIENNE

BAYESIAN ANALYSIS TO IDENTIFY NEW STAR CANDIDATES IN NEARBY YOUNG STELLAR KINEMATIC GROUPS

Lison Malo[1,2], René Doyon[2], David Lafrenière[2], Étienne Artigau[2], Jonathan Gagné[2], Frédérique Baron[2], and Adric Riedel[3]

Abstract

We present a new method based on a Bayesian analysis to identify new members of nearby young kinematic groups. The analysis minimally takes into account the position, proper motion, magnitude, and color of a star, but other observables can be readily added (e.g., radial velocity, distance). We use this method to find new young low-mass stars in the β Pictoris and AB Doradus moving groups and in the TW Hydrae, Tucana-Horologium, Columba, Carina, and Argus associations. Starting from a sample of 758 mid-K to mid-M (K5V-M5V) stars showing youth indicators such as Hα and X-ray emission, our analysis yields 215 new highly probable low-mass members of the kinematic groups analyzed. One is in TW Hydrae, 37 in β Pictoris, 17 in Tucana-Horologium, 20 in Columba, 6 in Carina, 50 in Argus, 33 in AB Doradus, and the remaining 51 candidates are likely young but have an ambiguous membership to more than one association. The false alarm rate for new candidates is estimated to be 5% for β Pictoris and

---

[1]Based on observations obtained at the Canada-France-Hawaii Telescope (CFHT) which is operated by the National Research Council of Canada, the Institut National des Sciences de l'"Univers of the Centre National de la Recherche Scientique of France, and the University of Hawaii.

[2]Département de physique and Observatoire du Mont-Mégantic, Université de Montréal, Montréal, QC H3C 3J7, Canada

[3]Department of Astrophysics, American Museum of Natural History, Central Park West at 79th Street, New York, NY 10024, USA

TW Hydrae, 10% for Tucana-Horologium, Columba, Carina, and Argus, and 14% for AB Doradus. Our analysis confirms the membership of 58 stars proposed in the literature. Firm membership confirmation of our new candidates will require measurement of their radial velocity (predicted by our analysis), parallax and lithium 6708 Å equivalent width. We have initiated these follow-up observations for a number of candidates, and we have identified two stars (2MASSJ01112542+1526214, 2MASSJ05241914-1601153) as very strong candidate members of the β Pictoris moving group and one strong candidate member (2MASSJ05332558-5117131) of the Tucana-Horologium association ; these three stars have radial velocity measurements confirming their membership and lithium detections consistent with young age. Finally, we proposed that six stars should be considered as *bona fide* members of βPMG and ABDMG, one of which being first identified in this work, the others being known candidates from the literature.

2.1 Introduction

Nearby young co-moving groups are sparse, gravitationally unbound stellar associations comprising a few dozens of stars scattered within ~ 100 pc of the Sun with ages ranging from 5 to a few hundred Myr. Co-moving group members are characterized by a common position and space motion within the Galaxy. As a result of a projection effect, they display an organized motion on the sky moving towards a convergent point (apex; Montes et al., 2001) and this can be used to discriminate genuine members from field stars. To identify new associations and/or new members of a given association, Eggen (1958, 1995) used the convergent point criterion, which is based on the direction of motion of group members on the celestial sphere, together with new criteria based on the amplitude of the stars' motion. The latter are known as Eggen's criteria. Eggen's method was slightly modified by Montes et al. (2001) to take into account the three-dimensional space motion dispersion of the stars. They used proper motion, radial velocity, and distance uncertainties to measure the galactic space velocities and their dispersion among the members of an association. Generally, proper motion, radial velocity, and distances constitute minimal information needed for identifying young stars from

co-moving groups.

In the last decade, several new associations have been identified, thanks mostly to *Hipparcos* (Perryman et al., 1997) and other large-scale surveys like *Tycho* (Høg et al., 2000) and Two Micron All Sky Survey (Skrutskie et al., 2006). Zuckerman et al. (2001) improved the method to confirm candidate membership to young associations by including constraints on their photometric properties. Following the advent of the 2MASS point-source catalog (Cutri et al., 2003), Song et al. (2003) used an optical-infrared Color-Magnitude Diagram (CMD) to better discriminate between K and M dwarfs. The *Hipparcos* catalog made it possible to determine space velocities with good precision for approximately 20% of nearby young star candidates. For the remaining 80%, Song et al. (2004) used the "good box" method for finding other candidate young stars with photometric and kinematics properties similar to the known members. Similarly, Torres et al. (2006, 2008) led the development of a merit function for identifying new members (Search for Associations Containing Young stars ; SACY).

Although significant progress has been made in the last decade in finding young stars in co-moving groups, their identification remains challenging because they are sparsely dispersed over the celestial sphere. Moreover, the studies mentioned above have uncovered relatively few low-mass (K and M) stars in nearby young associations since they relied mostly on surveys in the V band with a limiting magnitude around V=14. However, some recent studies are now providing a substantial number of candidates in the low-mass regime (Desidera et al., 2011, Kiss et al., 2011, Lépine & Simon, 2009, Rodriguez et al., 2011, Schlieder et al., 2010, Shkolnik et al., 2012, 2011, Riedel et al., 2011, Torres et al., 2006, 2008, Schlieder et al., 2012a).

In this paper, we present a new method for identifying young low-mass stars in kinematic groups. More specifically, the method allows calculating an objective membership probability of a given candidate to an ensemble of moving groups. This method is applied to the seven youngest kinematic groups closest to the Sun. The paper is structured as follows. A brief description of the young associations analyzed is presented in Section 2, and more details on the kinematic properties, space location, and photometric properties of the known members of these associations are presented in Section 3. A

presentation of the kinematic model describing these associations follows in Section 4. The Bayesian method used for selecting new members is described in Section 5. Then the sample to which our method is applied is described in Section 6, followed by the results is Section 7. Follow-up observations (radial velocity and lithium absorption) for some candidates are presented and discussed in Section 8. Section 9 is devoted to a discussion of previously known members and new candidate members unveiled from this work. Concluding remarks and suggestions for future work follow in Section 10.

2.2 The young associations

Our search for young low-mass stars will be restricted to the seven closest co-moving groups : the β Pictoris Moving Group (βPMG), the TW Hydrae Association (TWA), the Tucana-Horologium Association (THA), the Columba Association (COL), the Carina Association (CAR), the Argus Association (ARG), and the AB Doradus Moving Group (ABDMG). The basic properties of these associations, which are detailed below, are summarized in Tables 2.I and 3.III. Thereafter in this paper, we consider as *bona fide members* of young kinematic groups all stars with a good measurement of trigonometric distance, proper motion, Galactic space velocity and other youth indicators such as Hα emission, X-ray emission, appropriate location in the HR diagram and lithium absorption ; those 177 stars are listed in Table 2.II.

Table 2.I.   Properties of young Local associations

Name of group	Age range (Myr)	Distance range (pc)	Number of stars[a]
β Pictoris (βPMG)	12-22	9-73	39
TW Hydrae (TWA)	8-20	28-92	10
Tucana-Horologium (THA)	10-40	36-71	44
Columba (COL)	10-40	35-81	21
Carina (CAR)	10-40	46-88	5
Argus (ARG)	30-50	8-68	11
AB Doradus (ABDMG)	50-120	7-77	47

[a]Members with published trigonometric distance only.

2.2.1 β Pictoris Moving Group

This group was proposed by Zuckerman et al. (2001) following the work of Barrado y Navascués et al. (1999). Members sharing the galactic motion of its namesake star were selected from the *Hipparcos* (Perryman et al., 1997) and Gliese & Jahreiss (1991) databases. The age of this association is estimated from CMDs (20 ± 10 Myr; Barrado y Navascués et al., 1999), stellar formation models (22 ± 12 Myr; Makarov, 2007), and Li abundance (12 ± 8 Myr; Zuckerman et al., 2001). Fernández et al. (2008) summarize the estimated ages published in the literature (see their Table 2). At present, the βPMG counts 39 *bona fide members* (Faherty et al., 2012, Kiss et al., 2011, Schlieder et al., 2010, Rice et al., 2010, Zuckerman & Song, 2004, Schlieder et al., 2012a, Teixeira et al., 2009) ranging from 9 to 73 pc. Rice et al. (2010) have identified the lowest mass, isolated, member of βPMG : an M8.5V brown dwarf. Faherty et al. (2012) have measured the trigonometric distance of this object and this measurement confirms its membership to this group. The members are scattered over the celestial sphere with a majority of them in the southern hemisphere. The observational properties of all *bona fide members* are listed in Table 2.II.

Torres et al. (2006) and Torres et al. (2008) identified, respectively, 9 and 6 new candidate members of this association from the minimization of a merit function described by space velocities, galactic positions, and theoretical isochrones (M_V versus $V - I$). Lépine & Simon (2009) and Schlieder et al. (2010) each introduced 4 new candidate members, selected from the LSPM (Lepine & Shara, 2005) and Tycho-2 catalogs according to kinematic and optical/IR photometric criteria. Kiss et al. (2011) proposed 5 new candidate members using the RAVE (Steinmetz et al., 2006, Zwitter et al., 2008) and *Hipparcos* catalogs. Nakajima et al. (2010) and Nakajima & Morino (2012) revisited the *Hipparcos* catalog with a new method to identify members to stellar kinematic groups within 20 pc and 30 pc of the Sun, respectively ; they proposed 5 candidates of βPMG within 30 pc. Recently, Schlieder et al. (2012a) identified 2 likely new members with a consistent *Hipparcos* distance.

2.2.2 TW Hydrae association

TWA was the first nearby association discovered, in the studies of de la Reza et al. (1989) and Gregorio-Hetem et al. (1992) following the work of Rucinski & Krautter (1983) on TW Hya. These studies used the *IRAS* (Helou & Walker, 1988) PSC to identify four other T Tauri systems in the same region of the sky (Webb et al., 1999). Kastner et al. (1997) concluded that TWA forms a physical association with five strong X-ray emitters. Webb et al. (1999) associated six more stellar systems (7 stars and 1 brown dwarf) to TWA using the X-ray properties of all stars within $12°$ around TW Hya. TWA now counts around 30 potential members (Mamajek, 2005) including 10 *bona fide members* (see Table 2.II). Recently, Nakajima & Morino (2012) proposed 7 candidates within 30 pc.

The age of TWA is estimated from HR diagram along with pre-main sequence tracks (8 Myr; Webb et al., 1999), HR diagram with Hα and lithium equivalent width (10^{+10}_{-7} Myr; Barrado Y Navascués, 2006) and the expansion age (20^{+25}_{-7} Myr; Mamajek, 2005). Using galactic dynamics, de la Reza et al. (2006) determined an age of 8 ± 0.8 Myr. Mamajek et al. (2000) and recently Song et al. (2012) suggested that TWA is likely the near edge of a larger population (i.e., Lower Centaurus Crux).

2.2.3 The Great Austral Young Association (GAYA)

Torres et al. (2006, 2003) identified many young stars with similar kinematic and photometric properties. This group of stars was proposed to be called the Great Austral Young Association (GAYA) and was later sub-divided into three groups : THA, COL, and CAR (Torres et al., 2008).

2.2.3.1 Tucana-Horologium association

Discovered simultaneously, the Tucana association (Zuckerman & Webb, 2000) and the Horologium association (Torres et al., 2000) were combined together because of their similar space motion, age and distance (de La Reza et al., 2001). In the first case, Zuckerman & Webb (2000) used the *Hipparcos* and the *IRAS* catalogs to find 10 stars having

a similar galactic motion in both catalogs. The Horologium association was identified by Torres et al. (2000) using the *ROSAT* (Voges, 1994) catalog in order to find X-ray emitting sources around the active star EP Eri.

The following work of Song et al. (2003) discovered 11 new members with a galactic motion similar to those discovered in previous studies. THA counts 44 *bona fide members* (Kiss et al., 2011, Torres et al., 2008, Zuckerman & Song, 2004, Zuckerman et al., 2011) ranging from 36 to 71 pc (see Table 2.II). More recently, Torres et al. (2008) and Kiss et al. (2011), respectively, identified 9 and 2 new candidate members. Zuckerman et al. (2011) proposed 8 new members to THA with spectral types between A1V and G8V. Nakajima & Morino (2012) proposed 4 more candidates within 30 pc.

The age of THA is estimated at 40 Myr (Zuckerman & Webb, 2000) based on various age indicators including Li equivalent width, Hα profile and gyrochronology. The kinematic evolution of the association with time provides further constraints on its age. Assuming a coeval formation with an initial velocity dispersion of 1.5 km s^{-1}, the group of stars should have dispersed over 70 pc after a period of 20 Myr (Torres et al., 2001). From the studies of Stelzer & Neuhäuser (2000) and Zuckerman et al. (2001b), they estimate the lower age limit at 10 Myr.

2.2.3.2 Columba association

COL includes 53 proposed members by Torres et al. (2008), Zuckerman et al. (2011), with 21 listed as *bona fide members* (see Table 2.II). Three stars proposed by Torres et al. (2008) to be members of COL were already proposed by Zuckerman & Song (2004) to be members of THA. Recently, Zuckerman et al. (2011) added 14 new members (B9V to M0.5V) including multiple planet host star HR 8799 (Marois et al., 2008) whose membership was also confirmed by Doyon et al. (2010) through a Bayesian analysis similar to the one presented in this paper. The age of COL is estimated to be similar to that of THA (Torres et al., 2008).

2.2.3.3 Carina association

This association was discovered by the same method as THA and COL (Torres et al., 2008). Torres et al. (2008) proposed 23 members, with only five listed as *bona fide members*. (see Table 2.II). They also showed that the stars in CAR have properties and age similar to THA and COL members. Given the small number of *bona fide members* identified in CAR, this association cannot be considered as well defined as others like βPMG, THA, and COL.

2.2.4 Argus association

This association was initially unveiled by Makarov & Urban (2000) using proper motion to identify a bulk of stars located in the Carina-Vela moving group. The IC 2391 open cluster was proposed to be part of this moving group by Makarov & Urban (2000), and Torres et al. (2003) used the convergence point method to show that the kinematics of these two groups are similar. Torres et al. (2003) identified this group as the Argus Association due to its special galactic space velocity U and proposed a different definition for this group. Riedel et al. (2011) proposed that the closest (8.4 pc) pre-main sequence star should be AP Col, a member of the Argus association. Zuckerman et al. (2011) proposed 6 new members with a spectral type between A0V and F4V. Recently, Desidera et al. (2011) proposed HIP 36948 as a candidate member of Argus association from several age-dating indicators. ARG counts 11 *bona fide members* (see Table 2.II). This association is not as well defined as other groups because the properties of all known members are not well measured. There is no parallax measurement for the IC 2391 members.

The age of the ARG members is similar to that of the IC 2391 members as inferred from the lithium equivalent width and position in the HR diagram (40 Myr; Torres et al., 2008). An age of 50 ± 5 Myr was inferred by Barrado y Navascués et al. (2004) using lithium depletion and Hα emission.

2.2.5 AB Doradus moving group

This group was identified by Zuckerman & Song (2004) by performing a kinematic analysis of the *Hipparcos* catalog. Forty-seven *bona fide members* are associated with this group (Torres et al., 2008, Zuckerman & Song, 2004, Zuckerman et al., 2011) and range in distance from 7 to 77 pc. Several new candidate members have been proposed recently : 43 by Torres et al. (2008), 6 by Schlieder et al. (2010), 6 by Schlieder et al. (2012a), and 1 by Bowler et al. (2012). Nakajima & Morino (2012) proposed 8 (2 F and 6 M stars) more candidates of ABDMG within 30 pc.

In addition to having a common motion, the members show signs of youth, such as strong Hα emission and/or the presence of Li. The observational properties of all members are listed in Table 2.II.

The age of ABDMG is estimated by various age indicators. An age of ~ 50 Myr is deduced by a CMD (M_V versus $V - K$; see Figure 1 of Zuckerman et al. 2004). Luhman et al. (2005) compared the same diagram for ABDMG and the open cluster IC 2391 (30-50 Myr) to deduce an age between 75 and 150 Myr. Using Li equivalent widths and the CMD M_V versus $V - I$, López-Santiago et al. (2006) estimated different ages for two subgroups of ABDMG : 30-50 Myr and 80-120 Myr. Recently, ages of 45 Myr (lower limit) and 70 Myr were estimated from Li equivalent widths by Mentuch et al. (2008) and da Silva et al. (2009), respectively.

Table 2.II. *BONA FIDE MEMBERS* of young kinematic groups

Name	Spt	α (J2000.0) hh mm ss.ss	δ (J2000.0) dd mm ss.s	$\mu_\alpha \cos\delta$[b] (mas yr⁻¹)	μ_δ[b] (mas yr⁻¹)	v_{rad}[c] (km s⁻¹)	π[d] (mas)	r[e] (mag)	J (mag)	X-ray[f] $\log(f_x)$	U (km s⁻¹)	V (km s⁻¹)	W (km s⁻¹)	X (pc)	Y (pc)	Z (pc)
						β Pictoris Moving Group										
HIP 560	F2IV	00 06 50.08	−23 06 27.1	97.81±0.42	−47.12±0.21	6.50±3.50[h]	25.39±0.38	5.74	5.45±0.02	−12.36	−11.0±0.4	−15.1±0.6	−10.2±3.4	4.5	5.9	−38.7
HIP 10679	G2V	02 17 24.72	+28 44 30.5	80.15±4.38	−78.40±4.91	4.99±1.26[h]	36.58±5.83	7.06	6.57±0.02	−11.53	−9.0±1.3	−10.1±2.2	−7.2±1.1	−19.3	13.6	−13.9
HIP 10680	F5V	02 17 25.27	+28 44 42.3	87.60±2.12	−72.40±2.46	4.87±1.37[m]	28.97±2.88	6.40	6.05±0.03	...	−11.4±1.3	−13.7±1.8	−7.2±0.9	−24.3	17.1	−17.5
HIP 11152	M3Ve	02 23 26.63	+22 44 06.9	92.43±3.05	−113.69±2.36	10.40±2.00[y]	34.86±2.84	9.44[ll]	8.18±0.02	−11.41	−12.2±1.5	−13.6±1.7	−13.1±1.3	−20.1	12.0	−16.6
HIP 11360[a]	F4IV	02 26 16.25	+06 17 33.1	86.31±0.71	−49.97±0.45	8.80±3.00[k]	22.11±0.64	6.33	6.03±0.02	−12.18	−13.3±1.9	−18.0±0.9	−5.9±2.3	−27.8	9.6	−34.4
HIP 11437 A	K8	02 27 29.24	+30 58 24.6	79.78±2.56	−70.02±1.73	6.74±0.03	25.03±2.25	8.78	7.87±0.03	−11.37	−13.4±0.8	−14.1±1.6	−8.4±0.6	−29.4	19.8	−18.5
HIP 11437 B	M0	02 27 28.04	+30 58 40.5	79.78±2.56	−70.02±1.73	5.96±0.04	25.03±2.25	10.11[p]	8.82±0.04	−11.39	−12.8±0.8	−14.5±1.6	−8.0±0.6	−29.4	19.8	−18.5
HIP 12545 AB[a]	K6Ve(sb1)	02 41 25.89	+05 59 18.1	79.47±3.05	−53.89±1.74	8.25±0.05	23.79±1.50	8.81	7.90±0.03	−11.39	−10.9±0.5	−16.9±1.2	−5.3±0.3	−27.5	7.0	−31.0
HIP 21547	F0V	04 37 36.13	−02 28 24.8	44.22±0.34	−64.39±0.27	21.00±4.50[p]	33.98±0.34	4.89	4.74±0.04	−10.81	−14.0±3.7	−16.2±1.2	−10.0±2.3	−24.0	−8.1	−15.0
GJ 3305 AB	M0.5*	04 37 37.46	−02 29 28.2	46.00±2.80	−64.80±3.00	20.10±0.01[p]	33.98±0.34	8.61[p]	7.30±0.02	−10.81	−13.3±0.2	−16.1±0.4	−9.4±0.3	−24.0	−8.1	−15.0
HIP 23200	M0Ve	04 59 34.83	+01 47 00.7	34.60±2.34	−94.27±1.44	19.82±0.04	38.64±2.54	8.21	7.12±0.02	−11.32	−12.7±0.3	−16.8±0.8	−10.1±0.3	−22.6	−7.2	−10.4
HIP 23309	M0.5 kee	05 00 47.14	−57 15 25.5	36.34±1.42	70.22±1.27	19.40±0.30[p]	37.34±1.13	8.21[p]	7.09±0.02	−11.53	−10.7±0.3	−16.8±0.3	−9.0±0.2	−1.5	−21.2	−16.3
HIP 25486	F7	05 27 04.77	−11 54 03.3	17.55±0.36	−50.23±0.36	21.12±1.64[n]	36.98±0.48	5.67	5.27±0.03	−10.58	−11.9±1.2	−16.3±0.8	−9.2±0.7	−20.4	−13.9	−11.0
HIP 27321	A5V	05 47 17.08	−51 03 59.4	4.65±0.11	83.10±0.15	20.00±3.70[n]	51.44±0.12	3.67	3.67±0.24	...	−11.0±0.6	−16.0±3.1	−9.1±1.9	−3.4	−16.4	−9.9
J0608-2753[a]	M8.5e	06 08 52.83	−27 53 58.3	8.90±3.50[i]	10.70±3.50[i]	24.00±1.00[v]	31.98±3.63[i]	17.10[jj]	13.60±0.03	...	−14.2±0.7	−18.1±0.8	−6.9±0.6	−17.0	−23.7	−11.2
HIP 29964	K4Ve	06 18 28.24	−72 02 41.6	−8.32±0.86	72.02±1.06	16.20±1.00[q]	25.94±0.90	8.48[p]	7.53±0.02	−11.09	−9.9±0.5	−16.2±0.9	−8.8±0.5	7.4	−33.1	−18.2
HIP 50156[a]	M1V	10 14 19.18	+21 04 29.7	−144.06±1.90	−154.79±1.10	5.80±0.80[ff]	43.32±1.80	8.24[kk]	7.07±0.02	−11.50	−10.0±0.5	−20.4±0.8	−7.2±0.8	−11.3	−7.6	18.6
TWA 22AB	M6Ve+M6Ve	10 17 26.89	−53 54 26.5	−175.80±0.80[g]	−21.30±0.80[g]	13.57±0.26[t]	57.00±0.70[g]	10.44[ii]	8.55±0.02	−11.87	−8.2±0.2	−15.9±0.3	−9.0±0.1	3.5	−17.2	0.7
HIP 76629 A	K0V	15 38 57.57	−57 42 27.3	−53.98±1.14	−106.00±1.27	3.60±0.95[h]	25.95±1.14	7.07[p]	6.38±0.02	−10.95	−8.8±0.9	−17.6±0.9	−9.8±0.5	31.1	−22.7	−1.2
HIP 76629 BC	M4.5*	15 38 56.79	−57 42 19.0	−53.98±1.14	−106.00±1.27	0.10±2.00[p]	25.95±1.14	11.90[p]	10.05±0.05	−10.95	−11.6±1.7	−15.6±1.4	−9.7±0.5	31.1	−22.7	−1.2
HIP 79881	A0	16 18 17.89	−28 36 50.2	−31.19±0.26	−100.92±0.18	−13.00±0.50[t]	24.22±0.22	4.81	4.86±0.04	...	−13.6±0.5	−16.1±0.2	−12.3±0.2	39.0	−7.9	11.0
HIP 84586 AB	G5IV+K0IV	17 17 25.50	−66 57 03.9	−21.83±0.39	−136.91±0.42	3.34±1.69[u]	31.80±0.50	6.04	5.29±0.03	−10.42	−10.2±1.3	−16.2±1.0	−8.6±0.5	24.7	−17.4	−8.8
HIP 84586 C	M3Ve	17 17 31.28	−66 57 05.5	−21.83±0.39	−136.91±0.42	2.70±1.80[p]	31.80±0.50	10.09[p]	8.54±0.03	−10.42	−10.7±1.4	−15.8±1.0	−8.4±0.5	24.7	−17.4	−8.8
HIP 86598	F9V	17 41 49.03	−50 43 27.9	−3.70±1.08	−65.70±0.85	2.40±1.10[w]	13.80±0.87	7.68	7.34±0.02	−11.51	−6.2±1.2	−19.2±1.3	−10.5±0.8	67.3	−23.4	−13.4
HIP 88399 A	F5V	18 03 03.41	−51 38 56.4	4.02±0.60	−86.46±0.36	0.50±0.40[p]	20.77±0.56	6.48	6.16±0.02	−11.87	−7.2±0.4	−15.8±0.3	−9.4±0.3	44.3	−14.7	−11.6
HIP 88726 AB	A5V+A5V	18 06 49.90	−43 25 29.7	10.73±1.05	−106.59±0.51	−7.80±0.40[p]	23.90±0.66	4.63	4.68±0.25	...	−12.9±0.4	−15.7±0.5	−9.9±0.4	40.4	−7.5	−7.9
HIP 89829	G5V	18 19 52.21	−29 16 32.7	3.60±1.29	−46.46±0.78	−7.00±2.60[p]	13.78±1.02	7.99	7.53±0.02	−11.27	−7.1±2.6	−14.1±1.1	−7.6±0.8	72.0	4.3	−8.4
HIP 92024 A	A7	18 45 26.91	−64 52 16.5	32.40±0.17	−149.48±0.17	3.80±4.50[p]	35.03±0.19	4.57	4.38±0.26	−12.16	−9.3±3.6	−16.2±2.0	−9.8±1.8	22.8	−12.8	−11.5
HIP 92024 BC	K7V(sb2)	18 45 37.04	−64 51 46.0	30.30±0.01	−153.10±0.01	1.00±3.00[p]	35.03±0.19	8.00[p]	6.91±0.02	−11.08	−11.7±2.4	−15.4±1.4	−8.5±1.2	22.8	−12.8	−11.5
HIP 92680	G9IV	18 53 05.87	−50 10 49.9	17.64±1.13	83.63±0.76	−4.20±1.00[ff]	19.42±0.98	7.61	6.86±0.02	−11.07	−11.7±0.4	−15.8±0.9	−8.2±0.6	46.8	−11.5	−18.2
HIP 95261 AB[a]	A0Vn+M7	19 22 51.22	−54 25 26.3	25.57±0.21	−82.71±0.14	13.00±2.50[t]	20.74±0.21	4.99	5.10±0.04	...	2.1±2.1	−18.9±0.7	−14.0±1.1	41.3	−12.7	−21.3
HIP 95270	F5.5	19 22 58.94	−54 32 17.0	23.99±0.65	−81.82±0.44	0.20±0.40[n]	19.30±0.65	6.49	6.20±0.02	...	−9.4±0.5	−16.6±0.6	−8.6±0.4	44.4	−13.8	−22.9
HIP 99273	F5V	20 09 05.21	−26 13 26.5	39.17±0.50	−68.25±0.36	−5.80±2.20[n]	19.15±0.45	6.63	6.32±0.02	−12.31	−7.9±1.9	−15.8±0.6	−10.1±1.1	44.4	12.7	−24.4
HIP 102141 B	M4Ve	20 41 51.11	−32 26 07.3	269.30±4.63	−365.70±3.50	−5.13±0.05	93.50±3.67	8.06[p]	6.56±0.03[l]	−10.54	−11.0±0.3	−17.9±0.7	−10.8±0.6	8.5	1.7	−6.3
HIP 102141 A	M4Ve	20 41 51.11	−32 26 07.3	269.30±4.63	−365.70±3.50	−3.73±0.04	93.50±3.67	8.00[p]	6.56±0.03[l]	−10.54	−9.9±0.3	−17.6±0.7	−11.6±0.6	8.5	1.7	−6.3
HIP 102409	M1Ve	20 45 09.49	−31 20 26.6	279.96±1.26	−360.61±0.73	−4.13±0.03	100.91±1.06	6.71	5.44±0.02	−10.33	−9.8±0.1	−16.3±0.2	−10.7±0.1	7.7	1.7	−5.9
HIP 103311	F8V*	20 55 47.67	−17 06 50.9	58.81±0.83	−62.83±0.73	−9.00±3.00[p]	21.90±0.77	6.65	6.21±0.02	−10.87	−10.7±2.1	−15.5±1.3	−8.6±1.8	32.3	18.9	−26.2
HIP 112312 B	M5IVe	22 45 00.04	−33 15 25.8	184.76±2.64	−119.76±2.31	2.03±0.04	42.84±3.61	10.27[p]	8.68±0.02	...	−12.6±1.2	−17.9±1.5	−10.9±0.8	10.7	2.4	−20.6
HIP 112312	M4IVe	22 44 57.94	−33 15 01.5	184.76±2.64	−119.76±2.31	3.09±0.04	42.84±3.61	9.27[p]	7.79±0.02	−11.13	−12.2±1.2	−17.8±1.5	−11.8±0.8	10.7	2.4	−20.6
						TW Hydrae Association										
TWA 1	K6Ve	11 01 51.91	−34 42 17.0	−66.19±1.90	−13.90±1.50	13.40±0.80[p]	18.62±2.14	9.38[p]	8.22±0.02	−11.19	−10.9±1.5	−18.3±1.0	−4.6±1.2	7.5	−48.9	20.9
TWA 4ABCD	K7+M1*	11 22 05.30	−24 46 39.3	−85.40±1.70	−33.10±2.10	9.30±1.00[p]	22.27±2.31	7.78	6.40±0.02	−11.25	−11.3±1.4	−17.3±1.3	−6.3±1.4	5.4	−36.9	25.0
TWA 8A	M3Ve	11 32 41.24	−26 51 55.9	−99.20±6.20[i]	−32.20±6.20[i]	8.68±0.02	21.28±1.00[i]	9.80[l]	8.34±0.02	−11.57	−14.5±1.6	−18.6±1.0	−7.6±1.3	8.2	−38.6	25.4

Table 2.II — continued

Name	Spt	α (J2000.0) hh mm ss.ss	δ (J2000.0) dd mm ss.s	μα cos δ[b] (mas yr⁻¹)	μδ[b] (mas yr⁻¹)	vrad[c] (km s⁻¹)	π[d] (mas)	I[e] (mag)	J (mag)	X-ray[f] log(fx)	U (km s⁻¹)	V (km s⁻¹)	W (km s⁻¹)	X (pc)	Y (pc)	Z (pc)
TWA 8B	M5.5	11 32 41.16	−26 52 09.0	−101.30±6.20[j]	−38.60±6.20[j]	8.61±0.03	21.28±1.00[l]	11.75[l]	9.84±0.02	...	−14.3±1.5	−19.3±1.0	−8.9±1.3	8.2	−38.6	25.4
TWA 26	M9Ve	11 39 51.13	−31 59 21.4	−75.20±4.40[j]	−10.40±4.50[j]	11.60±2.00[d]	35.10±4.30[j]	15.83[j]	12.69±0.03	...	−5.5±1.3	−14.4±1.8	1.6±1.2	6.8	−24.1	13.6
TWA 19[a]	G5V	11 47 24.54	−49 53 02.9	−33.34±0.77	−9.91±0.90	14.40±0.40[p]	10.91±1.28	8.41[p]	7.89±0.03	−11.35	−6.0±1.4	−19.4±0.8	−4.7±1.0	34.3	−82.9	18.6
TWA 9B	M1V	11 48 23.73	−37 28 48.5	−20.00±3.40[m]	−20.00±3.40[m]	12.23±0.03[p]	21.38±2.48	11.42[p]	9.98±0.03	...	−4.9±1.1	−16.7±0.8	−1.8±1.0	14.2	−40.4	18.8
TWA 9A	K5V	11 48 24.22	−37 28 49.1	−53.10±1.90[m]	−20.00±3.40[m]	11.65±0.02	21.38±2.48	9.64[p]	8.68±0.03	−11.57	−5.1±1.1	−16.2±0.8	−2.1±1.0	14.2	−40.4	18.8
TWA 27AB	M8Ve*	12 07 33.46	−39 32 53.9	−80.10±17.90[j]	−15.10±17.90[j]	11.20±2.00[j]	18.51±1.03[jj]	15.88[jj]	13.00±0.03	...	−12.5±4.4	−20.0±3.0	−2.7±4.3	20.1	−45.7	20.7
TWA 11A	A0	12 36 01.03	−39 52 10.2	−56.66±0.30	−25.00±0.20	6.90±1.00[p]	13.74±0.33	5.76	5.78±0.02	−12.10	−11.4±0.6	−18.3±0.9	−6.4±0.5	33.2	−58.2	28.3
						Tucana-Horologium Association										
HIP 490	G0V	00 05 52.55	−41 45 10.9	97.53±0.38	−76.27±0.44	2.30±1.50[p]	25.39±0.59	6.84	6.46±0.02	−11.93	−9.4±0.5	−21.2±0.5	−2.0±1.4	10.4	−5.4	−37.6
HIP 1113	G8V	00 13 53.00	−74 41 17.8	83.53±0.78	−47.89±0.75	9.30±0.20[p]	22.52±0.82	7.97	7.41±0.02	−11.38	−8.9±0.5	−20.4±0.6	−1.5±0.2	19.5	−26.5	−29.8
HIP 1481	F8	00 18 26.12	−63 28 38.9	89.37±0.48	−59.46±0.50	7.00±2.00[d]	24.07±0.52	6.85	6.46±0.02	−11.69	−8.8±0.8	−20.4±1.0	−1.0±1.6	15.7	−19.3	−33.3
HIP 1910 AB	M0Ve*	00 24 08.99	−62 11 04.2	90.91±2.37	−47.25±3.04	6.60±0.60[p]	18.88±2.72	9.49	8.39±0.03	...	−13.1±2.3	−23.1±3.0	−1.0±0.9	19.0	−24.0	−43.2
HIP 1993	M0Ve	00 25 14.65	−61 30 48.3	87.76±2.14	−57.48±2.37	6.40±0.10[d]	21.83±2.42	9.69	8.61±0.03	...	−9.6±1.4	−21.6±2.1	−0.2±0.6	16.2	−20.4	−37.7
HIP 2484 AbB[a]	B9V*	00 31 32.67	−62 57 29.7	83.64±0.19	−54.82±0.18	14.00±2.50[r]	24.15±0.20	4.38	4.66±0.25	...	−5.1±0.9	−22.7±1.2	−6.3±2.0	14.6	−19.5	−33.5
HIP 2487 AB	A2V+A7V	00 31 33.47	−62 57 56.0	93.97±2.86	−46.32±2.68	9.80±0.74[jj]	19.36±2.97	4.39	4.32±0.29	...	−12.0±2.5	−24.5±3.1	−3.1±1.0	18.2	−24.3	−41.8
HIP 2578	A0V	00 32 43.91	−63 01 53.3	86.66±0.18	−50.33±0.17	5.00±1.20[r]	21.95±0.19	5.02	5.06±0.04	...	−10.2±0.4	−19.7±0.6	0.9±1.0	16.0	−21.5	−36.8
HIP 2729	K5Ve	00 34 51.20	−61 54 58.3	88.28±0.92	−53.16±0.91	−1.00±2.00[d]	22.76±0.99	8.55	7.34±0.02	−11.41	−11.7±0.9	−17.0±1.2	5.9±1.7	14.9	−20.2	−36.0
HIP 3556[a]	M3	00 45 28.14	−51 37 33.9	95.74±1.92	−58.95±1.87	−1.60±19.99[t]	24.78±2.65	9.73	8.48±0.02	...	−10.5±4.9	−18.0±7.1	5.7±18.2	9.6	−13.7	−36.7
HIP 6485	G6V	01 23 21.26	−57 28 50.7	92.45±0.92	−38.00±0.72	8.30±0.40[r]	20.19±0.83	7.77	7.24±0.02	−11.35	−10.5±0.5	−22.6±0.8	0.0±0.5	10.6	−23.1	−42.5
HIP 6856	K1V	01 28 08.68	−52 38 19.1	106.09±1.02	−42.81±1.24	8.00±0.20[p]	27.76±1.00	8.35	7.41±0.02	−11.41	−8.7±0.4	−19.2±0.6	−1.5±0.3	5.6	−15.0	−32.3
HIP 9141 AB	G3V*	01 57 48.96	−21 54 05.2	105.08±0.72	−50.60±0.54	6.80±0.20[p]	24.45±0.67	7.36	6.86±0.02	−11.76	−10.6±0.3	−21.0±0.6	−2.4±0.2	−10.7	−3.4	−39.3
HIP 9685[a]	F2V	02 04 35.13	−54 52 54.0	75.74±0.45	−25.05±0.48	3.40±3.70[r]	20.94±0.46	6.00	5.70±0.04	...	−8.1±0.5	−15.9±1.9	4.3±3.2	5.2	−23.9	−41.0
HIP 9892 AB	G7V(sb1)	02 07 18.05	−53 11 56.5	86.06±0.58	−22.60±0.65	10.00±0.50[p]	19.63±0.64	7.88	7.35±0.02	−11.25	−10.2±0.4	−21.4±0.6	−0.5±0.5	4.3	−24.8	−44.3
HIP 9902	F8V	02 07 26.11	−59 40 45.9	91.11±0.47	−18.29±0.47	11.10±0.70[p]	22.64±0.45	6.88	6.53±0.02	...	−9.2±0.3	−20.4±0.5	−1.7±0.6	7.1	−24.4	−36.1
HIP 10602	B8IV	02 16 30.59	−51 30 43.7	91.03±0.12	−22.23±0.12	10.30±1.30[r]	21.22±0.12	3.67	4.03±0.30	...	−10.0±0.1	−21.1±0.6	−0.6±1.1	2.1	−22.9	−41.1
HIP 12394	B9Va	02 39 35.38	−68 16 00.8	87.30±0.09	0.09±0.10	6.20±2.20[r]	21.48±0.09	4.19	4.44±0.30	...	−10.8±0.5	−16.8±1.5	3.3±1.6	10.5	−30.7	−33.4
HIP 12925	F8V	02 46 14.62	+05 35 33.3	75.27±1.45	−44.78±0.83	4.30±1.10[cc]	18.41±1.04	7.26	6.86±0.04	−12.02	−10.0±0.9	−20.7±1.2	−1.0±0.8	−36.1	8.0	−39.8
HIP 14551[a]	A5V	03 07 50.83	−27 49 52.0	66.26±0.50	−19.09±0.49	13.80±0.80[cc]	18.30±0.50	6.00	5.89±0.02	...	−11.0±0.4	−19.4±0.5	−3.7±0.7	−20.3	−18.5	−47.2
HIP 14913 ABC	A0V+F7III+F5V	03 12 25.75	−44 25 11.1	81.63±0.55	−4.57±0.98	13.50±2.10[cc]	23.53±0.62	5.41	5.12±0.03	−10.97	−10.2±0.4	−18.5±1.1	−2.7±1.8	−6.5	−22.3	−35.6
HIP 15247	F5	03 16 40.66	−03 31 48.9	78.63±0.67	−43.82±0.71	7.20±3.80[r]	20.31±0.59	6.87	6.46±0.02	−11.45	−9.1±2.5	−20.2±0.6	0.1±2.8	−32.8	−2.9	−36.6
HIP 16853 AB	G2V(sb)	03 36 53.41	−49 57 28.8	89.74±0.75	0.29±0.84	14.40±0.90[r]	23.07±0.73	6.96	6.49±0.03	−11.73	−10.2±0.3	−21.1±0.7	−0.4±0.8	−4.6	−26.8	−33.8
HIP 17764	F3V	03 48 11.48	−74 41 38.8	63.46±0.39	24.86±0.49	15.50±1.30[cc]	18.50±0.40	6.67	6.37±0.02	−12.80	−8.4±0.5	−21.7±1.0	−2.5±0.8	14.3	−40.4	−32.9
HIP 17782 AB[a]	G8V*	03 48 23.01	+52 02 16.3	61.87±1.98	−70.99±1.67	−2.20±0.60[cc]	19.35±1.62	7.93	7.22±0.02	−11.15	−9.9±1.1	−20.5±1.7	−4.1±0.6	−44.0	27.1	−1.7
HIP 17797	A1V	03 48 35.87	−37 37 12.6	74.44±0.71	−9.09±0.87	15.60±0.40[cc]	19.71±0.86	4.32	3.90±1.05	...	−10.6±0.3	−21.3±0.6	−1.0±0.6	−15.7	−27.4	−39.7
HIP 18714 AB	G3V*	04 00 31.98	−41 44 54.4	69.46±0.81	−7.00±0.85	16.30±0.70[w]	20.62±0.71	7.68	7.20±0.02	...	−9.1±0.3	−20.9±0.6	−1.8±0.7	−12.8	−29.2	−36.6
HIP 21632	G3V	04 38 43.93	−27 02 01.8	56.03±0.51	−11.08±0.72	18.80±0.00[p]	17.80±0.89	7.79	7.27±0.02	−11.58	−11.3±0.2	−21.3±0.6	−1.5±0.5	−29.6	−31.4	−36.0
HIP 21965	F2V	04 43 17.20	−23 37 41.9	50.25±0.69	−11.84±0.78	19.30±2.90[r]	15.73±0.98	6.64	6.29±0.02	−11.79	−11.9±1.7	−21.7±1.7	−1.3±1.9	−36.8	−34.0	−39.1
HIP 22295	F7V	04 48 05.18	−80 46 45.2	46.66±0.49	41.30±0.56	11.50±2.00[r]	16.39±0.51	7.53	7.17±0.02	−11.71	−9.9±0.8	−18.9±1.6	−0.2±1.6	20.9	−47.6	−31.9
HIP 24947	F6V	05 20 38.03	−39 45 17.9	38.36±0.29	13.06±0.50	15.20±1.60[r]	20.70±0.41	6.81	6.42±0.02	−11.34	−9.1±0.6	−15.3±1.2	−0.8±0.9	−17.4	−36.2	−26.8
HIP 32435	F5V	06 46 13.48	−83 59 29.4	19.66±0.43	61.60±0.47	12.50±0.70[r]	17.85±0.36	6.93	6.55±0.03	−11.98	−8.5±0.4	−19.5±0.6	−0.6±0.4	22.0	−44.8	−25.5
HIP 83494[a]	A5V	17 03 53.58	+34 47 24.7	−60.92±0.26	−5.05±0.34	−21.50±1.40[cc]	18.19±0.31	5.86	5.65±0.02	...	−10.6±0.6	−24.6±1.0	−0.3±0.9	23.7	37.5	32.5
HIP 84642 AB[a]	G8V+M5V	17 18 14.64	−60 27 27.5	−54.62±1.09	−91.04±0.84	1.30±0.70[cc]	16.97±1.34	8.71	8.01±0.02	−11.69	−13.6±1.3	−26.3±2.1	−1.3±0.3	50.1	−28.2	−13.1
HIP 100751	B2IV	20 25 38.86	−56 44 06.2	6.90±0.44	−86.02±0.32	2.00±2.50[r]	18.24±0.52	2.04	2.30±0.31	...	−6.1±1.9	−21.6±0.9	−1.6±1.4	42.3	−14.7	−31.6
HIP 104308[a]	A5V	21 07 51.24	−54 12 59.4	26.07±0.53	−80.75±0.35	12.50±0.50[r]	14.11±0.44	6.41	6.21±0.02	−11.33	−8.5±0.4	−24.2±2.3	3.9±6.6	50.9	−15.4	−46.9
HIP 105388	G7V	21 20 49.94	−53 02 03.0	28.77±1.01	−94.19±0.55	0.10±0.20[r]	23.27±0.98	7.90	7.39±0.02	−11.33	−6.4±0.3	−19.0±0.8	−1.2±0.2	30.0	−8.5	−29.6
HIP 105404 AB[a]	G9V(eb)	21 20 59.80	−52 28 40.0	25.45±1.69	−103.88±1.93	6.00±2.00[d]	22.15±1.40	8.02	7.18±0.03	−11.21	−2.2±1.5	−23.1±1.4	−4.6±1.4	31.5	−8.5	−31.2
HIP 107345	M1	21 44 30.12	−60 58 38.9	39.98±2.35	−91.66±1.56	2.30±0.50[p]	22.91±2.58	9.88	8.75±0.03	−11.99	−7.7±1.1	−19.3±2.1	−1.0±0.5	27.8	−14.6	−30.3
HIP 107947	F6V	21 52 09.73	−62 03 08.5	44.05±0.41	−92.02±0.45	1.40±0.60[r]	22.06±0.66	6.64	6.36±0.03	−11.45	−9.2±0.5	−19.9±0.6	−0.1±0.4	28.2	−16.0	−31.7

49

Table 2.II — continued

Name	Spt	α (J2000.0) hh mm ss.ss	δ (J2000.0) dd mm ss.s	$\mu_\alpha \cos\delta$[b] (mas yr⁻¹)	μ_δ[b] (mas yr⁻¹)	v_{rad}[c] (km s⁻¹)	π[d] (mas)	I[e] (mag)	J (mag)	X-ray[f] log(f_x)	U (km s⁻¹)	V (km s⁻¹)	W (km s⁻¹)	X (pc)	Y (pc)	Z (pc)
HIP 108195 ABC	F3+F3+M6-7	21 55 11.40	−61 53 11.9	44.50±0.23	−91.07±0.27	1.00±3.00[p]	21.52±0.41	5.46	5.24±0.04	−11.82	−9.6±1.9	−20.2±1.1	0.2±2.1	28.7	−16.3	−32.7
HIP 108422 AB	G8V*	21 57 51.46	−68 12 50.1	41.73±0.87	−85.79±0.94	1.10±2.10[p]	17.23±1.06	8.09	7.31±0.03	−11.17	−12.8±1.5	−22.8±1.7	2.4±1.4	34.6	−26.2	−38.5
HIP 116748 AB	G5V+K3V	23 39 39.49	−69 11 44.8	79.30±0.80	−67.62±0.78	8.00±0.80[p]	21.89±0.84	7.35	7.12±0.02	−11.16	−9.1±0.6	−22.1±0.8	−1.3±0.6	21.0	−23.3	−33.2
HIP 118121	A1V	23 57 35.07	−64 17 53.6	79.12±0.47	−60.80±0.46	0.57±0.82[aa]	21.08±0.49	4.93	4.91±0.04	...	−11.9±0.5	−18.7±0.6	3.8±0.7	19.7	−21.7	−37.3
Columba Association																
HIP 1134	F5V	00 14 10.25	−07 11 56.9	102.79±0.78	−66.36±0.36	−2.20±1.20[cc]	21.21±0.64	6.73	6.40±0.02	−11.72	−12.5±0.4	−23.6±0.8	−6.3±1.1	−2.2	17.4	−43.8
HIP 12413 A[a]	A1V	02 39 47.96	−42 53 30.0	88.20±2.02	−17.82±1.98	18.00±4.20[cc]	28.02±2.19	4.65	4.68±0.27	−11.45	−9.2±0.8	−19.6±2.1	−9.4±3.8	−4.0	−15.7	−31.8
HIP 16449	A3V	03 31 53.64	−25 36 50.9	53.90±0.31	−14.90±0.45	17.30±0.80[p]	13.90±0.55	6.25	6.16±0.02	−11.97	−12.8±0.4	−22.0±0.7	−4.1±0.8	−32.3	−27.0	−58.3
HIP 17248	M0.5V	03 41 37.24	+55 13 06.8	96.17±2.49	−117.69±2.26	−3.20±0.60[cc]	28.40±2.18	9.60	8.35±0.03	...	−11.3±1.2	−22.1±1.6	−6.0±0.6	−29.1	19.9	0.0
HIP 19775	G3V	04 14 22.57	−38 19 01.6	39.70±0.39[m]	3.70±0.80[m]	20.80±0.30[p]	12.42±0.97	8.45	7.94±0.03	−11.64	−13.3±0.6	−21.6±0.8	−4.6±0.9	−26.8	−48.6	−58.3
HIP 22226	F3V	04 46 49.50	−26 18 08.7	34.52±0.39	−4.13±0.66	21.30±2.50[s]	12.46±0.71	7.39	7.10±0.02	...	−13.2±1.4	−21.0±1.5	−3.4±1.6	−43.7	−45.8	−49.3
HIP 23179	A1V	04 59 15.43	+37 53 25.1	46.35±0.63	−97.80±0.41	7.70±2.50[cc]	19.13±0.79	4.87	4.90±0.47	−11.24	−13.0±2.4	−23.9±1.2	−6.3±0.3	−50.9	11.6	−2.6
HIP 23316	G5V	05 00 51.86	−41 01 06.5	31.76±0.63	10.74±0.90	23.50±0.00[p]	13.10±0.78	8.79	8.13±0.02	...	−13.3±0.5	−22.3±0.4	−5.0±0.6	−25.2	−54.9	−46.6
HIP 23362	B9V	05 01 25.58	−20 03 06.7	36.43±0.19	−16.46±0.22	24.20±2.80[cc]	16.48±0.25	4.95	5.01±0.04	...	−13.7±1.8	−22.2±1.5	−6.2±1.5	−38.9	−33.0	−32.9
HIP 24947	F6V	05 20 38.03	−39 45 17.9	38.36±0.29	13.06±0.50	23.90±2.20[p]	20.70±0.41	6.81	6.42±0.02	−11.34	−12.2±0.8	−21.8±1.7	−5.7±1.2	−17.4	−36.2	−26.8
HIP 25709 AB	G3V(sb2)	05 29 24.09	−34 30 55.4	25.80±0.80[m]	5.70±0.70[m]	24.10±5.00[ff]	14.11±0.57	7.76	7.31±0.02	−12.32	−13.0±2.2	−21.6±3.7	−4.8±2.6	−31.5	−51.9	−36.5
HIP 26309	A2V	05 36 10.29	−28 42 28.9	25.80±0.31	−3.04±0.46	22.40±1.20[cc]	18.94±0.43	6.10	5.96±0.02	...	−11.6±0.6	−19.5±0.8	−5.3±0.6	−28.2	−37.1	−24.9
HIP 26453	F3V	05 37 39.62	−28 37 34.6	24.29±0.44	−4.06±0.74	23.50±0.40[cc]	17.61±0.62	6.79	6.47±0.02	−11.94	−11.9±0.3	−20.6±0.3	−5.7±0.3	−30.4	−40.0	−26.4
HIP 26966	A0V	05 43 21.66	−18 33 26.8	18.92±0.36	−13.99±0.30	25.20±0.60[c]	13.32±0.42	5.72	5.79±0.02	...	−13.4±0.4	−22.1±0.4	−5.9±0.3	−50.7	−46.9	−29.4
HIP 26990	G0V	05 43 35.80	−39 55 24.6	25.82±0.32	15.08±0.52	22.80±0.60[cc]	18.06±0.45	7.48	7.06±0.02	−11.83	−12.0±0.3	−20.4±0.5	−4.7±0.3	−20.0	−43.9	−27.2
HIP 28036	F7V	05 55 43.14	−38 06 16.2	20.49±0.44	9.34±0.44	24.70±0.80[p]	18.39±0.44	6.90	6.49±0.02	−11.71	−11.6±0.3	−21.7±0.6	−6.0±0.4	−21.2	−43.7	−24.5
HIP 28474	G8V	06 00 41.30	−44 53 50.0	18.02±0.59	23.85±0.75	23.80±0.40[cc]	19.03±0.60	8.33	7.73±0.02	−12.56	−12.0±0.3	−21.0±0.3	−6.0±0.3	−14.6	−44.3	−24.2
HIP 30030[a]	G0V	06 19 08.05	−03 26 20.3	10.90±0.75	−42.62±0.61	19.10±2.40[g]	20.31±0.81	7.29	6.85±0.02	−11.38	−10.3±2.0	−18.4±1.3	−5.1±0.4	−41.1	−26.0	−7.5
HIP 32104	A2V	06 42 24.31	+17 38 43.0	7.87±0.66	−84.32±0.48	15.00±4.20[cc]	22.92±0.67	5.14	5.03±0.04	−12.24	−10.4±4.0	−20.0±1.3	−4.7±0.5	−41.7	−12.1	4.6
HIP 114189	A5V	23 07 28.69	+21 08 03.3	107.93±0.60	−49.63±0.46	−12.60±1.40[cc]	25.38±0.70	5.68	5.38±0.03	−13.11	−12.2±0.4	−21.2±1.2	−7.1±0.9	−1.5	32.0	−22.9
HIP 116805	B9V	23 40 24.49	+44 20 02.1	80.73±0.14	−18.70±0.15	−12.70±0.60[cc]	19.37±0.19	4.75	4.62±0.26	...	−11.5±0.2	−20.1±0.5	−5.9±0.2	−16.7	46.5	−14.8
Carina Association																
HIP 30034 A[a]	K1Ve	06 19 12.91	−58 03 15.6	14.36±0.74	44.66±0.84	22.60±0.30[p]	21.71±0.69	8.23	7.58±0.02	−11.40	−10.3±0.3	−21.7±0.3	−6.2±0.2	−2.2	−41.0	−20.9
HIP 32235	G6V	06 43 46.25	−71 58 35.6	6.17±0.80	61.15±0.87	20.70±0.10[p]	17.17±0.72	8.18	7.69±0.03	−11.95	−11.7±0.7	−23.4±0.3	−5.7±0.2	11.5	−50.9	−25.8
HIP 33737	K2V	07 00 30.46	−79 41 45.9	1.56±0.94	59.94±1.00	17.60±0.10[p]	17.00±0.89	9.16	8.27±0.02	−11.81	−9.2±0.8	−21.8±0.4	−5.5±0.3	19.3	−49.1	−26.0
HIP 46063	K1Ve	09 23 34.98	−61 11 35.9	−28.30±0.99	17.98±1.04	20.80±0.40[p]	11.36±1.14	9.12	8.56±0.03	−11.80	−9.8±1.4	−22.3±0.5	−5.8±0.5	15.8	−85.8	−11.9
HIP 46720 AB	F0V+F2V	09 31 25.00	−73 44 49.6	−35.40±0.45	32.44±0.48	18.30±0.00[p]	11.98±0.51	6.86	6.47±0.02	−11.35	−11.9±0.8	−22.8±0.3	−5.9±0.2	27.5	−75.3	−23.2
Argus Association																
HIP 4448 AB[a]	K3Ve+K4Ve	00 56 55.46	−51 52 31.9	95.93±1.57	10.23±1.35	1.60±0.50[p]	24.61±1.64	7.92	7.04±0.03	−11.21	−16.1±1.1	−9.3±0.7	−1.9±0.5	8.7	−14.6	−36.9
AP COL	M5	06 04 52.15	−34 33 36.0	27.33±0.35[k]	340.92±0.35[k]	22.40±0.30[k]	119.21±0.98[k]	9.74[k]	7.74±0.03	−11.43	−22.0±0.2	−13.6±0.2	−4.5±0.1	−3.7	−6.7	−3.4
HIP 36948	G8Vk	07 35 47.47	−32 12 14.1	−55.71±0.59	74.58±0.62	22.57±0.18[gg]	28.29±0.85	7.45	6.91±0.03	...	−23.1±0.4	−14.2±0.3	−4.4±0.1	−14.1	−32.2	−3.5
HIP 47135	G1	09 36 17.83	−78 20 41.7	−74.85±0.59	50.62±0.59	5.20±0.10[dd]	14.71±0.60	7.93	7.47±0.03	−12.33	−24.9±1.1	−14.3±0.4	−7.0±0.3	25.8	−58.8	−22.3
HIP 50191	A2V	10 14 44.16	−42 07 18.9	−150.09±0.10	49.44±0.11	7.40±2.70[cc]	32.18±0.15	3.82	3.86±0.26	...	−21.6±0.2	−10.3±2.6	−5.1±0.6	2.3	−30.3	6.4
HIP 57632[a]	A3V	11 49 03.66	+14 34 19.7	−497.68±0.87	−114.67±0.44	−0.20±0.50[cc]	90.91±0.52	2.04	1.85±0.27	...	−19.9±0.1	−16.0±0.2	−7.7±0.5	−1.2	−3.4	10.4
HIP 68994	F4V	14 07 29.29	−61 33 44.1	−69.88±0.79	−29.87±0.60	−5.20±1.00[cc]	15.59±0.81	7.25	6.97±0.02	...	−20.6±1.1	−11.5±1.1	−2.5±0.2	42.8	−47.8	−0.0
HIP 74405	G9V	15 12 23.43	−75 15 15.6	−73.87±0.87	−73.08±0.92	−3.50±0.10[p]	19.88±1.06	8.56	7.84±0.03	−11.64	−21.2±1.0	−12.5±0.8	−4.3±0.3	32.3	−36.3	−12.9
HIP 79797	A4V	16 17 05.40	−67 56 28.5	−45.99±0.28	−84.00±0.35	−9.00±4.30[cc]	19.15±0.42	5.77	5.77±0.03	...	−22.4±3.3	−11.1±2.7	−4.4±0.9	39.3	−32.5	−11.2
HIP 98495	A0V	20 00 35.58	−72 54 38.0	81.78±0.11	−132.16±0.14	−6.70±0.70[cc]	31.04±0.17	4.01	3.80±0.25	...	−21.8±0.5	−10.6±0.4	−4.8±0.4	21.8	−17.0	−16.5
HIP 99770	A2V	20 14 32.03	+36 48 22.5	69.81±0.19	69.14±0.20	−17.30±2.80[cc]	23.42±0.22	4.72	4.89±0.31	...	−23.4±0.8	−11.4±2.7	−4.4±0.1	11.4	41.1	0.9
AB Doradus Moving Group																
HIP 3589 AB	F8V*	00 45 50.88	+54 58 40.2	96.81±0.65	−74.17±0.53	−14.80±1.70[f]	19.04±0.89	7.04	6.64±0.02	−11.59	−10.9±1.3	−27.2±1.6	−16.8±0.9	−27.7	44.1	−7.2

Table 2.II — continued

Name	Spt	α (J2000.0) hh mm ss.ss	δ (J2000.0) dd mm ss.s	$\mu_\alpha \cos\delta$[b] (mas yr^{-1})	μ_δ[b] (mas yr^{-1})	v_{rad}[c] (km s^{-1})	π[d] (mas)	I[e] (mag)	J (mag)	X-ray[f] log(f_x)	U (km s^{-1})	V (km s^{-1})	W (km s^{-1})	X (pc)	Y (pc)	Z (pc)
HIP 5191 AB	K1V*	01 06 26.14	−14 17 46.8	99.29 ± 1.23	−94.93 ± 0.74	6.00 ± 1.20[ee]	21.12 ± 1.23	8.55	7.91 ± 0.02	−12.05	−7.8 ± 0.5	−29.0 ± 1.8	−9.3 ± 1.2	−8.2	7.2	−46.1
HIP 6276	G0V	01 20 32.26	−11 28 03.5	110.59 ± 0.92	−138.43 ± 0.69	8.26 ± 0.44[hh]	29.07 ± 1.01	7.60	7.03 ± 0.02	−12.20	−4.2 ± 0.2	−27.2 ± 1.0	−12.0 ± 0.4	−8.6	5.4	−32.9
HIP 10272 AB	K1V*	02 12 15.35	+23 57 29.8	125.44 ± 1.45	−161.47 ± 0.98	−0.30 ± 0.20[f]	27.30 ± 1.19	6.49	6.20 ± 0.02	−11.84	−8.6 ± 0.4	−31.3 ± 1.4	−14.3 ± 0.7	−24.7	16.8	−21.2
HIP 12635	K3.5V	02 42 20.94	+38 37 21.2	75.73 ± 2.49	−111.45 ± 2.73	−4.10 ± 0.30[ee]	19.83 ± 2.62	9.32	8.38 ± 0.02	−11.97	−8.2 ± 1.6	−28.2 ± 3.5	−13.7 ± 2.1	−39.3	26.9	−16.7
HIP 12638	G5V	02 42 21.30	+38 37 07.3	79.20 ± 2.24	−107.49 ± 2.39	−4.20 ± 0.20[f]	22.00 ± 2.35	7.93	7.43 ± 0.02	−11.97	−7.5 ± 1.2	−25.8 ± 2.6	−11.2 ± 1.4	−35.4	24.2	−15.0
HIP 13027 AB	G0V+G5V	02 47 27.38	+19 22 19.2	117.91 ± 0.89	−161.81 ± 0.71	3.70 ± 0.30[f]	29.80 ± 0.82	6.16	5.87 ± 0.02	−11.63	−7.9 ± 0.3	−28.8 ± 0.8	−11.8 ± 0.3	−25.1	10.6	−19.6
HIP 13209	B8V	02 49 59.02	+27 15 38.1	66.81 ± 0.24	−116.52 ± 0.15	4.00 ± 4.10[cc]	19.69 ± 0.19	3.69	3.66 ± 0.29	...	−8.9 ± 3.2	−26.9 ± 1.7	−16.1 ± 2.0	−39.7	20.3	−24.3
HIP 14684	G0V	03 09 42.27	−09 34 46.3	91.01 ± 1.30	−112.21 ± 1.30	14.60 ± 0.70[f]	26.73 ± 1.12	7.64	7.16 ± 0.03	...	−5.8 ± 0.5	−27.1 ± 1.1	−10.0 ± 0.6	−22.1	−4.4	−29.9
HIP 14809	G5V	03 11 13.83	+22 24 57.1	54.04 ± 1.36	−126.09 ± 1.32	5.20 ± 0.20[ee]	18.62 ± 1.13	7.85	7.27 ± 0.02	−11.91	−5.8 ± 0.3	−29.8 ± 1.9	−18.0 ± 1.0	−43.9	15.4	−26.9
HIP 15353	A3V	03 17 59.07	−66 55 36.7	56.94 ± 0.30	12.68 ± 0.40	26.00 ± 0.50[cc]	18.20 ± 0.30	5.88	5.78 ± 0.02	...	−6.1 ± 0.2	−27.0 ± 0.4	−11.9 ± 0.4	9.4	−38.1	−38.4
HIP 16563 AB	G5V*M0V	03 33 13.47	+46 15 26.9	68.46 ± 0.96	−176.81 ± 0.76	−6.00 ± 0.30[ee]	29.08 ± 1.02	7.34	6.84 ± 0.02	−11.06	−5.8 ± 0.5	−26.5 ± 0.8	−15.9 ± 0.6	−29.5	17.1	−4.8
HIP 17695	M2.5V kee	03 47 23.33	−01 58 19.5	185.53 ± 3.77	−273.48 ± 3.95	16.00 ± 1.70[ee]	62.00 ± 2.88	9.11[kk]	7.80 ± 0.03	−11.49	−7.4 ± 1.3	−26.9 ± 1.2	−10.8 ± 1.1	−12.0	−2.1	−10.6
HIP 18859	F5V	04 02 36.75	−00 16 07.8	149.04 ± 0.42	−253.03 ± 0.43	17.60 ± 1.30[f]	53.10 ± 0.32	4.80	4.71 ± 0.24	−10.91	−7.9 ± 0.2	−28.1 ± 0.2	−12.0 ± 0.1	−14.8	−2.8	−11.3
HIP 19183	F5V	04 06 41.53	+01 41 02.0	37.08 ± 1.43	−94.59 ± 1.34	15.90 ± 1.30[f]	18.12 ± 0.92	7.28	6.89 ± 0.03	−12.18	−5.0 ± 1.1	−27.0 ± 1.3	−14.3 ± 0.8	−44.6	−7.5	−31.6
HIP 22738 A	M3Ve	04 53 31.19	−55 51 37.2	134.53 ± 2.39	72.68 ± 2.03	29.00 ± 0.00[p]	90.02 ± 1.98	8.58[p]	7.20 ± 0.03	−11.11	−7.4 ± 0.2	−26.1 ± 0.1	−13.0 ± 0.1	−0.9	−8.6	−6.9
HIP 22738 B	M3Ve	04 53 30.54	−55 51 31.8	134.53 ± 2.39	72.68 ± 2.03	30.00 ± 0.00[p]	90.02 ± 1.98	9.29[p]	7.80 ± 0.02	−11.11	−7.5 ± 0.2	−26.9 ± 0.1	−13.6 ± 0.1	−0.9	−8.6	−6.9
HIP 25283 AB	K6 ke*	05 24 30.16	−38 58 10.6	44.25 ± 0.67	−59.51 ± 1.13	31.70 ± 0.20[f]	55.55 ± 0.92	7.87	6.70 ± 0.02	−11.57	−7.4 ± 0.1	−27.7 ± 0.2	−14.8 ± 0.1	−6.7	−13.5	−9.8
HIP 25647 ABCD	K1(sb4)	05 28 44.84	−65 26 55.1	33.16 ± 0.39	150.83 ± 0.73	33.00 ± 0.30[ee]	65.93 ± 0.57	5.94	5.32 ± 0.02	−10.24	−8.4 ± 0.1	−29.2 ± 0.3	−17.1 ± 0.2	1.2	−12.7	−8.3
HIP 26369	K7V	05 36 55.09	−47 57 48.1	12.64 ± 10.36	24.53 ± 10.04	31.10 ± 1.10[ee]	39.01 ± 7.34	8.38[kk]	7.45 ± 0.03	−10.93	−10.0 ± 1.3	−25.6 ± 1.2	−14.9 ± 1.3	−5.8	−21.0	−13.6
HIP 26373	K0V	05 36 56.85	−47 57 52.8	25.40 ± 1.65	−3.38 ± 1.45	32.20 ± 0.20[f]	39.82 ± 1.36	7.09	6.37 ± 0.02	−10.93	−7.0 ± 0.2	−28.0 ± 0.2	−14.5 ± 0.2	−5.7	−20.5	−13.3
HIP 26401 AB	G7V+K1V	05 37 12.92	−42 42 55.6	11.01 ± 1.36	−15.02 ± 2.04	31.80 ± 0.00[p]	13.05 ± 1.51	8.52	8.08 ± 0.03	−11.97	−4.9 ± 0.9	−29.0 ± 0.5	−13.9 ± 0.5	−24.1	−61.0	−39.6
HIP 30314 AB	G1V*	06 22 30.97	−60 13 07.2	−11.29 ± 0.35	64.24 ± 0.30	31.20 ± 0.20[f]	42.05 ± 0.27	5.87	5.43 ± 0.04	−11.33	−7.6 ± 0.1	−27.7 ± 0.2	−14.3 ± 0.1	−0.2	−21.2	−10.7
HIP 31711 AB	G1.5V*	06 38 00.36	−61 32 00.1	−47.84 ± 1.04	72.73 ± 0.87	33.40 ± 1.00[ee]	46.96 ± 0.81	5.46	5.08 ± 0.27	−10.76	−7.5 ± 0.2	−29.0 ± 0.9	−17.2 ± 0.4	0.4	−19.3	−9.1
HIP 31878	K7V	06 39 50.03	−61 28 41.7	−27.92 ± 1.00	75.34 ± 1.13	30.50 ± 0.70[ee]	44.74 ± 0.91	8.18	7.30 ± 0.02	−11.94	−7.8 ± 0.2	−27.3 ± 0.6	−14.1 ± 0.3	0.4	−20.3	−9.4
HIP 36349 AB	M3V*	07 28 51.37	−30 14 49.0	−130.08 ± 1.36	−131.55 ± 1.73	26.60 ± 1.00[ee]	63.72 ± 1.76	7.39	6.61 ± 0.02	−10.88	−7.3 ± 0.5	−24.3 ± 0.9	−15.9 ± 0.4	−6.9	−14.0	−1.6
HIP 51317	M2V	10 28 55.55	+00 50 27.5	−603.75 ± 1.90	−728.94 ± 2.04	8.30 ± 0.50[ff]	141.50 ± 0.53	6.18	6.18 ± 0.02	−12.95	−7.5 ± 0.2	−28.0 ± 0.3	−15.3 ± 0.4	−2.1	−4.4	5.2
HIP 63742 AB	G5V*	13 03 49.67	−05 09 42.3	−191.13 ± 0.86	−218.73 ± 0.68	2.00 ± 0.50[ee]	46.10 ± 0.81	6.80	6.05 ± 0.02	−11.83	−5.3 ± 0.2	−27.9 ± 0.5	−9.4 ± 0.5	7.3	−9.1	18.3
HIP 76768 AB	K3V+K4V	15 40 28.40	−18 41 46.0	−70.13 ± 3.32	−159.81 ± 2.39	−8.90 ± 0.40[ee]	24.88 ± 2.69	8.75	7.73 ± 0.03	−11.44	−7.1 ± 0.5	−29.7 ± 3.4	−15.8 ± 1.4	34.7	−6.5	19.2
HIP 81084	M0.5V	16 33 41.61	−09 33 11.6	−70.05 ± 2.75	−177.52 ± 2.29	−15.00 ± 0.40[ee]	32.60 ± 2.47	9.53	8.38 ± 0.02	−12.07	−7.5 ± 0.6	−27.9 ± 2.0	−12.6 ± 0.6	27.6	3.2	12.9
HIP 82688	G0V	16 54 08.15	−04 20 24.8	−37.25 ± 1.01	−114.05 ± 0.73	−16.50 ± 0.40[f]	21.40 ± 0.92	7.16	6.70 ± 0.02	−11.89	−5.7 ± 0.5	−28.1 ± 1.1	−12.5 ± 0.4	41.5	10.7	18.7
HIP 86346 AB	M0V*	17 38 39.64	+61 14 16.0	−23.30 ± 2.03	47.71 ± 2.20	−26.70 ± 0.10[q]	30.19 ± 2.00	8.99[mm]	7.62 ± 0.02	−11.32	−7.5 ± 0.6	−24.4 ± 0.2	−11.3 ± 0.3	−0.1	28.0	17.7
HIP 93580[a]	A4V	19 03 32.24	+01 49 07.6	22.63 ± 0.26	−68.50 ± 0.20	−23.10 ± 2.30[cc]	18.22 ± 0.31	5.62	5.46 ± 0.02	−12.15	−11.3 ± 1.9	−24.5 ± 1.4	−12.6 ± 0.2	44.4	32.2	−1.8

Table 2.II — continued

Name	Spt	α (J2000.0) hh mm ss.ss	δ (J2000.0) dd mm ss.s	$\mu_\alpha \cos \delta$[b] (mas yr^{-1})	μ_δ[b] (mas yr^{-1})	v_{rad}[c] (km s^{-1})	I[e] (mag)	J (mag)	X-ray[f] log(f_x)	U (km s^{-1})	V (km s^{-1})	W (km s^{-1})	X (pc)	Y (pc)	Z (pc)
HIP 94235 AB	G1V*	19 10 57.82	−60 16 20.2	12.51±0.79	−100.15±0.68	8.70±0.30[ff]	7.62	7.20±0.02	−11.88	−7.6±0.8	−27.3±1.2	−11.7±0.4	50.6	−22.3	−26.6
HIP 95347	B8V	19 23 53.15	−40 36 57.1	30.49±0.35	−119.21±0.18	−0.70±4.10[cc]	4.06	4.17±0.25	−12.05	−8.3±3.8	−27.5±0.4	−15.2±1.6	51.2	−2.0	−21.9
HIP 106231	K8V	21 31 01.71	+23 20 07.4	133.38±0.97	−145.24±0.90	−17.40±1.00[q]	8.13	7.07±0.02	−11.16	−5.0±0.3	−23.8±0.9	−15.7±0.7	6.3	22.4	−8.5
HIP 109268	B6V	22 08 13.97	−46 57 39.3	126.69±0.14	−147.47±0.14	...	1.78	2.02±0.35	...	−6.9±1.0	−25.4±0.2	−15.5±1.3	18.6	−3.3	−24.6
HIP 110526 AB	M3V*	22 23 29.04	+32 27 33.4	251.31±5.54	−212.28±11.32	−20.60±2.10[ee]	8.58	6.90±0.02	−11.04	−6.2±0.9	−27.6±2.1	−14.5±2.4	−0.0	14.5	−5.5
HIP 113579	G3V	23 00 19.29	−26 09 13.5	110.02±0.83	−160.09±0.56	6.10±0.20[r]	6.75	6.29±0.02	−11.68	−3.2±0.2	−25.4±0.6	−13.6±0.3	11.3	6.2	−27.9
HIP 113597 AB	K8V*	23 00 27.91	−26 18 43.1	113.54±2.13	−162.04±1.52	8.40±1.50[ee]	7.98	7.05±0.02	−11.68	−2.6±0.7	−25.2±1.7	−15.8±1.5	11.2	6.1	−27.7
HIP 114066	M1V	23 06 04.82	+63 55 33.9	171.46±1.59	−58.55±1.57	−23.70±0.80[ee]	9.10	7.82±0.02	−11.43	−6.1±0.7	−27.0±0.8	−15.5±0.6	−9.0	22.7	1.4
HIP 114530 AB	G5V*	23 11 52.05	−45 08 10.6	87.53±1.39	−93.36±0.79	9.10±0.20[r]	8.02	7.47±0.03	−11.66	−8.3±0.7	−28.3±1.5	−10.3±0.3	21.4	−6.1	−44.1
HIP 115162	G4V	23 19 39.55	+42 15 09.8	77.52±0.73	−66.90±0.96	−19.70±0.20[ee]	8.15	7.61±0.02	−12.35	−4.3±0.6	−27.4±0.6	−14.6±1.2	−12.6	46.1	−15.0
HIP 115738	A0V	23 26 55.95	+01 15 20.1	86.68±0.31	−94.29±0.22	−4.40±0.60[cc]	4.94	5.32±0.27	...	−6.9±0.1	−25.1±0.5	−12.6±0.5	2.9	26.8	−38.6
HIP 116910	G8V	23 41 54.28	−35 58 39.7	69.49±1.18	−67.53±0.95	11.10±1.70[p]	8.67	8.10±0.02	−11.39	−7.3±1.0	−27.3±2.0	−13.5±1.6	18.8	−0.8	−60.8
HIP 117452 AB[a]	A0V*	23 48 55.54	−28 07 49.0	100.80±0.25	−105.34±0.23	8.70±2.00[cc]	4.60	4.80±0.26	−11.79	−6.6±0.4	−26.6±0.3	−13.2±1.9	9.1	4.3	−40.9
HIP 118008	K3V	23 56 10.67	−39 03 08.6	206.72±0.51	−185.07±0.54	12.10±0.50[ee]	7.22	6.51±0.03	−12.10	−7.8±0.3	−27.6±0.5	−12.5±0.5	6.0	−1.8	−21.1

[a] *bona fide members* with ambiguous membership, see section 9.

[b] Proper motion from van Leeuwen, 2007, unless stated otherwise.

[c] Radial velocity measurement from Bailey et al., 2012, unless stated otherwise.

[d] Parallax measurement from van Leeuwen, 2007, unless stated otherwise.

[e] I_c magnitude from Anderson & Francis, 2012, unless stated otherwise.

[f] ROSAT X-ray flux calculated from Riaz et al. (see Section 5.4; 2006) in erg s^{-1} cm^{-2}.

Note. — (g) Teixeira et al., 2009 ; (h) Teixeira et al., 2008 ; (i) Faherty et al., 2012 ; (j) PPMXL; Roeser et al., 2010 ; (k) Riedel et al., 2011 ; (l) Riedel (in prep.) ; (m) UCAC3; Zacharias et al., 2009 ; (n) Kharchenko et al., 2007 ; (o) Bobylev & Bajkova, 2007 ; (p) Torres et al., 2006 ; (q) Montes et al., 2001 ; (r) Bobylev et al., 2007 ; (s) Moór et al., 2006 ; (t) we add 0.75 mag to the J(2mass) magnitude; Cutri et al., 2003 ; (u) Shkolnik et al., 2011 ; (v) Rice et al., 2010; (w) Kiss et al., 2011 ; (x) Schlieder et al., 2012a; (y) Schlieder et al., 2010 ; (z) Mohanty et al., 2003 ; (aa) Grenier et al., 1999 ; (bb) Zuckerman & Webb, 2000 ; (cc) Zuckerman et al., 2011 ; (dd) Guenther et al., 2007 ; (ee) Zuckerman et al., 2004 ; (ff) Gontcharov, 2006 ; (gg) Anderson & Francis, 2012; (hh) White et al., 2007 ; (ii) Gizis et al., 2007 ; (jj) DENIS; Epchtein et al., 1997 ; (kk) Koen et al., 2010 ; (ll) Weis, 1987 ; (mm) Messina et al., 2010

2.3 Global properties of known members and field stars

This section summarizes the main kinematic and photometric properties for the known members of the seven associations studied here. As the Bayesian analysis performed later requires considering also that a star belongs to the field, as an hypothesis, the properties of field stars are also discussed. These properties will be used in the next section for constructing kinematic and photometric models for each association. For simplicity, we model these properties using simple functions : the Galactic space velocities and positions distributions are modeled by Gaussians whose parameters are inferred by fitting cumulative distribution functions while the CMD sequences are modeled with polynomials.

2.3.1 Kinematic properties

Because of the coeval formation of a given association, all members share, to within a few $km\,s^{-1}$, a common space velocity within the Galaxy. The galactic space motion of a star, UVW, is determined from its sky position (α, δ), radial velocity, proper motion and parallax, using the Johnson & Soderblom (1987) relations. Proper motion and parallax measurements come from several sources (Faherty et al., 2012, Gizis et al., 2007, Riedel et al., 2011, van Leeuwen, 2007, Teixeira et al., 2009, 2008, ; A. R. Riedel in preparation), while radial velocities are taken from various studies (see Table 2.II). The field star sample we used comprises 10094 stars within 150 pc with *Hipparcos* parallax known to an accuracy better than 5σ (from van Leeuwen, 2007) and radial velocities from Francis & Anderson (2009). Figure 2.1 shows the U cumulative distribution function for the seven associations and for the field stars sample, as an example. These distributions are reasonably well approximated by normal functions whose parameters are given in Table 3.III.

2.3.2 Galactic position

By virtue of their youth and their coeval formation, the members of young associations have had little time to disperse within the Galaxy. As a result, the positions XYZ

Table 2.III.   Mean galactic motion and position

Name of group	UVW (km s^{-1})	σ_{UVW} (km s^{-1})	XYZ (pc)	σ_{XYZ} (pc)
β Pictoris (βPMG)	$-10.94, -16.25, -9.27$	$2.06, 1.30, 1.54$	$9.27, -5.96, -13.59$	$31.71, 15.19, 8.22$
Tucana-Horologium (THA)	$-9.88, -20.70, -0.90$	$1.51, 1.87, 1.31$	$11.39, -21.21, -35.40$	$19.29, 9.17, 5.39$
AB Doradus (ABDMG)	$-7.12, -27.31, -13.81$	$1.39, 1.31, 2.16$	$-2.37, 1.48, -15.62$	$20.03, 18.83, 16.59$
Columba (COL)	$-12.24, -21.32, -5.58$	$1.03, 1.18, 0.89$	$-27.44, -31.32, -27.97$	$13.79, 20.55, 15.09$
Carina (CAR)	$-10.50, -22.36, -5.84$	$0.99, 0.55, 0.14$	$15.55, -58.53, -22.95$	$5.66, 16.69, 2.74$
TW Hydrae (TWA)	$-9.87, -18.06, -4.52$	$4.15, 1.44, 2.80$	$12.49, -42.28, 21.55$	$7.08, 7.33, 4.20$
Argus (ARG)	$-21.78, -12.08, -4.52$	$1.32, 1.97, 0.50$	$14.60, -24.67, -6.72$	$18.60, 19.06, 11.43$
Field stars	$-10.92, -13.35, -6.79$	$23.22, 13.44, 8.97$	$-0.18, 2.10, 3.27$	$53.29, 51.29, 50.70$

of the members of a young association are relatively well confined within the Galaxy. The XYZ frame of reference is centered on the position of the Sun and follows the same sign convention as the galactic velocities UVW, i.e., X positive towards the center of the Galaxy, Y positive in the direction of galactic rotation and Z positive towards the north galactic pole. Table 3.III gives the mean values and dispersions for the XYZ distribution of the young kinematic group members and field stars. The X cumulative distributions of the known members of the seven associations and the field stars are presented in Figure 2.2.

2.3.3   Photometric properties

CMDs have been a crucial tool for identifying young stars. Since our goal is to search for low-mass stars, color indices as red as possible are desirable and we opted for the $I_c - J$ index. A color index based on V-band magnitudes, largely used in previous studies to search for young stars, is impractical for many objects later than M5V.

For the *bona fide members* and the field stars, the I_c magnitudes come from *Hipparcos* (Anderson & Francis, 2012), DENIS (Epchtein et al., 1997), SDSS-DR8 (Adelman-McCarthy & et al., 2011), and other studies. We transformed the Gunn-*i* DENIS and Sloan Digital Sky Survey (SDSS) magnitudes to I_c using conversions derived using the
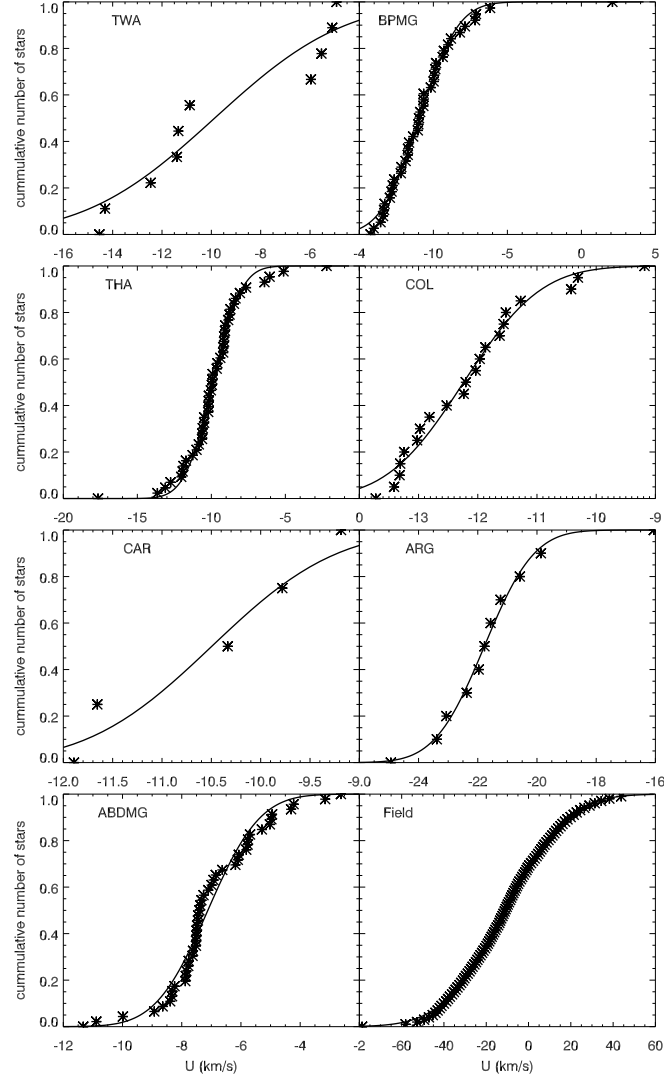
Figure 2.1 *U* cumulative distribution functions of *bona fide members* of young kinematic groups and the field stars. The black line represents the adopted parametrization (see Table 3.III).

standards of Landolt (Landolt, 2009). These transformations are

$$I_c = i_{DENIS} + 0.01 \tag{2.1}$$

$$I_c = i_{SDSS-DR8} - 0.67. \tag{2.2}$$

and accurate within 0.2 mag over $-0.10 < I_c - J < 3.25$.
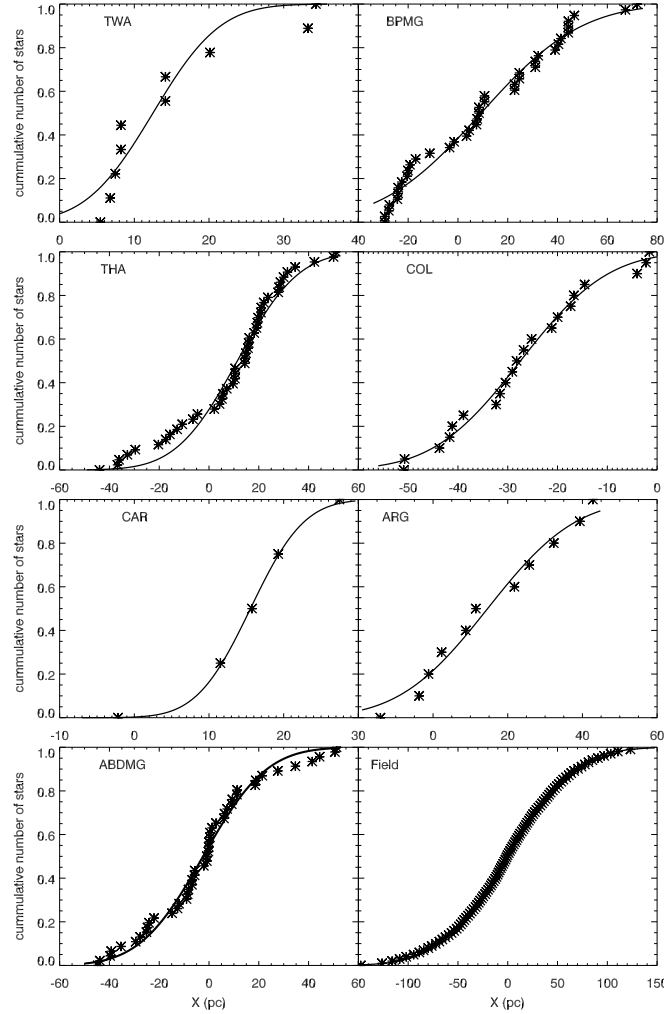
Figure 2.2 *X* cumulative distribution functions of the known members of young kinematic groups and the field stars. The black line represents the adopted parametrization (see Table 3.III).

The *J* magnitude is taken from the 2MASS PSC (Cutri et al., 2003). Field stars are taken from the samples of Francis & Anderson (2009) and Phan-Bao et al. (2003). The first includes 10094 stars within 150 pc with radial velocity and trigonometric distance measurements. The second includes 64 M dwarfs with parallax measurements from various studies.

The least massive known members of the seven young groups studied are M8.5V (βPMG and TWA) and M3V (ABDMG) dwarfs. Thus, to extend the color sequence of the young associations beyond M3V up to M9V, we used the evolutionary models of

Baraffe et al. (2002, 1998), shifting the isochrones (typically by 0.5 mag) to match the known members between K5V and M5V dwarfs.

For the purpose of the current analysis, the association members are merged into four groups : <10 Myr-old (TWA), 10 Myr to 20 Myr-old (βPMG), 20 Myr to 50 Myr-old (THA, COL, CAR and ARG) and >50 Myr-old (ABDMG). Since ABDMG lacks massive (A0V dwarf) known members, a sample of 33 early-type Pleiades members (with *Hipparcos* parallax) were used to reproduce the trend of the color sequence from A0V to M9V for the ABDMG.

We used the 8 Myr model for TWA, 12 Myr for βPMG and 40 Myr for the THA, COL, CAR and ARG groups. The oldest groups (including ABDMG and Pleiades members) were approximated as a 80 Myr model. For the field star sample, we used the 5 Gyr model. We corrected the magnitudes of the models to match the 2MASS color system. All known binaries were excluded for the determination of the color sequences. Figure 2.3 shows the resulting CMD sequences adopted, for the association members and old field stars. For $I_c - J > 0.8$, young stars are significantly overluminous compared to field stars. The absolute magnitude M_J of those four groups are well described, within a dispersion of 0.3 mag, using polynomials. Similarly, one can construct an empirical sequence for old field stars. This sequence is represented by the dashed line in Figure 2.3. The 1σ dispersion, represented by the gray envelope, varies with color and is typically $\sim$0.5 mag.

2.4   Kinematic model

A key element of our analysis for identifying new members of young associations is to build a kinematic model of a given association. For a star at a given position on the sky and given the mean and dispersion of the galactic space velocity of an association, this model should reliably predict the radial and tangential velocities and the direction of proper motion that the star would have if it were an actual member of the association. For a given distance, the tangential velocity translates into a proper motion amplitude. The direction and amplitude of the proper motion predicted by this model restrict considera-
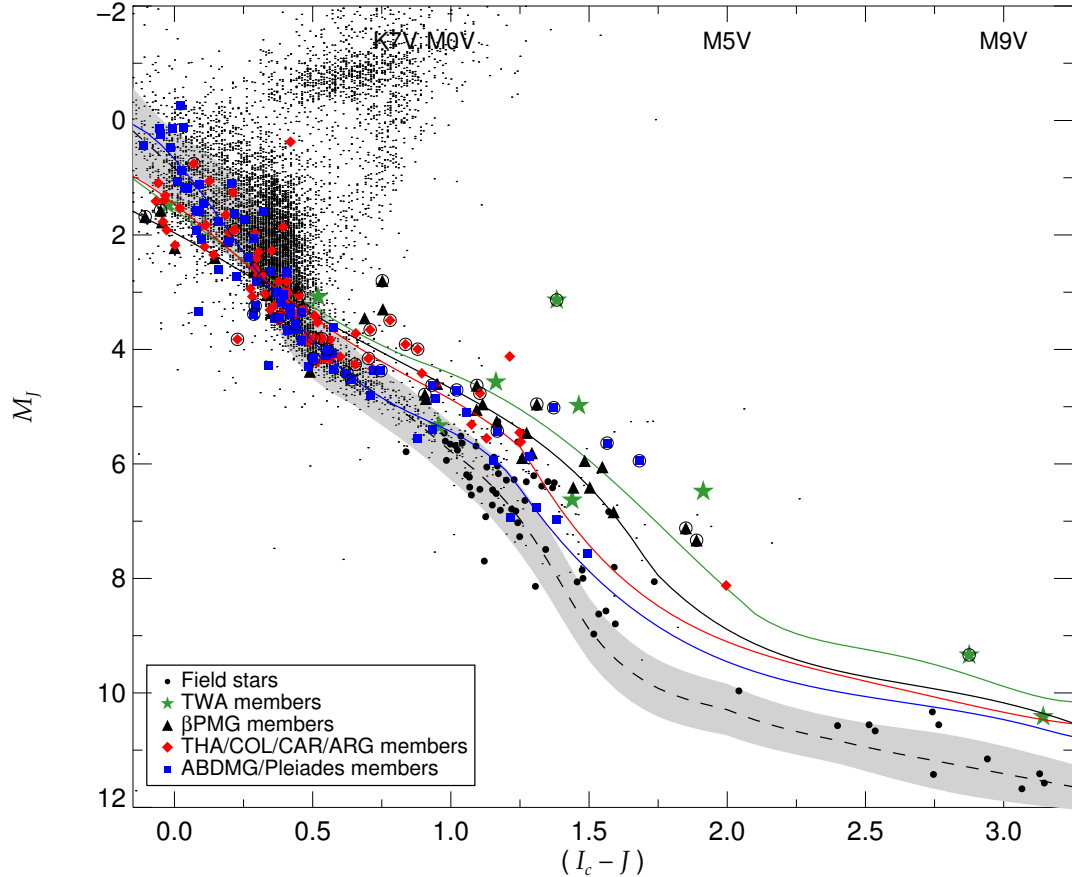
Figure 2.3 Color-magnitude diagram (M_J vs $I_c - J$) for members of TWA (green stars), βPMG (black triangles), THA, COL, CAR and ARG (red diamonds) and ABDMG and Pleiades (blue squares). Fields stars (dots and filled black circles) are from Francis & Anderson (2009) and Phan-Bao et al. (2003). The dashed line and shaded area represent the locus of old field stars. K5V-M5V, representative of our search sample (see §6), have $0.8 < I_c - J < 2.0$. On average, young late-type stars are brighter than field stars, a property that can be used, along with other kinematic properties, to discriminate young stars from old ones. Binary stars are those with black circles superposed on their own symbol.

bly the number of potential members of a young association, and even help constraining their distance.

The kinematic model is built by inverting the procedure described in Section 4.3. For a specific group and a position in the sky (right ascension and declination), we create virtual stars having UVW velocities and dispersions as given in Table 3.III. The radial and tangential velocities of these stars are calculated and their mean and dispersion are obtained. Then given a distance, the tangential velocity is used to estimate the amplitude of the proper motion.
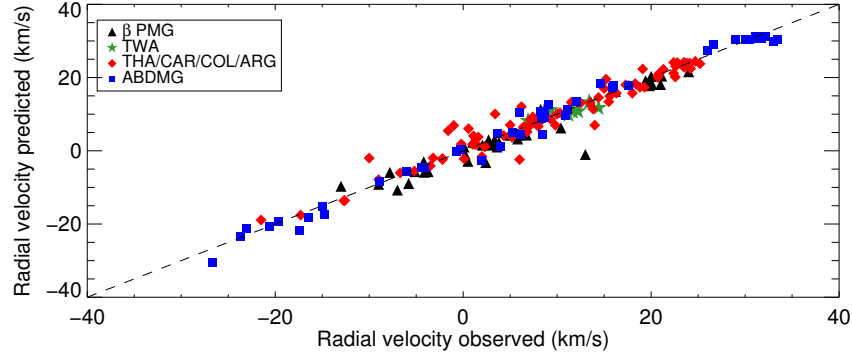
Figure 2.4 Comparison between estimated radial velocities by the kinematic model and those observed for the known members of βPMG (black triangles), TWA (green stars), THA, COL, CAR, and ARG (red asterisks), and ABDMG (blue diamonds).

The robustness of this kinematic model can be gauged by comparing the measured and predicted radial velocities for *bona fide members*. This comparison is presented in Figure 2.4 for the seven associations. There is an excellent correlation between the predicted and observed values, with an rms of 1.9 km s^{-1}.

2.5 Selection of candidates - Bayesian statistical analysis

2.5.1 General formalism

Based on a set $\{\theta\}$ of observables, a Bayesian analysis is used to select stars potentially members of a young kinematic group. From this analysis, a membership probability and a statistical distance are determined for each star and each group considered. In this study, the observables are the amplitude of proper motion in right ascension and declination, the apparent I_c and J magnitudes and the position (α, δ) of the star on the sky. It is possible to add more observables in the analysis (e.g., radial velocity), but in practice they are limited. Let $\{H_k\}$ be a set of hypotheses $H_{d_n}^{g_m}$

$$\{H_k\} = \{(H_{d_1}^{g_1}), (H_{d_2}^{g_1}), ..., (H_{d_n}^{g_1}), (H_{d_1}^{g_2}), (H_{d_2}^{g_2}), ..., (H_{d_n}^{g_m})\} \tag{2.3}$$

that a candidate is a member of a group (g_m) at a given distance d_n. The set contains $m \times n$ hypotheses where m represents the number of groups considered and n the number of distances. Given the observable θ, the probability that a candidate star is a member of group g_i at distance d_j is $P(H_{d_j}^{g_i}|\theta)$. In what follows, the symbol "|" means "given".

According to Bayes' theorem, we have :

$$P(H_{d_j}^{g_i}|\theta) \;=\; \frac{P(\theta|H_{d_j}^{g_i})P(H_{d_j}^{g_i})}{P(\theta)} \tag{2.4}$$

with,

$$P(\theta) \;=\; \sum_{k=1}^{m\times n} P(\theta|H_k)P(H_k)$$

where $P(\theta|H_k)$ is the probability to obtain the observable θ under a given hypothesis. This quantity can be easily determined with a model representative of the observable θ. In the denominator of Equation (2.4), $P(\theta)$ is the marginal probability to obtain the observable θ independently of the hypothesis considered. This term normalizes the numerator by summing over all possibilities. $P(H_k)$ is the prior probability that the hypothesis is true. Since these prior probabilities are unknown, an equal weight is given to them : $P(H_k) = (1/m \times n)$.

Equation (2.4) is a probability density function whose maximum gives the most likely hypothesis and the most likely distance (hereafter referred to as the *statistical* distance), while its sum over all distances (for each group hypothesis) gives the membership probability irrespective of the distance :

$$P(H^{g_i}|\theta) = \sum_{j=1}^{n} P(H_{d_j}^{g_i}|\theta). \tag{2.5}$$

As mentioned before, the probabilities $P(\theta|H_k)$ needed in Equation (2.4) are derived from a Gaussian distribution with mean $\bar{\theta}$ and standard deviation σ :

$$P(\theta|H) = \frac{1}{\sqrt{2\pi}\sigma} e^{-\frac{1}{2}\left(\frac{(\theta-\bar{\theta})}{\sigma}\right)^2} \tag{2.6}$$

By considering two observables and applying Bayes' theorem iteratively, equation (2.4) becomes :

$$P(H_{d_j}^{g_i}|\theta_1 \cap \theta_2) = \frac{P(\theta_1|H_{d_j}^{g_i})P(\theta_2|H_{d_j}^{g_i})P(H_{d_j}^{g_i})}{\sum_{k=1}^{m \times n} P(\theta_1|H_k)P(\theta_2|H_k)P(H_k)},$$

(2.7)

The generalization of this expression for f observables is :

$$P(H_{d_j}^{g_i}|\theta_1 \cap \theta_2 \cap ... \cap \theta_f) = \frac{P(H_{d_j}^{g_i})\prod_{l=1}^{f}P(\theta_l|H_{d_j}^{g_i})}{\sum_{k=1}^{m \times n} P(H_k)\prod_{l=1}^{f}P(\theta_l|H_k)}$$

(2.8)

2.5.2 Practical application of the formalism

Now consider the application of this formalism to the specific observables of our problem, starting with the apparent J magnitude. Given an association and a distance, the expected absolute J magnitude ($\bar{\theta}$) is deduced from the $I_c - J$ color of the candidate and the empirical sequence (M_J versus $I_c - J$) of the association. The parameter σ represents the dispersion in magnitude for a given color index.

Next consider the amplitude of the proper motion as a second observable. For a given association and position of a candidate on the sky, the kinematic model discussed in Section 4 predicts the expected mean tangential velocity and its dispersion from the mean and dispersion of UVW of a group (Section 4). Given this tangential velocity and the distance considered, the amplitude of the proper motion ($\bar{\theta}$) is calculated along with its dispersion (σ). These quantities are compared to the observed proper motion using Equation (2.6). We apply this methodology for the amplitude of the proper motion in both right ascension and in declination.

The last two observables to consider are the right ascension and declination, $\theta = (\alpha, \delta)$. Given the position ($\alpha, \delta$) of a candidate and a distance, the corresponding galactic positions XYZ of the candidate are determined and compared to the mean ($\bar{\theta}$) and dispersion (σ) from the kinematic model.

All the parameters used in the analysis are given in Table 3.III. In practice, the analysis was carried out for distances ranging from 1 to 200 pc, by increment of 0.5 pc. To handle the impact of biased photometry from possibly unresolved binary stars, we added

an extra hypothesis for each group wherein the photometric sequences was shifted by 0.75 mag, thus correcting for equal luminosity binarity. In what follows, the probabilities reported for a given group are the sum of the probabilities for the nominal and shifted photometric sequence hypotheses. Finally, in calculating Equation 2.8, we raised the probabilities for the three galactic positions (X, Y, Z) to the power 2/3 to ensure that all observables carry an equal weight. A web-based tool of the Bayesian technique presented here is available at `http://www.astro.umontreal.ca/%7emalo/banyan.php`. For simplicity, the online version does not include the photometry observables.
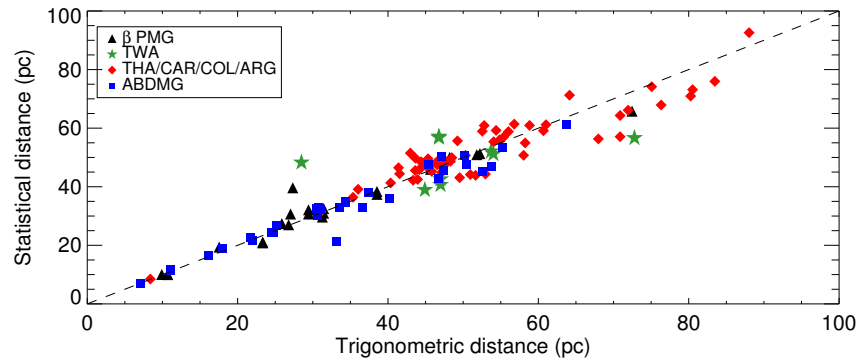
Figure 2.5 Comparison between the statistical distance from Bayesian analysis and the trigonometric distance for the known members of young associations.

To illustrate the robustness of the Bayesian analysis, this method was applied to known members of the young associations considered. Adopting a membership probability threshold of 90%, 72% of the *bona fide members* are recovered (see Table 2.IV).

Figure 2.5 presents a comparison between the observed trigonometric distance (d_p) and the *statistical* distance (d_s) estimated by the Bayesian analysis. The statistical distances agree with the trigonometric distances within 10%.

We applied this method to the sample of field stars from Phan-Bao et al. (2003), and adopting the same membership threshold ($P_{field} > 90\%$), 98% of these stars are found to be member of the field.

It should be stressed that the method above does not make use of the radial velocity as an input observable. Table 2.IV shows the resulting probabilities when the radial velocity is included in the analysis. In general, as expected, the probability slightly increases with

this additional knowledge but this is not always the case ; this will be discussed later in Section 2.9.

Table 2.IV. Membership probabilities of all bona fide members[a]

Name	βPMG			TWA			THA			COL			CAR			ARG			ABDMG			Field		
	P	P_ν	$P_{\nu+\pi}$	P	P_ν	$P_{\nu+\pi}$	P	P_ν	$P_{\nu+\pi}$	P	P_ν	$P_{\nu+\pi}$	P	P_ν	$P_{\nu+\pi}$	P	P_ν	$P_{\nu+\pi}$	P	P_ν	$P_{\nu+\pi}$	P	P_ν	$P_{\nu+\pi}$
β Pictoris moving group																								
HIP 560	74	98	99	0	0	0	15	0	0	6	0	0	0	0	0	0	0	0	0	0	0	4	1	0
HIP 10679	98	99	99	0	0	0	0	0	0	0	0	0	0	0	0	0	0	0	0	0	0	0	0	0
HIP 10680	66	99	99	0	0	0	0	0	0	32	0	0	0	0	0	0	0	0	0	0	0	1	0	0
HIP 11152	80	99	99	0	0	0	1	0	0	0	0	0	0	0	0	0	0	0	18	0	0	0	0	0
HIP 11360	4	6	12	0	0	0	0	0	0	93	93	87	0	0	0	0	0	0	0	0	0	0	0	0
HIP 11437 A	65	99	99	0	0	0	0	0	0	33	0	0	0	0	0	0	0	0	0	0	0	0	0	0
HIP 11437 B	77	99	99	0	0	0	0	0	0	22	0	0	0	0	0	0	0	0	0	0	0	0	0	0
HIP 12545 AB	2	0	11	0	0	0	0	0	0	96	99	88	0	0	0	0	0	0	0	0	0	0	0	0
HIP 21547	98	99	99	0	0	0	0	0	0	1	0	0	0	0	0	0	0	0	0	0	0	0	0	0
GJ 3305 AB	99[b]	99[b]	99[b]	0	0	0	0	0	0	0	0	0	0	0	0	0	0	0	0	0	0	0	0	0
HIP 23200	99	99	99	0	0	0	0	0	0	0	0	0	0	0	0	0	0	0	0	0	0	0	0	0
HIP 23309	96	99	99	0	0	0	0	0	0	0	0	0	0	0	0	0	0	0	3	0	0	0	0	0
HIP 25486	99	99	99	0	0	0	0	0	0	0	0	0	0	0	0	0	0	0	0	0	0	0	0	0
HIP 27321	63	95	99	0	0	0	0	0	0	0	0	0	0	0	0	0	0	0	0	0	0	0	0	0
J0608-2753	90	73	95	0	0	0	0	0	0	9	26	4	0	0	0	35	0	0	38	0	0	4	12	2
HIP 29964	58	99	99	0	0	0	0	0	0	0	0	0	0	0	0	2	0	0	11	0	0	0	0	0
HIP 50156	1	10	4	0	0	0	0	0	0	81	60	93	0	0	0	0	0	0	0	16	0	0	0	0
TWA 22AB	99[b]	99[b]	99[b]	0	0	0	0	0	0	0	0	0	0	0	0	0	0	0	0	0	0	0	0	0
HIP 76629 A	99[b]	99[b]	99[b]	0	0	0	0	0	0	0	0	0	0	0	0	0	0	0	0	0	0	0	0	0
HIP 76629 BC	99[b]	99[b]	99[b]	0	0	0	0	0	0	0	0	0	0	0	0	0	0	0	0	0	0	0	0	0
HIP 79881	80	96	99	0	0	0	0	0	0	0	0	0	0	0	0	0	0	0	0	0	0	0	0	0
HIP 84586 AB	92[b]	99[b]	99[b]	0	0	0	0	0	0	0	0	0	0	0	0	7[b]	0	0	0	0	0	8	3	0
HIP 84586 C	98[b]	99[b]	99[b]	0	0	0	0	0	0	0	0	0	0	0	0	1	0	0	0	0	0	0	0	0
HIP 86598	94	98	99	0	0	0	0	0	0	0	0	0	0	0	0	5	0	0	0	0	0	0	0	0
HIP 88399 A	80	99	99	0	0	0	0	0	0	0	0	0	0	0	0	19	0	0	0	0	0	0	1	0
HIP 88726 AB	87	99	99	0	0	0	0	0	0	0	0	0	0	0	0	12	0	0	0	0	0	0	0	0
HIP 89829	88	99	99	0	0	0	0	0	0	0	0	0	0	0	0	11	0	0	0	0	0	0	0	0
HIP 92024 A	56[b]	99[b]	99[b]	0	0	0	0	0	0	0	0	0	0	0	0	42[b]	0	0	1	0	0	0	0	0
HIP 92024 BC	43	99	99	0	0	0	0	0	0	0	0	0	0	0	0	56	0	0	0	0	0	0	0	0
HIP 92680	76[b]	99[b]	99[b]	0	0	0	0	0	0	0	0	0	0	0	0	23[b]	0	0	0	0	0	0	0	0
HIP 95261 AB	95	0	0	0	0	0	0	0	0	0	0	0	0	0	0	4	0	0	0	0	0	0	99	99
HIP 95270	95	99	99	0	0	0	0	0	0	0	0	0	0	0	0	3	0	0	0	0	0	0	99	0
HIP 99273	99	99	99	0	0	0	0	0	0	0	0	0	0	0	0	0	0	0	0	0	0	0	0	0
HIP 102141 B	99	99	99	0	0	0	0	0	0	0	0	0	0	0	0	0	0	0	0	0	0	0	0	0
HIP 102141 A	99	99	99	0	0	0	0	0	0	0	0	0	0	0	0	0	0	0	0	0	0	0	0	0
HIP 102409	99	99	99	0	0	0	0	0	0	0	0	0	0	0	0	0	0	0	0	0	0	0	0	0
HIP 103311	99	99	99	0	0	0	0	0	0	0	0	0	0	0	0	0	0	0	0	0	0	0	0	0
HIP 112312 B	99	99	99	0	0	0	0	0	0	0	0	0	0	0	0	0	0	0	0	0	0	0	0	0
HIP 112312	99	99	99	0	0	0	0	0	0	0	0	0	0	0	0	0	0	0	0	0	0	0	0	0
TW Hydrae Association																								
TWA 1	0	0	0	99[b]	99	99	0	0	0	0	0	0	0	0	0	0	0	0	0	0	0	0	0	0
TWA 4ABCD	0	0	0	99[b]	99[b]	99[b]	0	0	0	0	0	0	0	0	0	0	0	0	0	0	0	0	0	0
TWA 8A	0	0	0	99[b]	99[b]	99[b]	0	0	0	0	0	0	0	0	0	0	0	0	0	0	0	0	0	0
TWA 8B	0	0	0	99[b]	99[b]	99[b]	0	0	0	0	0	0	0	0	0	0	0	0	0	0	0	0	0	0
TWA 26	0	0	0	99[b]	99[b]	99[b]	0	0	0	0	0	0	0	0	0	0	0	0	0	0	0	0	0	0
TWA 19	0	0	0	83	94	75	0	0	0	0	0	0	0	0	0	0	0	0	0	0	0	16	5	24

Table 2.IV — continued

Name	βPMG P	P_v	$P_{v+\pi}$	TWA P	P_v	$P_{v+\pi}$	THA P	P_v	$P_{v+\pi}$	COL P	P_v	$P_{v+\pi}$	CAR P	P_v	$P_{v+\pi}$	ARG P	P_v	$P_{v+\pi}$	ABDMG P	P_v	$P_{v+\pi}$	Field P	P_v	$P_{v+\pi}$
TWA 9B	0	0	0	99	99	99	0	0	0	0	0	0	0	0	0	0	0	0	0	0	0	0	0	0
TWA 9A	0	0	0	99	99	99	0	0	0	0	0	0	0	0	0	0	0	0	0	0	0	0	0	0
TWA 27AB	0	0	0	99	99	99	0	0	0	0	0	0	0	0	0	0	0	0	0	0	0	0	0	0
TWA 11A	0	0	0	99	99	99	0	0	0	0	0	0	0	0	0	0	0	0	0	0	0	0	0	0
Tucana-Horologium Association																								
HIP 490	0	0	0	0	0	0	65	99	99	0	0	0	0	0	0	0	0	0	34	0	0	0	0	0
HIP 1113	0	0	0	0	0	0	99	99	99	0	0	0	0	0	0	0	0	0	0	0	0	0	0	0
HIP 1481	0	0	0	0	0	0	99	99	99	0	0	0	0	0	0	0	0	0	0	0	0	0	0	0
HIP 1910 AB	0	0	0	0	0	0	97	99	99	0	0	0	0	0	0	0	0	0	2	0	0	0	0	0
HIP 1993	0	0	0	0	0	0	99	99	99	0	0	0	0	0	0	0	0	0	0	0	0	0	50	9
HIP 2484 AbB	0	0	0	0	0	0	99	48	90	0	0	0	0	0	0	0	0	0	0	0	0	0	0	0
HIP 2487 AB	0	0	0	0	0	0	98[b]	99[b]	99[b]	0	0	0	0	0	0	0	0	0	1	0	0	0	0	0
HIP 2578	0	0	0	0	0	0	99	99	99	0	0	0	0	0	0	0	0	0	0	0	0	0	0	0
HIP 2729	0	0	0	0	0	0	99[b]	11[b]	99[b]	0	0	0	0	0	0	0	0	0	2	0	0	0	88[b]	9
HIP 3556	0	0	0	0	0	0	97	53	90	0	0	0	0	0	0	0	0	0	0	0	0	0	46	9
HIP 6485	0	0	0	0	0	0	93	99	99	0	0	0	0	0	0	0	0	0	6	0	0	0	0	0
HIP 6856	0	0	0	0	0	0	95	99	99	0	0	0	0	0	0	0	0	0	4	0	0	0	0	0
HIP 9141 AB	0	0	0	0	0	0	50	99	99	0	0	0	0	0	0	0	0	0	0	0	0	0	0	0
HIP 9685	0	0	0	0	0	0	91[b]	45[b]	74[b]	0	0	0	0	0	0	0	0	0	8[b]	0	0	0	54[b]	25[b]
HIP 9892 AB	0	0	0	0	0	0	90	99	99	0	0	0	0	0	0	0	0	0	9	0	0	0	0	0
HIP 9902	0	0	0	0	0	0	97	99	99	0	0	0	0	0	0	0	0	0	2	0	0	0	0	0
HIP 10602	0	0	0	0	0	0	98	99	99	0	0	0	0	0	0	0	0	0	1	0	0	0	1	0
HIP 12394	0	0	0	0	0	0	99	98	99	0	0	0	0	0	0	0	0	0	0	0	0	0	2	0
HIP 12925	0	0	0	0	0	0	2	97	99	95	0	0	0	0	0	0	0	0	0	0	0	0	0	0
HIP 14551	0	0	0	0	0	0	4	37	50	94	61	49	0	0	0	0	0	0	0	0	0	0	0	0
HIP 14913 ABC	2[b]	0	0	0	0	0	74[b]	99[b]	99[b]	22[b]	0	0	0	0	0	0	0	0	0	0	0	0	0	0
HIP 15247	1	0	0	0	0	0	19	99	99	79	0	0	0	0	0	0	0	0	0	0	0	0	0	0
HIP 16853 AB	0	0	0	0	0	0	98	99	99	0	0	0	0	0	0	0	0	0	0	0	0	0	0	0
HIP 17764	1	0	0	0	0	0	99	99	99	0	0	0	0	0	0	0	0	0	1	0	0	0	0	0
HIP 17782 AB	1[b]	0	0	0	0	0	0	0	0	66	96	98	0	0	0	20	0	0	0	0	0	12	2	2
HIP 17797	3[b]	0	0	0	0	0	73[b]	99[b]	99[b]	22[b]	0	0	0	0	0	0	0	0	0	0	0	0	0	0
HIP 18714 AB	0	0	0	0	0	0	98	99	98	1	0	0	0	0	0	0	0	0	0	0	0	0	0	0
HIP 21632	0	0	0	0	0	0	32	95	98	67	4	1	0	0	0	0	0	0	0	0	0	0	0	0
HIP 21965	0	1	0	0	0	0	15[b]	58[b]	90[b]	84[b]	40[b]	9[b]	0	0	0	0	0	0	0	0	0	0	0	0
HIP 22295	0	0	0	0	0	0	99	99	99	0	0	0	0	0	0	0	0	0	0	0	0	0	0	0
HIP 24947	0	0	0	0	0	0	1	97	98	0	0	0	0	0	0	0	0	0	0	0	0	2	2	0
HIP 32435	0	0	0	0	0	0	99	99	99	0	0	0	0	0	0	0	0	0	0	0	0	0	99	99
HIP 83494	0	0	0	0	0	0	0	0	0	0	0	0	0	0	0	0	0	0	0	0	0	98	81	86
HIP 84642 AB	0	0	0	0	0	0	1	18	13	0	0	0	0	0	0	0	0	0	0	0	0	0	0	0
HIP 100751	0	0	0	0	0	0	99[b]	99[b]	99[b]	0	0	0	0	0	0	0	0	0	0	0	0	0	0	0
HIP 104308	0	0	0	0	0	0	99	0	0	0	0	0	0	0	0	0	0	0	0	0	0	99	99	99
HIP 105388	0	0	0	0	0	0	99	99	99	0	0	0	0	0	0	0	0	0	0	0	0	0	0	0
HIP 105404 AB	0	0	0	0	0	0	99[b]	0	0	0	0	0	0	0	0	0	0	0	0	0	0	99[b]	99[b]	99[b]
HIP 107345	0	0	0	0	0	0	99	99	99	0	0	0	0	0	0	0	0	0	0	0	0	0	0	0
HIP 107947	0	0	0	0	0	0	99	99	99	0	0	0	0	0	0	0	0	0	0	0	0	0	0	0
HIP 108195 ABC	0	0	0	0	0	0	99[b]	99[b]	99[b]	0	0	0	0	0	0	0	0	0	0	0	0	0	0	0
HIP 108422 AB	0	0	0	0	0	0	99[b]	99[b]	99[b]	0	0	0	0	0	0	0	0	0	0	0	0	0	0	0
HIP 116748 AB	0	0	0	0	0	0	96	99	99	0	0	0	0	0	0	0	0	0	0	0	0	3	0	0
HIP 118121	0	0	0	0	0	0	99	99	99	0	0	0	0	0	0	0	0	0	0	0	0	0	0	0

Table 2.IV — continued

Name	βPMG			TWA			THA			COL			CAR			ARG			ABDMG			Field		
	P	P_v	$P_{v+\pi}$	P	P_v	$P_{v+\pi}$	P	P_v	$P_{v+\pi}$	P	P_v	$P_{v+\pi}$	P	P_v	$P_{v+\pi}$	P	P_v	$P_{v+\pi}$	P	P_v	$P_{v+\pi}$	P	P_v	$P_{v+\pi}$
Columba Association																								
HIP 1134	17	0	0	0	0	0	2	0	0	73	99	99	0	0	0	0	0	0	0	0	0	5	0	0
HIP 12413 A	1	53	96	0	0	0	90	0	0	7	46	3	0	0	0	0	0	0	0	0	0	0	0	0
HIP 16449	0	0	0	0	0	0	0	0	0	99	99	99	0	0	0	0	0	0	0	0	0	0	0	0
HIP 17248	1	0	0	0	0	0	0	0	0	71	99	99	0	0	0	26	0	0	0	0	0	1	0	0
HIP 19775	0	0	0	0	0	0	0	0	0	99	99	99	0	0	0	0	0	0	0	0	0	0	0	0
HIP 22226	1	0	0	0	0	0	0	0	0	99	99	99	0	0	0	0	0	0	0	0	0	0	0	0
HIP 23179	1	0	0	0	0	0	0	0	0	72	98	99	0	0	0	19	0	0	0	0	0	6	0	0
HIP 23316	0	0	0	0	0	0	0	0	0	99	99	99	0	0	0	0	0	0	0	0	0	0	0	0
HIP 23362	0	0	0	0	0	0	1	0	0	97	99	99	0	0	0	0	0	0	0	0	0	0	0	0
HIP 24947	0	0	0	0	0	0	1	0	0	97	99	99	0	0	0	0	0	0	0	0	0	0	0	0
HIP 25709 AB	0	0	0	0	0	0	0	0	0	99	99	99	0	0	0	0	0	0	0	0	0	0	0	0
HIP 26309	0	0	0	0	0	0	0	0	0	99	99	99	0	0	0	0	0	0	0	0	0	0	0	0
HIP 26453	0	0	0	0	0	0	0	0	0	99	99	99	0	0	0	0	0	0	0	0	0	0	0	0
HIP 26966	0	0	0	0	0	0	0	0	0	99	99	99	0	0	0	0	0	0	0	0	0	0	0	0
HIP 26990	0	0	0	0	0	0	0	0	0	99	99	99	0	0	0	0	0	0	0	0	0	0	0	0
HIP 28036	0	0	0	0	0	0	0	0	0	99[b]	99[b]	99[b]	0	0	0	0	0	0	0	0	0	0	0	0
HIP 28474	0	0	0	0	0	0	0	0	0	99	99	99	0	0	0	0	0	0	0	0	0	0	0	0
HIP 30030	0	7	14	0	0	0	0	0	0	99	91	85	0	0	0	0	0	0	0	0	0	0	0	0
HIP 32104	0	7	0	0	0	0	0	0	0	98	99	99	0	0	0	0	0	0	0	0	0	0	0	0
HIP 114189	93	1	0	0	0	0	0	0	0	5	95	98	0	0	0	0	0	0	0	0	0	1	2	0
HIP 116805	35[b]	1	0	0	0	0	0	0	0	20[b]	81[b]	95[b]	0	0	0	0	0	0	0	0	0	43[b]	17[b]	4[b]
Carina Association																								
HIP 30034 A	0	0	0	0	0	0	0	0	0	61	49	27	37	50	71	0	0	0	0	0	0	0	0	0
HIP 32235	0	0	0	0	0	0	0	0	0	0	0	0	99	99	99	0	0	0	0	0	0	0	0	0
HIP 33737	0	0	0	0	0	0	0	0	0	0	0	0	99	99	99	0	0	0	0	0	0	1	0	0
HIP 46063	0	0	0	0	0	0	0	0	0	0	0	0	98	99	99	0	0	0	0	0	0	1	0	0
HIP 46720 AB	0	0	0	0	0	0	0	0	0	0	0	0	99[b]	99[b]	99[b]	0	0	0	0	0	0	0	0	0
Argus Association																								
HIP 4448 AB	36[b]	0	0	0	0	0	0	0	0	0	0	0	0	0	0	59[b]	91[b]	86[b]	0	0	0	4[b]	8[b]	13[b]
AP COL	0	0	0	0	0	0	0	0	0	0	0	0	0	0	0	99[b]	99[b]	99[b]	0	0	0	0	0	0
HIP 36948	0	0	0	0	0	0	0	0	0	0	0	0	0	0	0	99	99	99	0	0	0	0	0	0
HIP 47135	0	0	0	0	0	0	0	0	0	0	0	0	0	0	0	97	99	99	2	0	0	0	0	0
HIP 50191	0	0	0	0	0	0	0	0	0	0	0	0	0	0	0	99	99	99	0	0	0	0	0	0
HIP 57632	0	0	0	0	0	0	0	0	0	0	0	0	0	0	0	64[b]	42[b]	77[b]	0	0	0	35[b]	57[b]	22[b]
HIP 68994	0	0	0	0	0	0	0	0	0	0	0	0	0	0	0	98	98	99	0	0	0	1	0	0
HIP 74405	0	0	0	0	0	0	0	0	0	0	0	0	0	0	0	99	99	99	0	0	0	0	0	0
HIP 79797	11	0	0	0	0	0	0	0	0	0	0	0	0	0	0	88	99	99	0	0	0	0	0	0
HIP 98495	53[b]	0	0	0	0	0	0	0	0	0	0	0	0	0	0	45[b]	99[b]	99[b]	0	0	0	0	1	0
HIP 99770	0	0	0	0	0	0	0	0	0	0	0	0	0	0	0	87	98	99	0	0	0	11	1	0
AB Doradus moving group																								
HIP 3589 AB	0	0	0	0	0	0	0	0	0	0	0	0	0	0	0	0	0	0	98	99	99	0	0	0
HIP 5191 AB	0	0	0	0	0	0	0	0	0	0	0	0	0	0	0	0	0	0	99	99	99	0	0	0
HIP 6276	0	0	0	0	0	0	0	0	0	0	0	0	0	0	0	0	0	0	99	99	99	0	0	0
HIP 10272 AB	0	0	0	0	0	0	0	0	0	0	0	0	0	0	0	0	0	0	98	98	99	1	0	0
HIP 12635	0	0	0	0	0	0	0	0	0	0	0	0	0	0	0	0	0	0	99	99	99	0	0	0

Table 2.IV — continued

Name	βPMG P	P_v	P_{v+π}	TWA P	P_v	P_{v+π}	THA P	P_v	P_{v+π}	COL P	P_v	P_{v+π}	CAR P	P_v	P_{v+π}	ARG P	P_v	P_{v+π}	ABDMG P	P_v	P_{v+π}	Field P	P_v	P_{v+π}
HIP 12638	0	0	0	0	0	0	0	0	0	0	0	0	0	0	0	0	0	0	98	99	99	1	0	0
HIP 13027 AB	0	0	0	0	0	0	0	0	0	0	0	0	0	0	0	0	0	0	99	99	99	0	0	0
HIP 13209	16^b	22^b	0	0	0	0	0	0	0	0	0	0	0	0	0	0	0	0	82^b	76^b	99^b	1	0	0
HIP 14684	0	0	0	0	0	0	0	0	0	0	0	0	0	0	0	0	0	0	99	99	99	0	0	0
HIP 14809	0	0	0	0	0	0	0	0	0	0	0	0	0	0	0	0	0	0	98	99	99	1	0	0
HIP 15353	0	0	0	0	0	0	96	0	0	0	0	0	0	0	0	0	0	0	2	98	99	0	1	0
HIP 16563 AB	0	0	0	0	0	0	0	0	0	0	0	0	0	0	0	0	0	0	99	99	99	0	0	0
HIP 17695	0	0	0	0	0	0	0	0	0	0	0	0	0	0	0	0	0	0	99	99	99	0	0	0
HIP 18859	11	9	0	0	0	0	0	0	0	0	0	0	0	0	0	0	0	0	88	90	99	0	0	0
HIP 19183	0	0	0	0	0	0	0	0	0	0	0	0	0	0	0	0	0	0	99	99	99	0	0	0
HIP 22738 A	0	0	0	0	0	0	0	0	0	3^b	0	0	0	0	0	0	0	0	96^b	99^b	99^b	0	0	0
HIP 22738 B	0	0	0	0	0	0	0	0	0	2^b	0	0	0	0	0	0	0	0	97^b	99^b	99^b	0	0	0
HIP 25283 AB	18	0	0	0	0	0	0	0	0	0	0	0	0	0	0	0	0	0	99^b	99^b	99^b	0	0	0
HIP 25647 ABCD	89	0	0	0	0	0	0	0	0	0	0	0	0	0	0	0	77	0	4	99	99	0	0	0
HIP 26369	0	0	0	0	0	0	0	0	0	2	0	0	0	0	0	0	0	0	7	99	99	0	0	0
HIP 26373	0	0	0	0	0	0	0	0	0	0	0	0	0	0	0	0	0	0	99^b	99^b	99^b	0	0	0
HIP 26401 AB	0	0	0	0	0	0	0	0	0	0	0	0	0	0	0	0	0	0	89	99	98	10	0	1
HIP 30314 AB	74	0	0	0	0	0	0	0	0	0	0	0	0	0	0	0	0	0	25	99	99	0	0	0
HIP 31711 AB	68	0	0	0	0	0	0	0	0	0	0	0	0	0	0	0	0	0	31	99	99	0	0	0
HIP 31878	68	0	0	0	0	0	0	0	0	0	0	0	0	0	0	0	0	0	31	99	99	0	0	0
HIP 36349 AB	74^b	0	0	0	0	0	0	0	0	0	3^b	0	0	0	0	0	0	0	24^b	96^b	99^b	0	0	0
HIP 51317	0	0	0	0	0	0	0	0	0	0	0	0	0	0	0	0	0	0	98	99	99	1	0	0
HIP 63742 AB	0	0	0	0	0	0	0	0	0	0	0	0	0	0	0	0	0	0	99^b	99^b	99^b	0	0	0
HIP 76768 AB	0	0	0	0	0	0	0	0	0	0	0	0	0	0	0	0	0	0	98^b	99^b	99^b	1	0	0
HIP 81084	0	0	0	0	0	0	0	0	0	0	0	0	0	0	0	0	0	0	98	99	99	1	0	0
HIP 82688	0	0	0	0	0	0	0	0	0	0	0	0	0	0	0	0	0	0	95	99	99	4	0	0
HIP 86346 AB	0	0	0	0	0	0	0	0	0	0	0	0	0	0	0	0	0	0	99^b	99^b	99^b	4	4	19
HIP 93580	84	23	0	0	0	0	0	0	0	0	0	0	0	0	0	0	0	0	10	71	80	4	4	0
HIP 94235 AB	19	0	0	0	0	0	0	0	0	0	0	0	0	0	0	0	0	0	74	99	99	5	0	0
HIP 95347	87	18	0	0	0	0	0	0	0	0	0	0	0	0	0	0	0	0	11	81	99	0	0	0
HIP 106231	0	0	0	0	0	0	0	0	0	0	0	0	0	0	0	0	0	0	99^b	99^b	99^b	0	0	0
HIP 109268	2^b	0	0	0	0	0	0	0	0	0	0	0	2^b	0	0	0	0	0	93^b	99^b	99^b	4^b	31^b	92
HIP 110526 AB	94^b	0	0	0	0	0	0	0	0	0	0	0	0	0	0	0	0	0	0	68^b	99^b	0	0	0
HIP 113579	0	0	0	0	0	0	0	0	0	0	0	0	0	0	0	0	0	0	99	99	99	0	0	0
HIP 113597 AB	0	0	0	0	0	0	0	0	0	0	0	0	0	0	0	0	0	0	99^b	99^b	99^b	0	0	0
HIP 114066	0	0	0	0	0	0	0	0	0	0	0	0	0	0	0	0	0	0	99^b	99^b	99^b	0	0	0
HIP 114530 AB	0	0	0	0	0	0	19	0	0	0	0	0	0	0	0	0	0	0	79	99	99	0	0	0
HIP 115162	0	0	0	0	0	0	0	0	0	0	0	0	0	0	0	0	0	0	97	99	99	2	0	0
HIP 115738	0	0	0	0	0	0	0	0	0	0	0	0	0	0	0	0	0	0	99	99	99	0	0	0
HIP 116910	0	0	0	0	0	0	1	0	0	0	0	0	0	0	0	0	0	0	97	99	99	1	0	0
HIP 117452 AB	0	7	0	0	0	0	96	0	0	0	0	0	0	0	0	0	0	0	0	3	7	2	89	92
HIP 118008	0	0	0	0	0	0	0	0	0	0	0	0	0	0	0	0	0	0	99	99	99	0	0	0

[a] Membership probability (P), membership probability including radial velocity information (P$_v$), or membership probability including radial velocity and parallax informations (P$_{v+\pi}$).

[b] Membership probability (P or P$_v$ or P$_{v+\pi}$) for which the binary hypothesis has a higher probability.

2.6 Low-mass star search sample

For our search for new late-type members of young associations, we wanted to start with a sample of low-mass stars showing chromospheric X-ray and Hα emissions, which are both indicator of youth. We used the sample of Riaz et al. (2006), consisting of 1061 spectroscopically confirmed K5V to M5V dwarfs, supplemented with 43 K5V-M5V young star candidates previously identified by Kastner et al. (1997), Webb et al. (1999), Torres et al. (2000), Zuckerman & Song (2004), Torres et al. (2006), Torres et al. (2008), Lépine & Simon (2009), Looper et al. (2010), Schlieder et al. (2010), Kiss et al. (2011), Rodriguez et al. (2011), Schlieder et al. (2012a), and Bowler et al. (2012).

The I-band photometric data come from the DENIS and SDSS-DR8 catalogs and several other studies (Casagrande et al., 2008, Koen et al., 2010, Reid & Cruz, 2002, Reid et al., 2003, 2004, Torres et al., 2006, A. R. Riedel (in preparation)).

We have removed stars with I_c magnitude uncertainties larger than 0.2 mag from our search sample. Also photometric observations of 7 stars with uncertain/missing I-band measurements were obtained on 2010 August 23-25 (NOAO-2010B-0449) at the CTIO 0.9m telescope using the full $(13.7' \times 13.7')$ Tek 2048×2046 CCD camera with $0.401''$ pixel^{-1}. The observations were made using a Gunn-i filter (8200/1500). Photometric calibration was done using observations of fields containing several stars with known magnitudes and available spectroscopy from SDSS. Since the SDSS-i filter is not exactly the same as the Gunn-i filter, synthetic magnitudes were extracted from the spectra of the SDSS stars. One standard field was observed after each target observation. The I_c magnitudes are given in Table 4.III (see note e). Finally, the J-band data are taken from the 2MASS PSC.

The proper motion data mainly come from the NOMAD (Zacharias et al., 2005), UCAC3 (Zacharias et al., 2009), PPMXL (Roeser et al., 2010), and other catalogs. From the original sample of 1104 stars, we kept 758 stars with proper motion measured at a significance of more than four sigma and a good I_c magnitude measurement. Of these 758 stars, 71 K5V-M5V were previously identified as young stars in the literature.

2.7 Results

2.7.1 Identification of new candidates

As described in the last section, our initial search sample is subject to the Bayesian analysis using as observables the apparent I_c and J magnitudes, the amplitude of proper motion in right ascension and declination, and the right ascension and declination. We will see later (Section 2.8) how other observables, in particular the radial velocity, can be used to better constrain the membership probability of a candidate. Figure 3.7 presents, for the entire search sample, the membership probability distribution for three of the seven young associations considered. As expected, the vast majority of stars have very low membership probabilities, but there is a significant population of objects with a probability higher than 90%. We set a threshold at 90% to qualify a candidate as a "high probability member" of a given association (see the next section for a discussion of false positives). Overall, our analysis has identified a total of 215 highly probable members including 58 young candidate identified in the literature.

The sample of new candidates (215) from our study includes one star in TWA, 37 in βPMG, 17 in THA, 20 in COL, 6 in CAR, 50 in ARG, and 33 in ABDMG. The properties of all candidates are presented in Table 4.III. We note that 51 of our candidates have an ambiguous membership, i.e., they are probable candidates in more than one association with a combined probability over all young groups above 90%. A radial velocity measurement is needed to remove this ambiguity (see Tables 2.VII, 3.X).

Figure 2.7 presents the position on the sky as well as the amplitude and the direction of the proper motion for both *bona fide members* and new highly probable candidate members of βPMG, THA, and ABDMG. The overall trend in amplitude and direction of the proper motion for the candidate members agree well with the *bona fide members*. Although the majority of the candidates (164) are located in the southern hemisphere, 13 candidates are in the northern hemisphere : 4 in βPMG, 4 in ARG, and 5 in ABDMG.

Figure 3.5 shows the spectral type distribution of the new candidates compared to the em bona fide members of βPMG, THA, and ABDMG. All the distributions show a maximum between spectral types M0V and M5V. Excluding ambiguous members, our
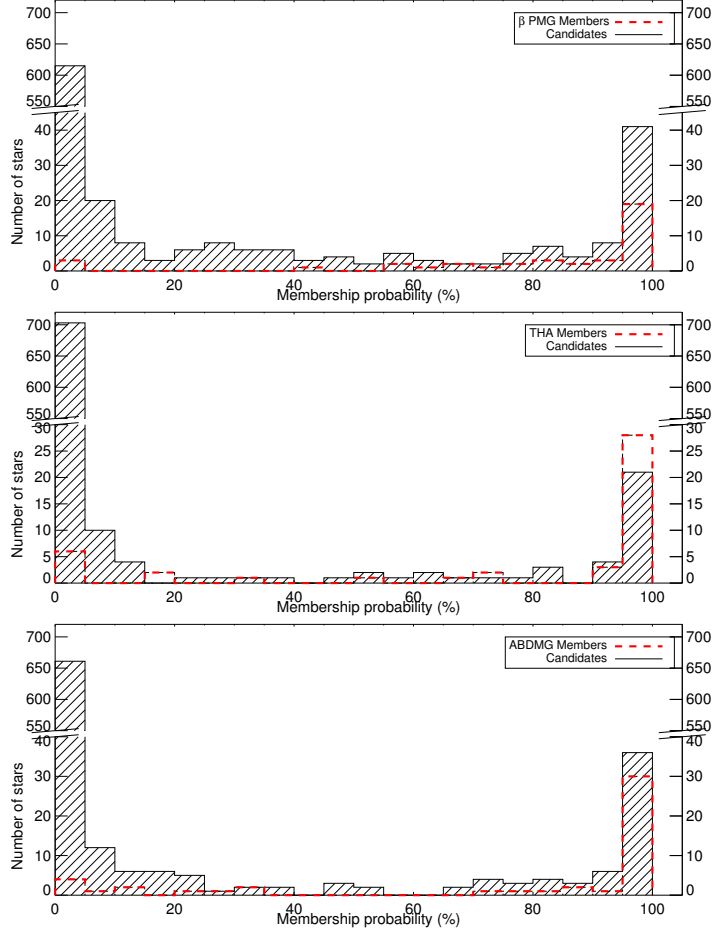
Figure 2.6 Distribution of membership probability for the entire search sample for each young associa-
tion (black histogram). The *bona fide members* are shown with a red dashed histogram. The vast majority
of the 758 stars have probabilities close to 0% as one expects.

analysis have unveiled 164 new late type (K5V-M5V) candidates. Compared to the 43
bona fide K5V-M5V dwarfs already catalogued in the seven kinematic groups under
study here, this new sample of young M dwarfs, if confirmed, would roughly quadruple
the known population of late type dwarfs of these associations.

The distance distributions for the *bona fide members* of βPMG, THA, and ABDMG
are superimposed to those of the candidates in Figure 3.6. Overall, the distance distri-
butions for both *bona fide members* and candidates are very similar. For ABDMG, our
analysis finds a tail of a few candidates between 55 and 80 pc. Our analysis also identi-
fies a few candidates that are relatively close (<20 pc) to the Sun. In general, candidates
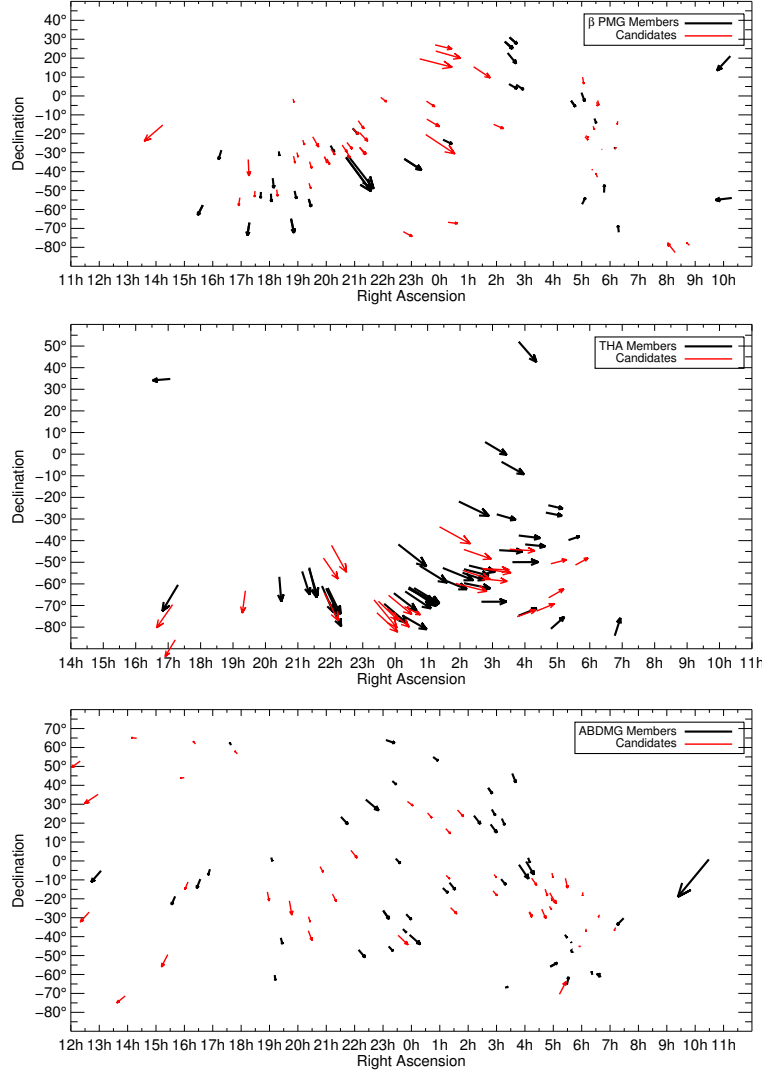
Figure 2.7 Position on the sky and vector of proper motion for the *bona fide members* (bold black arrows) and the new candidates (red arrows) resulting from this study.

found at relatively large distances should be taken with caution as they may well be members of more distant (>100 pc) young co-moving groups not considered in our analysis. One such example is the 8 Myr εCha association which could be easily confused with βPMG since both associations have very similar *UVW* (Torres et al., 2008). This emphasizes the need for a trigonometric parallax as a necessary criterion for confirming the *bona fide* status of a candidate.
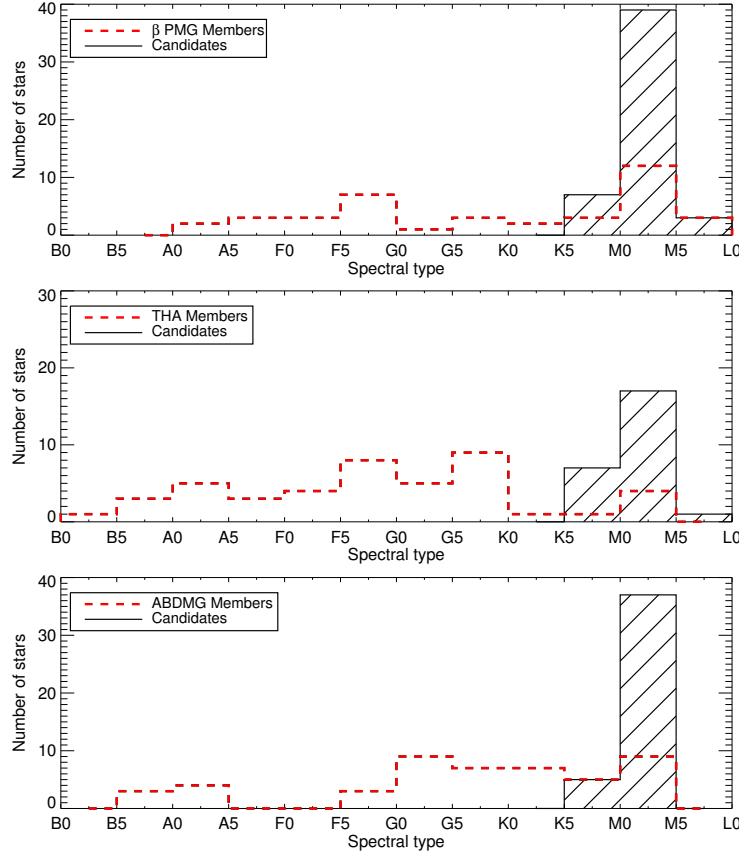
Figure 2.8 Spectral type distribution of previously known members (red dashed lines) and candidates (bold black lines) from this work.

The galactic positions *XYZ* of the candidates are presented in Figure 2.10. The dispersion of the *bona fide members* and the new candidates are very similar, in particular for *Y* and *Z*. This is expected since the candidates were chosen to be within the parameters of the *bona fide members*.

2.7.2   Quantifying the contamination

It is expected, that some field stars will have a high membership probability by pure chance. One thus needs to estimate the number of such contaminant in our sample. To quantify the number of false positives, we repeated our analysis 200 times by considering, each time, seven fake young associations with *UVW* and *XYZ* distributions similar
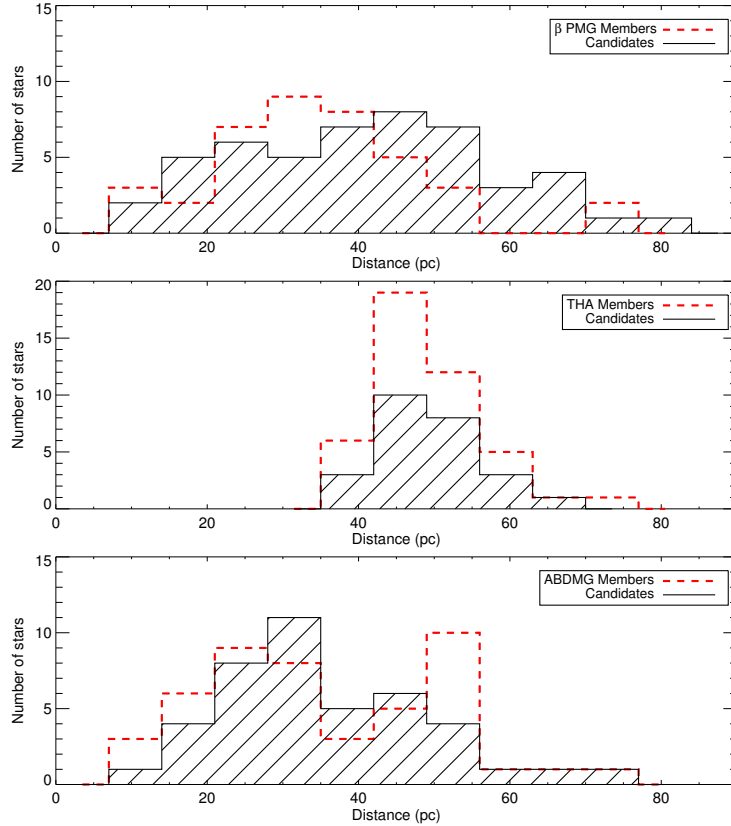
Figure 2.9 Distance distribution for the *bona fide members* (red dashed lines) and for candidates (bold black lines) from this study.

to, but not overlapping with, those of the seven young associations studied here. The seven fake associations were divided into three representative age groups : group 1 (8-20 Myr ; BPMG, TWA), group 2 (20-50 Myr ; COL, THA, CAR, ARG), and group 3 (>50 Myr ; ABDMG). As before, the candidate membership probability threshold was set to 90%.

These Monte Carlo simulations allow determining the median number of false positives. The results of this procedure are presented in Figure 2.11. The contamination is relatively modest for groups 1 and 2 with typically (median) only a few false positives, which is about an order of magnitude less than the real number of candidates. For false associations in the group 1 (8-20 Myr), the number of expected false positives is also smaller than the number of candidates by a factor of 10. The number of contaminants

73
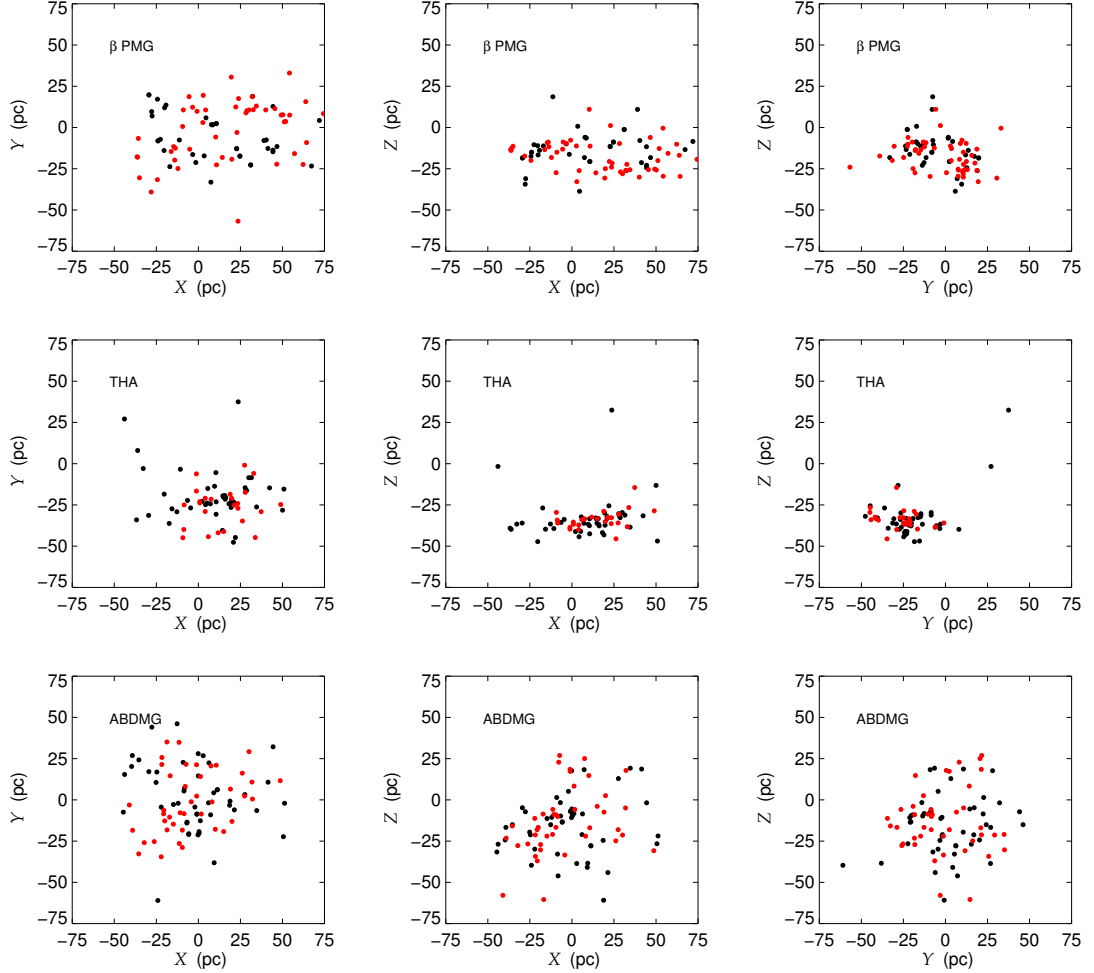
Figure 2.10 Galactic position *XYZ* of the *bona fide members* (black circles) and new candidates (red circles) from this study.

is significantly larger for ABDMG (group 3), as one would expect given that the CMD sequence for the older (>50 Myr) association lies closer to that of field stars compared to younger sequences. Based on this analysis, we can estimate a typical (median) false alarm rate of $\sim 5\%$ for group 1, $\sim 10\%$ for group 2, and $\sim 14\%$ for group 3, suggesting that a large fraction of our candidates are likely to be genuine members.
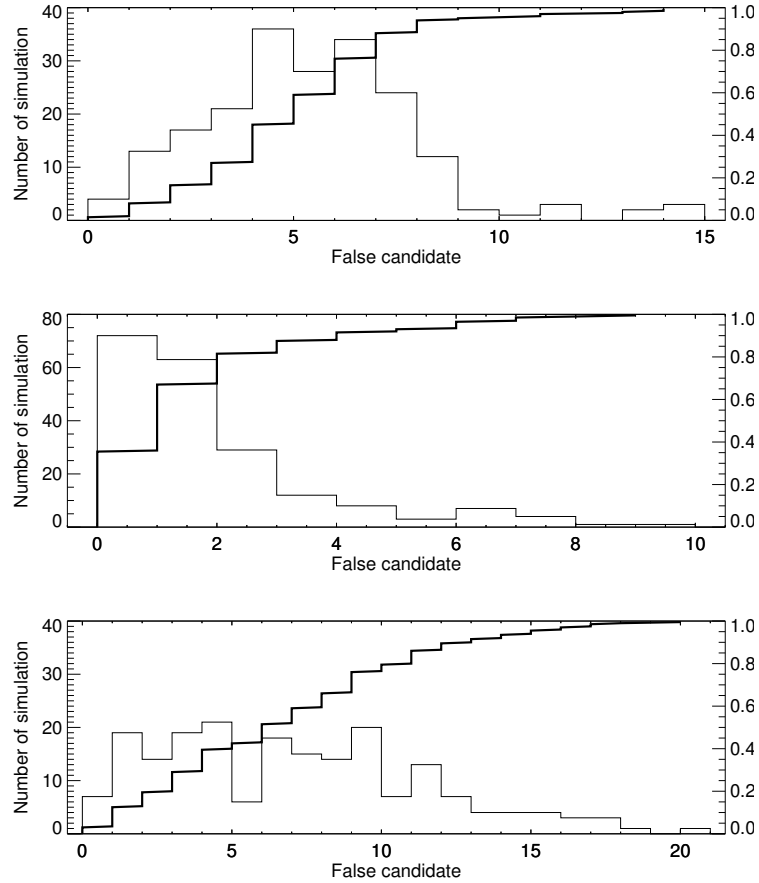
Figure 2.11 Distribution of number of candidates in fake associations (thin line and left axis) for various age groups : 8-20 Myr (top), 20-50 Myr (middle), and >50 Myr (bottom). The thick solid line is the corresponding cumulative distribution (right axis).

2.8 Radial velocity and lithium follow-up

As pointed out above, the statistical analysis can be performed with other observables, for example the radial velocity (RV). The previous analysis was performed without prior knowledge of this measurement. It is of course desirable to add this observable to the Bayesian analysis if the information is available.

Furthermore, while the kinematics of these stars indicate membership in these associations, their youth should be confirmed through the measurement of other spectroscopic age indicators such as lithium (Li) absorption at 6707.8 Å , a youth indicator for K-M dwarfs less than 70 Myr (see Figure 5, Mentuch et al., 2008). This section presents (on-

going) follow-up observations (RV and Li) of a subset of the highly probable members identified by our analysis.

2.8.1 Radial velocity follow-up

We initiated a program to obtain near-infrared high-resolution spectroscopy of some of our highly probable members to measure their radial velocities. The observations were performed using the PHOENIX (Hinkle et al., 2003) spectrograph at the Gemini South telescope (GS-2009A-Q-89, GS-2009B-Q-45, GS-2010A-Q-32, GS-2010B-Q-18, GS-2010B-Q-89). We used a $0.34''$-wide slit in combination with the H6420 filter (1.547μm-1.568μm) for a resolving power of R$\sim$ 30000. The instrument setup was inspired by the work of Mazeh et al. (2002) on low-mass binaries. The observations were obtained with a typical ABBA dither pattern along the slit with individual exposures of 60 to 300 s depending on the target brightness. Flat field and dark images were used to correct for detector cosmetics and OH night-sky emission lines were used for wavelength calibration. A set of radial velocity standards were observed and served as cross-correlation spectra for radial-velocity measurements.

To date, we have obtained RV measurements at one epoch for 101 candidates. The results show that 50% of them are fast rotators which, by itself, is an indication of youth, but makes the measurement of a radial velocity difficult. For 14 of the slow rotators we have obtained a second epoch of RV measurement (to assess spectroscopic binarity); these measurements are presented in Table 4.III. As discussed in Section 2.9, all 14 slow rotators have radial velocities in good agreement with the expected values for their respective association.

2.8.2 Lithium follow-up

As low-mass stars have a convective outer envelope, the primordial lithium in their photosphere is, with time, transported to the center of the star, where it is quickly destroyed. The presence of lithium in the photosphere of a low-mass star is thus indicative of youth. Lithium absorption at 6707.8 Å is indeed seen for young low-mass members
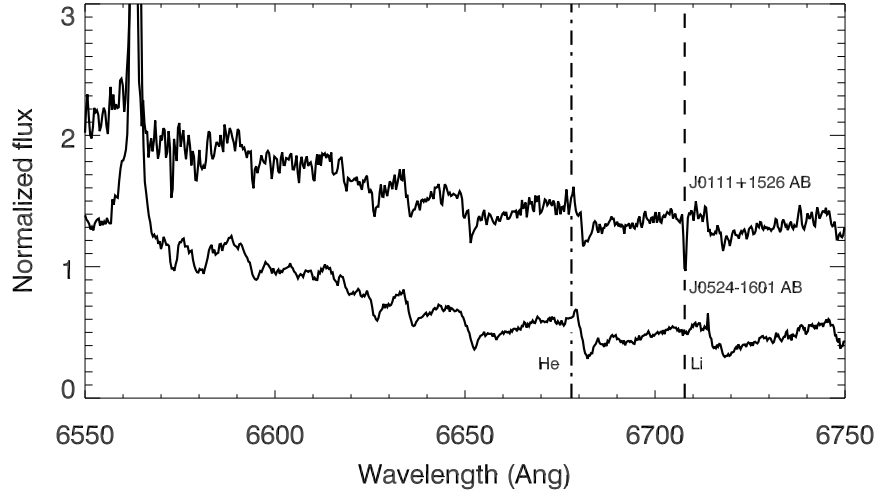
Figure 2.12 High-resolution optical ESPaDOnS spectra of two young binary candidate members showing lithium absorption (unresolved spectra). The Li feature of J0524-1601 is clearly broadened due to relatively fast rotation.

of βPMG, THA, and ABDMG. While our candidates are highly probable new members of these young associations, measurements of various age-dating indicators, such as the presence of lithium, is valuable to confirm their membership. We have initiated a program to obtain these measurements for the candidate members with a membership probability >90%. High-resolution optical spectroscopy was obtained in queue service observing (QSO) mode with ESPaDOnS (Donati et al., 2006) on CFHT. ESPaDOnS was used in a "star + sky" mode combined with the "slow" CCD readout mode, to get a resolving power of R $\sim$ 68000 covering the 3700 to 10500 Å over 40 grating orders. The data were reduced by the QSO team using the CFHT pipeline called UPENA 1.0. This pipeline uses J-F. Donati's software Libre-ESpRIT (Donati et al., 1997). The total integration time per target is between 30 and 80 minutes. So far 28 candidates have been observed and we have analyzed the spectrum for 10 stars, two of which (J0111+1526 and J0524-1601) show clear lithium absorption, confirming their youth. The spectra of these two stars are shown in Figure 2.12 and further discussed in the next section. The results of the remaining stars with follow-up spectroscopy will be published in a forthcoming paper.

The lithium detection limit is around K7V at an age of ABDMG, M0V for THA, and M3V for βPMG (Mentuch et al., 2008). From our 164 candidate members, we expected to detect lithium for 22, 16, and 1 stars in βPMG-TWA,THA-COL-CAR-ARG, and ABDMG, respectively. For star with a mass lower than the limit detection, we need to find a better age-dating indicator, such as surface gravity.

2.9   Discussion

In light of the statistical analysis presented above, we discuss the membership of specific stars drawn from three samples : *bona fide members*, new highly probable low-mass star candidates identified for the first time as part of this work, and the other 71 young low-mass star candidates previously identified in the literature (see Section 4.6). For the latter sample, only spectral types later than K5V are considered ; the most massive ones will be the subject of a future publication.

We should note that some *bona fide members* show a high membership probability when considering the binary hypothesis. This hypothesis should be interpreted as an overluminosity compared to other young stars, which could be due to the presence of a binary companion, chromospheric activity, or peculiar colors of the star.

2.9.1   Bona fide members

Since the observational properties of *bona fide members* form the basis of our Bayesian tool, one should expect our analysis to yield a high membership probability for these stars. This is indeed the case. Table 2.IV gives the membership probability obtained for these stars for three cases : (1) without considering the RV or parallax information (P), (2) considering the RV but not the parallax (P_v), and (3) considering both the RV and parallax ($P_{v+\pi}$). For all cases, a binary hypothesis is also considered and whenever it yields a higher probability than the single hypothesis, this is noted in Table 2.IV. Assuming that a member is recovered when its probability is higher than 90%, our analysis correctly recovers 72% (128/177) of all *bona fide members* for case 1. This fraction increases to 88% (155/177) when RV is included (case 2) and to 91% when both RV and

parallax information are used (case 3). This large recovery rate is expected but there remains a few cases (16 out of 177) that have ambiguous or uncertain membership. Those are discussed below.

2.9.1.1 βPMG

HIP 12545 AB : This star is a K6Ve spectroscopic binary (sb1; Torres et al., 2008) that was proposed by Zuckerman & Song (2004) to be a member of βPMG. From our analysis, this star seems to be a member of COL (P_v=99%, $P_{v+\pi}$=88%, P_π=48%). The Galactic positions (*XZ*) of this star are much similar to COL *bona fide members*. Its measured RV (8.25$\pm$0.05 km s^{-1}) is closer to that predicted for COL (8.6 km s^{-1}) compared to βPMG (11.3 km s^{-1}). However, this difference of 2.7 km s^{-1} is marginal, especially since this star is a fast rotator (vsini=40 km s^{-1}; Torres et al., 2006) as well as a spectroscopic binary ; its RV may thus be somewhat uncertain. Our analysis favors a membership in COL due to its position on the CMD which is marginally more consistent (by $\sim$ 0.7 mag) with COL compared to βPMG. However, when the photometry and the RV are excluded, our analysis favors a membership in βPMG (P_π=66%). We should note that this star has an EW_{Li}=433$\pm$23 mÅ (Mentuch et al., 2008) that may be too high to be a member of COL for an age of 20-40 Myr. For this reason, HIP 12545 AB is a *bona fide member* of βPMG.

HIP 11360 : This star (F4IV) was proposed by Moór et al. (2006) to be a member of βPMG. Torres et al. (2008) also proposed this star as a candidate member of βPMG since its kinematic is similar to HIP 12545 AB. Our analysis suggests this star to be in COL (P_v=93% and $P_{v+\pi}$=87%), but as for HIP 12545 AB, there is a difference of only 3.1 km s^{-1} between the predicted radial velocities for βPMG (10.3 km s^{-1}) and COL (7.2 km s^{-1}). A membership in COL is favored since the Galactic position of this star is closer to that of COL compared to βPMG.

HIP 95261 AB : This binary A0V+M7V was originally proposed by Zuckerman & Webb (2000) to be a member of THA, but its membership was revised to βPMG one year later by Zuckerman et al. (2001). Without RV information, our analysis yields a membership probability (P_π) of 99% in βPMG but it decreases to 0% when RV and parallax

information are included ($P_{v+\pi}$). The reason for this drop is its radial velocity (13.0±2.5 km s^{-1}) that is 15 km s^{-1} off from that predicted for βPMG (-1.0±2.0 km s^{-1}). Since this star has a low-mass (M7V) companion that could also affect the systemic velocity, the current RV measurement should be taken with caution. Another likely explanation is that the RV may be erroneous since this star is a very fast rotator (vsini = 330 km s^{-1} ; da Silva et al., 2009). To confirm this hypothesis, spectroscopic follow-up of the companion should be sought, in particular to search for low surface gravity indicators which should be significant if the star is a member of βPMG. Also, new RV measurements would be highly desirable to better determine the systemic velocity of the system.

2MASSJ06085283-2753583 : This young brown dwarf (M8.5) was proposed by Rice et al. (2010) to be a member of βPMG which is confirmed by our analysis (P_v=75% and $P_{v+\pi}$=95%). We should note that our analysis is not optimal for this object because its $I_c - J > 3.25$ is beyond the limit of our sequences. If we do not consider the photometry in our analysis, but consider the radial velocity and the trigonometric distance, the membership probability is 93% in βPMG. Since the IR spectrum shows telltale signatures of low-gravity (*H*-band shape, KI lines), this target should be warranted the status of *bona fide member* of βPMG.

HIP 23418 ABCD : This quadruple system was proposed to be in βPMG by Song et al. (2003) but does not appear in our *bona fide member* list because the uncertainty on its *Hipparcos* trigonometric distance is larger than our adopted criterion (5σ). Recently, a better parallax was measured by A. R. Riedel et al. (in preparation) at 40.18±2.07 mas. This star has a membership probability of P_v=99% to be member of βPMG (see 2MASSJ05015881+0958587 ; Table 4.III) and $P_{v+\pi}$=99%. This system should be included in the list of *bona fide members* of βPMG.

HIP 50156 : This star (M1V) was proposed by Schlieder et al. (2012a) to be a member of βPMG. From our analysis, this star seems to be a member of COL ($P_{v+\pi}$=93%). However, the radial velocity of this star is somewhat ambiguous : 6.9±1.0 (Kharchenko et al., 2007), 10±1 (Montes et al., 2001), 5.8±0.8 (Gontcharov, 2006) and 2.7±0.1 (López-Santiago et al., 2010) km s^{-1}. It is unclear why the RVs differ so much from these measurements. One possibility is that their radial velocity measurements are ske-

wed by (unknown) binary orbital motion. The predicted radial velocity is 3.2, 8.4, and 1.3 km s^{-1} for membership in βPMG, COL, and ABDMG, respectively. Spectroscopy from Shkolnik et al. (2009) and López-Santiago et al. (2010) did not unveil any lithium detection which would point to a relatively old association such as ABDMG. If we do not consider the radial velocity information in our analysis, but still consider the photometry and the trigonometric distance, the membership probability (P$_\pi$) is 99% in COL. This star appears young but more RV measurements are desirable to better assess its membership.

2.9.1.2   TWA

TWA 19 : This star (G5V) was rejected as a member of TWA and suggested instead to be member of the Scorpius-Centaurus complex by Mamajek (2005) and Torres et al. (2008). Recently, Chen et al. (2011) proposed this star as a member of Lower Centaurus Crux (LCC). While our analysis yields a membership probability in TWA of P=83%, (P$_v$=94%, P$_{v+\pi}$=75%), it would be interesting to add the Scorpius-Centaurus complex into our analysis but this is beyond the scope of the current paper since we restrict our search to relatively nearby co-moving groups within 100 pc from the Sun.

2.9.1.3   THA

HIP 14551 : This star (A5V) was proposed by Zuckerman et al. (2011) to be a member of THA. From our analysis, this star has an ambiguous status, with a membership probability P$_{v+\pi}$=50% in THA and 49% in COL.

HIP 17782 AB : This binary (G8V*) was proposed by Zuckerman et al. (2011) to be a member of THA. From our analysis, this star seems to be a member of COL (P$_{v+\pi}$=98%). The main reason for the higher probability in COL is the better agreement of its Galactic positions *XZ* with the members of COL. We propose that HIP 17782 AB be assigned as *bona fide member* of COL.

HIP 2484 AbB : This star was proposed by Zuckerman & Song (2004) to be a member of THA. From our analysis, this star seems to be a member of THA (P$_{v+\pi}$=90%),

however the probability without parallax (P_v=48%) is low because there is a 7 km s^{-1} difference between the measured and predicted radial velocities. We should note that HIP 2484 AbB and HIP 2487 AB form a quintuple system. The measured and predicted radial velocities for HIP 2487 AB are almost the same. We thus conclude that the measured radial velocity of HIP 2484 AbB is affected by the binary components and that HIP 2484 AbB is very likely a *bona fide member* of THA.

HIP 105404 AB : This binary (G9V(eb)) was proposed by Zuckerman & Song (2004) to be a member of THA. Our analysis also assigns this star in THA (P=99%) with a higher probability to be a binary, which is indeed the case. However, the membership (P_v) decreases to 0% when the RV is included. The reason is that measured RV is incompatible with the association, differing by 8 km s^{-1} from the predicted value. However, the companion of this star could have an impact on the measured radial velocity. If we do not consider the radial velocity information in our analysis, but still consider the photometry and the trigonometric distance, the membership probability is 99% in THA. Mentuch et al. (2008) measured an EW_{Li}=171$\pm$22 mÅ suggestive of youth. This star is also known to have a circumstellar disk detected at 24 μm (Zuckerman et al., 2011). More radial velocity monitoring of this star is needed to better assess its membership.

HIP 3556, HIP 9685, HIP 104308 : These stars (M3V, F2V, A5V) were proposed by Zuckerman & Song (2004) to be members of THA. From our analysis, the inclusion of the radial velocity causes a decrease of their membership probabilities. For HIP 3556, HIP 9685 and HIP 104308, there is a 7-8 km s^{-1} difference between the measured and predicted radial velocities. It is unclear why the RV differ so much from the expected values. One possibility is that their radial velocity measurements are skewed by (unknown) binary orbital motion, whereas the true system radial velocities would be consistent with the predicted values. However, no binary component are known to be orbiting around these stars. It is also possible that these objects just happen to have space motions relatively far from the bulk motion of the association. We should note that there is a rather large uncertainty on the radial velocity measurements for these stars. For HIP 104308, Zuckerman & Webb (2000) noted that the measurement of the radial velocity was difficult (early type star, vsini > 100 km s^{-1}). To confirm the membership of these stars, we

need better radial velocity monitoring.

HIP 83494 and HIP 84642 AB : These stars (A5V, G8V+M5V) were proposed by Zuckerman et al. (2011) to be members of THA. From our analysis, these stars seem to be field dwarfs. The main reason is that the Galactic positions (*XYZ*) of these stars are very different of the bulk position of the association. These stars are young as revealed by the presence of a circumstellar disk (Zuckerman et al., 2011) and lithium absorption for HIP 84642 AB (228 mÅ; Torres et al., 2006). It is possible that these objects just happen to have space motions relatively far from the bulk motion of the associations considered in this work.

2.9.1.4   COL

HIP 12413 A : This star (A1V) was proposed by Zuckerman et al. (2011) to be a member of COL. From our analysis, this star seems to be a member of βPMG ($P_{v+\pi}$=96%). There is a difference of only 0.9 km s^{-1} between the predicted radial velocities for βPMG (16.6 km s^{-1}) and COL (15.7 km s^{-1}). If we do not consider the RV information in our analysis, but still consider the photometry and trigonometric distance, the membership probability is 88% in THA. Zuckerman et al. (2011) note that HIP 12413 is a triple system (HIP 12413 A is a tight binary and HIP 12413 C a more distant (ρ=25$''$) M dwarf). Spectroscopic follow-up of the M dwarf, in particular to measure the Li absorption, would be very useful for constraining the age and the membership of this system.

HIP 30030 : This star (G0V) was proposed by Zuckerman & Song (2004) to be member of THA. From our analysis, this star has $P_{v+\pi}$=85% in COL. There is a difference of only 2.9 km s^{-1} between the predicted radial velocities for THA (19.3 km s^{-1}) and COL (22.2 km s^{-1}). The main reason for the higher probability in COL is its Galactic positions *XYZ* which are much similar to COL than THA.

2.9.1.5   CAR

HIP 30034 A : This star (K1Ve) was originally proposed by Zuckerman & Song (2004) to be a member of THA and by Torres et al. (2008) to be a member of CAR.

Our analysis favors a membership in CAR albeit with a modest probability ($P_{v+\pi}$=71%, 27% in COL). There is a difference of only 1.0 km s^{-1} between the predicted radial velocities for COL (22.0 km s^{-1}) and CAR (23.0 km s^{-1}). The main reason for the higher probability in CAR is the Galactic positions YZ that are more similar to CAR than THA.

2.9.1.6 ARG

HIP 4448 AB : This binary (K3Ve+K4Ve) was proposed by Torres et al. (2008) to be member of ARG which is confirmed by our analysis ($P_{v+\pi}$=86%). The probability below 90% is explained by its *U* velocity of -16.1 km s^{-1} which is somewhat different from the average value of -22 km s^{-1} for ARG *bona fide members*.

HIP 57632 : This star (A3V) was proposed by Zuckerman et al. (2011) to be a member of ARG which is confirmed by our analysis albeit with a modest probability ($P_{v+\pi}$=77%; 22% in the field). The relatively large uncertainty on the *J* band photometry does not explain this low probability since the latter remains low even when the photometry is excluded from the analysis. The main reason for its low probability is the Galactic space velocity *V* of this star (*V*=-16.0) which has a difference of 4 km s^{-1} with the average of ARG *bona fide members*.

2.9.1.7 ABDMG

HIP 93580 : This star (A4V) was proposed by Zuckerman et al. (2011) to be a member of ABDMG. Our analysis also puts this object in ABDMG, but with a somewhat low probability ($P_{v+\pi}$=80%). The Galactic space velocity *U* (-11.3 km s^{-1}) is somewhat different from the bulk motion of ABDMG members (*U*=-7.1 km s^{-1}). It is possible that this object just happens to have space motions relatively far from the bulk motion of the association.

HIP 117452 AB : This binary (A0V*) was proposed by Zuckerman et al. (2011) to be a member of ABDMG. From our analysis, this star has a membership probability of $P_{v+\pi}$=92% in the field. We should note that our analysis is not optimal for this object

because its $I_c - J <$ -0.1 is beyond the limit of our calculated sequences. If we do not consider the photometry in our analysis, but consider the radial velocity and the trigonometric distance, the membership probability changes to 99% in ABDMG. Zuckerman et al. (2011) detected a circumstellar disk excess at 24 and 70 μm. The tertiary companion of this system, HD 223340, is an early-K-type star about $75''$ away that shows Li absorption with an EW_{Li}=148 mÅ (Zuckerman et al., 2011) that is intermediate between that observed in stars of similar spectral types in ABDMG and THA (see Figure5, Mentuch et al., 2008). Thus, we confirm HIP 117452 AB as a *bona fide member* of ABDMG.

HIP 14807 : This star was proposed by Zuckerman & Song (2004) to be a member of ABDMG. HIP 14809 and HIP 14807 are a binary system. HIP 14807 is not listed as a *bona fide member* because no I_c and RV measurements are available for this star. However, if we do not consider the RV and photometry information in our analysis, but still consider the trigonometric distance, the membership probability is 96% in ABDMG. Furthermore, the other binary component (HIP 14809) is confirmed to be in ABDMG with $P_{v+\pi}$=99%. Our analysis confirms that both stars are *bona fide members* of ABDMG.

2.9.2 Candidate members

To confirm the membership of our 164 candidate members, we should include other observables in our analysis, such as radial velocity or parallax measurements. In addition to performing our own radial velocity measurements for a number of our candidates, we searched in the literature and compiled all radial velocity measurements from the previous studies of Bowler et al. (2012), Gizis et al. (2002), Hawley et al. (1996), Kiss et al. (2011), Lépine & Simon (2009), Looper et al. (2010), Montes et al. (2001), Rodriguez et al. (2011), Schlieder et al. (2010), Moór et al. (2006), Shkolnik et al. (2012), Torres et al. (2006), Schlieder et al. (2012a, b), Siebert et al. (2011). A good RV measurement ($\pm$2 km s^{-1}, not known to be spectroscopic binaries) is available for 35 of our 164 candidates, and Table 3.X shows the membership probability before and after the inclusion of the radial velocity in our Bayesian analysis. In general, the membership probability increases or remains high after inclusion of the radial velocity measurement; thus, these

stars (21/35) are strong candidate members of these seven young kinematic groups. For the other stars, the radial velocity measurement differs from those predicted for the seven young kinematic groups and need spectroscopic follow-up to search for various youth indicators. We searched the literature and compiled all available parallax measurements ; we found this information for 16 candidates either from the literature (Shkolnik et al., 2012, van Leeuwen, 2007, Wahhaj et al., 2011) and ongoing work (Riedel et al.), and Table 3.X shows the membership probability before and after the inclusion of the radial velocity and the parallax in our Bayesian analysis.. Finally, we also compiled all available Li measurements, in addition to our own measurements ; Li was measured for 12 candidates. Here we discuss the most promising candidates deserving more observations to confirm their status as young stars. We should note that full confirmation of the membership of these candidate members will require complete $UVWXYZ$, hence accurate proper motion, radial velocity and parallax measurements, and observation of signs of youth.

Table 2.V.   Candidate members with parallax measurement

Name	d_s[c] (pc)	d_π[d] (pc)	P_v[a] (%)	$P_{v+\pi}$[a] (%)	Group
J00503319+2449009	22.5 ± 1.3	11.8 ± 0.7[f]	99.99[b]	0.00	
J01034210+4051158	33.5 ± 1.6	29.9 ± 2.0	95.64	96.67	ABDMG
J01112542+1526214	20.5 ± 1.5	21.8 ± 0.8[e]	99.99[b]	99.99[b]	β PMG
J01351393-0712517	35.5 ± 3.1	37.9 ± 2.4	99.99[b]	99.99[b]	β PMG
J01365516-0647379	21.1 ± 1.7	24.0 ± 0.4	99.99	99.99	β PMG
J04141730-0906544	28.7 ± 1.9	23.8 ± 1.4	99.99	99.99	ABDMG
J04522441-1649219	16.0 ± 1.2	16.3 ± 0.4	99.99[b]	99.99[b]	ABDMG
J05015881+0958587	38.4 ± 3.9	24.9 ± 1.3[e]	99.99[b]	99.99[b]	β PMG
J05064946-2135038	21.9 ± 4.4	19.2 ± 0.5[e]	99.99[b]	99.99[b]	β PMG
J05064991-2135091	22.4 ± 0.7	19.2 ± 0.5[e]	4.35	99.99	β PMG
J05254166-0909123	21.8 ± 1.5	20.7 ± 2.2	99.99[b]	99.99[b]	ABDMG
J06091922-3549311	22.5 ± 4.5	21.3 ± 1.4[g]	99.99[b]	99.99[b]	ABDMG
J10121768-0344441	12.5 ± 0.0	7.9 ± 0.1[f]	0.14	0.00	
J14142141-1521215	16.2 ± 1.2	30.2 ± 4.5[f]	99.41	96.92	β PMG
J20434114-2433534	44.8 ± 3.2	28.1 ± 3.9	99.99[b]	99.99[b]	β PMG
J21212873-6655063	32.0 ± 2.0	30.2 ± 1.3[f]	99.99	99.99	β PMG
J21521039+0537356	29.0 ± 1.7	30.5 ± 5.3[f]	99.99[b]	99.99[b]	ABDMG
J23205766-0147373	29.6 ± 1.5	41.0 ± 2.7	96.16[b]	99.99[b]	ARG
J23301341-2023271	13.5 ± 0.6	16.2 ± 0.9[f]	75.69[b]	99.21[b]	COL

[a]Membership probability including radial velocity information (P_v) or membership probability including radial velocity and parallax information ($P_{v+\pi}$).

[b]Membership probability (P_v or $P_{v+\pi}$) for which the binary hypothesis has a higher probability.

[c]Statistical distance including radial velocity information.

[d]Trigonometric distance from Shkolnik et al. (2012), unless stated otherwise.

[e]Trigonometric distance from Riedel (in prep).

[f]Trigonometric distance from van Leeuwen (2007).

[g]Trigonometric distance from Wahhaj et al. (2011).

2.9.2.1 New highly probable candidate members

Of our 164 candidate members with P > 90%, 35 have a radial velocity measurement (of which 14 are from our work), 12 have Li detection (2 from our work), and 16 have a trigonometric parallax measurement. All new parallax measurements are compiled in Table 4.III. In general, there is a good agreement between the statistical distance inferred from our analysis and the true trigonometric one (see Table 2.V). We discuss below those candidate members with $P_v > 90\%$ and the presence of sign of youth or $P_\pi < 90\%$ or $P_{v+\pi} > 90\%$.

2MASSJ01112542+1526214 AB (GJ 3076) : We propose this binary (ρ=0.41″, M5V + M6V; Beuzit et al., 2004, Janson et al., 2012) as a highly probable member of βPMG with a P_v=99.99% at d_s=20±1 pc. Also, our analysis predicted the binary status of this star. Recently, a trigonometric distance (21.8±0.8 pc) was measured by A. R. Riedel et al. (in preparation), in very good agreement with our predicted statistical distance. Including this parallax in our analysis yields a $P_{v+\pi}$=99.99% (binary) for βPMG (see Table 2.V). Our ESPaDOnS spectrum of 2MASSJ01112542+1526214 AB (unresolved) is shown in Figure 2.12. It shows a strong EW_{Li} of 629±14 mÅ which is quite high for a candidate member of βPMG although there is no other known late-type dwarf in βPMG for comparison. Note that Montes et al. (2001) proposed this star as a young disk star, but did not assign it to any particular association. This star fits all requirements to be considered as a new *bona fide member* of βPMG.

2MASSJ05241914-1601153 AB : We propose this binary as a highly probable member of βPMG with a P_v=99.9% at d_s=20±5 pc. This candidate is a resolved binary system (M4.5V + M5.0V) that was discovered by Bergfors et al. 2010, with a separation of 0.639±0.001″. Our ESPaDOnS spectrum of 2MASSJ05241914-1601153 (unresolved) is shown in Figure 2.12. Li is clearly detected with an equivalent width of 223±27 mÅ. The broadened absorption line is an effect of the fast rotation of the star. This system is similar to the *bona fide βPMG member* M4Ve + M4.5V binary system HIP 112312 AB for which the latest spectral type object shows lithium absorption with an EW_{Li}=315±22 mÅ (Mentuch et al., 2008). This is a very strong candidate member of βPMG, and only

a trigonometric distance measurement is needed to fully confirm its *bona fide* status.

2MASSJ05332558-5117131 (TYC 8098-414-1) : We proposed this K7Ve star as a highly probable candidate member of THA with P_v=99.9% at d_s=54±4 pc. This candidate seems to be a young dwarf because Torres et al. (2006) measured an EW_{Li}= 50 mÅ consistent with other *bona fide members* of THA for an age between 10 and 40 Myr. A trigonometric parallax measurement is needed to confirm the *bona fide* status of this star.

2MASSJ05531299-4505119 : We propose this M0.5V star as a highly probable candidate member of ABDMG with P_v=99.9% at d_s=34±4 pc. This candidate seems to be a young dwarf because Torres et al. (2006) measured an EW_{Li}= 140 mÅ which is quite high for a candidate member of ABDMG. A trigonometric distance measurement and other youth indicators are needed to confirm its *bona fide* status.

2MASSJ18202275-1011131 (HIP 89874 AB) : From our analysis, this binary star (K5Ve+K7Ve; Tetzlaff et al., 2010) seems to be a highly probable candidate member of ARG with P=99% at d_s=34±4 pc. The membership probability with RV information is doubtful because there is a difference of 4.1 km s^{-1} between three published radial velocity measurements (-13.8, -9.7, -9.0 km s^{-1} Montes et al., 2001, López-Santiago et al., 2010, Torres et al., 2006). This large difference may come from the binary, or else it may reflect a large uncertainty due to the relatively fast rotation of the star (vsini = 20.1 km s^{-1}; López-Santiago et al., 2010). If we repeat our analysis with RV information (-13.8 km s^{-1}) and parallax measurement (13.17±3.81 mas; van Leeuwen, 2007), the membership probability changes to 94% (binary) in βPMG. The predicted radial velocity is -24.8 km s^{-1} for ARG and -16.2 km s^{-1} for βPMG. Also, this star has a relatively strong EW_{Li} of 530 mÅ (Torres et al., 2006) suggestive an age of 5-15 Myr. Montes et al. (2001) proposed this star as a young disk member. The Galactic positions (71.2, 26.4, 2.9 pc) of this star is very different from those of *bona fide members* of young co-moving groups listed in Table 2.II. Could this star be a member of the Scorpius-Centaurus complex ? Mamajek & Feigelson (2001) suggest that this is not the case since the star never had a close passage near Scorpius-Centaurus in the past.

2MASSJ13591045-1950034 (GJ 3820) : Without RV information, our analysis assigns this M4.5V flare star (Gizis et al., 2002) in ARG with P=95.6% at a statistical

distance of 8±1 pc, in fair agreement with the measured parallax of 10.7±0.1 pc (A. R. Riedel, in preparation). This star also has a measured RV of -15.8 km s^{-1} (Gizis et al., 2002). Including this RV and parallax in our analysis yields P$_v$=85% and P$_{v+\pi}$=99%, both in the field. This membership probability should be taken with caution, since Hawley et al. (1996) measured an RV of 35±10 km s^{-1} for this star, which is very different from the RV measurement of Gizis et al. (2002). These measurements suggest that this star may be a spectroscopic binary (sb1). Thus, although we cannot exclude that this star is young, it does not appear to be a likely member of any of the co-moving groups considered in this work. More RV monitoring is required to determine if this system is a binary. A measurement of EW$_{Li}$ would also provide a very useful constraint on the age.

2MASSJ00503319+2449009 (HIP 3937), 2MASSJ03033668-2535329 (HIP 14239) : Our analysis suggests membership in ARG for both stars with P=99.9%. However, each have a trigonometric distance in disagreement with our statistical distances (see Tables 2.VII, 3.X). When the parallax and radial velocity information are included into the analysis, both stars appear in the field (J0303-2535, P$_{v+\pi}$=99% ; J0050+2449, P$_{v+\pi}$=99%).

2MASSJ23301341-2023271 (HIP 116003 AB) : Our analysis suggests this M3V* star to be a candidate member of COL with P$_v$=76%. The P$_v$ should be taken with caution as this star is a known spectroscopic binary (Torres et al., 2006) which displays important RV variations. Indeed, Gizis et al. (2002) measured four times the RV of this star (11.7, -4.7, -16.7 and 30.1 km s^{-1}), and Torres et al. (2006) measured it three times with a mean RV=-5.7 km s^{-1}. The range of measured RVs includes our predicted value (-2.9 km s^{-1}) for COL. When the trigonometric distance (61.72±3.53 mas; van Leeuwen, 2007) is taken into account, but excluding the RV information for the reason just mentioned, P$_\pi$=99% (binary) in βPMG. Torres et al. (2006) did not detect lithium absorption, however the quality of their spectrum is not good. Better measurements of age-dating indicators and additional radial velocity monitoring of this star would be useful to verify its status.

2MASSJ10121768-0344441 (HIP 49986) : Our analysis suggests this (M1.5V) to be candidate member of ABDMG with P$_v$=91.4%. A parallax measurement is available for this star and the measured distance differs significantly from our predicted value (see

Table 2.V). Thus, this star appears to be in the field with $P_{v+\pi}$=99%. In addition, no youth indicators have been measured for this star yet.

2MASSJ01351393-0712517, 2MASSJ01365516-0647379, 2MASSJ05254166-0909123, 2MASSJ20434114-2433534 and 2MASSJ23205766-0147373 : Our analysis suggests these stars to be candidate members of βPMG (J0135-0712,M4V ; J0136-0647,M4V ; J2043-2433,M3.7+M4.1), ARG (J2320-0147,M4+M4) and ABDMG (J0525-0909,M3.5+M4) with a membership probability of $P_{v+\pi} > 99\%$ (see Table 2.V). Only age-dating indicators are needed to fully confirm their *bona fide* status.

2MASSJ06131330-2742054, 2MASSJ20100002-2801410 and 2MASSJ20333759-2556521 : From our analysis, we proposed these (M3.5 ; M2.5+M3.5 ; M4.5) stars to be candidate members of βPMG with a membership probability of P=99%. No RV measurement is available for these stars, however a trigonometric distance was measured by A. R. Riedel (in preparation) for each star. When the parallax information is included into the analysis, they all appear to be in βPMG with $P_{\pi} > 99\%$. To confirm the membership of these stars, we need measurements of radial velocity and age-dating indicators.

2.9.2.2 Previously identified in the literature

Of the 71 candidate members of the seven young kinematic groups identified in the literature, 58 have $P > 90\%$ or $P_v > 90\%$ (see Table 3.X) ; those are thus likely to be true members of the associations. We discuss below the remaining 13 stars and also those star for which we assign an association membership different from that previously proposed in the literature. Also, we discussed 5 new *bona fide members* of βPMG (2) and ABDMG (3).

2MASSJ00233468+2014282 (TYC 1186-706-1) : This star (K7.5V) was proposed by Lépine & Simon (2009) to be a member of βPMG. From our analysis, this star has an ambiguous membership (P_v) of 55% in the field and 35% in COL. If we exclude the photometry of the star from our analysis, but include the RV information, then it has a membership probability of 85% in the field. To confirm the membership of this star, we need a trigonometric distance and measurements of age-dating indicators.

2MASSJ01220441-3337036 (TYC 7002-2219-1) : This star (K7Ve) was proposed by Schlieder et al. (2010) to be candidate member of ABDMG. From our analysis, this star is a candidate member of THA (P_v =99%) due to RVs (4.8, 3.0±1.4 km s^{-1}; Schlieder et al., 2010, Torres et al., 2006) much closer to that predicted for THA (4.5±1.3 km s^{-1}) compared to ABDMG (18.2±2.1 km s^{-1}). Torres et al. (2006) did not detect lithium absorption for this star, however there is no other K7V in THA for comparison. To confirm our hypothesis, we need a trigonometric distance measurement.

2MASSJ03241504-5901125 : Torres et al. (2000) and de la Reza & Pinzón (2004) proposed this star (K7V) as a candidate member of THA. From our analysis, this star seems to be a highly probable candidate member of COL (P_v=99%) due to an RV (17.5±1.3 km s^{-1}; Torres et al., 2006) much closer to that predicted for COL (17.6±1.0 km s^{-1}) compared to THA (13.8±1.6 km s^{-1}). This candidate seems to be a young star with an EW_{Li} = 235 mÅ (Torres et al., 2006), consistent with the *bona fide members* of young associations with an age less than 40 Myr.

2MASSJ09361593+3731456 (HIP 47133) : This binary star (M2+M2) was proposed by Schlieder et al. (2012a) to be a member of the βPMG. From our analysis, this star is a likely member of the field with P=99%, P_v=99%, P_π=99%, and $P_{v+\pi}$=99%. (Schlieder et al., 2012b) found that this star is a spectroscopic binary (M2+M2) and have measured an RV of -2.5±1.0 km s^{-1}). The main reason for this star to be in the field is that its Galactic position Z (25.1 pc) is far (39 pc away) from the center of βPMG *bona fide members*. A measurement of EW_{Li} would also provide a very useful constraint on the age.

2MASSJ11254754-4410267 : This binary M4+M4.5 star was proposed by Rodriguez et al. (2011) to be a candidate member of TWA. From our analysis, this star has a membership probability of P_v=99.9% (binary) in ABDMG. This star has an EW_{Li} = <30 mÅ (Rodriguez et al., 2011), which is consistent with members of ABDMG of similar spectral type. A parallax measurement is needed to confirm the membership of this star in ABDMG.

2MASSJ11455177-5520456 (CD-54 4320) : This star (K5Ve) was proposed by Torres et al. (2008) to be a member of CAR. From our analysis, this star has an ambiguous

membership (P_v) of 46% in TWA and 48% in COL. The measured RV (16.1 km s^{-1}) falls slightly closer to the predicted value for COL, although there is a difference of only 2.0 km s^{-1} between the predicted radial velocities for TWA (11.8 km s^{-1}) and COL (13.9 km s^{-1}). da Silva et al. (2009) measured an EW$_{Li}$=190 mÅ, which confirm its age similar to THA/COL/CAR *bona fide members*.

2MASSJ11493184-7851011 (V* DZ Cha) : Torres et al. (2008) proposed this star (M1V) as a candidate member of ε Cha. From our analysis, this star is a highly probable candidate member of βPMG with P_v=91%. Our analysis gives a statistical distance of 71±6 pc, which would make this star as one of the most distant members of βPMG. As noted earlier, caution should be applied for our candidates with large statistical distances as we did not include the associations beyond 100 pc in our analysis. It is thus possible that this star is a member of the more distant ($\sim$110 pc) ε Cha association ($\sim$8 Myr), whose spatial velocity is close to that of βPMG. The EW$_{Li}$ of this star was measured by da Silva et al. (2009, ;560 mÅ), and it is somewhat larger than those of βPMG members of similar spectral types. This is clearly a young star, but a parallax measurement is needed to confirm its membership. And ideally we should add the ε Cha association in our analysis.

2MASSJ12151838-0237283 (TYC 4943-192-1) : This star (M0Ve) was proposed by Schlieder et al. (2010) to be a member of ABDMG. From our analysis, this star has an ambiguous membership (P_v) of 83% in ABDMG and 17% in the field. Although a promising candidate for ABDMG, age-dating indicators and a trigonometric parallax are needed to confirm its membership.

TWA 15 A (2MASSJ12342064-4815135) and TWA 15 B (2MASSJ12342047-4815195) These stars (M1.5V and M2V) were proposed by de la Reza et al. (2006) to be members of TWA. Torres et al. (2008) rejected these stars as TWA members but suggested that they could be members of the Scorpius-Centaurus complex. From our analysis, these stars have membership probabilities (P) of 99% and P_v =99% in the field. We repeated our analysis without considering the photometry of the star and the membership probabilities are still 99% for the field. However, these stars appear to be young since Mentuch et al. (2008) unveiled lithium absorption for all of them (EW$_{Li}$=494 and 484 mÅ for

TWA 15A and 15B, respectively). To confirm their membership, we should add in our analysis the Scorpius-Centaurus complex.

TWA 18 (2MASSJ13213722-4421518) : This star (M0Ve) was proposed by de la Reza et al. (2006) to be a member of TWA. From our analysis, this candidate member has a membership probability (P_v) of 89.2% at d_s=60±5 pc for TWA. This star is confirmed to be young since Mentuch et al. (2008) measured an EW_{Li}= 464 mÅ, consistent with the age of TWA. A trigonometric distance measurement is needed to confirm its membership.

2MASSJ16430128-1754274 : This star (M0.5V) was proposed by Kiss et al. (2011) to be a member of βPMG. From our analysis, this star has an ambiguous membership (P_v) of 65% in the field and 35% in βPMG. However, Kiss et al. (2011) measured EW_{Li}=300±20 mÅ confirming that the age of this star is similar to that of βPMG *bona fide members*. To confirm the membership, we need a trigonometric distance measurement.

2MASSJ20072376-5147272 (CD-52 9381) : This star (K6Ve) was proposed by Torres et al. (2008) to be a member of ARG. From our analysis, this star has a membership probability (P_v) of 89.5% in ARG at d_s=31±1 pc. This star shows EW_{Li}=60 mÅ (da Silva et al., 2009), consistent with an age less than 70 Myr. To confirm the membership of this star, we need a parallax measurement.

2MASSJ21212446-6654573 (HIP 105441 A,B) : This system (K2V+K7V, ρ=26″) was proposed by Zuckerman et al. (2001b) to be a member of THA, and by Ortega et al. (2009) to be a member of βPMG. From our analysis, this system seems to be a member of βPMG with P_v=99%. If we take into account the trigonometric distance of HIP 105441 A (π=33.14±1.45 mas; van Leeuwen, 2007), the membership probability $P_{v+\pi}$ is 99% for βPMG. We should note that its radial velocity is quite uncertain from previous studies (A :6.4±14.8,-24.1,Kharchenko et al. (2007), Torres et al. (2006), B :3.3 km s^{-1},Torres et al. (2006). HIP 105441 A could thus be a spectroscopic binary (Torres et al., 2006). The predicted radial velocity measurement is 5.7 km s^{-1} for βPMG. When the trigonometric distance is taken into account, but excluding the RV information for the reason just mentioned, P_{π}=99% in βPMG. However, Torres et al. (2006) showed

that HIP 105441 A does not have a Li detection but measured an EW_{Li}=15 mÅ for HIP 105441 B (K7V). To confirm membership, we need more radial velocity measurements and other age-dating measurements for the two stars.

2MASSJ22424884+1330532 (TYC 1158-1185-1 N,S) : This binary (K5Ve*) was proposed by Schlieder et al. (2010) to be a candidate member of βPMG, however this star was ruled out after RV measurement. From our analysis, this star has an ambiguous membership (P) of 46% in βPMG and 48% in the field. There is a difference of only 0.7 km s^{-1} between the predicted radial velocities for βPMG (-8.0 km s^{-1}) and the field (-7.3 km s^{-1}). If we exclude the photometry of the star from our analysis, but include the RV information, then it has a membership probability of 60% in COL and 40% in the field. The RV measurement (-14.9 km s^{-1}) is much closer to the predicted radial velocity for COL (-14.4 km s^{-1}) compared to the field or βPMG. To confirm the membership, we need a trigonometric distance and measurements of age-dating indicators.

2MASSJ05064991-2135091 A, 2MASSJ05064946-2135038 BC (GJ 3332) : This close visual binary (A: M1Ve and BC:M3.5V+M4V, ρ=1.2$''$; Torres et al., 2008) was proposed by Torres et al. (2008) to be a member of βPMG. From our analysis, the membership probability P_v is 96% in COL for the component A and 99% in βPMG (component BC). The higher probability in COL for component A is mainly due to a difference in space velocity, which could be the result of orbital motion. This system is known to be young as da Silva et al. (2009) measured EW_{Li}=20 mÅ, for both components A and BC ; these values are consistent with the age of βPMG, and the component's spectral types, although it is a bit low for the A component. Recently, a trigonometric distance (19.2$\pm$0.5 pc) was measured by A. R. Riedel (in preparation) which is consistent with our predicted statistical distances for βPMG. With the parallax measurement included into our analysis, both components appear to be in βPMG with a very high membership probability of $P_{v+\pi}$=99.9% (see Table 2.V). This close visual binary fits all requirements to be considered as a new *bona fide member* of βPMG.

2MASSJ06091922-3549311 (CD-35 2722) : We confirm the membership of this M0.5Ve star in ABDMG, as previously proposed by Torres et al. (2008). Recently, the NICI Planet-Finding Campaign confirmed that this star has a L4$\pm$1 companion physi-

cally associated with the primary star (Wahhaj et al., 2011). From this study, a trigono-metric distance was measured at 21.3±1.4 pc. From our analysis, we obtain P_ν = 99.9% and $P_{\nu+\pi}$ = 99.9% for ABDMG. This star shows many signs of youth such as EW_{Li} =10 mÅ, X-ray and Hα emission, consistent with *bona fide members* of ABDMG. This star fits all requirements to be considered as a new *bona fide member* of ABDMG. Thereby, the L4±1 companion is the lowest mass *bona fide member* of ABDMG.

2MASSJ04522441-1649219 (TYC 5899-26-1) : We confirm the membership of this M3Ve* star in ABDMG, as previously proposed by Torres et al. (2008) and confirmed by Schlieder et al. (2010) with RV measurement. Recently, a trigonometric distance was measured at 16.3±0.4 pc by Shkolnik et al. (2012). From our analysis, we obtain P_ν = 99.9% (binary) and $P_{\nu+\pi}$ = 99.9% (binary) for ABDMG. This star shows many signs of youth such as EW_{Li} =20 mÅ, X-ray and Hα emission, consistent with *bona fide members* of ABDMG. This star fits all requirements to be considered as a new *bona fide member* of ABDMG.

2MASSJ21521039+0537356 (HIP 107948) : This star (M2Ve) was proposed by Torres et al. (2008) to be a member of ABDMG. Shkolnik et al. (2012) measured a radial velocity of -15.1±1.5 km s^{-1} and a trigonometric distance at 30.5±5.3 pc. With this new measurements, our analysis gives a P_ν = 99.9% (binary) and $P_{\nu+\pi}$ = 99.9% (binary) for ABDMG. This star shows many signs of youth such as EW_{Li} =10 mÅ, X-ray and Hα emission, consistent with *bona fide members* of ABDMG. Shkolnik et al. (2009) estimated the age of this star between 20 and 150 Myr from various spectroscopic indices. This star fits all requirements to be considered as a new *bona fide member* of ABDMG.

2.10   Summary and conclusion

The study presented in this paper aims at extending the census of low-mass star members of seven young associations of the solar neighborhood : the β Pictoris and AB Doradus moving groups, the TW Hydrae, Tucana-Horologium, Columba, Carina, and Argus associations. To identify new members in these associations, we developed a

Bayesian statistical analysis which, based on the values of 6 observables (I_c and J magnitudes, amplitude of proper motion in right ascension and declination, right ascension and declination), computes a membership probability to a given association as well as the most probable (statistical) distance.

Starting from a sample of 758 stars, all showing indicators of youth such as Hα and X-rays emission, our analysis selected 164 young stars of spectral type between K5V and M5V with a membership probability over 90%. We find 1 of theses candidates in the TWA, 37 in the β PMG, 17 in the THA, 20 in the COL, 6 in the CAR, 50 in the ARG, and 33 in the ABDMG. We also quantified the reliability of our analysis by determining the recovery rate of known members of these associations ; the recovery rate is better than 90%. We also performed a Monte Carlo analysis to determine the expected number of false detections. The false alarm rate is typically between 5 and 15% depending on the association, thus showing that our method is very effective at identifying genuine members of young associations.

The kinematic models used in our statistical analysis predict the radial velocity of a candidate member, thus radial velocity follow-ups provide a powerful tool to further confirm membership. We initiated a program to measure the radial velocity of our new candidates. The first results for 14 candidates show that adding their radial velocity measurement to the analysis yields probabilities above 99%. To clearly establish the young age of the candidate members of βPMG and THA, we initiated a program to detect the presence of photospheric lithium. Early results allowed us to detect lithium for 2 of our candidate members of βPMG : 2MASSJ05241914-1601153 (M4.5V+M5V) and 2MASSJ01112542+1526214 (M5V+M6V). Also another of our candidates in THA, 2MASSJ05332558-5117131 (K7Ve), has both a radial velocity confirmation (from Torres et al. 2006 and our work) and a lithium detection (from Torres et al. 2006). Finally, we propose that six stars should be considered as *bona fide* members of βPMG (2MASSJ01112542+1526214, J05064991-2135091 and J05064946-2135038) and ABDMG (2MASSJ06091922-3549311, J04522441-1649219 and J21521039+0537356).

Table 2.VI. Candidate members of young kinematic groups

Name (2MASS)	I[a] (mag)	J (mag)	$\mu_\alpha \cos\delta$[b] (mas yr^{-1})	μ_δ[b] (mas yr^{-1})	Spt	X-ray[c] log(f_x)	Hα[d] (Å)	Li[e] (m Å)	v_{rad}^{meas}[f] (km s^{-1})	v_{rad}^{pred}[g] (km s^{-1})	d_π[h] (pc)	d_s[g] (pc)	P[i] (%)	Refs.
					β-Pictoris moving group									
J00172353-6645124	9.94±0.05	8.56±0.02	104.30±1.00	-13.50±1.00	M2.5V	-11.77	6.0	...	11.4±0.8[o]	11.0±1.6	...	35±3	99.9	18
J01112542+1526214	10.98±0.00[f]	9.08±0.03	180.00±2.00[y]	-120.00±5.00[y]	M5V+M6V	-12.13	9.3	629[o]	4.0±0.1	3.1±1.6	21.8±0.8[vv]	20±1	99.9[j]	18
J01351393-0712517	10.53±0.08	8.96±0.02	96.00±3.00[y]	-50.00±4.00[y]	M4V	-11.92	15.3	...	11.7±5.3[uu]	9.4±1.6	37.9±2.4[uu]	35±3	33.2[j]	18
J01365516-0647379	11.22±0.06	9.71±0.02	175.10±4.40[y]	-98.80±4.40[y]	M4V	-12.03	6.0	...	12.2±0.4[uu]	9.5±1.6	24.0±0.4[uu]	21±1	27.4	18
J01535076-1459503	9.82±0.06	7.94±0.03	105.00±1.40	-45.70±1.40	M3V+M3V	-11.54	6.6	...	...	12.0±1.6	...	28±2	99.9[j]	18
J05015881+0958587	8.74±0.04[vv]	7.21±0.02	12.09±9.92[n]	-74.41±5.71[n]	M3V(sb2)*	-11.37	6.0[ll]	0[ii]	14.9±3.5[j]	16.0±2.0	24.9±1.3[vv]	38±3	99.9[j]	5
J05064946-2135038	8.45±0.07[vv]	7.00±0.02	34.20±1.20	-33.80±2.10	M3.5Ve+M4V	-11.06	2.4[ll]	20[ii]	21.2±0.9[ll]	21.1±1.7	19.2±0.5[vv]	21±4	99.9[j]	7
J05082729-2101444	11.61±0.06	9.72±0.02	31.40±2.30	-16.00±2.30	M5V	-12.44	24.9	...	...	21.0±1.7	...	25±5	99.9[j]	18
J05224571-3917062	9.66±0.06	8.31±0.02	-1.90±0.90	8.80±0.80	K7V	-11.41	1.6	85[k]	36.4±0.0[k]	21.3±1.5	...	33±6	99.9	18
J05241914-1601153	10.59±0.06	8.67±0.03	14.00±5.00[y]	-36.00±2.00[y]	M4.5+M5.0	-11.99	11.7	223[o]	20.5±4.0[o]	20.8±1.8	...	20±5	99.9[j]	18
J05320450-0305291	9.26±0.06	7.88±0.02	7.20±2.00	-45.50±2.80	M2Ve+M3.5	-11.43	4.8	100[ii]	...	19.1±1.9	...	42±6	99.9[j]	7
J05332802-4257205	9.71±0.06	8.00±0.03	-19.70±6.10	43.60±5.80	M4.5V	-11.69	3.9	...	...	21.1±1.5	...	16±4	99.9	18
J05335981-0221325	9.90±0.06	8.56±0.02	10.00±1.00[y]	-50.00±1.00[y]	M3V	-11.54	6.1	...	...	19.0±1.9	...	42±5	99.9	18
J05422387-2758031	12.95±0.06	11.41±0.03	1.30±3.70	-4.20±1.70	M4.5V	-12.21	8.5	...	...	21.6±1.6	...	44±9	99.3	18
J06131330-2742054	9.55±0.02[vv]	8.00±0.03	-14.90±1.00	-2.10±1.00	M3.5V*	-11.51	5.1	...	...	21.6±1.6	29.2±0.8[vv]	25±6	99.9[j]	18
J06135773-2723550	10.97±0.06	9.74±0.02	-3.70±0.80	2.70±0.90	K5V	-12.12	-0.8	170[k]	-6.8±0.0[k]	21.6±1.6	...	51±8	97.3	18
J06161032-1320422	12.85±0.05	11.35±0.03	-5.40±2.70	-33.80±2.80	M3.5+M5.0	-12.22	4.2	...	...	20.6±1.8	...	47±7	97.9	18
J08173943-8243298	9.08±0.06	7.47±0.02	-81.90±0.90	102.60±1.50	M4	-11.24	7.6	...	...	12.9±1.5	...	27±2	99.9[j]	18
J08475676-7854532	10.84±0.06	9.32±0.02	-32.10±1.80	26.80±1.80	M3V	-12.03	6.6	...	...	13.4±1.5	...	66±7	93.8[j]	18
J11493184-7851011	10.73±0.00[k]	9.45±0.02	-43.40±2.90	-8.10±1.80	M1V	-12.07	4.7	560[k]	13.4±1.3[k]	10.9±1.5	...	71±6	78.3	7
J14142141-1521215	8.95±0.02[n]	7.43±0.02	-199.90±8.70[y]	-172.80±6.90[y]	K5V	-11.24	2.3	...	-4.1±0.0[ll]	-7.5±1.7	30.2±4.5	16±1	99.9	18
J16572029-5343316	9.97±0.07	8.69±0.02	-14.70±6.10	-85.90±2.20	M3V	-12.24	2.5	...	...	-1.8±1.9	...	51±3	99.5	18
J17150219-3333398	9.32±0.06	7.92±0.02	7.60±5.30	-176.90±1.20	M0V	-11.46	3.0	...	...	-9.2±2.0	...	23±1	96.9	18
J17292067-5014529	10.30±0.00[k]	8.87±0.03	-6.30±1.50	-63.50±4.10	M3Ve	-12.13	6.7	50[k]	-0.4±0.0[k]	-3.3±2.0	...	66±4	99.9[j]	6
J18142207-3246100	10.64±0.00[k]	9.44±0.02	7.30±4.70[y]	-39.90±4.70[y]	M1.5V*	-11.66	3.1	200[k]	-5.7±0.0[k]	-9.6±2.1	...	97±6	87.9[j]	6
J18151564-4927472	10.36±0.06	8.92±0.02	8.30±1.60	-71.50±1.60	M3V	-11.96	7.6	...	...	-3.6±2.0	...	61±4	91.2[j]	18
J18420694-5554254	10.88±0.06[o]	9.49±0.02	11.20±5.30	-81.40±2.70	M3.5V	-11.79	6.9	...	1.0±0.7[o]	-1.0±1.9	...	54±3	76.2	18
J18465255-6210366	9.99±0.00[k]	8.75±0.02	14.60±1.40	-81.10±1.30	M1Ve	-12.01	1.9[k]	332[k]	2.4±0.1[k]	1.3±1.9	...	54±3	58.2	6
J18495543-0134087	11.20±0.09[o]	9.78±0.03	9.00±9.00[y]	-35.90±9.00[y]	M2.5V	-12.05	5.8	...	...	-17.7±1.9	...	63±7	97.9	18
J18504448-3147472	9.44±0.00[k]	8.31±0.02	16.60±1.80	-74.70±0.70	K7Ve	-11.65	1.8[k]	492[k]	-6.0±1.0[k]	-9.5±2.0	...	53±3	92.5	6
J18580415-2953045	9.98±0.00[k]	8.86±0.02	11.50±1.40	-49.50±1.40	M0Ve	-11.76	2.8[k]	483[k]	-4.9±1.0[k]	-10.0±2.0	...	77±4	98.9[j]	6
J19102820-2319486	10.59±0.06	9.10±0.02	17.60±1.90	-51.60±1.50	M4V	-11.86	8.2	...	...	-11.7±2.0	...	67±5	99.9[j]	18
J19233820-4606316	10.19±0.05	9.11±0.03	17.90±0.90	-57.90±0.90	M0V	-12.07	2.0	...	-0.7±0.7[o]	-3.9±2.0	...	71±4	98.9	18
J19243494-3442392	11.29±0.05	9.67±0.02	23.20±1.80	-72.10±1.80	M4V	-12.50	13.9	...	...	-7.8±2.0	...	55±3	99.9[j]	18
J19312434-2134226	10.04±0.06	8.69±0.02	63.00±1.60	-110.10±1.60	M2.5V	-11.97	8.9	...	-26.0±1.8[uu]	-11.7±2.0	26.0±2.0[uu]	31±2	98.6	18
J19560294-3207186	10.85±0.06	8.96±0.03	32.60±1.90	-61.00±1.20	M4V	-11.76	6.2	-100[ff]	-11.0±5.0[ff]	-7.7±2.0	...	56±4	98.8[j]	8,12
J19560438-3207376	10.13±0.06	8.71±0.03	30.30±1.50	-66.60±1.00	M0V	-11.76	0.7[ff]	110[ff]	-7.2±0.4[ff]	-7.6±2.0	...	55±3	99.9[j]	8,12

Table 2.VI — continued

Name (2MASS)	I[a] (mag)	J (mag)	$\mu_\alpha \cos\delta$[b] (mas yr⁻¹)	μ_δ[b] (mas yr⁻¹)	Spt	X-ray[c] log(f_x)	Hα[d] (Å)	Li[e] (m Å)	v_{rad}^{meas}[f] (km s⁻¹)	v_{rad}^{pred}[g] (km s⁻¹)	d_π[h] (pc)	d_s[g] (pc)	P[i] (%)	Refs.
J20013718-3313139	10.27±0.05	9.15±0.02	27.10±2.60	-60.90±1.80	M1V	-12.23	2.6	-100[ff]	-5.6±1.8[ff]	-7.1±1.9	...	62±3	98.9	12
J20100002-2801410	10.20±0.02[vv]	8.65±0.02	40.40±0.90	-62.70±0.90	M2.5+M3.5	-11.84	10.1	...	...	-8.4±1.9	48.0±3.1[vv]	53±3	99.9[j]	18
J20333759-2556521	11.57±0.01[vv]	9.71±0.02	51.80±1.70	-76.80±1.40	M4.5V	-12.42	11.4	...	...	-7.9±1.9	48.3±3.3[vv]	40±3	99.9[j]	18
J20431469-2925217	13.16±0.06	11.42±0.04	36.80±6.00	-68.90±5.60	K5V	-12.92	-2.0	...	...	-6.5±1.9	...	51±3	96.9	18
J20434114-2433534	10.11±0.05	8.60±0.02	56.20±1.30	-72.00±1.30	M3.7+M4.1	-11.71	6.5	...	...	-7.8±1.8	28.1±3.9[uu]	44±3	99.9[j]	18
J20560274-1710538	9.26±0.06	7.85±0.02	59.30±3.00[n]	-63.00±3.20[n]	K7V+M0V	-11.78	1.4	420[k]	-6.0±0.9[uu]	-9.1±1.8	...	45±3	99.9[j]	5
J2073678-1304581	10.11±0.06	8.73±0.02	60.60±1.60	-86.60±1.60	M3V	-11.88	5.4	...	-6.9±0.6[k]	-9.4±1.7	...	36±2	91.4	18
J21100535-1919573	9.57±0.06	8.11±0.03	88.60±1.20	-92.50±1.20	M2V	-11.44	5.4	...	-5.1±1.0[o]	-7.8±1.8	...	32±2	99.9[j]	18
J21103096-2710513	13.30±0.06	11.20±0.03	60.30±4.20	-79.70±4.10	M5V	-12.48	11.3	...	...	-5.7±1.8	...	40±2	99.9[j]	18
J21103147-2710578	12.02±0.05	10.30±0.02	70.60±1.90	-72.30±2.80	M4.5V	-12.48	9.0	...	...	-5.7±1.8	...	42±3	99.9[j]	18
J21212873-6655063	8.90±0.00[k]	7.88±0.03	98.20±1.10	-105.70±1.80	K7V	...	...	15[k]	3.3±0.0[k]	5.7±1.7	30.2±1.3	32±1	57.6	4,9
J21551741-0045478	12.79±0.17[v]	11.09±0.02	62.00±0.00[y]	-48.00±1.00[y]	M4.5V	-12.36	12.5	...	...	-9.0±1.6	...	47±4	95.9	18
J22004158+2715135	9.54±0.17[v]	8.56±0.03	75.30±1.00	-16.70±1.20	M0.0Ve	-11.80	2.6[bb]	...	-13.3±2.4[bb]	-12.8±1.4	...	44±4	81.5	8
J22424896-7142211	8.87±0.00[k]	7.79±0.02	95.20±0.80	-52.30±0.80	K7Ve+K5V	-11.28	1.9[k]	440[k]	8.6±0.5[k]	8.8±1.7	...	37±2	94.8	6
J23172807+1936469	9.51±0.17[v]	8.02±0.02	350.00±2.00[y]	-90.00±3.00[y]	M3.5+M4.5	-11.70	3.6	...	-3.7±0.0[ll]	-6.4±1.4	...	12±1	94.4	18
J23301341-2023271	9.02±0.06[n]	7.20±0.03	314.50±7.20[y]	-208.10±6.10[y]	M3V	-11.44	3.3	0[k]	-5.7±0.6[k]	2.2±1.6	16.2±0.9	11±1	99.9[j]	18
J23314492-0244395	11.24±0.07[o]	9.51±0.02	90.00±2.00[y]	-60.00±1.00[y]	M4.5V	-11.95	19.0	...	...	-1.1±1.5	...	38±3	95.0[j]	18
J23323085-1215513	8.56±0.00[k]	7.45±0.02	137.90±1.00	-81.00±1.00	M0Ve	-11.32	2.8	185[k]	1.8±0.7[k]	0.8±1.5	...	28±1	95.9	6
J23500639+2659519	12.13±0.17[v]	10.14±0.02	182.00±2.00[y]	-44.00±0.00[y]	M3.5V	-12.27	9.8	...	-0.7±2.8[uu]	-5.2±1.4	...	23±2	92.8[j]	18
J23512227+2344207	11.68±0.17[v]	9.68±0.02	269.80±4.20[y]	-77.30±4.20[y]	M4V	-12.37	7.3	...	-2.1±0.5[uu]	-4.5±1.4	...	16±1	95.0	18
TW Hydrae Association														
J10182870-3150029	8.87±0.03	8.87±0.03	-55.50±3.20	-22.60±3.70	M0Ve*	-11.70	3.8[k]	510[k]	20.7±1.5[k]	15.5±1.7	...	54±5	99.9	2
J10252092-4241539	10.64±0.06	9.50±0.03	-46.80±1.20	-2.20±1.20	M1V	-12.08	4.1	490[xx]	...	15.5±1.6	...	58±5	97.4	13
J10423011-3340162	9.21±0.06[k]	7.79±0.02	-122.20±2.20[y]	-29.30±2.20[y]	M2Ve	-11.59	6.5	530[k]	11.4±0.0[k]	14.3±1.7	...	37±4	96.9[j]	2
J11102788-3731520	9.29±0.06	7.65±0.02	-107.30±0.90	-18.00±1.10	M4Ve+M4Ve	-11.64	12.7	710[k]	15.6±0.2[k]	13.0±1.8	...	41±4	99.9[j]	1
J11132622-4523427	10.71±0.06	9.41±0.03	-44.10±1.40	-8.10±1.30	M0Ve*	-12.00	17.7	589	15.8±2.0[ee]	13.2±1.9	...	58±5	99.9	5
J11210549-3845163	10.49±0.00[k]	9.00±0.03	-68.30±2.70	-12.10±1.50	M1Ve	-12.02	3.5[k]	550[k]	12.7±0.0[k]	12.5±1.9	...	52±5	99.9[j]	5
J11211723-3446454	9.66±0.05	8.43±0.04	-67.40±0.00[k]	-17.00±0.00[k]	M1Ve	-11.47	2.3[k]	580[k]	11.3±0.0[k]	12.2±1.9	...	52±5	99.9	5
J11211745-3446497	9.73±0.05	8.43±0.04	-67.40±0.00[k]	-17.00±0.00[k]	M1Ve	-11.47	1.5[k]	550[k]	11.6±0.0[k]	12.2±1.9	...	51±5	99.9	5
J11315526-3436272	9.27±0.06	7.67±0.03	-82.60±0.80	-22.60±1.00	M2+M2.5+M9	-11.36	8.7	629[k]	12.7±3.8[k]	11.5±2.0	...	46±5	99.9[j]	1
J11321831-3019518	11.31±0.06	9.64±0.02	-89.60±1.30	-25.80±1.30	M5Ve	...	6.8[bb]	600[bb]	12.3±1.5[bb]	11.1±2.0	...	45±4	99.9	10
J12072738-3247002	10.14±0.06	8.62±0.03	-72.70±0.90	-29.30±0.90	M3Ve+M3Ve	-12.04	2.4[pp]	500[ee]	8.5±1.2[ee]	9.1±2.3	...	48±4	99.9[j]	5
J12153072-3948426	9.50±0.00[k]	8.17±0.03	-74.00±0.80	-27.70±0.80	M1Ve	-11.60	2.6[k]	555[k]	7.5±0.1[k]	9.4±2.3	...	50±4	99.9[j]	5
J12313807-4558593	10.72±0.07	9.33±0.03	-64.40±3.10	-28.60±1.00	M3Ve*	-12.40	3.1[pp]	160[ii]	8.1±4.0[q]	9.1±2.4	...	54±5	99.9	5
J12350424-4136385	10.49±0.00[k]	9.12±0.02	-70.50±1.10	-29.90±1.10	M2Ve	-11.98	7.5	500[k]	6.6±0.0[k]	8.5±2.5	...	53±4	99.9	2
J13142668-4341522	12.41±0.06	10.75±0.02	-107.00±3.00	-60.80±3.00	M3.5V	-12.31	8.4	...	...	4.9±3.0	...	42±3	96.3	18
Tucana-Horologium Association														
J00171443-7032021	10.17±0.06	9.00±0.03	55.30±2.30	-28.40±14.40	M0.5V	-12.04	2.4	...	...	8.0±1.5	...	63±4	99.2[j]	18
J01220441-3337036	9.34±0.06	8.31±0.02	107.20±1.00	-59.00±1.00	K7Ve	-11.65	0.8	0[k]	4.8±0.0[k]	4.5±1.3	...	39±2	98.3	11
J01521830-5950168	10.26±0.06	8.94±0.02	107.80±1.80	-27.00±1.80	M2-3V	...	2.3[ff]	-20[ff]	7.9±1.6[ff]	9.9±1.5	...	40±2	95.3	12

Table 2.VI — continued

Name (2MASS)	I^a (mag)	J (mag)	$\mu_\alpha \cos\delta^b$ (mas yr^{-1})	μ_δ^b (mas yr^{-1})	Spt	X-ray^c log(f_x)	Hα^d (Å)	Li^e (m Å)	$v_{rad}^{meas\,f}$ (km s^{-1})	$v_{rad}^{pred\,g}$ (km s^{-1})	d_π^h (pc)	d_t^g (pc)	P^i (%)	Refs.
J02045317-5346162	12.08±0.06^o	10.44±0.02	95.60±2.90	−30.90±3.10	K5V	−11.84	−1.8	...	...	10.0±1.5	...	42±2	94.9^j	18
J02070176-4406380	10.68±0.05	9.27±0.03	95.70±3.60	−32.80±13.40	M3.5V	−12.22	4.1	...	...	9.1±1.4	...	43±2	98.9^j	18
J02414683-5259523	8.62±0.00^k	7.58±0.02	98.50±1.60	−14.00±1.30	K6Ve	−11.28	1.2^k	298^k	12.5±1.6^k	11.8±1.5	...	42±2	96.5^j	5
J02414730-5259306	9.79±0.00^k	8.48±0.03	92.20±1.10	−4.20±1.50	M2.5V	−11.28	5.5	10^k	12.7±1.2^k	11.8±1.5	...	43±3	94.7^j	5
J02423301-5739367	9.51±0.00^k	8.56±0.02	83.80±0.90	−8.80±1.30	K5Ve	−12.22	0.4^k	120^k	12.4±0.1^k	12.0±1.5	...	49±3	90.8	5
J03190864-3507002	9.60±0.06	8.58±0.03	89.70±1.60^y	−19.40±1.60^y	K7Ve	−12.13	1.3	65^k	13.5±0.2^k	12.9±1.5	...	44±3	84.4	7
J03331564-4359135	9.32±0.00^k	8.30±0.02	87.40±1.70^y	−5.60±1.20^y	K6Ve	−11.85	1.9	251^k	15.5±0.3^k	14.2±1.5	...	44±2	96.3	7
J03454058-7509121	12.39±0.05	10.82±0.02	64.30±5.60	23.00±2.50	M4V	−12.24	3.1	...	...	13.3±1.7	...	55±3	99.9^j	18
J04213904-7233562	11.20±0.05	9.87±0.02	62.20±1.30	25.40±1.30	M2.5V	−12.15	3.5	...	...	14.4±1.7	...	54±3	99.9	18
J04440099-6624036	10.53±0.05	9.47±0.02	53.00±4.00	30.20±4.00	M0.5V	−12.37	2.6	...	...	15.8±1.7	...	56±3	97.5	18
J04480066-5041255	9.79±0.00^k	8.74±0.03	54.30±1.80	14.10±1.80	K7Ve	−11.94	1.7	40^k	19.3±0.1^k	17.7±1.7	...	53±3	95.9	7
J05332558-5117131	10.00±0.00^k	8.99±0.02	44.00±1.80	24.20±1.70	K7V	−12.38	1.6	50^k	19.6±0.3^o	19.2±1.7	...	54±4	98.5	18
J17080882-6936186	10.51±0.06	9.06±0.02	−55.60±1.70	−80.20±1.70	M3.5V	−12.12	8.1	...	...	5.0±1.6	...	49±3	93.2^j	18
J17130733-8552105	9.69±0.06	8.59±0.03	−35.20±0.90	−58.10±0.90	M0V	−11.86	3.9	...	...	9.9±1.7	...	62±4	98.5^j	18
J19225071-6310581	0.89±0.05	9.45±0.02	−10.70±1.90	−77.40±1.90	M3V	−11.89	8.2	...	...	0.9±1.5	...	61±4	99.9^j	18
J21471964-4803166	12.29±0.06	10.73±0.02	50.40±3.20	−72.90±2.50	M4V	−12.41	6.4	...	...	−3.3±1.4	...	50±3	96.7^j	18
J21490499-6413039	12.18±0.06	10.35±0.02	47.80±1.90	−96.50±2.00	M4.5V	−12.10	11.4	...	...	2.5±1.5	...	44±2	99.9^j	18
J22021626-4210329	10.08±0.06	8.93±0.03	51.80±0.90	−93.30±1.00	M1V	−11.90	2.8	...	−2.0±1.1^o	−4.9±1.4	...	45±2	98.4	18
J23204705-6723209	11.34±0.06	9.99±0.04	80.00±1.60	−97.10±9.90	M5V	−12.08	11.5	...	...	5.7±1.5	...	39±2	99.9	18
J23261069-7323498	9.91±0.00^k	8.84±0.03	72.10±1.00	−66.80±1.00	M0V(sb)	−11.80	5.1	123^k	7.8±1.6^k	7.4±1.5	...	48±2	99.9	7
J23285763-6802338	10.52±0.06^o	9.26±0.02	67.90±1.70	−65.60±3.20	M2.5V	−11.98	6.0	...	...	6.1±1.5	...	49±3	99.9	18
J23452225-7126505	11.78±0.06	10.19±0.02	76.50±1.80	−64.00±1.80	M3.5V	−12.19	11.1	...	...	7.3±1.5	...	46±2	99.9^j	18
J23474694-6517249	10.36±0.06	9.10±0.02	80.70±1.20	−66.40±1.20	M1.5V	−12.24	2.5	...	6.4±0.7^o	6.0±1.5	...	45±2	99.9	18
Columba Association														
J02303239-4342232	8.88±0.08	8.02±0.03	81.40±0.80	−13.50±1.00	K5Ve	−11.85	0.0^k	50^k	16.3±1.1^k	15.2±1.0	...	51±2	38.3	7
J03050976-3725058	10.83±0.09	9.54±0.02	51.60±1.30	−11.50±1.30	M1.5+M3.0	−12.53	5.2	...	...	17.1±1.0	...	72±4	98.1^j	18
J03241504-5901125	10.55±0.00^k	9.55±0.02	37.80±1.20	10.50±1.10	K7V	−12.40	1.6	235^k	17.5±1.3^k	17.7±1.0	...	91±4	61.6	3
J03320347-5139550	11.48±0.06	10.23±0.03	37.10±4.30	10.80±1.40	M2V	−12.19	4.1	...	...	18.5±1.0	...	88±5	94.7	18
J04071148-2918342	10.14±0.06	9.06±0.02	41.60±1.10	−6.10±1.00	K7.5+M1.0	−11.98	3.2	...	...	20.4±1.0	...	72±4	99.4	18
J04091413-4008019	12.04±0.05	10.65±0.02	46.40±1.90	8.10±1.70	M3.5V	−12.40	16.9	...	...	20.7±1.0	...	63±4	99.1	18
J04240094-5512223	11.16±0.09	9.80±0.02	41.60±2.10	17.20±2.10	M2.5V	−12.39	3.7	...	20.5±0.7^o	20.2±1.1	...	68±4	55.4^j	18
J04313859-3042509	11.61±0.06	10.18±0.02	33.60±1.50	−5.80±1.50	M3.5V	−12.32	8.5	...	...	21.7±1.0	...	75±5	97.3^j	18
J04515303-4647309	10.95±0.00^k	9.80±0.02	29.00±3.00^y	14.50±2.70^y	M0V	−11.63	1.0^k	80^k	24.0±0.0^k	22.1±1.1	...	77±5	99.9	7
J05064991-2135091	8.25±0.02^{vv}	7.05±0.02	53.10±1.90	−23.40±1.00	M1Ve	−11.06	2.4^{ll}	20^{ii}	23.7±1.7^{ll}	22.8±1.0	19.2±0.5^{vv}	37±3	84.8^j	7
J05100427-2340407	10.52±0.06	9.24±0.03	43.40±4.40	−13.00±0.90	M3+M3.5	−11.75	5.4	...	...	23.1±1.1	...	48±4	94.5	18
J05100488-2340148	10.80±0.06	9.60±0.04	35.60±1.60	−13.10±1.50	M2+M2.5	−11.75	6.6	...	...	23.1±1.1	...	57±5	98.8	18
J05111098-4903597	12.05±0.06	10.64±0.03	33.00±2.50	20.40±2.10	M3.5V	−11.99	6.8	...	...	22.4±1.1	...	62±5	98.4	18
J05164586-5410168	11.80±0.05	10.43±0.02	26.30±1.90	26.60±2.40	M3V	−12.25	2.7	...	15.1±3.9^{kk}	21.9±1.1	...	69±5	92.1	18
J05195412-0723359	12.58±0.06	11.07±0.02	49.70±4.10^z	−38.00±4.10^z	M4V	−12.31	7.9	...	...	21.5±1.0	...	43±3	90.3	18
J05195695-1124440	11.75±0.06	10.37±0.02	24.00±2.00^y	−18.00±3.00^y	M3.5V	−12.19	11.8	...	...	22.2±1.0	...	76±6	98.4^j	18
J05241317-2104427	11.81±0.06	10.21±0.02	33.10±3.70	−16.00±4.80	M4V	−12.37	8.3	...	...	23.4±1.1	...	52±5	98.2^j	18

Table 2.VI — continued

Name (2MASS)	I^a (mag)	J (mag)	$\mu_\alpha \cos\delta^b$ (mas yr^{-1})	μ_δ^b (mas yr^{-1})	Spt	X-ray^c log(f$_x$)	Hα^d (Å)	Li^e (m Å)	$v_{rad}^{meas\,f}$ (km s^{-1})	$v_{rad}^{pred\,g}$ (km s^{-1})	d_π^h (pc)	d_s^g (pc)	P^i (%)	Refs.
J05395494-1307598	12.17±0.06	10.60±0.02	26.40±8.50	-18.90±8.50	M3V	-12.45	5.6	...	...	23.1±1.1	...	61±5	99.0^j	18
J05425587-0718382	11.52±0.05	10.10±0.03	19.10±2.10	-22.20±2.00	M3V	-12.21	7.0	...	...	22.3±1.1	...	75±6	98.2^j	18
J05432676-3025129	11.53±0.06	10.41±0.02	11.60±2.60	-0.30±1.20	M0.5V	-12.05	4.5	...	...	24.3±1.1	...	91±10	99.9	18
J05470650-3210413	11.36±0.06	9.86±0.02	23.90±0.90	6.80±0.90	M2.5V	-12.22	5.6	...	...	24.4±1.1	...	52±7	99.3^j	18
J06002304-4401217	11.67±0.06	10.31±0.04	24.40±4.30	15.30±3.60	M4V+M4V	-12.05	12.2	...	...	24.0±1.1	...	54±6	97.7	18
J06012186-1937547	12.88±0.06	11.37±0.03	10.40±3.40	-9.00±3.50	M3.5V	-12.10	10.3	...	...	24.3±1.1	...	79±10	99.9^j	18
J06511418-4037510	9.19±0.06	8.17±0.02	0.00±2.80^y	8.00±1.40^y	K5V	-11.97	-0.8	0^k	13.6±0.6^k	24.8±1.1	...	71±11	99.9^j	18
J07065772-5353463	9.62±0.06	8.54±0.03	-7.80±1.10	40.40±1.30	M0V	-11.77	2.7	...	...	23.0±1.2	...	53±4	99.9	18
J09331427-4848331	9.99±0.06	8.94±0.03	-46.50±1.20	23.40±2.60	K7V	-11.93	2.7	0^k	22.0±0.6^k	20.5±1.2	...	58±3	13.2	18
Carina Association														
J06112997-7213388	11.00±0.05	9.55±0.02	23.40±1.60	60.80±1.60	M4V+M5V	-12.33	9.0	...	...	19.9±0.5	...	45±1	90.4^j	18
J06234024-7504327	11.23±0.05	9.88±0.03	13.90±1.80	47.20±1.80	M3.5+M5	-11.94	8.0	...	...	19.1±0.5	...	60±2	90.4^j	18
J07540718-6320149	11.66±0.06	10.33±0.03	-10.80±2.40	30.00±2.40	M3V	-12.23	8.5	...	...	21.9±0.5	...	83±4	99.9^j	18
J08185942-7239561	10.86±0.06	9.78±0.02	-24.30±0.90	54.00±0.90	M0V	-12.44	2.1	...	...	19.5±0.6	...	60±2	99.9	18
J08422284-8345248	10.45±0.06	9.45±0.03	-49.50±1.30	91.20±1.20	K7V	-11.99	2.1	...	...	16.3±0.6	...	41±1	90.4	18
J10140807-7636327	11.34±0.06	9.75±0.02	-47.20±1.70	30.60±3.60	M4V+M5V	-12.17	11.0	...	...	17.1±0.6	...	69±2	99.9^j	18
Argus Association														
J00503319-2449009	9.42±0.00^s	7.95±0.02	223.70±2.30^y	-40.86±2.30^y	M3.5+M4.5	-11.49	5.8	...	6.0±1.1^{ll}	4.0±1.5	11.8±0.7	22±1	99.9^j	18
J03033668-2535329	9.29±0.04^n	8.00±0.02	213.20±1.90^y	94.50±1.80^y	M0.0+M6.0	-12.03	0.4	0^k	20.1±0.6^k	16.1±0.9	38.6±3.8	18±1	99.9	18
J03146689-0640242	9.47±0.00^u	7.86±0.03	322.70±2.70^y	-48.50±3.00^y	M2V	-13.10	0.0	...	29.7±0.0^{ll}	18.9±1.0	...	10±1	99.9	18
J03282609-0537361	12.15±0.17^v	10.29±0.02	118.00±1.00^y	-18.00±2.00^y	M4V	-12.44	5.2	...	...	19.4±1.0	...	27±2	98.4^j	18
J03415581-5542287	11.89±0.06	10.19±0.03	231.70±9.00^y	250.90±9.00^y	M4.5+M6	-12.53	10.9	...	...	11.9±1.4	...	14±1	98.9	18
J04132663-0139211	10.96±0.06	9.38±0.02	132.00±4.00^y	-6.00±4.00^y	M4+M5.5	-12.09	9.8	60^{dd}	31.7±0.3^{uu}	22.2±1.2	26.2±1.7^{uu}	19±2	99.9	18
J04244260-0647313	11.09±0.06	9.57±0.03	146.00±1.00^y	8.00±2.00^y	M4V	-11.92	4.3	...	...	22.7±1.2	...	16±1	99.4	18
J04464970-6034109	9.82±0.05	8.55±0.02	56.80±1.40	109.50±1.40	M1.5V	-12.00	5.3	...	...	12.1±1.6	...	37±2	92.3	18
J04595855-0333123	11.19±0.06	9.76±0.02	72.00±0.00^y	48.00±1.00^y	M4+M5.5	-12.25	5.5	...	...	24.2±1.3	...	19±2	90.8	18
J06134539-2352077	10.16±0.06	8.37±0.03	-28.00±3.90	105.30±1.30	M3.5+M5	-11.39	6.1	...	...	23.4±1.7	...	16±2	99.9^j	18
J06380031-4056011	11.89±0.05	10.35±0.03	-1.00±2.00	97.40±1.90	M3.5V	-12.30	4.7	...	...	19.3±1.8	...	35±2	93.9	18
J07140101-1945332	12.31±0.05	10.81±0.02	-22.50±4.90	25.10±3.40	M4.5V	-12.15	7.0	...	...	23.0±1.8	...	61±6	99.9^j	18
J07343426-2401353	12.24±0.05	10.65±0.02	-22.00±2.00^y	30.00±4.00^y	M3.5V	-12.29	8.2	...	...	21.7±1.8	...	71±5	94.2^j	18
J08031018+2022154	10.88±0.17^v	9.24±0.02	-104.00±2.00^y	-58.00±3.00^y	M3V+M4V	-11.62	...	...	35.5±1.5^{uu}	20.6±1.3	...	25±1	99.9^j	18
J09423823-6229028	11.82±0.05	10.21±0.03	-150.30±3.20	79.50±5.30	M3.5+M3.5	-12.20	3.7	...	...	7.4±1.9	...	30±1	97.2	18
J09445422-1220544	10.39±0.00^t	8.50±0.02	-328.80±4.60^y	33.30±4.60^y	M5V	-11.67	15.3	...	...	14.5±1.7	...	12±1	99.9^j	18
J10252563-4918389	10.52±0.06	9.12±0.04	-182.10±6.70	54.50±6.40	M4V	-12.05	8.3	...	...	7.5±1.9	...	27±1	99.9	18
J11200609-1029468	9.27±0.06	7.81±0.03	-202.50±1.50^y	19.80±2.70^y	M2V	-11.64	2.4	...	...	5.2±1.4	...	25±1	99.9^j	18
J12092998-7505400	11.29±0.05	9.91±0.02	-65.30±2.50	-0.60±2.50	M3V	-12.41	7.5	...	...	0.5±1.8	...	78±4	99.1^j	18
J12233860-4606203	10.96±0.06	9.53±0.02	-235.10±6.80	-7.40±7.90	M4V	-12.20	7.5	...	...	-0.8±1.8	...	23±1	99.9	18
J13283294-3654233	11.22±0.05	9.83±0.03	-192.00±3.00^y	-36.00±24.00^y	M3.5V	-12.53	3.8	...	...	-6.7±1.6	...	27±1	99.2	18
J13382562-2516466	10.14±0.06	8.66±0.02	-295.56±12.10^{aa}	-76.33±9.40^{aa}	M3.5V	-11.87	6.7	...	...	-8.6±1.4	...	16±1	99.9	18
J13493313-6818291	10.79±0.05	9.50±0.03	-51.00±9.90	-26.50±7.70	M2+M4+M3.5	-12.03	7.7	...	...	-3.5±1.7	...	84±3	96.4^j	18
J13591045-1950034	9.90±0.03^{vv}	8.33±0.04	-552.70±5.50^{cc}	-183.10±5.50^{cc}	M4.5V	-11.89	3.1	...	-15.8±0.0^{ll}	-10.9±1.2	10.7±0.1^{vv}	8±1	95.6	18

Table 2.VI — continued

Name (2MASS)	I^a (mag)	J (mag)	$\mu_\alpha \cos\delta^b$ (mas yr^{-1})	μ_δ^b (mas yr^{-1})	Spt	X-ray^c log(f_x)	Hα^d (Å)	Li^e (m Å)	$v_{rad}^{meas\,f}$ (km s^{-1})	$v_{rad}^{pred\,g}$ (km s^{-1})	d_π^h (pc)	d_s^g (pc)	P^i (%)	Refs.
J14284804-7430205	10.46±0.06	9.26±0.02	-62.20±1.60	-36.30±1.60	M1V	-12.01	4.8	...	...	-3.4±1.7	...	76±3	97.0^j	18
J14563812-6623419	11.76±0.05	10.40±0.03	-60.90±5.20^y	-40.40±5.20^y	M1.5V	-12.34	-0.8	...	...	-6.3±1.7	...	73±3	95.3^j	18
J15163224-5855237	10.05±0.05	9.10±0.03	-42.80±3.40^y	-44.20±3.20^y	K7V	-11.92	1.9	...	...	-9.1±1.6	...	77±3	98.5	18
J15553178-3512028	10.66±0.00^f	8.93±0.02	-226.00±3.00^y	156.00±2.00^y	M4+M7	-11.87	8.1	...	-15.5±0.7^{uu}	-17.6±1.2	...	13±1	99.9	18
J17115853-2530585	11.12±0.06	9.90±0.02	-15.10±2.50	-34.00±2.70	M1V	-12.11	3.1	...	...	-21.9±1.3	...	65±7	92.1	18
J18083702-0426259	6.78±0.03^n	5.77±0.03	-8.40±1.10^y	-16.10±0.70^y	K5V	-11.92	-0.9	...	...	-25.2±1.4	167.5±29.5	19±3	99.9^j	18
J18202275-1011131	8.67±0.00^f	7.64±0.02	10.51±5.95^n	-33.91±4.03^n	K5Ve+K7Ve	-11.67	9.8	530^k	-13.8±0.6^k	-24.8±1.4	...	34±4	99.5	18
J18450097-1409053	10.25±0.06	8.47±0.04	46.00±6.00^y	-84.00±13.00^y	M5V	-11.74	8.8	...	...	-24.1±1.4	...	16±2	95.5^j	18
J19224278-0515536	11.36±0.06	9.92±0.02	30.90±5.20	-15.60±5.20^y	K5V	-12.10	-1.0	...	...	-23.8±1.5	...	50±5	99.3^j	18
J19432464-3722108	10.73±0.06	9.20±0.03	172.00±8.00^y	-182.00±15.00^y	M3.5+M6.0	-12.21	8.2	...	...	-18.1±1.2	...	13±1	98.8	18
J19435432-0546363	11.21±0.06	9.74±0.02	66.00±3.00^y	14.00±3.00^y	M4V	-12.10	5.7	...	...	-22.9±1.5	...	32±2	90.5	18
J20163382-0711456	9.76±0.07	8.59±0.03	84.60±8.10	-0.60±23.60	M0V+M2V	-12.35	1.7	...	...	-21.2±1.5	...	33±2	95.8	18
J20515256-3046329	11.41±0.06	10.11±0.02	104.00±1.00	-48.30±1.00	M1.5V	-12.55	2.3	...	...	-16.1±1.1	...	34±1	92.9	18
J20531465-0221218	10.65±0.06	9.33±0.02	189.40±4.10^y	15.10±4.10^y	M3+M4	-12.36	3.1	...	-39.9±1.1^{uu}	-18.9±1.5	37.9±5.7^{uu}	18±1	90.2	18
J21342935-1840372	11.72±0.06	10.05±0.02	79.00±1.80	-11.40±2.10	M4V	-12.40	10.5	...	...	-14.7±1.2	...	51±2	93.7^j	18
J22174316-1546452	12.39±0.06	10.79±0.02	110.00±0.00^y	-14.00±2.00^y	M4V	-12.52	7.5	...	...	-11.1±1.1	...	42±2	98.4	18
J22274882-0113527	11.06±0.17^v	9.48±0.02	170.10±5.40	-20.70±10.90	M3.5V	-12.20	5.2	...	...	-10.7±1.3	...	27±1	99.9^j	18
J22332264-0936537	10.08±0.06	8.53±0.02	148.00±1.80	4.90±1.30	M3+M3	-11.61	6.1	...	-4.4±1.4^{uu}	-9.9±1.1	...	32±1	99.9^j	18
J22371494-2622332	10.60±0.06	9.16±0.03	145.30±1.50	-12.80±1.50	M3.5V	-11.77	7.1	...	...	-8.5±0.9	...	33±1	99.2^j	18
J22505766-0147373	10.87±0.00^f	9.35±0.02	171.90±4.30^y	27.90±4.30^y	M4+M4	-12.13	6.7	...	-7.2±0.4^{uu}	-5.1±1.1	41.0±2.7^{uu}	29±1	92.8^j	18
J23331860-2714219	10.89±0.17^y	9.35±0.02	343.20±5.50^{cc}	22.10±5.50^{cc}	M3V	-12.37	2.6	...	...	-3.6±1.7	...	15±1	99.3	18
J23332198-1240072	11.84±0.00^f	10.28±0.02	164.20±4.50^y	9.00±4.40^y	K5V	-12.28	-1.1	...	...	-3.6±0.9	...	31±1	98.6	18
J23532520-7056410	10.34±0.05	8.68±0.02	306.70±8.80^{aa}	46.35±8.80^{aa}	M3.5V	-12.22	4.8	...	0.6±2.4^{kk}	0.0±1.3	...	17±1	92.2^j	18
J23555512-1321238	10.72±0.00^f	9.26±0.02	308.80±4.40^y	12.50±4.40^y	M2.5V	-12.41	7.4	...	-9.0±2.8^{kk}	-1.1±0.8	...	18±1	97.3	18
J23572056-1258487	10.18±0.00^f	8.64±0.02	201.40±4.50^y	17.40±4.50^y	M4V	-11.76	4.3	...	17.4±0.0^{ll}	-1.0±0.8	...	25±1	99.9^j	18
J23581366-1724338	9.62±0.00^f	8.31±0.02	221.20±4.20^y	15.40±4.20^y	M2+M2	-11.68	4.8	...	-8.7±1.8^{uu}	-0.8±0.7	39.1±5.3^{uu}	24±1	99.2	18
AB Doradus moving group														
J00340843-2523498	9.37±0.17^v	8.48±0.03	83.40±1.60	-98.20±1.40	K7Ve*	-11.90	2.1^{oo}	...	-12.4±2.0^{oo}	-8.1±1.7	...	50±2	98.9	11
J01034210-4051158	10.50±0.00^u	9.37±0.04	118.60±4.00^y	-162.30±4.00^y	M2.6+M3.8	-11.50	1.9	...	-10.9±0.4^{uu}	-11.6±1.5	29.9±2.0^{uu}	33±1	65.7	14,17
J01123504+1703557	11.74±0.17^v	10.21±0.02	92.00±1.00^y	-98.00±1.00^y	M3V	-12.31	5.7	...	...	-1.6±1.8	...	48±2	96.9^j	18
J01132958-0738088	10.39±0.05	9.36±0.02	69.40±1.20	-67.40±1.20	K7V+M5.5	-12.03	2.1	...	...	8.6±2.1	...	64±2	97.0	18
J01225093-2439505	11.48±0.06	10.08±0.03	120.10±2.60	-121.50±1.70	M3.5V	-12.46	9.7	...	...	15.5±2.1	...	33±1	99.9	18
J01372322-2657119	9.26±0.17^v	8.43±0.02	116.70±1.10^y	-129.20±0.70^y	K5Ve	-11.70	...	...	-5.9±3.0^{oo}	-3.7±1.7	...	37±1	98.1	11
J02523096-1548357	12.21±0.17^v	10.54±0.02	78.00±3.00^y	-92.00±3.00^y	M2.5V	-12.64	4.0	...	...	19.4±2.0	...	42±2	99.9^j	18
J02545247-0709255	11.46±0.07	10.00±0.03	44.00±2.00^y	-62.00±4.00^y	M3V	-12.37	3.5	...	...	16.6±1.9	...	71±4	95.2^j	18
J04084031-2705473	12.42±0.06	10.81±0.02	52.00±1.90	-96.00±1.40	M4V	-12.32	3.6	...	...	26.7±1.8	...	30±2	99.9	18
J04093930-2648489	10.65±0.06	9.51±0.03	47.20±0.90	-77.80±0.90	M1.5V	-12.11	2.8	...	...	26.7±1.8	...	37±3	98.1	18
J04141730-0906544	11.09±0.05	9.63±0.02	96.00±6.00^y	-138.00±3.00^y	M3.5V	-11.80	6.1	...	23.4±0.3^{uu}	21.8±1.7	23.8±1.4^{uu}	28±1	99.2	17
J04355618-2527347	9.74±0.00^f	8.24±0.02	78.40±7.00	-182.40±9.90	M3.5V	-11.79	5.2	78^{hh}	...	27.4±1.7	...	15±1	99.9^j	18
J04424932-1452268	11.71±0.06	10.24±0.03	42.00±3.00^y	-132.00±3.00^y	M4V	-12.24	14.8	...	...	24.9±1.7	...	29±2	99.9	18
J04514615-2400087	11.87±0.06	10.56±0.03	41.80±1.20	-56.90±1.50	M3V	-12.29	7.3	...	...	27.6±1.7	...	45±4	98.9	18
J04522441-1649219	9.10±0.00^f	7.74±0.02	123.40±3.40^y	-210.60±3.50^y	M3Ve*	-11.51	6.3	20^{ii}	26.7±1.5^{oo}	25.7±1.6	16.3±0.4^{uu}	16±1	99.9^j	7,11,17

Table 2.VI — continued

Name (2MASS)	I (mag)	J (mag)	$\mu_\alpha \cos\delta$ (mas yr^{-1})	μ_δ (mas yr^{-1})	Spt	X-ray log(f_x)	Hα (Å)	Li (m Å)	v_{rad}^{meas} (km s^{-1})	v_{rad}^{pred} (km s^{-1})	d_π (pc)	d_s (pc)	P (%)	Refs.
J04554034-1917553	10.91±0.05	9.78±0.02	21.80±1.60	-66.10±1.60	M0.5V	-12.20	4.4	...	...	26.5±1.6	...	49±4	98.3	18
J04571728-0621564	10.55±0.05	9.51±0.02	18.00±2.00[y]	-92.00±5.00[y]	M0.5V	-12.33	3.1	...	23.2±0.6[o]	22.5±1.6	...	49±3	96.2	18
J05130132-7027418	10.77±0.05	9.21±0.03	127.30±12.50[z]	246.00±12.50[z]	M3.5+M5.5	-11.96	7.9	...	...	28.7±1.6	...	10±1	91.6	18
J05254166-0909123	9.91±0.00[t]	8.45±0.03	39.90±4.60[y]	-189.70±4.60[y]	M3.5+M4	-11.82	3.3	...	28.4±0.5[uu]	24.1±1.5	20.7±2.2[uu]	21±1	99.9[j]	18,17
J05531299-4505119	9.67±0.00[k]	8.60±0.03	32.80±1.40[y]	-4.90±1.40[y]	M0.5V	-11.94	1.4	140[l]	31.7±0.6[k]	31.3±1.6	...	34±4	98.7	18
J06021455-1634494	10.07±0.05	8.99±0.03	-6.80±1.60	-64.60±1.30	M0V	-12.09	2.2	...	...	26.9±1.5	...	50±4	97.7	18
J06091922-3549311	9.35±0.06	7.92±0.02	-5.60±0.90	-56.60±0.90	M0.5V+L4	-11.56	3.4	10[k]	31.4±0.4[k]	30.7±1.5	21.3±1.4[yy]	22±4	99.9[j]	7,16,17
J06373215-2823125	10.89±0.07	9.60±0.02	-20.80±2.00	-47.20±2.00	M2.5V	-12.38	3.5	...	...	29.5±1.4	...	42±5	99.0	18
J07115917-3510157	0.96±0.05	9.63±0.02	-28.60±1.20	-57.90±1.60	M3V+M3V	-12.14	4.8	...	...	30.1±1.4	...	29±4	99.9	18
J10121768-0344441	7.08±0.00[n]	5.89±0.02	-152.90±1.30[y]	-242.90±1.00[y]	M1.5V	-12.51	-0.4	...	9.0±1.4[jj]	12.1±1.7	7.9±0.1	19±1	87.0[j]	18
J11254754-4410267	11.91±0.05	10.34±0.03	-84.50±2.70	-57.70±7.70	M4+M4.5	-11.74	10.7	-30[xx]	19.5±2.0[xx]	19.2±1.4	...	49±3	54.4[j]	13
J12194808+5246450	9.25±0.17[v]	8.28±0.02	-169.94±1.90[n]	-121.50±1.79[n]	K7V	-12.36	0.0	...	-4.9±1.2[qq]	-18.9±2.0	28.0±1.7	25±1	95.0	14
J12383713-2703348	10.07±0.05	8.73±0.04	-172.00±3.00[y]	-188.00±6.00[y]	M2.5V	-12.06	3.1	...	...	8.4±1.7	...	25±1	99.3	18
J12574030-3513306	8.84±0.02[n]	7.40±0.02	-264.16±2.95[n]	-176.16±2.26[n]	M4V	-11.22	1.4[ll]	...	-9.5±0.6[ss]	-16.8±2.1	19.3±1.1	17±1	99.9[j]	14
J13545390-7121476	9.80±0.06	8.55±0.02	-165.00±6.50	-132.70±6.80	M2.5V	-12.02	3.3	...	...	19.1±1.4	...	24±1	91.0	18
J14190331+6451463	11.98±0.17[v]	10.39±0.02	-104.00±2.00[y]	12.00±2.00[y]	M3V	-12.43	11.2	...	...	-25.8±1.9	...	35±2	98.3[j]	18
J15244849-4929473	9.45±0.06	8.16±0.03	-121.10±3.00[y]	-238.90±2.70[y]	M2V	-12.49	0.5	...	6.7±0.9[o]	7.5±1.4	...	23±1	95.1[j]	18
J15594729+4403595	9.76±0.17[v]	8.51±0.02	-71.90±0.90[y]	-11.20±1.10[y]	M1V	-11.83	3.3	...	...	-28.9±1.8	...	33±4	92.8[j]	18
J16074132-1103073	11.29±0.06	9.82±0.02	-64.00±4.00[y]	-148.00±5.00[y]	M4V	-12.45	7.1	...	...	-13.3±1.6	...	36±2	98.4[j]	18
J16232165+6149149	11.62±0.17[v]	10.06±0.02	-42.00±3.00[y]	54.00±2.00[y]	M2.5+M3.5	-12.32	5.6	...	...	-29.4±1.7	...	28±4	93.9	18
J17520294+5636278	10.73±0.17[v]	9.23±0.02	-50.00±2.00[y]	56.00±2.00[y]	M3.5V	-12.25	...	...	...	-31.0±1.6	...	16±3	99.9	18
J18553176-1622495	10.26±0.06	9.13±0.03	32.60±4.70	-175.60±4.70	M0.5V	-12.21	4.2	...	...	-13.4±1.4	...	34±1	98.5	18
J19420065-2104051	10.31±0.00[t]	8.69±0.02	48.00±1.00[y]	-276.00±1.00[y]	M3.5V	-12.45	2.6	...	...	-9.9±1.5	...	21±1	97.4[j]	18
J20220177-3653014	12.31±0.06	10.71±0.02	72.00±13.00[y]	-188.00±29.00[y]	M4.5V	-12.48	5.8	...	...	-0.3±1.7	...	33±1	99.4	18
J20223306-2927499	11.81±0.06	10.41±0.02	32.00±2.00[y]	-104.00±1.00[y]	M3.5V	-12.30	9.4	...	...	-4.1±1.6	...	58±2	95.6[j]	18
J20465795-0259320	10.15±0.05	9.12±0.03	59.10±2.40	-108.40±2.40	M0V	-12.22	1.6	...	-13.8±0.9[o]	-15.3±1.6	...	47±2	99.2	18
J21130526-1729126	9.22±0.00[k]	8.35±0.03	74.40±0.80	-145.10±0.80	K6Ve	-12.07	0.1[k]	20[k]	-7.4±0.6[k]	-7.2±1.7	...	39±1	99.9	7
J21521039+0537356	9.75±0.00[w]	8.25±0.03	119.17±7.95[n]	-150.29±4.89[n]	M2Ve*	-11.68	4.2[hh]	10[dd]	-15.1±1.5[uu]	-14.3±1.7	30.5±5.3	28±1	91.1[j]	7,17
J23320018-3917368	10.28±0.06	8.90±0.03	189.50±4.20	-183.70±7.90	M3V	-11.63	5.7	...	11.6±0.7[o]	11.9±2.1	...	23±1	99.9	18
J23513366-3127229	11.35±0.17[v]	9.82±0.02	108.00±1.00[y]	-84.00±1.00[y]	M2V+L0	-12.18	3.2	78[hh]	-13.5±0.6[tt]	-13.8±1.6	...	42±2	95.1[j]	15
Ambiguous candidate members														
J00281434-3227556	11.86±0.06[o]	10.12±0.02	108.00±3.80	-42.60±2.10	M5V	-12.30	10.6	...	...	...	...	...	...	18
J00551501+3015156	11.43±0.17[v]	10.05±0.02	74.00±3.00[y]	-36.00±2.00[y]	M2V	-12.28	3.6	...	...	...	...	...	...	18
J01071194-1935359	9.43±0.06	8.15±0.02	63.10±1.20	-39.80±1.20	M0.5V+M2.5	-11.58	2.9	302[ff]	11.5±1.4[ff]	...	...	...	...	12
J01132817-3821024	9.66±0.07[o]	8.49±0.02	123.00±1.10	-38.30±1.20	M0.0+M1.0	-11.77	2.5	...	...	...	...	...	...	18
J01484087-4830519	10.42±0.06	9.19±0.03	111.20±1.20	-51.00±1.20	M1.5V	-11.96	3.1	...	...	...	...	...	...	18
J02001277-0840516	10.05±0.05	8.77±0.02	108.00±3.00[y]	-62.00±2.00[y]	M2.5V	-11.84	4.2	...	...	...	...	...	...	18
J02155892-0929121	9.80±0.06	8.43±0.03	92.00±3.00[y]	-38.00±5.00[y]	M2.5+M5+M8	-11.71	6.9	...	...	...	...	...	...	18
J02224418-6022476	10.51±0.05	8.99±0.02	136.90±1.70	-14.40±1.70	M4V	-11.53	8.1	...	...	...	...	...	...	18
J02365171-5203036	9.78±0.00[k]	8.42±0.02	102.60±0.80	0.80±0.80	M2Ve	-11.57	5.8	380[k]	16.0±0.1[k]	...	...	...	...	5
J02442137+1057411	9.31±0.04[n]	7.97±0.02	68.43±3.14[n]	-37.36±2.44[n]	M0Ve	-11.70	3.4[n]	...	...	...	34.9±3.7	...	...	8

Table 2.VI — continued

Name (2MASS)	I^a (mag)	J (mag)	$\mu_\alpha \cos\delta^b$ (mas yr^{-1})	μ_δ^b (mas yr^{-1})	Spt	X-ray^c log(f$_x$)	Hα^d (Å)	Li^e (m Å)	$v_{rad}^{\mathrm{meas}\,f}$ (km s^{-1})	$v_{rad}^{\mathrm{pred}\,g}$ (km s^{-1})	d_π^h (pc)	d_s^g (pc)	p^i (%)	Refs.
J02564708-6343027	11.32±0.06	9.86±0.03	67.40±1.70	8.80±3.80	M4V	-12.26	9.4	...	...	...	...	...	...	18
J03494535-6730350	10.85±0.05	9.85±0.02	41.60±1.00	19.50±1.00	K7V	-12.30	1.7	...	16.3±3.2^{kk}	...	...	...	...	18
J04082685-7844471	10.31±0.05	9.28±0.02	55.70±2.30	42.80±1.40	M0V	-12.13	2.7	...	...	...	...	...	...	18
J04363294-7851021	12.53±0.05	10.98±0.02	32.80±2.80	47.40±2.70	M4V	-12.19	14.1	...	...	...	...	...	...	18
J04365738-1613065	10.53±0.06	9.12±0.03	70.00±5.00^y	-26.00±4.00^y	M3.5V	-11.54	5.1	...	...	...	...	...	...	18
J05090356-4209199	11.01±0.06	9.58±0.02	27.90±1.70	58.80±2.20	M3.5V	-12.16	8.2	...	...	...	...	...	...	18
J05142736-1514514	12.05±0.05	10.71±0.04	36.00±6.00^y	-16.00±2.00^y	M3.5V	-12.14	9.7	...	...	...	...	...	...	18
J05142878-1514546	12.44±0.06	10.95±0.02	34.10±8.10^y	-14.20±8.00^y	M3.5V	-12.14	5.7	...	...	...	...	...	...	18
J05195582-1124568	11.71±0.06	10.10±0.02	24.00±3.00^y	-20.00±3.00^y	M3V	-12.19	9.0	...	...	...	...	...	...	18
J05240991-4223054	11.74±0.06	10.58±0.02	4.90±1.90	-13.30±2.50	M0.5V	-12.34	2.8	...	...	...	...	...	...	18
J05301858-5358483	9.72±0.06	7.91±0.02	207.50±9.00^y	387.10±9.00^y	M3+M6+M4	-11.68	3.9	...	...	...	...	...	...	18
J05381615-6923321	10.14±0.06	8.96±0.02	65.50±4.40	108.90±4.40	M0.5V	-11.58	2.9	...	...	...	...	...	...	18
J05392505-4245211	10.72±0.06	9.45±0.02	40.60±1.20	15.90±3.00	M2V	-11.91	3.5	...	...	...	...	...	...	18
J05471788-2856130	11.60±0.06	10.08±0.02	17.20±3.30	30.20±2.20	M3.5V	-12.09	8.2	...	...	...	...	...	...	18
J06153953-8433115	10.60±0.05	9.25±0.03	-32.20±1.40	107.00±1.30	M3V	-12.00	5.1	...	...	...	...	...	...	18
J06262932-0739540	11.18±0.06	9.93±0.02	9.30±7.90	-17.80±7.80	M1V+M2V	-12.30	4.7	...	...	...	...	...	...	18
J06434532-6424396	10.67±0.09	9.29±0.02	2.30±2.40	54.50±2.40	M4+M3+M5	-11.97	6.3	...	...	...	...	...	...	18
J06475229-2523304	9.79±0.06	8.35±0.02	22.40±1.10^y	-70.30±1.30^y	K7V	-11.68	1.1	60^k	-56.5±0.0^k	...	...	...	...	18
J07170438-6311123	11.02±0.06	9.73±0.02	-13.10±1.50	48.00±1.40	M2V	-12.39	3.8	...	...	...	...	...	...	18
J07310129-4600266	11.64±0.17^v	9.95±0.02	-12.00±4.00^y	-98.00±2.00^y	M4V	-11.96	...	...	...	...	...	...	...	18
J07504838-2931126	11.37±0.06	9.83±0.02	-82.10±1.70	24.50±3.30	M4V	-11.56	22.1	...	...	...	...	...	...	18
J08224744-5726530	10.29±0.06	8.63±0.02	-481.40±9.00^y	159.00±9.00^y	M4.5+>L0	-11.97	7.3	...	...	...	...	...	...	18
J08412528-5736021	10.94±0.05	9.58±0.03	-20.70±3.70	26.50±2.00	M3V+M3V	-11.95	9.4	...	...	...	...	...	...	18
J08465879-7246588	9.53±0.06	8.49±0.02	-73.20±0.90	55.80±1.00	K7V	-12.25	1.7	20^k	...	...	...	...	...	18
J09032434-6348330	10.77±0.06	9.57±0.03	-34.50±1.40	35.40±1.40	M0.5V	-12.09	2.9	...	...	...	...	...	...	18
J09315840-6209258	11.42±0.06	9.95±0.02	-38.40±4.20	18.60±2.80	M3.5V	-11.96	9.1	...	-6.0±0.0^k	...	...	...	...	18
J09353126-2802552	9.85±0.06	8.51±0.02	-49.40±0.60	-57.40±0.70	K7V	-11.68	2.1	20^k	1.5±0.0^k	...	...	...	...	18
J11091606-7352465	11.22±0.06	9.86±0.03	-53.30±1.90	10.30±1.90	M3V	-12.10	6.2	...	...	...	...	...	...	18
J11455177-5520456	9.03±0.06	8.02±0.03	-97.70±1.60^y	-5.80±1.50^y	K5Ve	-11.44	0.4^k	190^k	16.1±0.0^k	...	...	...	...	7
J12103101-7507205	12.70±0.06	11.19±0.03	-66.50±3.50	-5.80±7.70	M4V	-12.54	8.4	...	...	...	...	...	...	18
J12170465-5743558	9.69±0.06	8.71±0.02	-92.70±1.30^y	-12.30±1.30^y	K7V	-11.63	1.4	160^k	-1.6±0.0^k	...	...	...	...	18
J12242443-5339088	12.17±0.05	10.51±0.02	-180.00±2.00^y	-60.00±4.00^y	M5V	-12.34	9.8	...	...	...	...	...	...	18
J13213722-4421518	10.99±0.06	9.74±0.02	-34.90±3.50	-18.80±3.50	M0.5V	-12.20	4.5	464	6.9±3.0^q	...	...	...	...	5
J17165072-3007104	11.78±0.06	10.37±0.03	-8.00±3.00^y	-36.00±2.00^y	M2.5V	-12.24	7.1	...	...	...	...	...	...	18
J17243644-3152484	10.06±0.06	9.00±0.02	-7.00±1.30	-34.60±1.60	K7V	-11.97	2.2	...	...	...	...	...	...	18
J17261525-0311308	11.99±0.06	10.38±0.02	-29.70±9.00^y	-112.10±9.00^y	M4.5V	-12.40	11.1	...	...	...	...	...	...	18
J17275761-4016243	11.65±0.06	10.04±0.02	-13.10±3.30	-50.40±3.30	M4V	-12.36	6.8	...	...	...	...	...	...	18
J17300060-1840132	11.33±0.06	9.92±0.02	-8.10±2.80	-39.30±9.00	M3.5V	-12.29	5.2	...	...	...	...	...	...	18
J17580616-2222238	11.04±0.06	9.72±0.02	-5.90±3.00	-44.10±2.30	M1V	-12.23	5.1	...	...	...	...	...	...	18
J18141047-3247344	9.16±0.07	8.07±0.02	3.30±1.70	-52.00±1.30	K6Ve(sb2)	-11.66	60.0^{gg}	440^{ii}	...	...	...	...	...	6
J20072376-5147272	9.07±0.00^k	8.16±0.02	86.90±0.70	-145.30±1.10	K6Ve	-11.39	1.0^k	60^k	-13.3±0.0^k	...	...	...	...	7
J21334415-3453372	11.47±0.06	10.24±0.02	40.40±1.30	-72.50±1.30	M1.5V	-12.35	5.6	...	...	...	...	...	...	18

Table 2.VI — continued

Name (2MASS)	I^a (mag)	J (mag)	$\mu_\alpha \cos\delta^b$ (mas yr⁻¹)	μ_δ^b (mas yr⁻¹)	Spt	X-ray^c log(f$_x$)	Hα^d (Å)	Li^e (m Å)	$v_{rad}^{meas\,f}$ (km s⁻¹)	$v_{rad}^{pred\,g}$ (km s⁻¹)	d_π^h (pc)	d_k^g (pc)	P^i (%)	Refs.
J21464282-8543046	10.43±0.05	8.84±0.02	184.00±5.00^y	−212.00±32.00^y	M3.5V	−11.67	12.7	...	...	...	...	...	...	18
J22294830-4858285	12.74±0.06	11.21±0.02	111.90±3.00	−64.10±3.00	M4.5V	−12.46	5.8	...	...	...	...	...	...	18
J22440873-5413183	10.71±0.06	9.36±0.03	70.90±9.10	−60.10±8.30	M4V	−11.97	6.1	...	−7.7±4.7^{kk}	...	...	...	...	18
J22470872-6920447	9.79±0.06	8.89±0.02	71.90±1.40	−59.90±1.40	K6Ve	−12.32	0.1^k	0^k	−2.2±0.0^k	...	...	...	...	11
J23495365+2427493	11.53±0.17^v	9.90±0.02	130.00±6.00^y	−40.00±3.00^y	M3.5+M4.5	−12.28	4.7	...	...	...	...	...	...	18
Other previously-proposed candidate members														
J00233468+2014282	9.05±0.17^v	8.14±0.02	61.40±1.80	−38.30±2.00	K7.5V	−11.87	0.7^{nn}	...	...	−5.0±1.5^{nn}	...	...	...	8
J09361593+3731456	9.03±0.17^v	8.09±0.02	−99.44±2.45^n	−89.51±1.42^n	M2+M2	−12.26	...	...	−2.5±1.0^{ww}	...	33.7±2.6	...	...	14
J12151838-0237283	9.82±0.06	8.67±0.03	−86.00±2.90	−113.00±1.90	M0Ve	−12.18	1.5^{oo}	...	1.4±4.6^{kk}	...	...	...	...	11
J12210499-7116493	10.09±0.06	9.09±0.02	−44.20±1.60	−12.40±1.60	K7V	−11.82	2.1	550^{ff}	8.1±0.6^{ff}	...	...	...	...	12
J12342047-4815195	11.81±0.00^p	10.49±0.04	95.60±9.00^y	95.60±9.00^y	M2V	−11.91	10.5^p	484	10.0±1.7^{ee}	...	...	...	...	5
J12342064-4815135	11.94±0.00^p	10.56±0.03	68.10±9.00^y	95.60±9.00^y	M1.5V	−11.91	9.0^p	494	11.2±2.0^q	...	...	...	...	5
J16430128-1754274	10.61±0.06	9.44±0.03	−27.80±1.40	−52.40±1.50	M0.5V	−12.09	3.2	300^{ff}	−11.3±3.5^{kk}	...	...	...	...	12
J22424884+1330532	9.30±0.17^v	8.63±0.02	73.70±1.80^v	−41.20±2.00^y	K5Ve*	−11.76	1.5^{oo}	...	−14.9±1.5^{oo}	...	...	...	...	11

^{a} I_c magnitude from *DENIS* catalog (Epchtein et al., 1997), unless stated otherwise.

^{b} Proper motion from *UCAC3* catalog (Zacharias et al., 2009), unless stated otherwise.

^{c} ROSAT X-ray flux calculated from Riaz et al. (see Section 5.4; 2006) in erg s⁻¹ cm⁻².

^{d} Hα EW from Riaz et al. (2006), unless stated otherwise.

^{e} Lithium EW from Mentuch et al. (2008), unless stated otherwise. Negative value means lower limit on the Lithium EW.

^{f} Radial velocity measurement from Montes et al. (2001), unless stated otherwise.

^{g} Radial velocity and statistical distance derived by our analysis (see Section 4.5).

^{h} Trigonometric distance from van Leeuwen (2007), unless stated otherwise.

^{i} Membership probability without considering the RV or parallax information (see Section 4.5).

^{j} Membership probability for which the binary hypothesis is higher.

References. — (1) Kastner et al., 1997 ; (2) Webb et al., 1999 ; (3) Torres et al., 2000 ; (4) Zuckerman et al., 2001b ; (5) Zuckerman & Song, 2004 ; (6) Torres et al., 2006 ; (7) Torres et al., 2008 ; (8) Lépine & Simon, 2009 ; (9) Ortega et al., 2009 ; (10) Looper et al., 2010 ; (11) Schlieder et al., 2010 ; (12) Kiss et al., 2011 ; (13) Rodriguez et al., 2011 ; (14) Schlieder et al., 2012a ; (15) Bowler et al., 2012 ; (16) Wahhaj et al., 2011 ; (17) Shkolnik et al., 2012 ; (18) this work.

Note. — (k) Torres et al., 2006 ; (l) magnitude without binary correction; Torres et al., 2006 ; (n) van Leeuwen, 2007 ; (o) this work; (p) Zuckerman et al., 2001c ; (q) Reid et al., 2003 ; (r) Reid & Cruz, 2002 ; (s) Koen et al., 2010 ; (t) Casagrande et al., 2008 ; (u) Reid et al., 2004 ; (v) SDSS-DR8; Adelman-McCarthy & et al., 2011 ; (w) Weis, 1991 ; (x) Koen et al., 2002 ; (y) NOMAD; Zacharias et al., 2005 ; (z) PPMXL; Roeser et al., 2010 ; (aa) PPMX; Roeser et al., 2008 ; (bb) Looper et al., 2010 ; (cc) Salim & Gould, 2003 ; (dd) Zickgraf et al., 2005 ; (ee) Shkolnik et al., 2011 ; (ff) Kiss et al., 2011 ; (gg) Herbig & Bell, 1988 ; (hh) Shkolnik et al., 2009 ; (ii) da Silva et al., 2009 ; (jj) Kharchenko et al., 2007 ; (kk) RAVE; Zwitter et al., 2008 ; (ll) Gizis et al., 2002 ; (mm) Hipparcos; Anderson & Francis, 2012 ; (nn) Lépine & Simon, 2009 ; (oo) Schlieder et al., 2010 ; (pp) Jayawardhana et al., 2006 ; (qq) Upgren & Harlow, 1996 ; (rr) Hawley et al., 1996 ; (ss) Schlieder et al., 2012a ; (tt) Bowler et al., 2012 ; (uu) Shkolnik et al., 2012 ; (vv) Riedel (inprep); (ww) Schlieder et al., 2012b ; (xx) Rodriguez et al., 2011 ; (yy) Wahhaj et al., 2011.

Table 2.VII.   Ambiguous candidate members
of young kinematic groups[a]

Name	Group	P (%)	d_s (pc)	v_{rad}^{pred} (km s^{-1})
J00281434-3227556	β PMG	88.7[b]	33 ± 3	8.4 ± 1.5
···	THA	10.3[b]	38 ± 2	0.4 ± 1.3
J00551501+3015156	β PMG	9.9	52 ± 4	−1.2 ± 1.6
···	COL	80.2[b]	61 ± 2	−6.1 ± 1.1
J01071194-1935359	β PMG	9.1[b]	43 ± 4	9.3 ± 1.5
···	THA	1.6[b]	52 ± 3	0.6 ± 1.3
···	COL	85.2[b]	68 ± 3	5.5 ± 0.9
J01132817-3821024	β PMG	22.2	29 ± 2	11.9 ± 1.5
···	THA	58.6	36 ± 2	4.7 ± 1.3
···	COL	19.0	38 ± 1	9.3 ± 0.9
J01484087-4830519	THA	77.0	38 ± 2	8.5 ± 1.4
···	ABDMG	23.0	36 ± 2	23.1 ± 2.0
J02001277-0840516	β PMG	13.4	31 ± 2	11.4 ± 1.6
···	THA	12.4	38 ± 2	3.0 ± 1.4
···	COL	74.2	40 ± 1	8.1 ± 0.9
J02155892-0929121	β PMG	35.4	34 ± 3	12.6 ± 1.7
···	THA	23.5[b]	44 ± 3	4.5 ± 1.4
···	COL	41.1[b]	48 ± 2	9.7 ± 0.9
J02224418-6022476	THA	67.4[b]	32 ± 2	11.3 ± 1.5
···	CAR	3.6[b]	29 ± 1	16.1 ± 0.4
···	ABDMG	28.9[b]	26 ± 2	25.8 ± 1.9
J02365171-5203036	β PMG	9.2	29 ± 2	16.3 ± 1.5
···	THA	62.4[b]	39 ± 2	11.5 ± 1.5
···	COL	28.3[b]	39 ± 2	15.8 ± 1.0
J02442137+1057411	β PMG	26.1[b]	46 ± 3	10.4 ± 1.8
···	THA	9.7[b]	56 ± 3	2.9 ± 1.4
···	COL	56.1[b]	63 ± 2	7.6 ± 1.0
J02564708-6343027	THA	82.9[b]	53 ± 3	12.7 ± 1.6
···	COL	1.4[b]	58 ± 3	16.2 ± 1.0
···	ABDMG	15.6[b]	47 ± 4	27.0 ± 1.8
J03494535-6730350	THA	2.1	66 ± 4	14.2 ± 1.6
···	COL	12.9	81 ± 4	17.4 ± 1.1
···	ABDMG	80.0	61 ± 6	28.1 ± 1.7
J04082685-7844471	THA	26.5	55 ± 3	13.2 ± 1.7
···	CAR	71.0	54 ± 1	17.0 ± 0.5
···	ABDMG	1.8	50 ± 4	26.3 ± 1.6
J04363294-7851021	β PMG	7.4	49 ± 5	14.3 ± 1.5
···	COL	7.2[b]	69 ± 3	15.8 ± 1.1
···	ABDMG	84.0[b]	57 ± 5	26.5 ± 1.6
J04365738-1613065	β PMG	3.0	24 ± 3	20.0 ± 1.8
···	THA	48.6[b]	47 ± 3	16.2 ± 1.5
···	COL	48.3[b]	39 ± 2	20.9 ± 1.0
J05090356-4209199	β PMG	27.3	26 ± 4	21.0 ± 1.5
···	ARG	72.5[b]	52 ± 4	18.5 ± 1.5
J05142736-1514514	THA	12.8	67 ± 5	18.3 ± 1.6
···	COL	86.6	58 ± 4	22.5 ± 1.0
J05142878-1514546	THA	11.9[b]	68 ± 6	18.3 ± 1.6
···	COL	87.1	61 ± 5	22.5 ± 1.0

Table 2.VII — continued

Name	Group	P (%)	d_s (pc)	v_{rad}^{pred} (km s^{-1})
J05195582-1124568	β PMG	24.0	39 ± 7	20.3 ± 1.8
⋯	COL	75.9 [b]	72 ± 6	22.2 ± 1.0
J05240991-4223054	ABDMG	89.4	53 ± 9	30.9 ± 1.6
J05301858-5358483	β PMG	78.4	5 ± 1	19.9 ± 1.4
⋯	COL	12.0	6 ± 1	22.2 ± 1.1
⋯	ABDMG	6.8	3 ± 1	31.0 ± 1.6
J05381615-6923321	COL	19.9	28 ± 1	19.0 ± 1.1
⋯	ABDMG	73.9	21 ± 2	29.1 ± 1.6
J05392505-4245211	THA	31.4	52 ± 5	20.1 ± 1.7
⋯	COL	68.3	41 ± 4	23.7 ± 1.1
J05471788-2856130	β PMG	86.8	24 ± 5	21.7 ± 1.6
⋯	ARG	10.0 [b]	53 ± 6	22.3 ± 1.6
J06153953-8433115	β PMG	75.7	33 ± 3	12.8 ± 1.5
⋯	ABDMG	22.8 [b]	35 ± 2	25.2 ± 1.5
J06262932-0739540	COL	89.4	81 ± 8	23.2 ± 1.1
J06434532-6424396	COL	38.2 [b]	55 ± 3	20.8 ± 1.1
⋯	CAR	54.0 [b]	52 ± 3	21.9 ± 0.5
⋯	ABDMG	7.4 [b]	33 ± 4	30.0 ± 1.5
J06475229-2523304	COL	75.2	10 ± 2	25.1 ± 1.1
⋯	ABDMG	21.5 [b]	30 ± 4	28.8 ± 1.4
J07170438-6311123	β PMG	2.1	49 ± 5	17.7 ± 1.3
⋯	COL	75.8	58 ± 4	21.0 ± 1.1
⋯	CAR	1.1	50 ± 3	22.2 ± 0.5
⋯	ABDMG	20.0	35 ± 5	29.9 ± 1.5
J07310129+4600266	COL	81.6 [b]	51 ± 2	6.0 ± 1.0
⋯	ABDMG	11.4 [b]	64 ± 2	−2.9 ± 1.6
J07504838-2931126	β PMG	75.9	23 ± 3	19.6 ± 1.5
⋯	COL	19.6	15 ± 2	24.6 ± 1.2
J08224744-5726530	β PMG	19.7	6 ± 1	17.3 ± 1.3
⋯	ABDMG	77.4	5 ± 1	29.2 ± 1.4
J08412528-5736021	COL	69.8 [b]	82 ± 5	21.0 ± 1.2
⋯	CAR	25.9 [b]	82 ± 4	22.2 ± 0.5
J08465879-7246588	β PMG	33.4	38 ± 3	14.6 ± 1.4
⋯	ABDMG	66.1	36 ± 3	27.1 ± 1.4
J09032434-6348330	COL	24.5	67 ± 3	19.4 ± 1.2
⋯	CAR	70.0	65 ± 2	20.8 ± 0.6
⋯	ARG	4.7 [b]	98 ± 4	8.5 ± 1.9
J09315840-6209258	β PMG	53.2	61 ± 7	14.8 ± 1.3
⋯	COL	19.4 [b]	78 ± 4	19.0 ± 1.2
⋯	CAR	19.6 [b]	77 ± 3	20.3 ± 0.6
J09353126-2802552	TWA	74.3	42 ± 5	17.4 ± 1.8
⋯	ABDMG	18.6 [b]	54 ± 4	22.7 ± 1.4
J11091606-7352465	β PMG	26.4	61 ± 6	11.6 ± 1.5
⋯	ARG	68.9 [b]	93 ± 4	2.3 ± 1.8
J11455177-5520456	β PMG	4.4	40 ± 3	9.4 ± 1.5
⋯	TWA	55.1	46 ± 4	12.0 ± 2.1
⋯	COL	29.5	45 ± 2	13.9 ± 1.2
J12103101-7507205	β PMG	18.4	57 ± 5	10.3 ± 1.5
⋯	ARG	77.4 [b]	75 ± 4	0.4 ± 1.8
⋯	ABDMG	2.9 [b]	64 ± 4	22.5 ± 1.4
J12170465-5743558	ARG	47.6	53 ± 3	−0.1 ± 1.8

Table 2.VII — continued

Name	Group	P (%)	d_s (pc)	v_{rad}^{pred} (km s^{-1})
J12242443-5339088	β PMG	87.9	23 ± 1	7.4 ± 1.5
...	COL	4.0	24 ± 1	11.7 ± 1.1
...	ABDMG	3.8	26 ± 1	18.1 ± 1.4
J13213722-4421518	TWA	57.1	60 ± 5	6.1 ± 2.8
J17165072-3007104	β PMG	70.2 [b]	102 ± 7	−10.4 ± 2.1
...	ARG	23.5 [b]	69 ± 7	−21.1 ± 1.3
J17243644-3152484	β PMG	53.5 [b]	107 ± 7	−9.9 ± 2.1
...	ARG	37.7 [b]	74 ± 7	−20.8 ± 1.3
J17261525-0311308	β PMG	24.6	23 ± 2	−17.9 ± 2.0
...	ABDMG	73.8 [b]	43 ± 2	−19.4 ± 1.5
J17275761-4016243	β PMG	35.1 [b]	80 ± 5	−7.0 ± 2.0
...	ARG	64.8 [b]	62 ± 5	−18.7 ± 1.4
J17300060-1840132	β PMG	12.8 [b]	80 ± 6	−14.0 ± 2.0
...	ARG	85.7	45 ± 7	−23.5 ± 1.3
J17580616-2222238	β PMG	12.6 [b]	78 ± 6	−13.0 ± 2.1
...	ARG	87.1	45 ± 6	−23.2 ± 1.3
J18141047-3247344	β PMG	61.3 [b]	76 ± 5	−9.6 ± 2.1
...	ARG	38.6 [b]	52 ± 6	−21.0 ± 1.3
J20072376-5147272	ARG	17.9	31 ± 1	−13.1 ± 1.2
J21334415-3453372	THA	74.1	52 ± 3	−8.3 ± 1.4
...	ABDMG	18.7 [b]	76 ± 3	2.3 ± 1.8
J21464282-8543046	β PMG	1.8	13 ± 1	10.3 ± 1.6
...	COL	21.4	17 ± 1	11.3 ± 1.1
...	ABDMG	76.6 [b]	16 ± 1	22.3 ± 1.6
J22294830-4858285	β PMG	71.7	36 ± 2	4.0 ± 1.7
...	ARG	22.0	41 ± 2	−6.5 ± 0.9
J22440873-5413183	β PMG	9.1	42 ± 3	5.8 ± 1.7
...	THA	83.5 [b]	48 ± 3	0.7 ± 1.4
...	ABDMG	6.8 [b]	62 ± 3	14.2 ± 1.9
J22470872-6920447	THA	53.3	50 ± 3	5.4 ± 1.5
...	ABDMG	45.8	55 ± 3	19.1 ± 1.8
J23495365+2427493	β PMG	81.7	32 ± 2	−4.8 ± 1.4
...	COL	16.1 [b]	35 ± 1	−10.6 ± 1.1

[a]Membership probability without considering the RV or parallax information (P).

[b]Membership probability (P) for which the binary hypothesis has a higher probability.

Table 2.VIII.   Membership probabilities of all candidates[a]

Name	βPMG P	P_ν	P_{ν+π}	TWA P	P_ν	P_{ν+π}	THA P	P_ν	P_{ν+π}	COL P	P_ν	P_{ν+π}	CAR P	P_ν	P_{ν+π}	ARG P	P_ν	P_{ν+π}	ABDMG P	P_ν	P_{ν+π}	Field P	P_ν	P_{ν+π}
J00171443-7032021	0.0	...	...	0.0	...	...	99.2^b	...	...	0.0	...	...	0.0	...	...	0.0	...	...	0.5	...	...	0.3	...	...
J00172353-6645124	99.9	99.9	...	0.0	0.0	...	0.0	0.0	...	0.0	0.0	...	0.0	0.0	...	0.4	0.0	...	0.1	0.0	...	0.0	0.0	...
J00233468+2014282	20.9	10.3	...	0.0	0.0	...	0.0	0.0	...	18.1^b	35.0^b	...	0.0	0.0	...	0.0	0.0	...	0.0	0.0	...	61.1	54.7	...
J00281434-3227556	88.7^b	...	...	0.0	...	...	10.3^b	...	...	0.9	0.0	...	0.0	...	...	0.0	...	...	0.0	...	...	0.1	...	...
J00340843+2523498	0.0	0.0	...	0.0	0.0	...	0.9	0.0	...	0.0	0.0	...	0.0	0.0	...	0.0	0.0	...	98.9	97.7	...	1.1	2.3	...
J00503319+2449009	0.0	0.0	0.0	0.0	0.0	0.0	0.0	0.0	0.0	0.0	0.0	0.0	0.0	0.0	0.0	99.9^b	99.9^b	0.0	0.0	...	0.0	0.3	0.1	99.9
J00551501+3015156	9.9	...	...	0.0	...	...	0.0	...	...	80.2^b	...	...	0.0	...	...	0.0	...	...	0.0	...	...	9.8	...	...
J01034210+4051158	0.0	0.0	0.0	0.0	0.0	0.0	0.0	0.0	0.0	0.0	0.0	0.0	0.0	0.0	0.0	0.0	0.0	0.0	65.7	95.6	96.7	34.3	4.4	3.3
J01071194-1935359	9.1^b	85.2^b	...	0.0	0.0	...	1.6	0.0	...	85.2^b	0.0	...	0.0	0.0	...	0.0	0.0	...	0.0	0.0	...	4.1	14.8	...
J01112542+1526214	99.9^b	99.9^b	99.9^b	0.0	0.0	0.0	0.0	0.0	0.0	0.1	0.0	0.0	0.0	0.0	0.0	0.0	0.0	0.0	0.0	0.0	0.0	0.0	0.0	0.0
J01122504+1703557	2.9	...	...	0.0	...	...	0.0	...	...	0.0	...	...	0.0	...	...	0.0	...	...	96.9^b	...	...	0.2	...	...
J01132817-3821024	22.2	...	...	0.0	...	...	58.6	...	...	19.0	...	...	0.0	...	...	0.0	...	...	0.0	...	...	0.2	...	...
J01132958-0738088	0.0	...	...	0.0	...	...	0.0	...	...	0.0	...	...	0.0	...	...	0.0	...	...	97.0	...	...	3.0	...	...
J01220441-3337036	0.1	0.0	...	0.0	0.0	...	98.3	99.9	...	1.0	0.0	...	0.0	0.0	...	0.0	0.0	...	0.6	0.0	...	0.1	0.0	...
J01225093-2439505	0.0	...	...	0.0	...	...	0.0	...	...	0.0	...	...	0.0	...	...	0.0	...	...	99.9	...	...	0.1	...	...
J01351393-0712517	33.2^b	99.9^b	99.9^b	0.0	0.0	0.0	6.0^b	0.0	0.0	60.8^b	0.0	0.0	0.0	0.0	0.0	0.0	0.0	0.0	0.0	0.0	0.0	0.0	0.0	0.0
J01365516-0647379	27.4	99.9	99.9	0.0	0.0	0.0	1.5	0.0	0.0	70.9	0.0	0.0	0.0	0.0	0.0	0.0	0.0	0.0	0.0	0.0	0.0	0.1	0.2	0.1
J01372322+2657119	1.4	0.0	...	0.0	0.0	...	0.0	0.0	...	0.0	0.0	...	0.0	0.0	...	0.0	0.0	...	98.1	99.9	...	0.5	0.1	...
J01484087-4830519	0.0	...	...	0.0	...	...	77.0	...	...	0.0	...	...	0.0	...	...	0.0	...	...	23.0	...	...	0.0	...	...
J01521830-5950168	0.0	0.0	...	0.0	0.0	...	95.3	99.9	...	0.0	0.0	...	0.0	0.0	...	0.0	0.0	...	4.6^b	0.0	...	0.2	0.0	...
J01535076-1459503	99.9^b	...	...	0.0	...	...	0.0	...	...	0.0	...	...	0.0	...	...	0.0	...	...	0.0	...	...	0.2	...	...
J02001277-0840516	13.4	...	...	0.0	...	...	12.4	...	...	74.2	...	...	0.0	...	...	0.0	...	...	0.0	...	...	0.1	...	...
J02045317-5346162	0.0	...	...	0.0	...	...	94.9^b	...	...	0.0	...	...	0.0	...	...	0.0	...	...	5.1^b	...	...	0.0	...	...
J02070176-4406380	0.1	...	...	0.0	...	...	98.9^b	...	...	0.3	...	...	0.0	...	...	0.0	...	...	0.7	...	...	0.0	...	...
J02155892-0929121	35.4	...	...	0.0	...	...	23.5^b	...	...	41.1^b	...	...	0.0	...	...	0.0	...	...	0.0	...	...	0.1	...	...
J02224418-6022476	0.1	...	...	0.0	...	...	67.4^b	...	...	0.1	...	...	3.6^b	...	...	0.0	...	...	28.9^b	...	...	0.0	...	...
J02303239-4342232	0.5	1.6	...	0.0	0.0	...	61.1	0.1	...	38.3	98.3	...	0.0	0.0	...	0.0	0.0	...	0.0	0.0	...	0.0	0.0	...
J02365171-5203036	9.2	17.6	...	0.0	0.0	...	62.4^b	1.3	...	28.3^b	81.1^b	...	0.0	0.0	...	0.0	0.0	...	0.2	0.0	...	0.0	0.0	...
J02414683-5259523	0.0	0.0	...	0.0	0.0	...	96.5^b	99.9^b	...	0.0	0.0	...	0.0	0.0	...	0.0	0.0	...	3.5^b	0.0	...	0.0	0.0	...
J02414730-5259306	0.3	0.0	...	0.0	0.0	...	94.7^b	99.9^b	...	4.2^b	0.0	...	0.0	0.0	...	0.0	0.0	...	0.8	0.0	...	0.0	0.0	...
J02423301-5739367	0.0	0.0	...	0.0	0.0	...	90.8	99.9	...	0.0	0.0	...	0.0	0.0	...	0.0	0.0	...	9.2	0.0	...	0.0	0.0	...
J02442137+1057411	26.1^b	...	0.0	0.0	...	0.0	9.7^b	...	0.0	56.1^b	...	0.0	0.0	...	0.0	0.0	...	0.0	0.0	...	0.0	8.1	...	0.0
J02523096-1548357	0.2	...	...	0.0	...	...	0.0	...	...	0.0	...	...	0.0	...	...	0.0	...	...	99.9^b	...	...	0.0	...	...
J02545247-0709255	2.9	...	...	0.0	...	...	0.0	...	...	0.0	...	...	0.0	...	...	0.0	...	...	95.2^b	...	...	1.9	...	...
J02564708-6343027	0.1	0.0	...	0.0	0.0	...	82.9^b	0.0	...	1.4	0.0	...	0.0	0.0	...	0.0	16.6	...	15.6^b	0.0	...	0.4	83.4	99.9
J03033668-2535329	0.0	0.0	0.0	0.0	0.0	0.0	0.0	0.0	0.0	0.0	0.0	0.0	0.0	0.0	0.0	99.9	99.9	0.0	0.0	0.0	0.0	0.2	0.0	...
J03050976-3725058	1.2	...	...	0.0	...	...	0.5	...	...	98.1^b	...	...	0.0	...	...	0.0	...	...	0.0	...	...	0.0	0.0	...
J03190864-3507002	0.1	0.0	...	0.0	0.0	...	84.4	99.9	...	15.4	0.0	...	0.0	0.0	...	0.0	0.0	...	0.0	0.0	...	0.0	0.0	...
J03214689-0640242	0.0	0.0	...	0.0	0.0	...	0.0	0.0	...	0.0	0.0	...	0.0	0.0	...	99.9	0.0	...	0.0	0.0	...	0.5	99.9	...

Table 2.VIII — continued

Name	βPMG P	βPMG P$_\nu$	βPMG P$_{\nu+\pi}$	TWA P	TWA P$_\nu$	TWA P$_{\nu+\pi}$	THA P	THA P$_\nu$	THA P$_{\nu+\pi}$	COL P	COL P$_\nu$	COL P$_{\nu+\pi}$	CAR P	CAR P$_\nu$	CAR P$_{\nu+\pi}$	ARG P	ARG P$_\nu$	ARG P$_{\nu+\pi}$	ABDMG P	ABDMG P$_\nu$	ABDMG P$_{\nu+\pi}$	Field P	Field P$_\nu$	Field P$_{\nu+\pi}$
J03241504-5901125	0.0	0.0	...	0.0	0.0	...	0.0	0.0	...	61.6	99.4	...	0.0	0.0	...	0.0	0.0	...	34.4	0.0	...	4.0	0.6	...
J03282609-0537361	0.1	...	...	0.0	...	...	0.1	...	...	0.0	...	...	0.0	...	...	98.4[b]	...	...	0.0	...	...	1.4	...	...
J03315564-4359135	0.0	0.0	...	0.0	0.0	...	96.3	99.9	...	3.7	0.0	...	0.0	0.0	...	0.0	0.0	...	0.0	0.0	...	0.0	0.0	...
J03320347-5139550	0.7	...	...	0.0	...	...	0.0	...	...	94.7	...	...	0.0	...	...	0.0	...	...	0.3	...	...	4.3	...	...
J03415581-5542287	0.6	...	...	0.0	...	...	0.0	...	...	0.0	...	...	0.0	...	...	98.9	...	...	0.0	...	...	0.5	...	...
J03454058-7509121	0.0	...	...	0.0	...	...	99.9[b]	...	...	0.0	...	...	0.0	...	...	0.0	...	...	0.0	...	...	0.0	...	...
J03494535-6730350	0.0	0.0	...	0.0	0.0	...	2.1	7.4	...	12.9	87.7	...	0.0	0.0	...	0.0	0.0	...	80.0	0.0	...	4.9	4.9	...
J04071148-2918342	0.4	...	...	0.0	...	...	0.1	...	...	99.4	...	...	0.0	...	...	0.0	...	...	0.0	...	...	0.0	...	...
J04082685-7844471	0.0	...	...	0.0	...	...	26.5	...	...	0.4	...	...	71.0	...	...	0.0	...	...	1.8	...	...	0.3	...	...
J04084031-2705473	0.2	...	...	0.0	...	...	0.0	...	...	0.0	...	...	0.0	...	...	0.0	...	...	99.9	...	...	0.4	...	...
J04091413-4008019	0.0	...	...	0.0	...	...	0.6	...	...	99.1	...	...	0.0	...	...	0.0	...	...	0.0	...	...	0.0	...	...
J04093930-2648489	0.0	...	...	0.0	...	...	0.0	...	...	0.0	...	...	0.0	...	...	0.0	...	...	98.1	...	...	1.9	...	...
J04132663-0139211	0.6	0.0	0.0	0.0	0.0	0.0	0.0	0.0	0.0	0.0	0.0	0.0	0.0	0.0	0.0	99.9	0.0	0.0	0.0	0.0	0.0	0.1	99.9	99.9
J04141730-0906544	0.0	0.0	0.0	0.0	0.0	0.0	0.0	0.0	0.0	0.0	0.0	0.0	0.0	0.0	0.0	0.0	0.0	0.0	99.2	99.9	99.9	0.3	0.0	0.1
J04213904-7233562	1.0	...	...	0.0	...	...	99.9	...	...	0.0	...	...	0.0	...	...	0.0	...	...	0.0	...	...	0.2	...	...
J04240094-5512223	0.0	...	...	0.0	...	...	4.9[b]	...	...	55.4[b]	99.0[b]	...	0.0	...	...	0.0	...	...	38.6[b]	...	...	0.1	...	...
J04244260-0647313	2.7	...	...	0.0	...	...	0.0	...	...	0.0	...	...	0.0	...	...	99.4	...	...	0.0	...	...	0.6	...	...
J04313859-3042509	0.0	...	...	0.0	...	...	0.1	...	...	97.3[b]	...	...	0.0	...	...	0.0	...	...	0.0	...	...	0.0	...	...
J04353618-2527347	7.4	...	...	0.0	...	...	0.0	...	...	0.0	...	...	0.0	...	...	0.0	...	...	99.9[b]	...	...	0.0	...	...
J04363294-7851021	3.0	...	...	0.0	...	...	0.8	...	...	7.2[b]	...	...	0.0	...	...	0.0	...	...	84.0[b]	...	...	0.6	...	...
J04365738-1613065	0.0	...	...	0.0	...	...	48.6[b]	...	...	48.3[b]	...	...	0.0	...	...	0.0	...	...	0.0	...	...	0.0	...	...
J04424932-1452268	6.8	...	...	0.0	...	...	0.0	...	...	0.0	...	...	0.0	...	...	0.0	...	...	99.9	...	...	0.3	...	...
J04440099-6624036	0.0	...	...	0.0	...	...	97.5	...	...	0.0	...	...	0.1	...	...	0.0	...	...	2.0	...	...	0.4	...	...
J04464970-6034109	0.0	...	...	0.0	...	...	0.0	...	...	0.0	...	...	0.0	...	...	92.3	...	...	0.8	...	...	0.1	...	...
J04480066-5041255	0.0	0.0	...	0.0	0.0	...	95.9	99.9	...	0.5	0.1	...	0.0	0.0	...	0.0	0.0	...	3.5	0.0	...	0.0	0.0	...
J04514615-2400087	0.0	...	...	0.0	...	...	0.0	...	...	0.1	...	...	0.0	...	...	0.0	...	...	98.9	...	...	0.0	...	...
J04515303-4647309	0.0	...	...	0.0	...	...	0.0	...	...	99.9	99.9	0.0	0.0	...	...	0.0	...	...	0.0	0.0	...	1.1	0.0	0.0
J04522441-1649219	0.0	...	...	0.0	...	...	0.0	...	...	99.9	...	...	0.0	...	...	0.0	...	...	0.0	99.9[b]	99.9[b]	0.0	0.0	0.0
J04554034-1917553	0.0	...	...	0.0	...	...	0.0	...	...	0.0	...	...	0.0	...	...	0.0	...	...	99.9[b]	...	...	0.1	...	...
J04571728-0621564	0.0	...	...	0.0	...	...	0.0	...	...	0.0	...	...	0.0	...	...	0.0	...	...	98.3	...	...	1.7	0.3	...
J04595855-0333123	0.0	...	...	0.0	...	...	0.0	...	...	0.0	...	...	0.0	...	...	90.8	...	...	96.2	99.9	...	3.8	...	...
J05015881+0958587	99.9[b]	99.9[b]	99.9[b]	0.0	0.0	0.0	0.0	0.0	0.0	0.0	0.0	0.0	0.0	0.0	0.0	0.0	0.0	0.0	0.0	0.0	0.0	9.2	0.0	0.0
J05064946-2135038	99.9[b]	99.9[b]	99.9[b]	0.0	0.0	0.0	0.0	0.0	0.0	0.0	0.0	0.0	0.0	0.0	0.0	0.0	0.0	0.0	0.0	0.0	0.0	0.0	0.0	0.0
J05064991-2135091	14.6	4.4	99.9	0.0	0.0	0.0	0.6	0.0	0.0	84.8[b]	95.6[b]	0.0	0.0	0.0	0.0	0.0	0.0	0.0	0.0	0.0	0.0	0.0	0.0	0.0
J05082729-2101444	99.9[b]	...	...	0.0	...	...	0.0	...	...	0.1	...	...	0.0	...	...	0.0	...	...	0.0	...	...	0.0	...	...
J05090356-4209199	27.3	...	...	0.0	...	...	5.3[b]	...	...	0.0	...	...	0.0	...	...	72.5[b]	...	...	0.0	...	...	0.2	...	...
J05100427-2340407	0.2	...	...	0.0	...	...	1.1	...	...	94.5	...	...	0.0	...	...	0.0	...	...	0.0	...	...	0.0	...	...
J05100488-2340148	0.1	...	...	0.0	...	...	0.7	...	...	98.8	...	...	0.0	...	...	0.0	...	...	0.0	...	...	0.0	...	...
J05111098-4903597	0.0	...	...	0.0	...	...	0.0	...	...	98.4	...	...	0.0	...	...	0.0	...	...	0.9	...	...	0.0	...	...
J05130132-7027418	1.2	...	...	0.0	...	...	12.8	...	...	6.5	...	...	0.0	...	...	0.2	...	...	91.6	...	...	0.5	...	...
J05142736-1514514	0.1	...	...	0.0	...	...	11.9[b]	...	...	86.6	...	...	0.0	...	...	0.0	...	...	0.0	...	...	0.5	...	...
J05142878-1514546	0.7	...	...	0.0	...	...	...	...	...	87.1	...	...	0.0	...	...	0.0	...	...	0.0	...	...	0.2	...	...

Table 2.VIII — continued

Name	βPMG P	βPMG P_ν	βPMG P_{ν+π}	TWA P	TWA P_ν	TWA P_{ν+π}	THA P	THA P_ν	THA P_{ν+π}	COL P	COL P_ν	COL P_{ν+π}	CAR P	CAR P_ν	CAR P_{ν+π}	ARG P	ARG P_ν	ARG P_{ν+π}	ABDMG P	ABDMG P_ν	ABDMG P_{ν+π}	Field P	Field P_ν	Field P_{ν+π}
J05164586-5410168	0.1	1.8	…	0.0	0.0	…	0.1	65.9	…	92.1	0.0	…	0.0	0.0	…	0.0	0.0	…	7.7	0.0	…	0.0	32.2	…
J05195412-0723359	0.0	…	…	0.0	…	…	9.1	…	…	90.3	…	…	0.0	…	…	0.0	…	…	0.0	…	…	0.5	…	…
J05195582-1124568	24.0	…	…	0.0	…	…	0.1	…	…	75.9[b]	…	…	0.0	…	…	0.0	…	…	0.0	…	…	0.0	…	…
J05195695-1124440	1.1	…	…	0.0	0.0	…	0.3	0.0	…	98.4[b]	0.0	…	0.0	0.0	…	0.0	0.0	…	0.0	0.2	…	0.2	…	…
J05224571-3917062	99.9	0.0	…	0.0	…	…	0.0	…	…	0.0	…	…	0.0	…	…	0.0	…	…	89.4	…	…	0.1	99.9	…
J05240991-4223054	0.0	…	…	0.0	…	…	0.0	…	…	0.0	…	…	0.0	…	…	0.0	…	…	0.0	…	…	10.6	…	…
J05241317-2104427	1.4	…	…	0.0	…	…	0.3	…	…	98.2[b]	…	…	0.0	…	…	0.0	…	…	0.0	0.0	…	0.0	0.0	…
J05241914-1601153	99.9[b]	99.9[b]	…	0.0	0.0	…	0.0	0.0	…	0.0	0.0	…	0.0	0.0	…	0.0	0.0	…	0.0	99.9[b]	…	0.0	0.1	…
J05254166-0909123	0.0	0.0	0.0	0.0	0.0	0.0	0.0	0.0	0.0	0.0	0.0	0.0	0.0	0.0	0.0	0.0	0.0	0.0	99.9[b]	99.9[b]	99.9[b]	0.0	0.1	…
J05301858-5358483	78.4	…	…	0.0	…	…	0.0	…	…	12.0	…	…	0.0	…	…	0.3	…	…	6.8	…	…	2.5	…	…
J05320450-0305291	99.9[b]	…	…	0.0	…	…	0.0	…	…	0.0	…	…	0.0	…	…	0.0	…	…	0.5	…	…	0.0	…	…
J05332558-5117131	0.0	0.0	…	0.0	0.0	…	98.5	99.9	…	0.3	0.0	…	0.0	0.0	…	0.0	0.0	…	0.1	0.0	…	0.6	0.1	…
J05332802-4257205	99.9[b]	…	…	0.0	…	…	0.0	…	…	0.0	…	…	0.0	…	…	0.0	…	…	0.1	…	…	0.0	…	…
J05335981-0221325	99.9	…	…	0.0	…	…	0.0	…	…	0.0	…	…	0.0	…	…	0.0	…	…	73.9	…	…	0.0	…	…
J05381615-6923321	0.0	…	…	0.0	…	…	0.6	…	…	19.9	…	…	0.1	…	…	0.0	…	…	0.1	…	…	5.5	…	…
J05392505-4245211	0.0	…	…	0.0	…	…	31.4	…	…	68.3	…	…	0.0	…	…	0.0	…	…	0.1	…	…	0.1	…	…
J05395494-1307598	0.6	…	…	0.0	…	…	0.3	…	…	99.0[b]	…	…	0.0	…	…	0.0	…	…	0.0	…	…	0.0	…	…
J05422287-2758031	99.3	…	…	0.0	…	…	0.0	…	…	0.0	…	…	0.0	…	…	0.2	…	…	0.0	…	…	0.7	…	…
J05425587-0718382	1.5	…	…	0.0	…	…	0.0	…	…	98.2[b]	…	…	0.0	…	…	0.0	…	…	0.0	…	…	0.2	…	…
J05432676-3025129	0.0	…	…	0.0	…	…	0.0	…	…	99.9	…	…	0.0	…	…	0.0	…	…	0.0	…	…	0.3	…	…
J05470650-3210413	0.6	…	…	0.0	…	…	0.0	…	…	99.3[b]	…	…	0.0	…	…	10.0[b]	…	…	3.2	…	…	0.0	…	…
J05471788-2856130	86.8	…	…	0.0	…	…	0.0	…	…	0.0	…	…	0.0	…	…	0.0	…	…	98.7	99.9	…	3.2	…	…
J05531299-4505119	0.0	0.0	…	0.0	0.0	…	0.1	0.0	…	0.0	0.0	…	0.0	0.0	…	0.0	0.0	…	0.5	…	…	1.2	…	…
J06002304-4401217	0.0	…	…	0.0	…	…	1.6	…	…	97.7	…	…	0.0	…	…	0.0	…	…	0.0	…	…	0.2	…	…
J06012186-1937547	0.4	…	…	0.0	…	…	0.0	…	…	99.9[b]	…	…	0.0	…	…	0.0	…	…	97.7	…	…	0.1	…	…
J06022455-1634494	0.3	…	…	0.0	…	…	0.0	…	…	0.0	…	…	0.0	…	…	0.0	…	…	99.9[b]	99.9[b]	…	2.0	0.0	…
J06091922-3549311	0.3	0.0	0.0	0.0	0.0	0.0	6.0[b]	0.0	0.0	0.0	0.0	0.0	90.4[b]	0.0	0.0	0.0	0.0	0.0	2.1[b]	99.9[b]	99.9[b]	0.0	0.0	0.0
J06112997-7213388	0.0	…	…	0.0	…	…	0.0	…	…	1.4	…	…	0.0	…	…	0.0	…	…	0.0	…	…	0.0	…	…
J06131330-2742054	99.9[b]	0.0	0.0	0.0	0.0	0.0	0.0	0.0	0.0	0.0	0.0	0.0	0.0	0.0	0.0	0.0	99.9[b]	0.0	0.0	0.0	0.0	0.0	0.0	0.0
J06134539-2352077	0.1	…	…	0.0	…	…	0.0	…	…	0.0	…	…	0.0	…	…	99.9[b]	…	…	0.0	…	…	2.6	…	…
J06135773-2723550	97.3	0.0	…	0.0	0.0	…	0.0	0.0	…	0.0	0.0	…	0.0	0.0	…	0.0	0.0	…	22.8[b]	0.0	…	1.4	99.9	…
J06153953-8433115	75.7	…	…	0.0	…	…	0.0	…	…	0.0	…	…	0.0	…	…	0.0	…	…	0.0	…	…	2.0	…	…
J06161032-1320422	97.9	…	…	0.0	…	…	0.0	…	…	0.0	…	…	0.0	…	…	0.0	…	…	2.4[b]	0.0	…	0.8	…	…
J06234024-7504327	0.0	…	…	0.0	…	…	4.9[b]	…	…	1.5	…	…	90.4[b]	…	…	0.0	…	…	0.0	…	…	10.4	…	…
J06262932-0739540	0.2	…	…	0.0	…	…	0.0	…	…	89.4	…	…	0.0	…	…	0.0	…	…	99.0	0.0	…	0.8	99.9	…
J06373215-2823125	0.2	…	…	0.0	…	…	0.0	…	…	0.0	…	…	0.0	…	…	0.0	…	…	0.0	0.0	…	4.3	99.9	…
J06380031-4056011	0.2	…	…	0.0	…	…	0.0	…	…	1.6	…	…	54.0[b]	…	…	93.9	…	…	0.0	…	…	0.0	…	…
J06434532-6424396	0.4	…	…	0.0	…	…	0.0	…	…	38.2[b]	…	…	0.0	…	…	0.0	…	…	7.4[b]	0.0	…	3.0	…	…
J06475229-2523304	0.2	0.0	…	0.0	0.0	…	0.0	0.0	…	75.2	0.0	…	0.0	0.0	…	0.0	0.0	…	21.5[b]	0.0	…	0.0	…	…
J06511418-4037510	0.1	0.0	…	0.0	0.0	…	0.0	0.0	…	99.9[b]	0.0	…	0.0	0.0	…	0.0	0.0	…	0.0	0.0	…	0.0	99.9	…
J07065772-5353463	0.2	…	…	0.0	…	…	0.0	…	…	99.9	…	…	0.0	…	…	0.0	…	…	0.2	…	…	0.0	99.9	…

Table 2.VIII — continued

Name	βPMG P	βPMG P_ν	βPMG P_{ν+π}	TWA P	TWA P_ν	TWA P_{ν+π}	THA P	THA P_ν	THA P_{ν+π}	COL P	COL P_ν	COL P_{ν+π}	CAR P	CAR P_ν	CAR P_{ν+π}	ARG P	ARG P_ν	ARG P_{ν+π}	ABDMG P	ABDMG P_ν	ABDMG P_{ν+π}	Field P	Field P_ν	Field P_{ν+π}
J07115917-3510157	0.0	⋮	⋮	0.0	⋮	⋮	0.0	⋮	⋮	0.0	⋮	⋮	0.0	⋮	⋮	0.0	⋮	⋮	99.9	⋮	⋮	0.4	⋮	⋮
J07140101-1945332	0.0	⋮	⋮	0.0	⋮	⋮	0.0	⋮	⋮	0.0	⋮	⋮	0.0	⋮	⋮	99.9^b	⋮	⋮	0.0	⋮	⋮	0.3	⋮	⋮
J07170438-6311123	2.1	⋮	⋮	0.0	⋮	⋮	0.0	⋮	⋮	75.8	⋮	⋮	1.1	⋮	⋮	0.6	⋮	⋮	20.0	⋮	⋮	0.4	⋮	⋮
J07310129+4600266	0.1	⋮	⋮	0.0	⋮	⋮	0.0	⋮	⋮	81.6^b	⋮	⋮	0.0	⋮	⋮	0.0	⋮	⋮	11.4^b	⋮	⋮	6.8	⋮	⋮
J07343426-2401353	0.0	⋮	⋮	0.0	⋮	⋮	0.0	⋮	⋮	0.0	⋮	⋮	0.0	⋮	⋮	94.2^b	⋮	⋮	0.0	⋮	⋮	5.8	⋮	⋮
J07504838-2931126	75.9	⋮	⋮	0.0	⋮	⋮	0.0	⋮	⋮	19.6	⋮	⋮	0.0	⋮	⋮	0.0	⋮	⋮	0.0	⋮	⋮	4.5	⋮	⋮
J07540718-6320149	0.0	⋮	⋮	0.0	⋮	⋮	0.0	⋮	0.0	0.0	⋮	⋮	99.9^b	⋮	⋮	0.0	⋮	⋮	0.0	⋮	⋮	0.0	⋮	⋮
J08031018+2022154	0.0	⋮	⋮	0.0	⋮	⋮	0.0	⋮	⋮	0.0	⋮	⋮	0.0	⋮	⋮	99.9^b	⋮	⋮	0.0	⋮	⋮	0.2	⋮	⋮
J08173943-8243298	99.9^b	⋮	⋮	0.0	⋮	⋮	0.0	⋮	⋮	0.0	⋮	⋮	0.0	⋮	⋮	0.1	⋮	⋮	0.2	⋮	⋮	0.0	⋮	⋮
J08185942-7239561	0.0	⋮	⋮	0.0	⋮	⋮	0.0	⋮	⋮	0.0	⋮	⋮	99.9	⋮	⋮	0.0	⋮	⋮	0.0	⋮	⋮	0.0	⋮	⋮
J08224744-5726530	19.7	⋮	⋮	0.0	⋮	⋮	0.0	⋮	⋮	0.0	⋮	⋮	0.0	⋮	⋮	0.0	⋮	⋮	77.4	⋮	⋮	2.9	⋮	⋮
J08412528-5736021	0.2	⋮	⋮	0.0	⋮	⋮	0.0	⋮	⋮	69.8^b	⋮	⋮	25.9^b	⋮	⋮	0.1	⋮	⋮	0.0	⋮	⋮	4.1	⋮	⋮
J08422284-8345248	0.0	⋮	⋮	0.0	⋮	⋮	0.0	⋮	⋮	1.5	⋮	⋮	90.4	⋮	⋮	0.1	⋮	⋮	2.1	⋮	⋮	5.9	⋮	⋮
J08465879-7246588	33.4	0.0	⋮	0.0	⋮	⋮	0.0	⋮	0.0	0.0	0.0	⋮	0.0	0.0	⋮	0.0	0.0	⋮	66.1	0.0	⋮	0.3	99.9	⋮
J08475676-7854532	93.8^b	⋮	⋮	0.0	⋮	⋮	0.0	⋮	⋮	0.0	⋮	⋮	0.0	⋮	⋮	4.7^b	⋮	⋮	2.7^b	⋮	⋮	3.6	⋮	⋮
J09032434-6348330	0.1	⋮	⋮	0.0	⋮	⋮	0.0	⋮	⋮	24.5	⋮	⋮	70.0	⋮	⋮	0.0	⋮	⋮	0.6	⋮	⋮	0.7	⋮	⋮
J09315840-6209258	53.2	⋮	⋮	0.1	⋮	⋮	0.0	⋮	⋮	19.4^b	⋮	⋮	19.6^b	⋮	⋮	81.7^b	⋮	⋮	0.0	⋮	⋮	7.3	⋮	⋮
J09331427-4848331	0.1	⋮	⋮	74.3	⋮	⋮	0.0	⋮	⋮	13.2	94.3	⋮	0.0	⋮	⋮	0.0	⋮	⋮	0.0	⋮	⋮	5.0	5.7	⋮
J09353126-2802552	0.0	⋮	⋮	0.0	⋮	⋮	0.0	⋮	⋮	0.0	⋮	⋮	0.0	⋮	⋮	0.1	⋮	⋮	18.6^b	⋮	⋮	7.1	99.9	⋮
J09361593-3731456	0.5	⋮	0.9	0.0	⋮	0.0	0.0	⋮	0.0	0.0	⋮	0.0	0.1	⋮	0.0	97.2	⋮	0.0	0.0	⋮	0.0	99.4	99.9	99.1
J09423823-6229028	0.5	⋮	⋮	0.0	⋮	⋮	0.0	⋮	⋮	2.2	⋮	⋮	97.2	⋮	⋮	99.9^b	⋮	⋮	0.0	⋮	⋮	0.0	⋮	⋮
J09445422-1220544	0.0	⋮	⋮	0.0	⋮	⋮	0.0	⋮	⋮	0.0	⋮	⋮	99.9^b	⋮	⋮	0.0	⋮	⋮	0.0	⋮	⋮	0.0	8.4	⋮
J10121768-0344441	0.0	0.1	0.0	0.0	⋮	0.0	0.0	⋮	0.0	0.0	⋮	0.0	0.0	⋮	0.0	0.0	⋮	0.0	87.0^b	91.4^b	0.0	12.9	⋮	99.9
J10140807-7636327	0.0	⋮	⋮	99.9^b	⋮	⋮	0.0	⋮	⋮	0.0	⋮	⋮	99.9^b	⋮	⋮	0.0	⋮	⋮	0.0	⋮	⋮	0.0	⋮	⋮
J10182870-3150029	0.0	⋮	⋮	97.4	98.0	⋮	0.0	⋮	⋮	1.3	⋮	⋮	0.0	⋮	⋮	0.0	⋮	⋮	0.0	⋮	⋮	0.2	1.9	⋮
J10252092-4241539	0.0	⋮	⋮	0.0	⋮	⋮	0.0	⋮	⋮	0.0	⋮	⋮	0.0	⋮	⋮	0.0	⋮	⋮	0.0	⋮	⋮	1.3	⋮	⋮
J10252563-4918389	0.0	⋮	⋮	96.9^b	88.7^b	⋮	0.0	⋮	⋮	0.6	⋮	⋮	0.0	⋮	⋮	99.9	⋮	⋮	0.0	⋮	⋮	0.1	⋮	⋮
J10423011-3340162	2.5^b	11.2^b	⋮	0.0	⋮	⋮	0.0	⋮	⋮	0.1	⋮	⋮	0.0	⋮	⋮	0.0	⋮	⋮	0.5	⋮	⋮	0.0	⋮	⋮
J11091606-7352465	26.4	⋮	⋮	99.9^b	99.9^b	⋮	0.0	⋮	⋮	0.0	⋮	⋮	0.0	⋮	⋮	68.9^b	⋮	⋮	0.5	⋮	⋮	4.0	⋮	⋮
J11102788-3731520	0.0	⋮	⋮	99.9	99.9^b	⋮	0.0	⋮	⋮	0.0	⋮	⋮	0.0	⋮	⋮	0.0	⋮	⋮	0.0	⋮	⋮	0.0	⋮	⋮
J11132622-4523427	0.0	⋮	⋮	99.9	99.9	⋮	0.0	⋮	⋮	0.0	⋮	⋮	0.0	⋮	⋮	0.0	⋮	⋮	0.0	⋮	⋮	0.1	⋮	⋮
J11200609-1029468	0.0	⋮	⋮	0.0	⋮	⋮	0.0	⋮	⋮	0.0	⋮	⋮	0.0	⋮	⋮	99.9^b	⋮	⋮	0.0	⋮	⋮	0.0	⋮	⋮
J11210549-3845163	0.0	⋮	⋮	99.9^b	99.9^b	⋮	0.0	⋮	⋮	0.0	⋮	⋮	0.0	⋮	⋮	0.0	⋮	⋮	0.0	⋮	⋮	0.0	⋮	⋮
J11211723-3446454	0.0	⋮	⋮	99.9	99.9	⋮	0.0	⋮	⋮	0.0	⋮	⋮	0.0	⋮	⋮	0.0	⋮	⋮	0.0	⋮	⋮	0.0	⋮	⋮
J11211745-3446497	0.0	⋮	⋮	99.9	99.9	⋮	0.0	⋮	⋮	0.0	⋮	⋮	0.0	⋮	⋮	0.0	⋮	⋮	0.0	⋮	⋮	0.0	⋮	⋮
J11254754-4410267	0.3	⋮	⋮	44.2	0.1	⋮	0.0	⋮	⋮	0.0	⋮	⋮	0.0	⋮	⋮	0.0	⋮	⋮	54.4^b	99.9^b	⋮	1.1	⋮	⋮
J11315526-3436272	0.0	⋮	⋮	99.9^b	99.9^b	⋮	0.0	⋮	⋮	0.0	⋮	⋮	0.0	⋮	⋮	0.0	⋮	⋮	0.0	⋮	⋮	0.0	⋮	⋮
J11321831-3019518	0.0	⋮	⋮	99.9	99.9	⋮	0.0	⋮	⋮	0.0	⋮	⋮	0.0	⋮	⋮	0.0	⋮	⋮	0.0	⋮	⋮	0.0	⋮	⋮
J11455177-5520456	4.4	⋮	⋮	55.1	45.7	⋮	0.0	⋮	⋮	29.5	47.7	⋮	0.0	⋮	⋮	0.1	⋮	⋮	0.0	⋮	⋮	10.8	6.6	⋮
J11493184-7851011	78.3	91.4	⋮	0.0	0.0	⋮	0.0	⋮	⋮	0.0	⋮	⋮	0.0	⋮	⋮	0.0	⋮	⋮	0.0	⋮	⋮	21.7	8.6	⋮
J12072738-3247002	0.0	⋮	⋮	99.9^b	99.9^b	⋮	0.0	⋮	⋮	0.0	⋮	⋮	0.0	⋮	⋮	0.0	⋮	⋮	0.0	⋮	⋮	0.0	⋮	⋮

Table 2.VIII — continued

Name	βPMG			TWA			THA			COL			CAR			ARG			ABDMG			Field		
	P	P_ν	$P_{\nu+\pi}$	P	P_ν	$P_{\nu+\pi}$	P	P_ν	$P_{\nu+\pi}$	P	P_ν	$P_{\nu+\pi}$	P	P_ν	$P_{\nu+\pi}$	P	P_ν	$P_{\nu+\pi}$	P	P_ν	$P_{\nu+\pi}$	P	P_ν	$P_{\nu+\pi}$
J12092998-7505400	0.7	⋯	⋯	0.0	⋯	⋯	0.0	⋯	⋯	0.0	⋯	⋯	0.0	0.0	⋯	99.1[b]	⋯	⋯	0.0	⋯	⋯	0.1	⋯	⋯
J12103101-7507205	18.4	⋯	⋯	0.0	⋯	⋯	0.0	⋯	⋯	0.0	⋯	⋯	0.0	⋯	⋯	77.4[b]	⋯	⋯	2.9[b]	⋯	⋯	1.3	⋯	⋯
J12151838-0237283	0.0	0.0	⋯	0.5	0.5	⋯	0.0	⋯	⋯	0.0	0.0	⋯	0.0	0.0	⋯	0.0	0.0	⋯	48.4[b]	82.9[b]	⋯	51.1	16.7	⋯
J12153072-3948426	0.0	0.0	⋯	99.9[b]	99.9[b]	⋯	0.0	0.0	⋯	0.0	0.0	⋯	0.0	0.0	⋯	0.0	0.0	⋯	0.0	0.0	⋯	0.0	0.0	⋯
J12170465-5743558	0.9	⋯	⋯	5.9	0.0	⋯	0.0	⋯	⋯	0.0	0.0	⋯	0.0	0.0	⋯	47.6	89.5	⋯	95.0	0.0	⋯	39.0	10.5	⋯
J12194808+5246450	0.0	83.8	0.0	0.0	0.0	0.0	0.0	0.0	0.0	0.0	0.0	0.0	0.0	0.0	0.0	0.0	0.0	0.0	0.2	0.0	0.0	5.0	99.9	99.9
J12210499-7116493	46.0	⋯	⋯	0.0	⋯	⋯	0.0	⋯	⋯	0.0	⋯	⋯	0.0	0.0	⋯	0.0	0.0	⋯	0.0	⋯	⋯	53.8	16.2	⋯
J12233860-4606203	0.0	⋯	⋯	0.0	⋯	⋯	0.0	⋯	⋯	0.0	⋯	⋯	0.0	⋯	⋯	99.9	⋯	⋯	0.0	⋯	⋯	0.2	⋯	⋯
J12242443-5339088	87.9	⋯	⋯	0.0	⋯	⋯	0.0	⋯	⋯	4.0	⋯	⋯	0.0	⋯	⋯	0.0	⋯	⋯	3.8	⋯	⋯	4.3	⋯	⋯
J12313807-4558593	0.0	⋯	⋯	99.9	99.9	⋯	0.0	⋯	⋯	0.0	⋯	⋯	0.0	0.0	⋯	0.0	⋯	⋯	0.0	⋯	⋯	0.0	0.0	⋯
J12342047-4815195	0.0	⋯	⋯	0.0	0.0	⋯	0.0	⋯	⋯	0.0	⋯	⋯	0.0	0.0	⋯	0.0	⋯	⋯	0.0	⋯	⋯	99.9	99.9	⋯
J12342064-4815135	0.0	⋯	⋯	99.9	99.9	⋯	0.0	⋯	⋯	0.0	⋯	⋯	0.0	⋯	⋯	0.0	⋯	⋯	0.0	⋯	⋯	99.9	99.9	⋯
J12350424-4136385	0.0	⋯	⋯	0.0	⋯	⋯	0.0	⋯	⋯	0.0	⋯	⋯	0.0	0.0	⋯	0.0	⋯	⋯	0.0	⋯	⋯	0.0	0.0	⋯
J12383713-2703348	0.0	⋯	⋯	0.0	⋯	⋯	0.0	⋯	⋯	0.0	⋯	⋯	0.0	⋯	⋯	0.0	⋯	⋯	99.3	⋯	⋯	0.7	⋯	⋯
J12574030+3513306	0.0	11.6	0.0	0.0	0.0	0.0	0.0	0.0	0.0	0.0	1.3	0.2	0.0	0.0	0.0	0.0	0.0	0.0	99.9[b]	67.0[b]	99.9[b]	0.4	20.2	0.1
J13213722-4421518	0.0	0.0	⋯	57.1	89.2	⋯	0.0	0.0	⋯	0.0	0.0	⋯	0.0	0.0	⋯	0.0	0.0	⋯	0.0	0.0	⋯	42.9	10.8	⋯
J13283294-3654233	0.0	⋯	⋯	0.0	⋯	⋯	0.0	⋯	⋯	0.0	⋯	⋯	0.0	⋯	⋯	99.2	⋯	⋯	0.0	⋯	⋯	0.8	⋯	⋯
J13382562-2516466	0.0	⋯	⋯	0.0	⋯	⋯	0.0	⋯	⋯	0.0	⋯	⋯	0.0	⋯	⋯	99.9	⋯	⋯	0.0	⋯	⋯	0.2	⋯	⋯
J13412668-4341522	1.6	⋯	⋯	96.3	⋯	⋯	0.0	⋯	⋯	0.4	⋯	⋯	0.4	⋯	⋯	0.1	⋯	⋯	0.0	⋯	⋯	1.6	⋯	⋯
J13493313-6818291	2.6	⋯	⋯	0.0	⋯	⋯	0.0	⋯	⋯	0.0	⋯	⋯	0.0	⋯	⋯	96.4[b]	⋯	⋯	0.0	⋯	⋯	1.0	⋯	⋯
J13545390-7121476	8.5	⋯	⋯	0.0	⋯	⋯	0.0	⋯	⋯	0.0	⋯	⋯	0.0	⋯	⋯	0.0	⋯	⋯	91.0	0.0	⋯	0.5	⋯	⋯
J13591045-1950034	99.9	99.4	96.9	0.0	0.0	0.0	0.0	0.0	0.0	0.0	0.0	0.0	0.0	0.0	0.0	95.6	15.0	0.1	0.0	0.0	0.0	4.4	85.0	99.9
J14142141-1521215	0.0	0.0	0.0	0.0	0.1	1.1	0.0	0.0	0.0	0.0	0.3	1.9	0.0	0.0	0.0	0.0	0.0	0.0	0.0	0.0	0.0	0.2	0.1	0.0
J14190331+6451463	0.0	⋯	⋯	0.0	⋯	⋯	0.0	⋯	⋯	0.1	⋯	⋯	0.0	⋯	⋯	0.0	⋯	⋯	98.3[b]	⋯	⋯	1.5	⋯	⋯
J14284804-7430205	1.8	⋯	⋯	0.0	⋯	⋯	0.0	⋯	⋯	0.0	⋯	⋯	0.2	⋯	⋯	97.0[b]	⋯	⋯	0.0	⋯	⋯	0.9	⋯	⋯
J14563812-6623419	0.1	⋯	⋯	0.0	⋯	⋯	0.0	⋯	⋯	0.0	⋯	⋯	0.0	⋯	⋯	95.3[b]	⋯	⋯	0.0	⋯	⋯	4.7	⋯	⋯
J15163224-5855237	0.5	⋯	⋯	0.0	⋯	⋯	0.0	⋯	⋯	0.0	⋯	⋯	0.0	⋯	⋯	98.5	⋯	⋯	0.0	⋯	⋯	1.0	⋯	⋯
J15244849-4929473	4.5	0.0	⋯	0.0	0.0	⋯	0.0	0.0	⋯	0.0	0.0	⋯	0.0	0.0	⋯	0.0	0.0	⋯	95.1[b]	99.9[b]	⋯	0.4	0.0	⋯
J15553178+3512028	0.0	0.0	⋯	0.0	0.0	⋯	0.0	0.0	⋯	0.0	0.0	⋯	0.0	0.0	⋯	99.9	99.9	⋯	0.0	⋯	⋯	0.2	0.1	⋯
J15594729+4403595	0.1	⋯	⋯	0.0	⋯	⋯	0.0	⋯	⋯	0.0	⋯	⋯	0.0	⋯	⋯	0.0	⋯	⋯	92.8[b]	⋯	⋯	7.0	⋯	⋯
J16074132-1103073	0.5	⋯	⋯	0.0	⋯	⋯	0.0	⋯	⋯	0.0	⋯	⋯	0.0	⋯	⋯	0.0	⋯	⋯	98.4[b]	⋯	⋯	1.1	⋯	⋯
J16232165+6149149	0.7	35.3	⋯	0.0	⋯	⋯	0.0	⋯	⋯	0.0	⋯	⋯	0.0	⋯	⋯	0.0	⋯	⋯	93.9	⋯	⋯	5.5	⋯	⋯
J16430128-1754274	7.5	⋯	⋯	0.0	0.0	⋯	0.0	0.0	⋯	0.0	⋯	⋯	0.0	0.0	⋯	9.2	0.0	⋯	0.0	0.0	⋯	83.2	64.7	⋯
J16572029-5343316	99.5	⋯	⋯	0.0	⋯	⋯	0.0	⋯	⋯	0.0	⋯	⋯	0.0	⋯	⋯	0.4	⋯	⋯	0.1	⋯	⋯	0.0	⋯	⋯
J17080882-6936186	0.0	⋯	⋯	0.0	⋯	⋯	93.2[b]	⋯	⋯	0.0	⋯	⋯	0.0	⋯	⋯	0.0	⋯	⋯	0.0	⋯	⋯	6.8	⋯	⋯
J17115853-2530585	0.2	⋯	⋯	0.0	⋯	⋯	0.0	⋯	⋯	0.0	⋯	⋯	0.0	⋯	⋯	92.1	⋯	⋯	0.0	⋯	⋯	7.7	⋯	⋯
J17130733-8552105	0.0	⋯	⋯	0.0	⋯	⋯	98.5[b]	⋯	⋯	0.0	⋯	⋯	0.4	⋯	⋯	0.0	⋯	⋯	0.0	⋯	⋯	1.0	⋯	⋯
J17150219-3333398	96.9	⋯	⋯	0.0	⋯	⋯	0.0	⋯	⋯	0.0	⋯	⋯	0.0	⋯	⋯	0.0	⋯	⋯	0.0	⋯	⋯	1.9	⋯	⋯
J17165072-3007104	70.2[b]	⋯	⋯	0.0	⋯	⋯	0.0	⋯	⋯	0.0	⋯	⋯	0.0	⋯	⋯	23.5[b]	⋯	⋯	1.3	⋯	⋯	6.3	⋯	⋯
J17243644-3152484	53.5[b]	⋯	⋯	0.0	⋯	⋯	0.0	⋯	⋯	0.0	⋯	⋯	0.0	⋯	⋯	37.7[b]	⋯	⋯	0.0	⋯	⋯	8.8	⋯	⋯
J17261525-0311308	24.6	⋯	⋯	0.0	⋯	⋯	0.0	⋯	⋯	0.0	⋯	⋯	0.0	⋯	⋯	0.0	⋯	⋯	73.8[b]	⋯	⋯	1.6	⋯	⋯

Table 2.VIII — continued

Name	βPMG P	βPMG P$_\nu$	βPMG P$_{\nu+\pi}$	TWA P	TWA P$_\nu$	TWA P$_{\nu+\pi}$	THA P	THA P$_\nu$	THA P$_{\nu+\pi}$	COL P	COL P$_\nu$	COL P$_{\nu+\pi}$	CAR P	CAR P$_\nu$	CAR P$_{\nu+\pi}$	ARG P	ARG P$_\nu$	ARG P$_{\nu+\pi}$	ABDMG P	ABDMG P$_\nu$	ABDMG P$_{\nu+\pi}$	Field P	Field P$_\nu$	Field P$_{\nu+\pi}$
J17275761-4016243	35.1[b]	...	...	0.0	...	...	0.0	...	...	0.0	...	...	0.0	...	...	64.8[b]	...	...	0.0	...	...	0.1	...	...
J17292067-5014529	99.9[b]	99.9[b]	...	0.0	0.0	...	0.0	0.0	...	0.0	0.0	...	0.0	0.0	...	0.4	0.0	...	0.0	0.0	...	0.0	0.0	...
J17300060-1840132	12.8[b]	...	...	0.0	...	...	0.0	...	...	0.0	...	...	0.0	...	...	85.7	...	...	0.0	...	...	1.5	...	...
J17520944-5636278	0.0	...	...	0.0	...	...	0.0	...	...	0.0	...	...	0.0	...	...	0.0	...	...	99.9	...	...	0.3	...	...
J17580616-2222238	12.6[b]	...	...	0.0	...	...	0.0	...	...	0.0	...	...	0.0	...	...	87.1	...	...	0.0	...	...	0.3	...	...
J18083702-0426259	0.0	...	0.0	0.0	0.0	0.0	0.0	0.0	0.0	0.0	0.0	0.0	0.0	0.0	0.0	99.9[b]	...	0.0	0.0	0.0	0.0	0.0	...	...
J18141047-3247344	61.3[b]	...	...	0.0	...	...	0.0	...	...	0.0	...	...	0.0	...	...	38.6[b]	...	...	0.0	...	...	0.1	0.2	...
J18142207-3246100	87.9[b]	99.9[b]	...	0.0	0.0	...	0.0	0.0	...	0.0	0.0	...	0.0	0.0	...	11.8	0.0	...	0.0	0.0	...	0.3	...	...
J18151564-4927472	91.2[b]	...	...	0.0	...	...	0.0	...	...	0.0	...	...	0.0	...	...	8.8[b]	...	...	0.0	0.0	...	0.0	5.5	...
J18202275-1011131	0.4	94.5[b]	...	0.0	0.0	...	0.0	0.0	...	0.0	0.0	...	0.0	0.0	...	99.5	0.0	...	0.0	0.0	...	0.1	0.0	...
J18420694-5554254	76.2	99.9	...	0.0	...	...	0.0	...	...	0.0	...	...	0.0	...	...	23.8[b]	...	...	0.0	...	...	0.0	...	...
J18450097-1409053	4.5[b]	...	...	0.0	...	...	0.0	...	...	0.0	...	...	0.0	...	...	95.5[b]	...	...	0.0	...	...	0.0	0.0	...
J18465255-6210366	58.2	99.9	...	0.0	...	...	0.0	...	...	0.0	...	...	0.0	...	...	41.8[b]	0.0	...	0.0	0.0	...	0.0	0.0	...
J18495543-0134087	97.9	...	...	0.0	...	...	0.0	...	...	0.0	...	...	0.0	...	...	0.1	...	...	0.0	...	...	2.0	0.0	...
J18504448-3147472	92.5	99.9	...	0.0	...	...	0.0	...	...	0.0	...	...	0.0	...	...	7.5	0.0	...	0.0	0.0	...	0.0	...	...
J18553176-1622495	0.0	...	...	0.0	...	...	0.0	...	...	0.0	...	...	0.0	...	...	0.0	...	...	98.5	0.0	...	1.5	0.2	...
J18580415-2953045	98.9[b]	99.9[b]	...	0.0	0.0	...	0.0	0.0	...	0.0	0.0	...	0.0	0.0	...	1.0	0.0	...	0.0	0.0	...	0.1	0.0	...
J19102820-2319486	99.9[b]	...	...	0.0	...	...	0.0	...	...	0.0	...	...	0.0	...	...	0.2	...	...	0.0	...	...	0.0	...	...
J19224278-0515536	0.0	...	...	0.0	...	...	0.0	...	...	0.0	...	...	0.0	...	...	99.3[b]	...	...	0.0	...	...	0.7	...	...
J19225071-6310581	0.0	...	...	0.0	...	...	99.9[b]	...	...	0.0	...	...	0.0	...	...	0.0	0.0	...	0.0	0.0	...	0.0	0.2	...
J19233820-4606316	98.9	99.9	...	0.0	...	...	0.0	...	...	0.0	...	...	0.0	...	...	0.5	0.0	...	0.0	0.0	...	0.6	0.2	...
J19243494-3442392	99.9[b]	...	...	0.0	...	...	0.0	...	...	0.0	...	...	0.0	...	...	0.0	...	...	0.0	...	...	0.0	...	...
J19312434-2134226	98.6	0.0	0.0	0.0	0.0	0.0	0.0	0.0	0.0	0.0	2.2	0.0	0.0	0.0	0.0	1.3	64.1	85.9	0.0	0.0	0.0	0.1	35.9	14.1
J19420065-2104051	0.1	...	...	0.0	...	...	0.0	...	...	0.0	...	...	0.0	...	...	0.0	...	...	97.4[b]	...	...	0.3	...	...
J19432464-3722108	0.0	...	...	0.0	...	...	0.0	...	...	0.0	...	...	0.0	...	...	98.8	...	...	0.0	...	...	1.2	...	...
J19435432-0546363	0.0	...	...	0.0	...	...	0.0	...	...	0.0	...	...	0.0	...	...	90.5	...	...	0.0	...	...	9.5	0.5	...
J19560294-3207186	98.8[b]	99.5[b]	...	0.0	0.0	...	0.0	0.0	...	0.0	0.0	...	0.0	0.0	...	0.0	0.0	...	0.0	0.0	...	1.2	0.5	...
J19560438-3207376	99.9[b]	99.9[b]	...	0.0	0.0	...	0.0	0.0	...	0.0	0.0	...	0.0	0.0	...	0.0	0.0	...	0.0	0.0	...	0.0	0.0	...
J20013718-3313139	98.9	99.9	...	0.0	0.0	...	0.0	0.0	...	0.0	0.0	...	0.0	0.0	...	0.0	0.0	...	0.0	0.0	...	1.1	0.1	...
J20072376-5147272	2.6	0.0	0.0	0.0	0.0	0.0	0.0	0.0	0.0	0.0	0.0	0.0	0.0	0.0	0.0	17.9	89.5	0.0	39.0	0.0	0.0	40.5	10.5	0.0
J20100002-2801410	99.9[b]	...	...	0.0	...	...	0.0	...	...	0.0	...	...	0.0	...	...	0.0	...	...	0.0	...	...	0.0	0.0	...
J20163382-0711456	0.0	...	...	0.0	...	...	0.0	...	...	0.0	...	...	0.0	...	...	95.8	...	...	0.0	...	...	4.2	...	...
J20220177-3653014	0.4	...	...	0.0	...	...	0.0	...	...	0.1	...	...	0.0	...	...	0.0	...	...	99.4	...	...	0.1	...	...
J20223306-2927499	0.5	...	...	0.0	...	...	0.3	...	...	0.0	...	...	0.0	...	...	0.0	...	...	95.6[b]	...	...	3.5	...	...
J20333759-2556521	99.9[b]	...	0.0	0.0	...	...	0.0	...	...	0.0	...	...	0.0	...	...	0.0	...	...	0.0	...	...	0.2	...	...
J20431469-2925217	96.9	...	...	0.0	...	...	0.6	...	...	0.0	...	...	0.0	...	...	0.0	...	...	1.0	1.0	...	1.5	...	...
J20434114-2433534	99.9[b]	99.9[b]	99.9[b]	0.0	0.0	0.0	0.0	0.0	0.0	0.0	0.0	0.0	0.0	0.0	0.0	0.0	0.0	0.0	0.0	0.0	0.0	0.0	0.0	0.0
J20465795-0259320	0.0	0.0	...	0.0	0.0	...	0.0	0.0	...	0.0	0.0	...	0.0	0.0	...	0.0	0.0	...	99.2	99.9	...	0.8	0.1	...
J20515256-3046329	0.0	...	...	0.0	...	...	0.0	...	...	0.0	...	...	0.0	...	...	92.9	0.0	...	0.0	0.0	...	7.1	0.0	...
J20531465-0221218	0.0	...	0.0	0.0	0.0	0.0	0.0	0.0	0.0	0.0	0.0	0.0	0.0	0.0	0.0	90.2	0.0	0.0	0.0	0.0	0.0	9.8	99.9	99.9

Table 2.VIII — continued

Name	βPMG P	βPMG P_ν	βPMG $P_{\nu+\pi}$	TWA P	TWA P_ν	TWA $P_{\nu+\pi}$	THA P	THA P_ν	THA $P_{\nu+\pi}$	COL P	COL P_ν	COL $P_{\nu+\pi}$	CAR P	CAR P_ν	CAR $P_{\nu+\pi}$	ARG P	ARG P_ν	ARG $P_{\nu+\pi}$	ABDMG P	ABDMG P_ν	ABDMG $P_{\nu+\pi}$	Field P	Field P_ν	Field $P_{\nu+\pi}$
J20560274-1710538	99.9[b]	99.9[b]	…	0.0	0.0	…	0.0	0.0	…	0.0	0.0	…	0.0	0.0	…	0.0	0.0	…	0.0	0.0	…	0.0	0.0	…
J21073678-1304581	91.4	…	…	0.0	…	…	0.0	…	…	0.2	…	…	0.1	…	…	0.0	…	…	8.0[b]	…	…	0.4	…	…
J21100535-1919573	99.9[b]	99.9[b]	…	0.0	0.0	…	0.0	0.0	…	0.0	0.0	…	0.0	0.0	…	0.0	0.0	…	0.0	0.0	…	0.0	0.0	…
J21103096-2710513	99.9[b]	99.9[b]	…	0.0	0.0	…	0.0	0.0	…	0.0	0.0	…	0.0	0.0	…	0.0	0.0	…	0.0	0.0	…	0.1	0.0	…
J21103147-2710578	99.9[b]	…	…	0.0	…	…	0.0	…	…	0.0	…	…	0.0	…	…	0.0	…	…	0.0	…	…	0.0	…	…
J21130526-1729126	0.0	0.0	…	0.0	0.0	…	0.0	0.0	…	0.0	0.0	…	0.0	0.0	…	0.0	0.0	…	99.9	99.9	…	0.3	0.1	…
J21212873-6655063	57.6	99.9	99.9	0.0	0.0	0.0	0.0	0.0	0.0	0.0	0.0	0.0	0.0	0.0	0.0	29.3	0.0	0.0	12.8[b]	0.0	0.0	0.3	0.1	0.1
J21334415-3453372	0.0	…	…	0.0	…	…	74.1	…	…	0.0	…	…	0.0	…	…	0.0	…	…	18.7[b]	…	…	7.2	…	…
J21342935-1840372	0.0	…	…	0.0	…	…	0.0	…	…	0.0	…	…	0.0	…	…	93.7[b]	…	…	0.0	…	…	6.3	…	…
J21464282-8543046	1.8	…	…	0.0	…	…	0.0	…	…	21.4	…	…	0.0	…	…	0.0	…	…	76.6[b]	…	…	0.2	…	…
J21471964-4803166	0.4	…	…	0.0	…	…	96.7[b]	…	…	0.0	…	…	0.0	…	…	0.0	…	…	2.8[b]	…	…	0.1	…	…
J21490499-6413039	0.0	…	…	0.0	…	…	99.9[b]	…	…	0.0	…	…	0.0	…	…	0.0	…	…	0.0	…	…	0.0	…	…
J21521039+0537356	8.0	0.1	0.0	0.0	0.0	0.0	0.0	0.0	0.0	0.0	0.0	0.0	0.0	0.0	0.0	0.0	0.0	0.0	91.1[b]	99.9[b]	99.9[b]	0.9	0.1	0.0
J21551741-0045478	95.9	…	…	0.0	…	…	0.0	…	…	0.0	…	…	0.0	…	…	0.0	…	…	0.0	…	…	3.3	2.0	…
J22004158+2715135	81.5	98.0	…	0.0	0.0	…	0.0	0.0	…	3.4	0.0	…	0.0	0.0	…	0.0	0.0	…	1.5	0.0	…	15.1	0.1	…
J22021626-4210329	0.0	0.0	…	0.0	0.0	…	98.4	99.9	…	0.0	0.0	…	0.0	0.0	…	0.0	0.0	…	0.0	0.0	…	0.1	0.1	…
J22174316-1546452	0.0	…	…	0.0	…	…	0.0	…	…	0.0	…	…	0.0	…	…	98.4	…	…	0.0	…	…	1.6	…	…
J22274882-0113527	0.0	…	…	0.0	…	…	0.0	…	…	0.0	…	…	0.0	…	…	99.9[b]	…	…	0.0	…	…	0.5	…	…
J22294830-4858285	71.7	0.0	…	0.0	0.0	…	0.0	0.0	…	0.0	0.0	…	0.0	0.0	…	22.0	2.3[b]	…	0.0	0.0	…	6.3	97.7	…
J22332264-0936537	0.0	…	…	0.0	…	…	0.0	…	…	0.0	…	…	0.0	…	…	99.9[b]	…	…	0.0	…	…	0.4	…	…
J22371494-262232	0.0	…	…	0.0	…	…	0.0	…	…	0.0	…	…	0.0	…	…	99.2[b]	…	…	0.0	…	…	0.8	…	…
J22424884+1330532	46.0	0.0	…	0.0	0.0	…	0.0	0.0	…	6.0	60.3	…	0.0	0.0	…	3.5[b]	0.0	…	1.6	0.0	…	48.0	39.7	…
J22424896-7142211	94.8	99.9	…	0.0	0.0	…	0.0	0.0	…	0.0	0.0	…	0.0	0.0	…	0.0	0.0	…	0.0	0.0	…	0.1	0.0	…
J22440873-5413183	9.1	0.0	…	0.0	0.0	…	83.5[b]	0.0	…	0.3	0.0	…	0.0	0.0	…	0.0	0.0	…	6.8[b]	0.0	…	0.4	99.9	…
J22470872-6920447	0.0	0.0	…	0.0	0.0	…	53.3	0.3	…	0.2	0.0	…	0.0	0.0	…	0.0	0.0	…	45.8	0.0	…	0.6	99.9	…
J23172807+1936469	94.4	96.1	…	0.0	0.0	…	0.0	0.0	…	0.3	0.0	…	0.0	0.0	…	0.0	0.0	…	0.0	0.0	…	5.3	3.9	…
J23204705-6723209	0.0	…	…	0.0	…	…	99.9	…	…	0.0	…	…	0.0	…	…	0.0	…	…	0.0	…	…	0.2	…	…
J23205766-0147373	0.0	0.0	0.0	0.0	0.0	0.0	0.0	0.0	0.0	0.0	0.0	0.0	0.0	0.0	0.0	92.8[b]	96.2[b]	99.9[b]	0.0	0.0	0.0	7.2	3.8	0.2
J23261069-7323498	0.0	0.0	…	0.0	0.0	…	99.9	99.9	…	0.0	0.0	…	0.0	0.0	…	0.0	0.0	…	0.0	0.0	…	0.0	0.0	…
J23285763-6802338	0.0	0.0	…	0.0	0.0	…	99.9	99.9	…	0.0	0.0	…	0.0	0.0	…	0.0	0.0	…	0.0	0.0	…	0.0	0.0	…
J23301341-2023271	99.9[b]	11.2[b]	0.7	0.0	0.0	0.0	0.1	1.5	0.1	0.1	75.7[b]	99.2[b]	0.0	0.0	0.0	0.0	0.0	0.0	0.0	0.0	0.0	0.0	11.6	0.0
J23314492-0244395	95.0[b]	…	…	0.0	…	…	0.1	…	…	4.2[b]	…	…	0.0	…	…	0.0	…	…	0.0	…	…	0.1	…	…
J23320018-3917368	0.0	0.0	…	0.0	0.0	…	0.3	0.0	…	0.0	0.0	…	0.0	0.0	…	0.0	0.0	…	99.9	99.9	…	0.1	0.0	…
J23323085-1215513	95.9	99.9	…	0.0	0.0	…	0.0	0.0	…	3.7	0.0	…	0.0	0.0	…	0.0	0.0	…	0.0	0.0	…	0.1	0.0	…
J23331860+2714219	0.0	…	…	0.0	…	…	0.0	…	…	0.0	…	…	0.0	…	…	99.3	…	…	0.0	…	…	0.7	…	…
J23332198-1240072	0.0	…	…	0.0	…	…	0.0	…	…	0.0	…	…	0.0	…	…	98.6	…	…	0.0	…	…	1.4	…	…
J23452225-7126505	0.0	0.0	…	0.0	0.0	…	99.9[b]	99.9	…	0.0	0.0	…	0.0	0.0	…	0.0	0.0	…	0.1	0.0	…	0.0	0.0	…
J23474694-6517249	0.0	0.0	…	0.0	0.0	…	99.9	99.9	…	0.0	0.0	…	0.0	0.0	…	0.0	0.0	…	0.0	0.0	…	0.0	0.0	…
J23495365+2427493	81.7	…	…	0.0	…	…	0.0	…	…	16.1[b]	…	…	0.0	…	…	0.0	…	…	0.0	…	…	2.2	…	…
J23500639+2659519	92.8[b]	61.6[b]	…	0.0	0.0	…	0.0	0.0	…	3.3[b]	0.0	…	0.0	0.0	…	0.0	0.0	…	0.0	0.0	…	3.9	38.4	…

Table 2.VIII — continued

Name	βPMG			TWA			THA			COL			CAR			ARG			ABDMG			Field		
	P	P_v	$P_{v+\pi}$	P	P_v	$P_{v+\pi}$	P	P_v	$P_{v+\pi}$	P	P_v	$P_{v+\pi}$	P	P_v	$P_{v+\pi}$	P	P_v	$P_{v+\pi}$	P	P_v	$P_{v+\pi}$	P	P_v	$P_{v+\pi}$
J23512227+2344207	95.0	99.3	...	0.0	0.0	...	0.0	0.0	...	3.5[b]	0.0	...	0.0	0.0	...	0.0	0.0	...	0.0	0.0	...	1.5	0.7	...
J23513366+3127229	4.8	0.0	...	0.0	0.0	...	0.0	0.0	...	0.0	0.0	...	0.0	0.0	...	0.0	0.0	...	95.1[b]	99.9[b]	...	0.2	0.0	...
J23532520-7056410	1.8	0.0	...	0.0	0.0	...	0.0	0.0	...	0.0	0.0	...	0.0	0.0	...	92.2[b]	99.4[b]	...	0.0	0.0	...	6.0	0.6	...
J23555512-1321238	0.0	0.0	...	0.0	0.0	...	0.0	0.0	...	0.0	0.0	...	0.0	0.0	...	97.3	0.0	...	0.0	0.0	...	2.7	99.9	...
J23572056-1258487	0.0	0.0	...	0.0	0.0	...	0.0	0.0	...	0.0	0.0	...	0.0	0.0	...	99.9[b]	0.0	...	0.0	0.0	...	0.2	99.9	...
J23581366-1724338	0.0	0.0	0.0	0.0	0.0	0.0	0.0	0.0	0.0	0.0	0.0	0.0	0.0	0.0	0.0	99.2	0.0	0.0	0.0	0.0	0.0	0.8	99.9	99.9

[a]Membership probability (P), membership probability including radial velocity information (P_v), or membership probability including radial velocity and parallax informations ($P_{v+\pi}$).

[b]Membership probability (P or P_v or $P_{v+\pi}$) for which the binary hypothesis has a higher probability.

BIBLIOGRAPHIE

Adelman-McCarthy, J. K., & et al. 2011, VizieR Online Data Catalog, 2306, 0

Anderson, E., & Francis, C. 2012, Astronomy Letters, 38, 331

Bailey, III, J. I., White, R. J., Blake, C. H., Charbonneau, D., Barman, T. S., Tanner, A. M., & Torres, G. 2012, ApJ, 749, 16

Baraffe, I., Chabrier, G., Allard, F., & Hauschildt, P. H. 1998, A&A, 337, 403

—. 2002, A&A, 382, 563

Barrado Y Navascués, D. 2006, A&A, 459, 511

Barrado y Navascués, D., Stauffer, J. R., & Jayawardhana, R. 2004, ApJ, 614, 386

Barrado y Navascués, D., Stauffer, J. R., Song, I., & Caillault, J. 1999, ApJ, 520, L123

Bergfors, C., et al. 2010, A&A, 520, A54+

Beuzit, J.-L., et al. 2004, A&A, 425, 997

Bobylev, V. V., & Bajkova, A. T. 2007, Astronomy Letters, 33, 571

Bobylev, V. V., Goncharov, G. A., & Bajkova, A. T. 2007, VizieR Online Data Catalog, 908, 30821

Bowler, B. P., Liu, M. C., Shkolnik, E. L., Dupuy, T. J., Cieza, L. A., Kraus, A. L., & Tamura, M. 2012, ArXiv e-prints

Casagrande, L., Flynn, C., & Bessell, M. 2008, MNRAS, 389, 585

Chen, C. H., Mamajek, E. E., Bitner, M. A., Pecaut, M., Su, K. Y. L., & Weinberger, A. J. 2011, ApJ, 738, 122

Cutri, R. M., et al. 2003, VizieR Online Data Catalog, 2246, 0

da Silva, L., Torres, C. A. O., de La Reza, R., Quast, G. R., Melo, C. H. F., & Sterzik, M. F. 2009, A&A, 508, 833

de La Reza, R., da Silva, L., Jilinski, E., Torres, C. A. O., & Quast, G. 2001, in Astronomical Society of the Pacific Conference Series, Vol. 244, Young Stars Near Earth : Progress and Prospects, ed. R. Jayawardhana & T. Greene, 37–+

de la Reza, R., Jilinski, E., & Ortega, V. G. 2006, AJ, 131, 2609

de la Reza, R., & Pinzón, G. 2004, AJ, 128, 1812

de la Reza, R., Torres, C. A. O., Quast, G., Castilho, B. V., & Vieira, G. L. 1989, ApJ, 343, L61

Desidera, S., et al. 2011, A&A, 529, A54

Donati, J.-F., Catala, C., Landstreet, J. D., & Petit, P. 2006, in Astronomical Society of the Pacific Conference Series, Vol. 358, Astronomical Society of the Pacific Conference Series, ed. R. Casini & B. W. Lites, 362–+

Donati, J.-F., Semel, M., Carter, B. D., Rees, D. E., & Collier Cameron, A. 1997, MNRAS, 291, 658

Doyon, R., Lafrenière, D., Artigau, E., Malo, L., & Marois, C. 2010, in In the Spirit of Lyot 2010

Eggen, O. J. 1958, MNRAS, 118, 65

—. 1995, AJ, 110, 2862

Epchtein, N., et al. 1997, The Messenger, 87, 27

Faherty, J. K., et al. 2012, ArXiv e-prints

Fernández, D., Figueras, F., & Torra, J. 2008, A&A, 480, 735

Francis, C., & Anderson, E. 2009, New Astronomy, 14, 615

Gizis, J. E., Jao, W.-C., Subasavage, J. P., & Henry, T. J. 2007, ApJ, 669, L45

Gizis, J. E., Reid, I. N., & Hawley, S. L. 2002, AJ, 123, 3356

Gliese, W., & Jahreiss, H. 1991, NASA STI/Recon Technical Report A, 92, 33932

Gontcharov, G. A. 2006, Astronomy Letters, 32, 759

Gregorio-Hetem, J., Lepine, J. R. D., Quast, G. R., Torres, C. A. O., & de La Reza, R. 1992, AJ, 103, 549

Grenier, S., et al. 1999, A&AS, 137, 451

Guenther, E. W., Esposito, M., Mundt, R., Covino, E., Alcalá, J. M., Cusano, F., & Stecklum, B. 2007, A&A, 467, 1147

Hawley, S. L., Gizis, J. E., & Reid, I. N. 1996, AJ, 112, 2799

Helou, G., & Walker, D. W., eds. 1988, Infrared astronomical satellite (IRAS) catalogs and atlases. Volume 7 : The small scale structure catalog, Vol. 7

Herbig, G. H., & Bell, K. R. 1988, Third Catalog of Emission-Line Stars of the Orion Population : 3 : 1988

Hinkle, K. H., et al. 2003, in Presented at the Society of Photo-Optical Instrumentation Engineers (SPIE) Conference, Vol. 4834, Society of Photo-Optical Instrumentation Engineers (SPIE) Conference Series, ed. P. Guhathakurta, 353–363

Høg, E., et al. 2000, A&A, 355, L27

Janson, M., et al. 2012, ArXiv e-prints

Jayawardhana, R., Coffey, J., Scholz, A., Brandeker, A., & van Kerkwijk, M. H. 2006, ApJ, 648, 1206

Johnson, D. R. H., & Soderblom, D. R. 1987, AJ, 93, 864

Kastner, J. H., Zuckerman, B., Weintraub, D. A., & Forveille, T. 1997, Science, 277, 67

Kharchenko, N. V., Scholz, R., Piskunov, A. E., Roeser, S., & Schilbach, E. 2007, VizieR Online Data Catalog, 3254, 0

Kiss, L. L., et al. 2011, MNRAS, 411, 117

Koen, C., Kilkenny, D., van Wyk, F., Cooper, D., & Marang, F. 2002, MNRAS, 334, 20

Koen, C., Kilkenny, D., van Wyk, F., & Marang, F. 2010, MNRAS, 403, 1949

Landolt, A. U. 2009, AJ, 137, 4186

Lepine, S., & Shara, M. M. 2005, VizieR Online Data Catalog, 1298, 0

Lépine, S., & Simon, M. 2009, AJ, 137, 3632

Looper, D. L., Bochanski, J. J., Burgasser, A. J., Mohanty, S., Mamajek, E. E., Faherty, J. K., West, A. A., & Pitts, M. A. 2010, AJ, 140, 1486

López-Santiago, J., Montes, D., Crespo-Chacón, I., & Fernández-Figueroa, M. J. 2006, ApJ, 643, 1160

López-Santiago, J., Montes, D., Gálvez-Ortiz, M. C., Crespo-Chacón, I., Martínez-Arnáiz, R. M., Fernández-Figueroa, M. J., de Castro, E., & Cornide, M. 2010, A&A, 514, A97+

Luhman, K. L., Stauffer, J. R., & Mamajek, E. E. 2005, ApJ, 628, L69

Makarov, V. V. 2007, ApJS, 169, 105

Makarov, V. V., & Urban, S. 2000, MNRAS, 317, 289

Mamajek, E. E. 2005, ApJ, 634, 1385

Mamajek, E. E., & Feigelson, E. D. 2001, in Astronomical Society of the Pacific Conference Series, Vol. 244, Young Stars Near Earth : Progress and Prospects, ed. R. Jayawardhana & T. Greene, 104–115

Mamajek, E. E., Lawson, W. A., & Feigelson, E. D. 2000, ApJ, 544, 356

Marois, C., Macintosh, B., Barman, T., Zuckerman, B., Song, I., Patience, J., Lafrenière, D., & Doyon, R. 2008, Science, 322, 1348

Mazeh, T., Prato, L., Simon, M., Goldberg, E., Norman, D., & Zucker, S. 2002, ApJ, 564, 1007

Mentuch, E., Brandeker, A., van Kerkwijk, M. H., Jayawardhana, R., & Hauschildt, P. H. 2008, ApJ, 689, 1127

Messina, S., Desidera, S., Turatto, M., Lanzafame, A. C., & Guinan, E. F. 2010, A&A, 520, A15+

Mohanty, S., Jayawardhana, R., & Barrado y Navascués, D. 2003, ApJ, 593, L109

Montes, D., López-Santiago, J., Gálvez, M. C., Fernández-Figueroa, M. J., De Castro, E., & Cornide, M. 2001, MNRAS, 328, 45

Moór, A., Ábrahám, P., Derekas, A., Kiss, C., Kiss, L. L., Apai, D., Grady, C., & Henning, T. 2006, ApJ, 644, 525

Nakajima, T., & Morino, J.-I. 2012, AJ, 143, 2

Nakajima, T., Morino, J.-I., & Fukagawa, M. 2010, AJ, 140, 713

Ochsenbein, F., Bauer, P., & Marcout, J. 2000, A&AS, 143, 23

Ortega, V. G., Jilinski, E., de la Reza, R., & Bazzanella, B. 2009, AJ, 137, 3922

Perryman, M. A. C., et al. 1997, A&A, 323, L49

Phan-Bao, N., et al. 2003, A&A, 401, 959

Reid, I. N., & Cruz, K. L. 2002, AJ, 123, 2806

Reid, I. N., et al. 2003, AJ, 126, 3007

—. 2004, AJ, 128, 463

Riaz, B., Gizis, J. E., & Harvin, J. 2006, AJ, 132, 866

Rice, E. L., Faherty, J. K., & Cruz, K. L. 2010, ApJ, 715, L165

Riedel, A. R., Murphy, S. J., Henry, T. J., Melis, C., Jao, W.-C., & Subasavage, J. P. 2011, AJ, 142, 104

Rodriguez, D. R., Bessell, M. S., Zuckerman, B., & Kastner, J. H. 2011, ApJ, 727, 62

Roeser, S., Demleitner, M., & Schilbach, E. 2010, AJ, 139, 2440

Roeser, S., Schilbach, E., Schwan, H., Kharchenko, N. V., Piskunov, A. E., & Scholz, R. 2008, VizieR Online Data Catalog, 1312, 0

Rucinski, S. M., & Krautter, J. 1983, A&A, 121, 217

Salim, S., & Gould, A. 2003, ApJ, 582, 1011

Schlieder, J. E., Lépine, S., & Simon, M. 2010, AJ, 140, 119

—. 2012a, ArXiv e-prints

Schlieder, J. E., Lepine, S., & Simon, M. 2012b, ArXiv e-prints

Shkolnik, E., Liu, M. C., & Reid, I. N. 2009, ApJ, 699, 649

Shkolnik, E. L., Anglada-Escude, G., Liu, M. C., Bowler, B. P., Weinberger, A. J., Boss, A. P., Reid, I. N., & Tamura, M. 2012, ArXiv e-prints

Shkolnik, E. L., Liu, M. C., Reid, I. N., Dupuy, T., & Weinberger, A. J. 2011, ApJ, 727, 6

Siebert, A., et al. 2011, AJ, 141, 187

Skrutskie, M. F., et al. 2006, AJ, 131, 1163

Song, I., Zuckerman, B., & Bessell, M. 2012, ArXiv e-prints

Song, I., Zuckerman, B., & Bessell, M. S. 2003, ApJ, 599, 342

—. 2004, ApJ, 614, L125

Steinmetz, M., et al. 2006, AJ, 132, 1645

Stelzer, B., & Neuhäuser, R. 2000, A&A, 361, 581

Teixeira, R., Ducourant, C., Chauvin, G., Krone-Martins, A., Bonnefoy, M., & Song, I. 2009, A&A, 503, 281

Teixeira, R., Ducourant, C., Chauvin, G., Krone-Martins, A., Song, I., & Zuckerman, B. 2008, A&A, 489, 825

Tetzlaff, N., Neuhaeuser, R., & Hohle, M. M. 2010, VizieR Online Data Catalog, 741, 190

Torres, C. A. O., da Silva, L., Quast, G. R., de la Reza, R., & Jilinski, E. 2000, AJ, 120, 1410

Torres, C. A. O., Quast, G. R., da Silva, L., de La Reza, R., Melo, C. H. F., & Sterzik, M. 2006, A&A, 460, 695

Torres, C. A. O., Quast, G. R., de La Reza, R., da Silva, L., & Melo, C. H. F. 2001, in Astronomical Society of the Pacific Conference Series, Vol. 244, Young Stars Near Earth : Progress and Prospects, ed. R. Jayawardhana & T. Greene, 43–+

Torres, C. A. O., Quast, G. R., de La Reza, R., da Silva, L., Melo, C. H. F., & Sterzik, M. 2003, in Astrophysics and Space Science Library, Vol. 299, Open Issues in Local Star Formation, ed. J. Lépine & J. Gregorio-Hetem, 83

Torres, C. A. O., Quast, G. R., Melo, C. H. F., & Sterzik, M. F. 2008, Young Nearby Loose Associations, ed. B. Reipurth, 757–+

Upgren, A. R., & Harlow, J. J. B. 1996, PASP, 108, 64

van Leeuwen, F., ed. 2007, Astrophysics and Space Science Library, Vol. 350, Hipparcos, the New Reduction of the Raw Data

Voges, W. 1994, in New Horizon of X-Ray Astronomy. First Results from ASCA, ed. F. Makino & T. Ohashi, 197–+

Wahhaj, Z., et al. 2011, ApJ, 729, 139

Webb, R. A., Zuckerman, B., Platais, I., Patience, J., White, R. J., Schwartz, M. J., & McCarthy, C. 1999, ApJ, 512, L63

Weis, E. W. 1987, AJ, 93, 451

—. 1991, AJ, 102, 1795

White, R. J., Gabor, J. M., & Hillenbrand, L. A. 2007, AJ, 133, 2524

Zacharias, N., et al. 2009, VizieR Online Data Catalog, 1315, 0

Zacharias, N., Monet, D. G., Levine, S. E., Urban, S. E., Gaume, R., & Wycoff, G. L. 2005, VizieR Online Data Catalog, 1297, 0

Zickgraf, F.-J., Krautter, J., Reffert, S., Alcalá, J. M., Mujica, R., Covino, E., & Sterzik, M. F. 2005, A&A, 433, 151

Zuckerman, B., Rhee, J. H., Song, I., & Bessell, M. S. 2011, ApJ, 732, 61

Zuckerman, B., & Song, I. 2004, ARA&A, 42, 685

Zuckerman, B., Song, I., & Bessell, M. S. 2004, ApJ, 613, L65

Zuckerman, B., Song, I., Bessell, M. S., & Webb, R. A. 2001a, ApJ, 562, L87

Zuckerman, B., Song, I., & Webb, R. A. 2001b, ApJ, 559, 388

Zuckerman, B., & Webb, R. A. 2000, ApJ, 535, 959

Zuckerman, B., Webb, R. A., Schwartz, M., & Becklin, E. E. 2001c, ApJ, 549, L233

Zwitter, T., et al. 2008, AJ, 136, 421

CHAPITRE 3

CARACTÉRISATION DE LA VITESSE RADIALE, DE LA ROTATION ET DE L'ÉMISSION DE RAYONS X DES ÉTOILES DE FAIBLE MASSE CANDIDATES DANS LES ASSOCIATIONS CINÉMATIQUES JEUNES ET PROCHES

BANYAN. III. RADIAL VELOCITY, ROTATION AND X-RAY EMISSION OF LOW-MASS STAR CANDIDATES IN NEARBY YOUNG KINEMATIC GROUPS

Lison Malo[1,2], Étienne Artigau[2], René Doyon[2], David Lafrenière[2], Loïc Albert[2], and Jonathan Gagné[2]

Abstract

Based on high-resolution spectra obtained with PHOENIX at Gemini-South, CRIRES at VLT-UT1, and ESPaDOnS at CFHT, we present new measurements of the radial and projected rotational velocities of 219 low-mass stars. The target likely membership was initially established using the Bayesian analysis tool recently presented in Malo et al. (2013), taking into account only the position, proper motion and photometry of the stars to assess their membership probability. In the present study, we include radial velocity as an additional input to our analysis, and in doing so we confirm the high membership probability for 130 candidates : 27 in β Pictoris, 22 in Tucana-Horologium, 25 in Columba, 7 in Carina, 18 in Argus and 18 in AB Doradus and 13 with an ambiguous membership. Our analysis also confirms the membership of 57 stars proposed in the literature. A sub-sample of 16 candidates was observed at three or more epochs, allowing us to discover

---

6 new spectroscopic binaries. The fraction of binaries in our sample is 25%, consistent with values in the literature. Twenty percent of the stars in our sample show projected rotational velocities ($v \sin i$) higher than 30 km s^{-1} and therefore are considered as fast rotators. A parallax and other youth indicators are still needed to fully confirm the 130 highly probable candidates identified here as new *bona fide* members. Finally, based on the X-ray emission of *bona fide* and highly probable group members, we show that for low-mass stars in the 12-120 Myr age range, the X-ray luminosity is an excellent indicator of youth and better than the more traditionally used R$_X$ parameter, the ratio of X-ray to bolometric luminosity.

3.1 Introduction

The search for young low-mass stars in the solar neighborhood has gained tremendous momentum recently as the youth and intrinsic faintness of these objects make them prime targets for planet searches through high-contrast imaging. This is both because young planetary-mass companions shine brighter and because low-mass stars are less luminous, which loosens the imaging contrast requirements. Finding more Young Moving Group (YMG) members also has intrinsic interest : to refine these YMG characteristics (initial mass function, age, velocities, spatial extent), to complete the solar neighborhood census, and to improve and develop new youth indicators.

As YMG members share common kinematics and span similar age ranges, one can search for overlooked members through a detailed kinematic and photometric analysis of nearby stars. The Hipparcos mission, combined with multiple radial velocity studies (e.g., Anderson & Francis 2012, de Bruijne & Eilers 2012) led to the identification of the most massive members of these groups, but the relatively shallow completeness magnitude ($V = 7 - 9$) prevented the detection of low-mass members (i.e., later than M5). Assuming that YMG stars follow a typical Initial Mass Function (IMF), the vast majority of low-mass members are expected to have gone unnoticed. This led to a number of efforts to extend measurements of proper motion, radial velocity and parallax to the nearby low-mass dwarfs (e.g., Shkolnik et al. 2012).

Proper motion studies beyond the reach of *Hipparcos* also benefitted greatly from the advent other all-sky surveys (e.g., Lépine & Simon 2009, Zacharias et al. 2013) reaching fainter magnitudes. In particular, infrared proper motions can now be obtained by correlating the WISE and 2MASS (Cutri et al., 2012) surveys, which is ideally suited to measure proper motions well into the substellar regime (Gagné et al., 2013, Rodriguez et al., 2013). These all-sky photometric surveys have now been supplemented by radial velocity (RV) measurements coming from various works. Surveys like the Radial Velocity Experiment (RAVE; Steinmetz et al., 2006, Zwitter et al., 2008) and SDSS (York et al., 2000) performed RV measurements on a large sample of stars, while others were focussed on old low-mass dwarfs (Chubak et al., 2012, Delfosse et al., 1998, Jenkins et al., 2009, Soubiran et al., 2013). These RV studies are key for studying Galactic dynamics. Finally, and not least, parallax measurements of solar neighborhood stars is spear-headed by the CTIOPI and RECONS group (Riedel et al., 2014, 2011, 2010) and other works (Lépine & Simon, 2009, Liu et al., 2013, Shkolnik et al., 2012) focusing on the lowest mass component of the solar neighborhood.

To complete the census of nearby young kinematic group members, kinematics alone is not enough to confirm membership, independent youth indicators are also mandatory to confirm the age of these stars. The high magnetic activity of young stars gives rise to various indicators such as $H\alpha$ emission, X-ray and UV (Rodriguez et al., 2011, 2013, Preibisch & Feigelson, 2005, Shkolnik et al., 2011). Other spectroscopic indicators include the Li abundance (da Silva et al., 2009, Mentuch et al., 2008) and others like sodium and calcium doublets (Na ; 8183-8195Å, Ca : 8498-8542Å) that trace low-surface gravity (Mentuch et al., 2008, Lyo et al., 2004, Shkolnik et al., 2009, Slesnick et al., 2006). Stellar rotation and gyrochronology can also be used for constraining the age of an isolated star through a comparison with young stars in open clusters of known ages such as the Hyades, Pleiades and IC2391 (Irwin et al., 2011, López-Santiago et al., 2009, 2010, Messina et al., 2010). Recently, Reiners & Mohanty (2012) presented the angular momentum evolution in low-mass stars, which can also be used as a youth indicator. To assess the membership of a given star to the known YMGs, a complete description of these groups is essential : their space velocity, spatial extent, luminosity along

with appropriate youth indicators. Based on such YMG descriptions, any given star candidate member of a YMG can have its observational properties (proper motion, radial velocity, absolute magnitude) compared against actual observations.

In the present paper, we present the follow-up of the 130 highly candidate members of young kinematic groups identified or re-identified in a previous paper (Malo et al., 2013, hereafter Paper I). In that paper, we presented an analysis tool (BANYAN[1]) based on Bayesian inference to assess the membership probability of a given low-mass star to nearby YMGs. This analysis has unveiled a large population of potentially new young low-mass stars but those stars cannot be confirmed as *bona fide* members of their respective association until knowledge of their radial velocity, parallax measurements and signs of youth are secured. The present work focuses on the radial and projected rotational velocity measurements which were measured through the cross-correlation technique using the infrared and optical domain. The paper is structured as follows. The sample and the observations are presented in § 4.2 and data reduction is presented in § 4.3. A presentation of the radial and projected rotational velocity measurements follows in § 4. The identification and confirmation of highly candidate members is described in § 4.5 and § 4.6 is devoted to a discussion of rotation-age and X-ray luminosity relations. Concluding remarks follow in § 4.7.

3.2   Sample and Observations

A detailed account of our initial search sample has been presented in Paper I. In summary, our original sample of stars show chromospheric X-ray and Hα emissions, and have good I$_c$ photometry and proper motion measurements (<0.2mag and $>4\sigma$). In Paper I, the *I*-band photometric data came from several studies. Recently, the UCAC4 (Zacharias et al., 2013) catalog published *I*-band photometric data from the APASS[2] survey. For this paper, we use an uniform source of *I*-band photometric data by using APASS-i' instead of DENIS and SDSS-DR8 catalogs, when possible. We transform the APASS-i' magnitude from UCAC4 catalog to I_c using conversion derived from the stan-

---

[1]Bayesian Analysis for Nearby Young AssociatioNs : www.astro.umontreal.ca/∼malo
[2]www.aavso.org/apass

dards of Landolt (Landolt, 2009). The transformation is :

$$I_c = i_{APASS} - 0.546 \qquad (3.1)$$

and accurate within 0.05 mag over $0.9 < I_c - J < 2.0$.

Using *I*-band photometry from the UCAC4 catalog has added 141 stars that were not included in Paper I because the *I*-band photometry was not available. Our initial sample was thus increased to 920 low-mass (K5V-M5V) stars, of which 75 were previously identified as young stars in the literature. By applying our Bayesian analysis to this extended sample, we found 247 candidate members with a membership probability (*P*) over 90%, amongh which 50 were already proposed as candidate members in the literature. These candidates were restricted to the seven closest ($<100\,$pc) and youngest ($<100\,$Myr) co-moving groups considered in Paper I : TW Hydrae Association (TWA; de la Reza et al., 1989), β Pictoris Moving Group (βPMG; Zuckerman et al., 2001), Tucana-Horologium Association (THA; Torres et al., 2000, Zuckerman & Webb, 2000), Columba Association (COL; Torres et al., 2008), Carina Association (CAR; Torres et al., 2008), Argus Association (ARG; Makarov & Urban, 2000) and AB Doradus Moving Group (ABDMG; Zuckerman & Song, 2004).

3.2.1 Observations

As described in Paper I, our statistical analysis yields a membership probability, a prediction of the radial velocity and the most probable statistical distance for each star. Membership confirmation requires both a parallax and RV measurements consistent with prediction of the analysis. Some candidate members listed in Paper I present ambiguous memberships i.e. they could belong to two or more YMGs ; the radial velocities predicted for those groups differ by a few km s^{-1} . Therefore, high resolution spectroscopy with accuracy of a few km s^{-1} was required to clarify the membership of ambiguous candidates. Observations were performed using two near-infrared spectrographs, PHOENIX (Hinkle et al., 2003) and CRIRES (Kaeufl et al., 2004), and one optical spectrograph, ESPaDOnS (Donati et al., 2006). In all cases, a set of slowly rotating radial-velocity

standards were observed to calibrate our measurements. These template observations are summarized in Table 3.I.

3.2.1.1 PHOENIX

In 2009 and 2010[3], PHOENIX at Gemini-South was used with the 0.34″ wide slit in combination with the H6420 order-sorting filter (1.547 μm - 1.568 μm) to reach a resolving power of R $\sim$ 52,000 (4 pixels). This wavelength domain was selected as it is advantageously free of strong terrestrial absorption lines (Mazeh et al., 2002).

Observations were obtained with a typical ABBA dither pattern along the slit with individual exposures of 60 to 300 seconds depending on the target brightness. This observing strategy facilitates the removal of sky emission lines through the subtraction of two consecutive images. Along with each science target observation, a slowly radial velocity standard was observed immediately before or after. We also observed 12 M0-M3V slow rotators, which were used to calibrate measurements of rotational broadening. The typical signal-to-noise ratio (S/N) achieved was respectively 30-50 and 90-120 per spectral pixel for science targets and radial velocity standards. Using that setup, 243 observations of 155 stars were obtained with a S/N sufficient to extract radial velocity measurements with an accuracy better than 1 km s^{-1}.

We also used two archival radial velocity standards (GJ 382 and GJ 447) from the Gemini archive, which were observed during the GS-2002B-Q-11 program with the same setup. The reduction was done using the same method as explained above.

3.2.1.2 CRIRES

CRIRES was used at VLT-UT1[4] with the 0.4″ and 0.2″ wide slit in the order 36 (1.555 μm), resulting in a resolving power of 50,000 and 80,000, respectively. The dithering strategy and individual exposure times were similar to that used with PHOENIX. Each science program also included observations of radial velocity standards and slow

---

[3]Gemini ID program : GS-2009A-Q-89, GS-2009B-Q-45, GS-2010A-Q-32, GS-2010B-Q-18, QS-2010B-Q-89

[4]VLT Period : 087.D-0510, 088.D-0553, 089.D-0592, 091.D-0641

rotators. The achieved S/N was respectively 30-70 and 90-120 per spectral pixel for science targets and radial velocity standards. This observing strategy produced high S/N spectra allowing radial velocity measurements with accuracies better than $1\,\mathrm{km\,s^{-1}}$ for 105 observations of 88 stars.

3.2.1.3   ESPaDOnS

Starting in 2010, 53 stars were observed with ESPaDOnS, a visible light echelle spectrograph at CFHT[5]. Observations were done using the "star+sky" mode combined with the "slow" and "normal" CCD readout mode, to get a resolving power of R∼68,000 covering the 3700 to 10500 Åspectral domain over 40 grating orders. The total integration time per target was between 5 and 120 minutes.

3.3   Data reduction

3.3.1   Near-infrared Data

The data were reduced in a standard fashion for longslit spectroscopy, using custom *IDL* routines. The individual nods frames were first dark subtracted and divided by a normalized flat field (only for CRIRES data). For PHOENIX data, flat image contains fringe thus we do not use the flat images. The nods frames were then pair-subtracted, and we forced that dispersion to be perpendicular to the trace by correcting the slit inclinaison. The 1-D spectrum extraction was obtained from the intensity difference image, where a median Gaussian fitting in the spatial direction was used (in both positive and negative traces). Both the datasets were wavelength-calibrated using five strong OH emission lines (1.5539711, 1.5540945, 1.5545890, 1.5546393, 1.5570159 μm; Rousselot et al., 2000) that encompass the wavelength domain used.

The noise in each spectrum was determined by measuring the pixel-to-pixel scatter along the extracted 1-D spectrum. Each spectrum was corrected for the barycentric velocity component of the Earth using the *IDL* function *baryvel* which is available as part

---

[5]CFHT program : 11AC13, 11BC08, 11BC99, 12AC23, 12BC24, 13AC23, 13BC33

Table 3.I.   Properties of radial velocity standards

Name of template	Spectral Type	RV (km s^{-1})	$v\sin i$ (km s^{-1})	Ref.	Instrument
HIP 107345	M1V	2.3±0.5	8.2±0.1	1,1	PH,CR
HIP 1993	M0Ve	6.4±0.1	7.3±2.3	1,1	PH,CR
HIP 23309	M0Ve	19.4±0.3	5.8±0.3	1,1	PH,CR
GJ 806	M3V	-24.7±0.1	1.5	5,2	ESP
GJ 908	M2V	-71.3±0.1	3.0	5,2	ESP
GJ 382	M2V	7.9±0.1	<1.8	3,4	CR,PH,ESP
GJ 447	M4V	-31.1±0.1	<2.5	3,4	PH
GJ 729	M3Ve	-10.5±0.2	2.5	5,1	CR
HIP 67155	M2V	15.8±0.1	<1.4	3,2	CR,ESP
HIP 65859	M0.5V	14.56±0.1	<2.0	3,2	ESP
HIP 68469	M1V	-25.8±0.1	<2.0	3,2	ESP

References. — (1) Torres et al., 2006 ; (2) Jenkins et al., 2009 ; (3) Nidever et al., 2002 ; (4) Reiners et al., 2012 ; (5) de Bruijne & Eilers, 2012

Note. — Instrument : PHOENIX (PH), CRIRES (CR) and ESPaDOnS (ESP)

of the astrolib package [6]. For visual binary stars, we reduced each component by fitting two Gaussian profiles to the trace.

3.3.2   ESPaDOnS Data

The ESPaDOnS observations were reduced by CFHT using UPENA 1.0, an in-house software that calls the Libre-ESpRIT pipeline (Donati et al., 1997). In the present analysis, we used the processed spectra with the continuum normalized to 1 and automatic wavelength correction from telluric lines.

3.4   Results

The extracted high-resolution spectra enabled measurement of the science target radial velocity from the observed Doppler shift, and the projected rotational velocity ($v\sin i$) from the width of the absorption lines. All 403 observations were analysed using the procedure described in Section 3.4.1. Table 3.XI summarizes all measurements.

[6]idlastro.gsfc.nasa.gov

In addition, it was possible to investigate the multiplicity fraction of these stars by classifying them into three categories : 1) visual binaries (using the acquisition images) ; 2) double-line spectroscopic binaries (SB2) ; and 3) single-line spectroscopic binaries (SB1).

3.4.1 Radial and projected rotational velocity measurements

The radial velocity (RV) and projected rotational velocity ($v \sin i$) were measured through a cross-correlation between each individual spectrum and a template. The template consisted in radial velocity standard (see Table 3.I) convolved with rotational profiles and artificially Doppler shifted. All spectra were effectively re-sampled at equal steps of $\log \lambda$ to properly sample data in equal velocity bins. In artificially broadening standard star spectra, the rotational profiles defined in Gray (1992) were adopted, or more specifically we used the *IDL astrolib* routine *lsf_rotate*. The limb darkening was set to a typical value of 0.6. The RV and $v \sin i$ parameters were scanned between -150 and 150 km s^{-1} and between 1 and 120 km s^{-1}, respectively. The maximum of the Cross-Correlation Function (CCF) was found by fitting a Gaussian function to the central peak. That yielded the best value of RV and $v \sin i$. For each template, a χ^2 minimization map in 2-D (RV and $v \sin i$) was generated and the template producing the lowest χ^2 was adopted which yielded the final RV and $v \sin i$ measurements.

The wavelengths across which the analysis was performed were the same for all near-infrared datasets (between 1.553 and 1.5575 μm). For the optical data, cross-correlation was performed on an order by order basis between 531 to 793 nm. Only parts of orders devoid of strong telluric absorption were used, these are orders : 26, 27, 28, 29, 30, 31, 33, 35, 36, 37 and 42.

For double-line spectroscopic binary cases, the two peaks seen in the CCF map were both fitted by a Gaussian function.

Figure 3.1 presents a comparison between radial and projected rotational velocity measurements from this analysis and those compiled from the literature. There is an excellent correlation between the literature values and those observed from this work, with a standard deviation of 1.3, 1.9 and 0.8 km s^{-1} for PHOENIX, CRIRES and ESPa-

DOnS, respectively. Except for one star (J05332558-5117131), we have similar results for projected rotational velocity measurements. We cannot exclude that this exception is a spectroscopic binary, which was unresolved during our observations but mostly resolved during Torres et al. (2006) observation.

3.4.1.1 Uncertainty on radial and projected rotational velocity measurements

Our sources of uncertainty on radial velocity measurement (similar for $v\sin i$ measurements) fall into three categories, which are expressed in the Equation 3.2 :

$$\sigma_{RV}^2 = \sigma_{noise}^2 + \sigma_{rvstd}^2 + \sigma_{rvvsini}^2 \tag{3.2}$$

where σ_{noise} is the statistical spectrum noise, σ_{rvstd} is the uncertainty of the RV standard and $\sigma_{rvvsini}$ is the systematic error as a function of $v\sin i$. The σ_{noise} was determined by repeating, through a Monte Carlo analysis, the procedure explained in Section 4, this time adding Gaussian noise to each spectral pixel and measuring the standard deviation of the resulting distribution. The second source of uncertainty taken into account is the error on RV and $v\sin i$ of the slowly-rotating radial velocity templates, whose values are tabulated in Table 3.I. The third source is the systematic uncertainty from the RV offset which is effectively measured when comparing RV of an artificially broadened slowly-rotating template to its original self. That RV offset as a function of $v\sin i$ was determined for each template. Figure 3.2 presents the systematic RV offset as a function of $v\sin i$ when GJ 382 is used as a radial velocity template for the three instruments. The correction is significant for $v\sin i > 30$ km s^{-1} . For example, a target spectrum correlated with that of GJ 382 with a $v\sin i$ of 30 km s^{-1} introduces a systematic RV offset of 1.6 km s^{-1}, 1.1 km s^{-1} and 0.2 km s^{-1} with PHOENIX, CRIRES and ESPaDOnS, respectively.
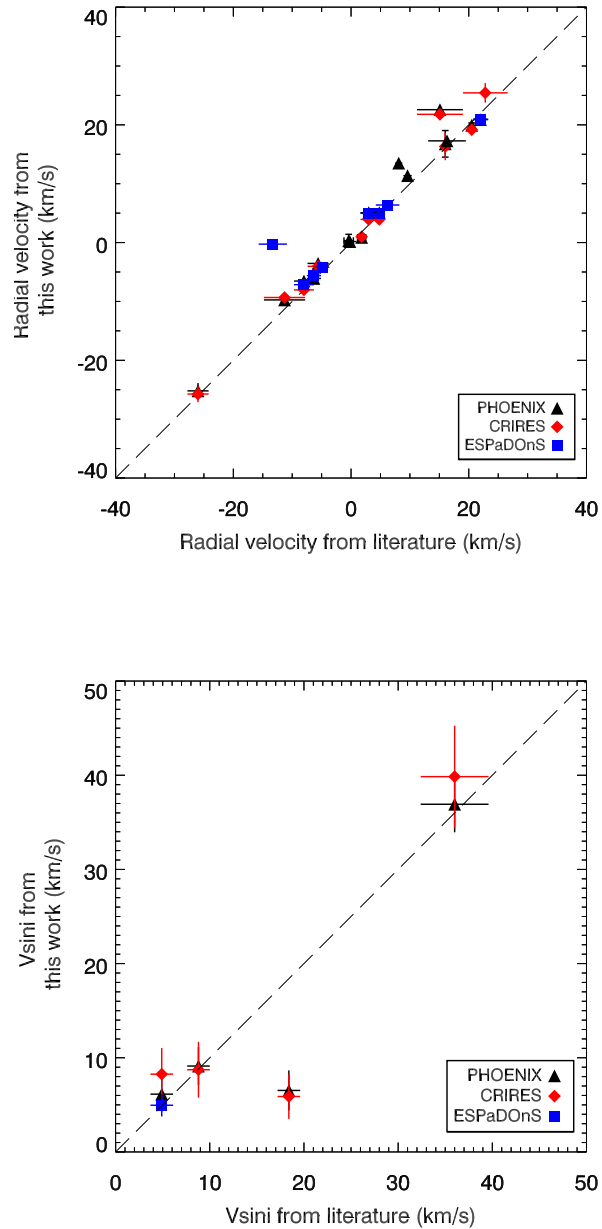
Figure 3.1 Radial and projected rotational velocity measurements for PHOENIX (black triangles), CRIRES (red diamonds) and ESPaDOnS (blue squares) compared to compiled measurements from the literature. The dotted line illustrates the one-to-one relation between literature and measured velocities.
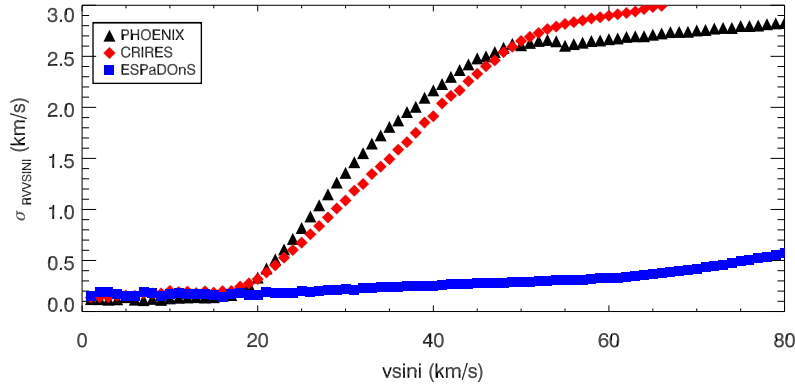
Figure 3.2 Systematic radial velocity offset induced by the convolution of a slowly rotating RV templates (GJ 382) as a function of $v\sin i$. The CRIRES and PHOENIX datasets (red diamonds, black triangles) show a $> 1\,\mathrm{km\,s^{-1}}$ systematic errors for $v\sin i$ values above $\sim 30\,\mathrm{km\,s^{-1}}$, while ESPaDOnS data set (order42 : blue squares), which covers a much broader wavelength domain, is almost immune to this effect.

3.4.2 Multiplicity fraction

Properties of multiple systems provide strong empirical constraints on star formation theories and evolution. Moreover, double-lined spectroscopic binaries allow precise determination of dynamical properties of the components, including the mass ratio (Gálvez-Ortiz et al., 2010). One clear observational trend, which has gradually emerged is that the multiplicity fraction gradually decreases with decreasing stellar mass (Janson et al., 2012).

During our follow-up program, a sample of hiterto unidentified visual or spectroscopic binaries was uncovered. From the 219 observed stars, we found 37 visual binary (VB), 12 double-lined spectroscopic binaries (SB2) and 6 single-lined spectroscopic binaries (SB1) showing radial velocity variations of more than $5\,\mathrm{km\,s^{-1}}$. Table 3.II lists the properties of the binary systems found within our program.

It is worthwhile to note that for 78% of the βPMG and ABDMG candidate binary systems, our statistical analysis predicted an overluminosity compared to *bona fide* members. This overluminosity prediction decreases to 33% for THA, COl, CAR and ARG candidates. As stated in Paper I, this overluminosity could be the result of unresolved binarity. For βPMG and ABDMG, our follow-up observations give credence to our ana-

lysis for identifying binary systems.

We find a binary fraction for the low-mass components of 25%, which is consistent with the value published in the literature (25%,42% Delfosse et al., 2004, Leinert et al., 1997). Shkolnik et al. (2010) find from a sample of 185 X-ray M dwarfs a spectroscopic binary fraction of 16%. Janson et al. (2012) find a multiplicity fraction for M0V-M5V dwarfs and separations between $0.08''$ and $6''$ of $27\pm 3\%$. Bergfors et al. (2010) estimated the multiplicity fraction for young M0V-M6V dwarfs (<600 Myr) with an angular separation $0.1''$ to $6''$ to be $32\pm6\%$.

We note that ultrafast rotators ($v\sin i > 50\,\text{km s}^{-1}$) could be unresolved spectroscopic binaries with two rapidly rotating components. Therefore, a second epoch of measurements is needed to rule out the binary status. An example of such behaviour is the TWA candidate member SCR 1425-4113 (see Riedel et al., 2014). While the CRIRES observation did not enable us to detect the two binary components, we measured a $v\sin i$ of 95 km s^{-1}. The second observation with ESPaDOnS enabled us to resolve the two components of the system.

3.5 Candidates Membership

The statistical analysis presented in Paper I assumed no prior knowledge of the radial velocity information for most systems[7]. The radial velocity obtained in this work can be used to further constraint their membership. Our analysis is based on a kinematical model that takes into account the mean Galactic space velocities (UVW) and Galactic positions (XYZ) along with their dispersion. Those parameters, given in Paper I, have been slightly modified to take into account several new proposed members from recent studies (Riedel et al., 2014, Shkolnik et al., 2012, Wahhaj et al., 2011, Weinberger et al., 2013). The following stars are considered new *bona fide* members ; in βPMG : 2MASSJ01112542+1526214 (LP 467-16AB), 2MASSJ05064946-2135038 (GJ 3332BC), 2MASSJ05064991-2135091 (GJ 3331A), HIP 23418ABCD and 2MASSJ03350208+2342356 ; in TWA : TWA2 and TWA12 ; and in ABDMG :

---

[7]BANYAN web tool : www.astro.umontreal.ca/∼malo

Table 3.II.   Properties of binary systems

Name (2MASS)	Sep. (arcsec)	q2/q1 (flux ratio)	Type of binary[a]	Instr.	Refs.[b]
J00233468+2014282AB	…	…	VB	ESP	1
J00281434-3227556	0.6	0.71	VB	PH	1
J00340843+2523498W	…	…	VB	ESP	5
J01132817-3821024	1.3	0.72	VB	PH	4
J01535076-1459503	2.7	0.80	VB	PH	4
J04480066-5041255A	…	…	VB	PH	1
J05045462-1415337	0.5	0.76	VB	PH	1
J05100488-2340148	1.7	0.63	VB	PH	4
J05100427-2340407A	…	…	VB	PH	4
J05130132-7027418	1.6	0.2	VB	CR	4
J05142736-1514514	2.5	0.3	VB	PH	1
J05241914-1601153AB	…	…	VB	PH	6
J05254166-0909123AB	…	…	VB	PH	7
J05301858-5358483	4.3	0.04	VB	CR	4
J06002304-4401217	1.9	0.97	VB	CR	4
J06153953-8433115	1.1	1.0	VB	CR	1
J06434532-6424396AB	…	…	VB	PH,CR	4
J07105990-5632596	0.9	0.35	VB	PH	1
J07523324-6436308A	…	…	VB	PH	1
J08224744-5726530	8.1	0.2	VB	CR	4
J08412528-5736021	1.4	0.97	VB	PH	4
J08472263-4959574	1.7	0.84	VB	PH	1
J09032434-6348330	7.9	0.11	VB	CR	1
J09423823-6229028	1.3	0.90	VB	CR	4
J10120908-3124451	1.1	0.96	VB	CR	1,3
J11102788-3731520	1.4	0.70	VB+SB2	PH	4
J14142141-1521215	1.3	0.34	VB	PH	1
J16074132-1103073AB	…	…	VB	PH	1
J17104431-5300250A	…	…	VB	PH	1
J17165072-3007104	1.6	0.92	VB	CR	1
J17243644-3152484	0.9	0.74	VB	CR	1
J17494867-4005431A	…	…	VB	PH	1
J18450097-1409053A	…	…	VB	PH	1
J20434114-2433534	1.3	0.98	VB	PH	8
J21103096-2710513	…	…	VB	CR	1
J23002791-2618431	2.1	0.54	VB	PH	1
J23204705-6723209	2.6	0.55	VB	PH	1
Double-line binary					
J01351393-0712517	…	…	SB2	ESP	1
J06131330-2742054	…	…	SB2	PH	3
J07282116+3345127	…	…	SB2	ESP	9
J08185942-7239561	…	…	SB2	CR	1
J08422284-8345248	…	…	SB2	PH,CR	1
J08465879-7246588	…	…	SB2	PH	1
J09361593+3731456	…	…	SB2	ESP	5
J14252913-4113323	…	…	SB2	ESP	1,3
J17462934-0842362	…	…	SB2	PH	1
J18141047-3247344	…	…	VB+SB2	CR	10
J19420065-2104051	…	…	SB2	CR	1
J20100002-2801410	…	…	SB2	ESP	4
Single-line binary					
J01132958-0738088	…	…	SB1	…	4
J02070176-4406380	…	…	SB1	…	1
J02485260-3404246	…	…	SB1	…	1
J15244849-4929473	…	…	SB1	…	1
J18495543-0134087	…	…	SB1	…	1
J22470872-6920447	…	…	SB1	…	1

[a] Visual binary (VB), Single-line binary (SB1), Double-line binary (SB2).

[b] (1) this work ; (2) Torres et al. (2006) ; (3) Riedel et al. (2014) ; (4) Janson et al. (2012) ; (5) Skiff (2010) ; (6) Bergfors et al. (2010) ; (7) Daemgen et al. (2007) ; (8) Shkolnik et al. (2009) ; (9) Shkolnik et al. (2010) ; (10) Messina et al. (2010).

Table 3.III. Main properties of young kinematic groups

Name of group	UVW (km s^{-1})	σ_{UVW} (km s^{-1})	XYZ (pc)	σ_{XYZ} (pc)	Number of objects	Age[a] range (Myr)	Distance[b] range (pc)
TW Hydrae (TWA)	$-10.53, -18.27, -5.00$	$3.50, 1.17, 2.15$	$12.17, -43.23, 21.90$	$6.14, 7.30, 3.06$	12	8-12[c]	42-92
β Pictoris (βPMG)	$-11.16, -16.19, -9.27$	$2.06, 1.32, 1.35$	$4.35, -5.82, -13.29$	$31.43, 15.04, 7.56$	44	12-22[d]	9-73
Tucana-Horologium (THA)	$-9.93, -20.72, -0.89$	$1.55, 1.79, 1.41$	$11.80, -20.79, -35.68$	$18.57, 9.14, 5.29$	42	20-40[e]	36-71
Columba (COL)	$-12.24, -21.27, -5.56$	$1.08, 1.22, 0.94$	$-28.22, -29.74, -28.07$	$13.68, 23.70, 16.09$	20	20-40[e]	35-81
Carina (CAR)	$-10.50, -22.36, -5.84$	$0.99, 0.55, 0.14$	$15.55, -58.53, -22.95$	$5.66, 16.69, 2.74$	5	20-40[e]	46-88
Argus (ARG)	$-21.78, -12.08, -4.52$	$1.32, 1.97, 0.50$	$14.60, -24.67, -6.72$	$18.60, 19.06, 11.43$	11	30-50[f]	8-68
AB Doradus (ABDMG)	$-7.11, -27.21, -13.82$	$1.39, 1.31, 2.26$	$-2.25, 2.93, -15.42$	$20.10, 18.97, 15.37$	48	70-120[g]	11-64
Field stars	$-10.92, -13.35, -6.79$	$23.22, 13.44, 8.97$	$-0.18, 2.10, 3.27$	$53.29, 51.29, 50.70$	10094		3-150

[a] Age range from the literature. Note that relative ages between moving groups are more accurate than absolute ones.

[b] Members with published trigonometric distance only.

[c] Age reference from Barrado Y Navascués (2006), Webb et al. (1999)

[d] Age reference from βPMG Makarov (2007), Song et al. (2003)

[e] Age reference from Zuckerman & Webb (2000), Torres et al. (2001)

[f] Age reference from Barrado y Navascués et al. (2004), Torres et al. (2008)

[g] Age reference from Mentuch et al. (2008), López-Santiago et al. (2006), Luhman et al. (2005)

2MASSJ06091922-3549311 (CD-35 2722 AB), J07234358+2024588 (BD+20 1790) and HIP 107948. For the sole purpose of establishing the core membership of the association, two outlier stars were removed from the *bona fide* member list. We removed HIP 51317 (M2V) from the ABDMG *bona fide* member list because its X-ray luminosity appears to be much more compatible with a field star (see Section 4.6.1.1). HIP 24947 in THA was also excluded because it has ambiguous radial velocity measurements (15.2, 23.9 km s^{-1}; Bobylev & Bajkova, 2007, Bobylev et al., 2007) that place it either in THA or COL. Table 3.III summarizes the main properties of YMGs.

This study presents RV measurements for 368 low-mass stars, of which 202 are new measurements and 166 are compiled from the literature. We also presents $v \sin i$ measurements for 270 stars, of which 202 are new measurements and 68 are compiled from the literature A weighted average of all RV and $v \sin i$ measurements was adopted for stars with multiple measurements (see Tables 3.IV and 3.V). Adding the RV information in our Bayesian tool, we found 130 highly-probable YMG candidates with membership probabilities (P_v) in excess of 90%. Of these, a subgroup of 117 can be uniquely associated with a single existing YMG, and the remaining 13 have high membership probabilities to two or more YMGs. A trigonometric distance is required to assign membership without ambiguity. The 117 candidates are divided the following way between

parent YMGs : 27 in βPMG, 22 in THA, 25 in COL, 7 in CAR, 18 in ARG and 18 in ABDMG. In addition, we confirmed the high membership probability of 57 candidates previously proposed in the literature. Table 4.III presents the properties of the strong YMG candidates which have a P_v above 90%.

For fast rotators with $v \sin i > 30$ km s^{-1} the RV becomes more uncertain which prevents significant constraints on the membership to be set. However, the rapid rotation deduced from the large $v \sin i$ when combined with other youth indicators (Malo et al. in prep) help constrain the age within certain broad limits (see Section 4.5.1). Candidates whose membership probability decreases when RV is included in the analysis but have a high projected rotational velocity (> 30 km s^{-1}) are tabulated in Table 4.III.

Table 3.IV. Compilation of RV from the literature

Name 2MASS	Spectral Type	RV (km s^{-1})	RV (km s^{-1})	RV (km s^{-1})
J00340843+2523498	K7Ve*	-12.4 ± 2.0^c	-8.8 ± 0.2^a	...
J01220441-3337036	K7Ve	4.8 ± 0.8^e	3.0 ± 1.4^c	4.7 ± 0.3^a
J01225093-2439505	M3.5V	9.6 ± 0.7^g	11.4 ± 0.2^a	...
J01521830-5950168	M2-3V	8.5 ± 2.3^h	7.9 ± 1.6^d	...
J02303239-4342232	K5Ve	16.3 ± 1.1^e	14.5 ± 2.4^h	...
J02365171-5203036	M2Ve	16.0 ± 0.1^e	14.6 ± 2.1^a	...
J03494535-6730350	K7V	16.3 ± 3.2^h	16.8 ± 0.2^a	...
J04435686+3723033	M3Ve	6.2 ± 2.0^c	6.4 ± 0.2^a	...
J04480066-5041255	K7Ve(vb)	19.3 ± 0.1^e	19.2 ± 0.3^a	...
J05082729-2101444	M5V	22.8 ± 3.8^b	23.6 ± 1.5^a	...
J05164586-5410168	M3V	15.1 ± 3.9^h	21.9 ± 0.4^a	...
J05254166-0909123	M3.5+M4	28.4 ± 0.5^i	25.7 ± 0.3^a	...
J05332558-5117131	K7V	20.5 ± 0.0^e	19.6 ± 0.4^a	...
J05335981-0221325	M3V	22.0 ± 1.3^b	20.9 ± 0.2^a	...
J11102788-3731520	M4Ve+M4Ve	15.6 ± 0.2^e	10.2 ± 0.4^a	...
J11254754-4410267	M4+M4.5	19.5 ± 2.0^l	20.9 ± 0.8^a	...
J17292067-5014529	M3Ve	-0.4 ± 0.8^e	0.3 ± 1.1^a	...
J18202275-1011131	K5Ve+K7Ve	-13.8 ± 0.8^e	-9.0 ± 1.0^k	...
J19102820-2319486	M4V	-8.0 ± 1.7^b	-6.9 ± 0.3^a	...
J19233820-4606316	M0V	-0.2 ± 1.1^j	-0.0 ± 0.3^a	...
J19312434-2134226	M2.5V	-26.0 ± 1.8^i	-25.5 ± 1.4^a	...
J19560438-3207376	M0V	-7.1 ± 2.2^h	-7.2 ± 0.4^d	...
J20013718-3313139	M1V	-5.6 ± 1.8^d	-3.6 ± 0.2^a	...
J20434114-2433534	M3.7+M4.1	-6.0 ± 0.9^i	-5.7 ± 0.5^a	...
J21100535-1919573	M2V	-6.3 ± 1.2^j	-5.7 ± 0.3^a	...
J23261069-7323498	M0V(sb)	7.8 ± 1.6^e	8.9 ± 3.3^a	...
J23323085-1215513	M0Ve	1.8 ± 0.7^e	0.9 ± 0.5^a	...
J23513366+3127229	M2V+L0	-13.5 ± 0.6^f	-13.6 ± 0.3^a	...

Note. — (a) this work ; (b) Binks & Jeffries, 2013 (c) Schlieder et al., 2010 ; (d) Kiss et al., 2011 ; (e) Torres et al., 2006 ; (f) Bowler et al., 2012 ; (g) Bowler et al., 2013 ; (h) RAVE; Zwitter et al., 2008 ; (i) Shkolnik et al., 2012 ; (j) Moór et al., 2013 ; (k) Montes et al., 2001 ; (l) Rodriguez et al., 2011.

Table 3.V.   Compilation of $v \sin i$ from the literature

Name 2MASS	Spectral Type	$v \sin i$ (km s^{-1})	$v \sin i$ (km s^{-1})
J01220441-3337036	K7Ve	4.9 ± 1.2^b	$< 5.8^a$
J02365171-5203036	M2Ve	36.0 ± 3.6^b	38.1 ± 3.5^a
J02414683-5259523	K6Ve	80.4 ± 3.8^b	80.0^c
J02414730-5259306	M2.5V	10.4 ± 1.9^b	8.0^c
J04480066-5041255	K7Ve(vb)	5.4 ± 1.2^b	$< 5.9^a$
J05332558-5117131	K7V	18.4 ± 1.2^b	$< 6.2^a$
J11102788-3731520	M4Ve+M4Ve	11.6 ± 1.2^b	$< 12.4^a$
J11211723-3446454	M1Ve	12.3 ± 1.2^b	10.0^c
J11211745-3446497	M1Ve	12.0 ± 1.2^b	10.0^c
J17130733-8552105	M0V	85.0^c	99.2 ± 9.3^a
J21100535-1919573	M2V	5.0^c	9.7 ± 1.2^a
J23261069-7323498	M0V(sb)	61.0 ± 0.8^b	64.1 ± 8.6^a
J23323085-1215513	M0Ve	8.8 ± 1.2^b	$< 9.0^a$

Note. — (a) this work ; (b) Torres et al., 2006 ; (c) Glebocki & Gnacinski, 2005.

3.5.1 Kinematic model prediction

As explained in Section 4 of Paper I, predicted radial velocity for candidate members are derived from a kinematic model, using Galactic space velocities of *bona fide* members as input parameters. One way to assess the accuracy of this model is to look for systematic differences between predicted and observed radial velocity measurements. Figure 3.3 presents a comparison between predicted and observed radial velocities for 111 candidate members with $P_v > 90\%$; as expected, the agreement between model predictions and observations is excellent.
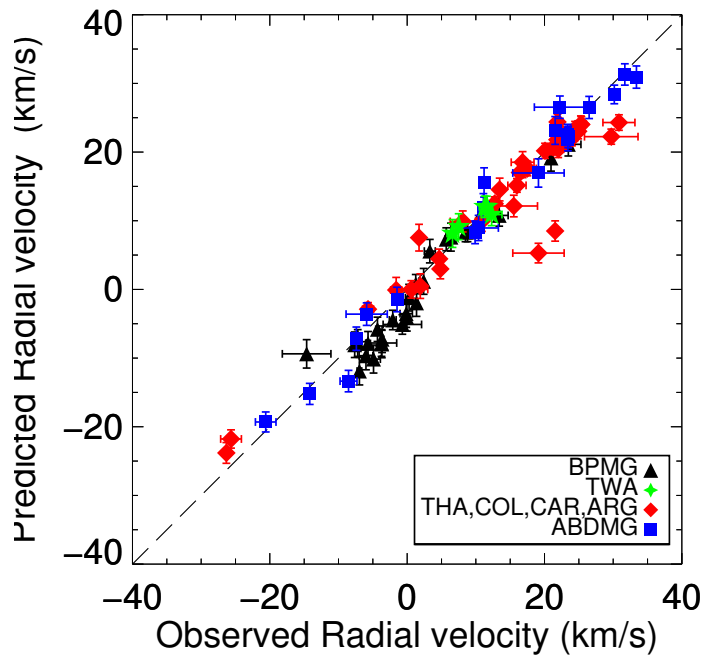
Figure 3.3 Comparison between predicted and observed radial velocities for the 111 candidate members ($P_v > 90\%$ and excluding known binary).

For βPMG candidate members, we observe a systematic difference of 3-5 km s^{-1} for a radial velocity range between -10 and 0 km s^{-1}. This systematic difference is also shown in Figure 3.4 and seem to increase as a function of distance. This may be a hint that the kinematic properties of low-mass members of βPMG differ slightly from that of

the bulk population.
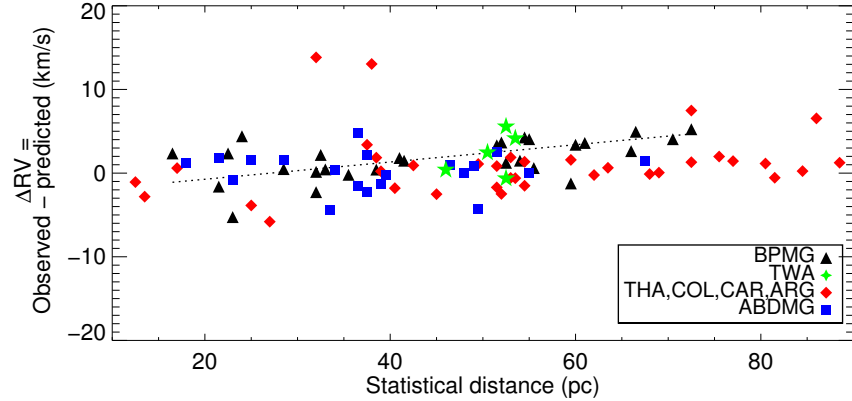
Figure 3.4 Comparison between predicted and observed radial velocities for YMGs as a function of the statistical distance.

3.5.2 New bona fide members

Although our observations and analysis unveiled 117 new highly probable candidate members to YMGs, a word of caution is necessary before assigning a firm membership to these objects. These candidates will be attributed the status of *bona fide* members only after their parallax is measured and shown to be consistent with the statistical distance predicted by our analysis. These candidates should also show evidence of youth through other indicators, e.g. lithium EW strength, low-surface gravity, and - as argued in the next section - relatively strong X-ray luminosity.

Recent parallax and radial velocity measurements along with spectroscopic obser-vations provide evidence for adding three new low-mass stars to the list of *bona fide* members. Those systems are briefly discussed below.

2MASSJ00275035-3233238 (GJ 2006A) and 2MASSJ00275035-3233238 (GJ 2006B). This binary system (ρ=18″, M3.5Ve+M3.5Ve) was first proposed to be a member of βPMG by Riedel et al. (2014) who measured a trigonometric distance of 32.3$\pm$1.8 pc, consistent with our predicted statistical distance of 32$\pm$2 pc. Its spectrum shows sign of low gravity (hence youth) as evidenced by the strength of the NaI8200 index. Our

radial velocity measurements (8.8 ± 0.2 km s^{-1} and 8.5 ± 0.2 km s^{-1}) are consistent with the prediction (8.4 ± 1.5 km s^{-1}) of our kinematic model and yield a very high membership probability in βPMG : $P_v = 99.9\%$ and $P_{v+\pi} = 99.9\%$.

2MASSJ06131330-2742054 (SCR 0613-2742AB). This is another binary system (ρ=0.093$''$, M4V unresolved) proposed to be a member of βPMG by Riedel et al. (2014) at a trigonometric distance of 29.4 ± 0.9 pc, consistent with our statistical distance of 25 ± 6 pc. Our RV (22.5 ± 0.2 km s^{-1}) is also consistent with that measured by Riedel et al. (22.54 ± 1.16 km s^{-1}), all of which yield a very high membership probability ($P_{v+\pi}$ = 99.9%) in βPMG. The system also shows low-surface gravity based on the NaI8200 index. There is no lithium absorption which is expected for βPMG *bona fide* members near the lithium depletion boundary (Riedel et al., 2014, Yee & Jensen, 2010) for βPMG. It is interesting to note that our analysis correctly predicts the binary nature of this star without knowledge of the parallax and the RV.

2MASSJ14252913-4113323 (SCR 1425-4113AB). This spectroscopic binary system (M2.5(sb)) was first proposed to be a potential member of TWA (with a marginal kinematic fit) by Riedel et al. (2014). Its NaI8200 index is consistent with a low-gravity object. It shows EW Li absorption (595 mÅ) consistent with a membership in TWA. However, our radial velocity (-2.0$\pm$1.6 km s^{-1}) is more consistent with a membership in βPMG with a predicted RV of -1.5$\pm$1.8 km s^{-1} compared to 1.5$\pm$2.8 km s^{-1} for TWA. When constrained with the trigonometric distance (66.9$\pm$4.3 pc) measured by Riedel et al., our analysis yields a membership probability of 89.2% in βPMG assuming a binary system. This star is yet another system for which our analysis correctly predicts its binary nature without RV and parallax measurements. If in βPMG, this star would be the most distant M dwarf of the βPMG. However, given its relatively large distance combined with a large Li EW much more consistent with an association younger than βPMG (e.g TWA), one should be cautious before assigning a *bona fide* membership to βPMG for SCR 1425-4113AB. This is beyond the scope of this paper but one should consider other distant associations (e.g the Scorpius-Centaurus complex; Song et al., 2012) in our

Bayesian analysis to firmly establish the membership of this young system. It is interesting to note that the star HIP 86598 (F9V) at 72 pc, formerly identified in βPMG by Kiss et al. (2011), was recently proposed by Song et al. (2012) to be a member of the Scorpius-Centaurus region.

3.6 Discussion

Kinematics and Galactic positions alone are not sufficient to ascertain YMG membership, youth also needs to be established by verifying that candidates and *bona fide* members share similar measurements. Here we discuss how stellar rotation and X-ray luminosity can be used for constraining the age of young low-mass stars.

3.6.1 Rotation-Age Relation

Past studies of the rotation periods of stars in young clusters and in the field have established that stellar rotation is a function of mass, age and magnetic activity, and that the rotation rates generally decrease with age (Soderblom, 2010). The first parametrization of the empirical stellar rotation spin-down was introduced by Skumanich (1972), using projected rotational velocity as a proxy of the rotation rate. This parametrization takes the form of a power law, with an index of -0.5 ($v \sin i \; \alpha$ to $t^{-1/2}$). More recently, much attention has been paid to studying the stellar rotation rate evolution in the low-mass regime ($<1 \; M_\odot$), which eventually led to the development of gyrochronology (Barnes, 2003, 2007).

One of the main outstanding problems within this area of research in understanding the angular momentum evolution of young late-type stars (K7V-M6V), for which the spin-up due to contraction competes with the spin-down due to magnetic braking (Reiners & Mohanty, 2012). The stellar rotation rate evolution of M0V-M3V dwarfs can be broadly broken down into three main phases. During the first few million years, after the star is formed, the stellar rotation slows down due to interactions with the circumstellar disk. After the primordial disk dissipates, the stellar rotation rate increases until the star reaches the zero-age main sequence, and then finally decreases over time according to

Table 3.VI.   log L_X and $v \sin i$ average properties

Group of stars	log L_X (erg s^{-1})	$\sigma_{\log L_X}$ (erg s^{-1})	$v \sin i$ (km s^{-1})	$\sigma_{v \sin i}$ (km s^{-1})	Number[a] of stars
		βPMG			
M0-M5 *Bona fide*	29.6	0.1	8.0	1.4	7,7
M0-M5 Candidate	29.4	0.4	14.6	1.7	25,15
M0-M2 Candidate	29.5	0.2	$\cdots$	$\cdots$	10
M3-M5 Candidate	29.3	0.5	$\cdots$	$\cdots$	15
		THA, COL, CAR and ARG			
M0-M5 *Bona fide*	$\cdots$	$\cdots$	$\cdots$	$\cdots$	2
M0-M5 Candidate	29.4	0.3	22.5	2.5	42,31
		ABDMG			
M0-M5 *Bona fide*	29.0	0.1	10.0	1.4	4,4
M0-M5 Candidate	29.1	0.2	16.0	1.9	17,14
M0-M2 Candidate	29.2	0.1	$\cdots$	$\cdots$	7
M3-M5 Candidate	29.0	0.2	$\cdots$	$\cdots$	10
		Field			
M0-M5	27.5	0.6	3.1	1.4	39,39

[a]Number of stars with L_x and $v \sin i$ measurements, respectively.

the power-law relation of Skumanich (1972). However, given the dispersion of rotation periods for old M dwarfs (Irwin et al., 2011), the exact exponent of the power law may depend on the magnetic field geometry of the stars. Observational data on the stellar rotation of low-mass stars at different ages and masses thus provide key insignts into their evolution (Reiners & Mohanty, 2012).

To help investigate how stellar rotation evolves as a function of age, we compiled measurements of $v \sin i$ for the M0V-M5V *bona fide* members of YMGs (see Table 3.VIII), which include 7 stars from βPMG, 4 stars from ABDMG and 2 stars for all THA, COL, CAR, and ARG YMGs. We excluded the binary systems from this analysis because their $v \sin i$ measurements could potentially be biased by blended line profiles, for spectroscopic binaries, and because stellar rotation evolution in binary systems could be affected by angular momentum exchanges between their components. We also compiled $v \sin i$ measurements for old M0V-M5V stars with a trigonometric parallax and X-ray detection from several sources (Delfosse et al., 1998, Glebocki & Gnacinski, 2005, Jenkins et al., 2009, Lépine et al., 2013, Reiners & Basri, 2008). This old sample comprises 39 stars and their properties are presented in Table 3.VII.

Table 3.VII.   Compilation of X-ray emission from field M dwarfs

Name 2MASS	Spectral Type	$\log f_x$ [a] (erg s^{-1} cm^{-2})	plx (mas)	$\log L_x$ [b] (erg s^{-1})	R_x	vsini (km s^{-1})
J01123052-1659570	M4.5V	-11.73 ± 0.07	269.10 ± 7.60[c]	27.49 ± 0.05	-3.54	2.50[i]
J02001278+1303112	M4.5V	-11.94 ± 0.11	222.00 ± 5.00[d]	27.45 ± 0.09	-3.64	3.80[j]
J02164119-3059181	M3V	-11.87 ± 0.08	69.81 ± 3.10[c]	28.52 ± 0.04	-3.37	5.00[k]
J02441537+2531249	M3V	-12.52 ± 0.23	133.16 ± 2.26[c]	27.31 ± 0.21	-4.55	2.80[g]
J05015746-0656459	M4V	-12.31 ± 0.14	163.00 ± 26.00[e]	27.35 ± 0.00	-3.96	3.20[e]
J06000351+0242236	M4V	-11.53 ± 0.08	190.90 ± 1.90[f]	27.98 ± 0.07	-3.49	7.40[j]
J10112218+4927153	M0V	-12.02 ± 0.09	205.21 ± 0.54[c]	27.44 ± 0.09	-5.26	2.80[j]
J10121768-0344441	M1.5V	-12.51 ± 0.19	127.08 ± 1.90[c]	27.37 ± 0.18	-4.90	1.80[i]
J11474440+0048164	M4V	-12.28 ± 0.16	300.00 ± 1.50[g]	26.84 ± 0.16	-4.41	2.00[g]
J11510737+3516188	M1V	-12.30 ± 0.16	116.48 ± 1.19[c]	27.65 ± 0.15	-4.46	3.30[g]
J11314655-4102473	M3.5V	-11.38 ± 0.07	96.56 ± 2.39[c]	28.73 ± 0.04	-3.14	18.00[j]
J13295979+1022376	M0.5V	-12.44 ± 0.22	138.70 ± 2.90[c]	27.35 ± 0.20	-4.83	1.30[g]
J17283991-4653424	M3V	-11.86 ± 0.13	220.24 ± 1.42[c]	27.53 ± 0.12	-4.33	3.20[k]
J18073292-1557464	M4.5V	-11.90 ± 0.11	130.00 ± 3.70[g]	27.95 ± 0.08	-3.12	3.00[i]
J18185725+6611332	M4.5V	-12.49 ± 0.04	137.50 ± 27.50[h]	27.31 ± 0.14	-3.67	14.60[i]
J18494929-2350101	M3.5V	-11.25 ± 0.06	336.72 ± 2.03[c]	27.78 ± 0.06	-3.50	4.00[i]
J19510930+4628598	M4V	-12.16 ± 0.09	84.10 ± 2.40[h]	28.06 ± 0.06	-3.40	22.00[i]
J20303207+6526586	M2.5V	-12.11 ± 0.07	120.00 ± 3.10[g]	27.81 ± 0.04	-4.14	3.20[g]
J20531977+6209156	M0.5V	-12.34 ± 0.09	130.00 ± 3.60[g]	27.51 ± 0.06	-4.93	2.80[g]
J22011310+2818248	M4V	-11.55 ± 0.05	112.30 ± 3.00[c]	28.43 ± 0.03	-3.19	35.10[i]
J23415498+4410407	M5V	-11.79 ± 0.09	320.00 ± 1.10[g]	27.28 ± 0.09	-3.76	1.20[g]
J23430628+3632132	M4V	-12.20 ± 0.13	120.00 ± 2.90[g]	27.72 ± 0.11	-3.64	2.60[g]
J23491255+0224037	M1V	-12.47 ± 0.20	177.90 ± 5.60[g]	27.11 ± 0.17	-4.89	3.00[i]
J04374092+5253372	M0.5V	-12.40 ± 0.13	98.91 ± 1.01[c]	27.68 ± 0.13	-4.81	2.60[j]
J05420897+1229252	M4V	-13.08 ± 0.39	171.60 ± 4.00[c]	26.53 ± 0.36	-4.95	2.90[g]
J09411033+1312344	M1.5V	-12.39 ± 0.20	88.81 ± 1.68[c]	27.79 ± 0.19	-4.32	2.50[i]
J09535523+2056460	M4.5V	-12.87 ± 0.34	108.40 ± 2.30[c]	27.13 ± 0.32	-3.85	16.50[g]
J09560868+6247185	M0V	-12.49 ± 0.16	94.68 ± 1.26[c]	27.64 ± 0.14	-4.82	2.50[i]
J10251088-1013434	M1V	-13.13 ± 0.53	81.00 ± 1.91[c]	27.13 ± 0.51	-5.09	2.50[i]
J11023832+2158017	M0V	-11.84 ± 0.13	84.95 ± 1.05[c]	28.39 ± 0.12	-3.96	2.50[i]
J11474440+0048164	M4V	-12.28 ± 0.16	298.04 ± 2.30[c]	26.85 ± 0.15	-4.41	2.00[g]
J11510737+3516188	M1V	-12.30 ± 0.16	116.48 ± 1.19[c]	27.65 ± 0.15	-4.46	2.50[i]
J12375231-5200055	M3V	-12.14 ± 0.13	103.18 ± 2.31[c]	27.91 ± 0.11	-4.12	2.90[k]
J14021961+1341229	M0.5V	-12.91 ± 0.36	50.36 ± 2.04[c]	27.76 ± 0.32	-4.59	4.00[i]
J15215291+2058394	M1.5V	-11.16 ± 0.06	87.63 ± 1.81[c]	29.04 ± 0.04	-3.24	6.50[i]
J16252459+5418148	M2V	-13.00 ± 0.29	153.46 ± 0.99[c]	26.71 ± 0.28	-5.08	2.50[i]
J16570570-0420559	M3.5V	-11.66 ± 0.09	115.40 ± 1.50[f]	28.30 ± 0.08	-3.16	10.70[i]
J17435595+4322441	M2.5V	-13.01 ± 0.21	105.50 ± 1.18[c]	27.02 ± 0.20	-5.01	2.50[i]
J18050755-0301523	M1.0V	-12.62 ± 0.31	128.89 ± 1.43[c]	27.24 ± 0.30	-4.90	2.50[i]

[a]ROSAT X-ray flux calculated from Riaz et al. (2006, Section 5.4) in erg s^{-1} cm^{-2}.

[b]ROSAT X-ray luminosity calculated using ROSAT website formulae (see text).

Note. — (c) van Leeuwen (2007) ; (d) Houdebine (2012) ; (e) Delfosse et al. (1998) ; (f) Lépine & Gaidos (2011), (g) Jenkins et al. (2009) ; (h) Lepine & Shara (2005) ; (i) Reiners et al. (2012) ; (j) Glebocki & Gnacinski (2005) ; (k) Torres et al. (2006)
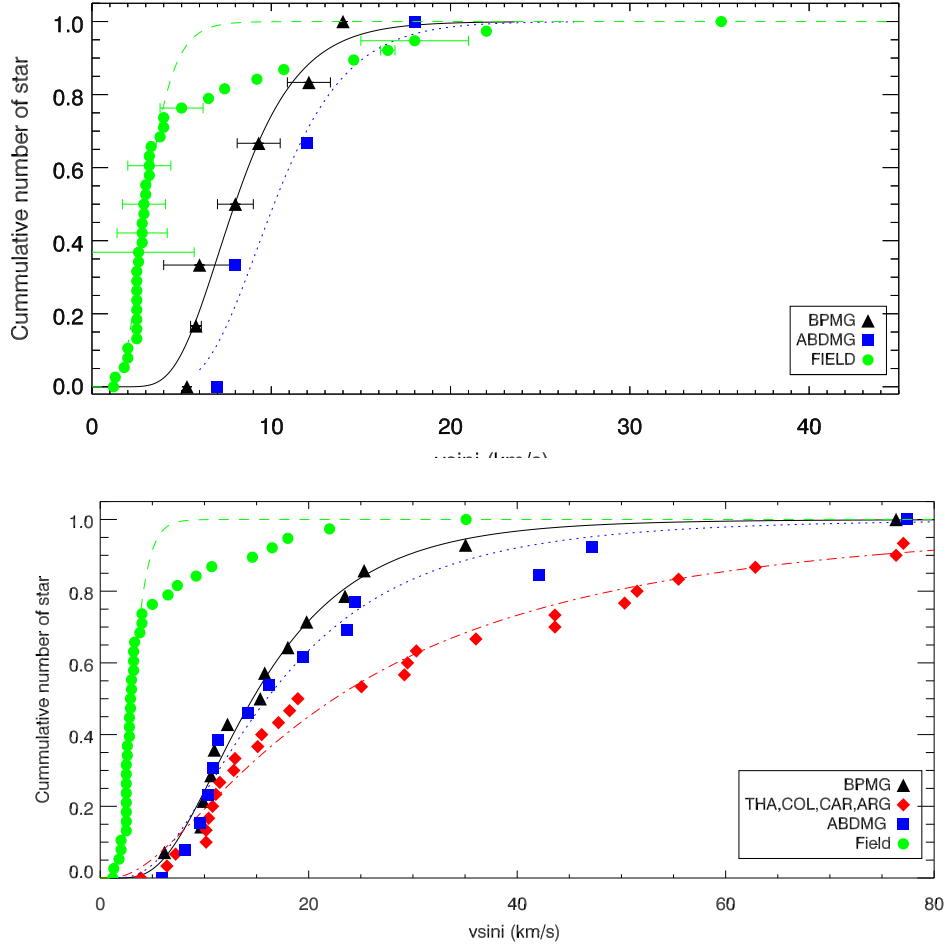
Figure 3.5 Top panel : $v\sin i$ cummulative distribution of M0V-M5V *bona fide* members excluding binaries (all kinds) compared to field distribution (filled green cercles). The lines represent the adopted parameterization (see Table 3.VI). Bottom panel : $v\sin i$ cummulative distribution of candidate members excluding binary systems.

Figure 3.5 (top) presents the cumulative distribution of $v\sin i$ for the M0V-M5V *bona fide* members of βPMG and ABDMG compared to that of the old sample. We estimated the median and dispersion of these distributions by fitting a log-normal function, as proposed by Weise et al. (2010). Table 3.VI summarises the median $v\sin i$ along with their dispersion for YMG and field stars. As visible in Figure 3.5, there is a trend for $v\sin i$ to decrease with age between βPMG and field stars. We compared the distributions of $v\sin i$ pairwise by performing a double-sided Kolmogorov-Smirnov (K-S) test using the

IDL routine *kstwo*. We found that field $v \sin i$ measurements are clearly not drawn from the same distribution as that of βPMG; the K-S probability that both distributions are the same is only 0.1%. The bottom panel of the Figure 3.5 presents the cumulative distributions of $v \sin i$ for our candidate members of the different YMGs with $P_v > 90\%$, along with the distribution for the old sample. Since our detection limits are between 3 and 8 km s^{-1}, depending on the slowly-rotating standard stars used, we reached only upper limits on $v \sin i$ for 28 candidates (see Table 4.III); these candidates were excluded from the figure.

To quantify the similarity between our samples of candidates and the *bona fide* members, we once again performed a K-S test as above. Overall the candidate distributions are very similar to the *bona fide* YMG distributions with K-S probabilities of 20-73%. Accordingly, the probabilities that the $v \sin i$ of our candidates were drawn from the same distribution as those of the field sample are very low, 0.0002-0.0003%. Similar results were also found by Scholz et al. (2007). It thus appears empirically that young low-mass stars in the age range defined by βPMG and ABDMG have larger $v \sin i$ than their old counterparts in the field. In our candidates sample, there are 22 ultrafast rotators (> 50 km s^{-1}), including 8 stars that were identified as binary systems; for the 14 remaining fast rotators we cannot rule out the possibility that they are also unresolved binary systems.

3.6.2 X-ray luminosity-Age Relation

Past studies on stellar activity of low-mass stars have shown a saturation limit when the $v \sin i$ is compared to the R_X parameter, the ratio of X-ray to bolometric luminosity (Mamajek & Hillenbrand, 2008, Preibisch & Feigelson, 2005). This parameter is convenient as an activity proxy because it is independent of distance but it must rely on an estimate of the bolometric flux of the star. In order to quantify the sensitivity of the R_X parameter vs age for YMG stars, we have compiled ROSAT X-ray luminosities of all known *bona fide* low-mass members with spectral type later than M0V. This sample comprises 13 M stars. The bolometric luminosities are determined using the *J*-band bolometric correction presented in Pecaut & Mamajek (2013, see their Table 6, using $J - H$

Table 3.VIII.   Properties of *bona fide* members

Name of star	$v \sin i$[a] (km s^{-1})	π[b] (mas)	R_x	$\log L_x$ (erg s^{-1})
βPMG				
HIP 11152	6.0±2.0[c]	34.86±2.84	-2.85	29.58±0.08
HIP 23200	14.0	38.64±2.54	-3.15	29.58±0.01
HIP 23309	5.8±0.3	37.34±1.13	-3.37	29.40±0.08
HIP 50156	8.0±1.0[d]	43.32±1.80	-3.35	29.31±0.03
HIP 102409	9.3±1.2	100.91±1.06	-2.98	29.75±0.01
HIP 112312	12.1±1.2	42.84±3.61	-2.68	29.69±0.03
GJ 3331 A	5.3[e]	51.98±1.30[f]	-2.91	29.58±0.04
ABDMG				
HIP 17695	18.0[g]	62.00±2.88	-3.07	29.00±0.02
HIP 31878	12.0[g]	44.74±0.91	-3.70	28.84±0.05
HIP 81084	7.0[g]	32.60±2.47	-3.40	28.98±0.04
HIP 114066	8.0[g]	40.81±1.60	-3.00	29.42±0.01

[a]Projected rotation velocity measurement from Torres et al. (2006), unless stated otherwise.

[b]Parallax measurement from van Leeuwen (2007), unless stated otherwise.

[c]Schlieder et al. (2010)

[d]Herrero et al. (2012)

[e]Reiners et al. (2012)

[f]Riedel et al. (2014)

[g]da Silva et al. (2009)

index) for βPMG members and the *J*-band bolometric correction from Casagrande et al. (2008, see their Equation 5) for ABDMG members and field dwarfs. Again, all binary systems were excluded.

The upper panel of Figure 3.6 presents the cumulative distribution of R_X for young *bona fide* members and old field dwarfs. While one can see a clear difference between young and old stars, there is no obvious distinction between βPMG and ABDMG members.

The bottom panel of Figure 3.6 presents the cumulative distribution of $\log L_X$ for M0V-M5V *bona fide* members compared to the old low-mass population. The X-ray luminosity is calculated using this formulae[8] : $L_x = 1.2e^{38} f_x d_\pi^2$. One clearly see a difference of ~ 0.6 dex between βPMG and ABDMG members. Even if we take into account the uncertainties on the *ROSAT* counts, HR1 ratio and parallax (error bar on Figure 3.6), the difference between the two young samples is significant. A K-S test performed on both distributions shows that they are different at a confidence level of 94.4%. We estimated the mean and dispersion of each distribution by fitting error functions (see the Table 3.VI). We note that Preibisch & Feigelson (2005) found similar results for Chamaeleon association and the Pleiades group, where these two groups have similar ages compared to βPMG and ABDMG. Overall, relatively young stars represented by βPMG members are two orders of magnitude more luminous than M dwarfs in the field and this luminosity excess remains significant (a factor of ~ 4) compared to older AMDMG members. This analysis shows that the X-ray luminosity is an excellent youth indicator for M dwarfs in the age range defined by βPMG and ABDMG members. This youth diagnostic is very complementary to the common method of using the presence of the lithium resonance line at 6707.8 . However, since lithium is rapidly depleted in M dwarfs, especially fully convective ones ($\sim$M3V), lithium is a useful youth indicator only for low-mass stars younger than a few 10^7 yrs. Using the X-ray luminosity as youth indicator extends by roughly an order of magnitude the age range covered by the lithium method.

We performed the same analysis on our candidate members, where the X-ray luminosity was determined using the statistical distance (see Table 4.III), as a proxy of the

---

[8]http ://heasarc.gsfc.nasa.gov/W3Browse/all/rassdsstar.html

parallax (log L_X^s). As shown in Paper I, the statistical distance is a reliable estimate of the true distance within an uncertainty of $\sim$10%. Figure 3.7 presents the cumulative distribution of log L_X^s for our highly probable members compared to the low-mass field dwarfs. The amplitude of the error bars is $\sim$0.3 dex and take into account the uncertainties on both the *ROSAT* flux and the statistical distance. The same trend for the X-ray luminosity to increase at young ages is confirmed with the candidates. One can see in Figure 3.7 that the βPMG distribution shows an excess of low-luminosity objects which could find an explanation if the statistical distance of these objects is somewhat different from reality. In fact, we do have a parallax for one βPMG candidate member and indeed, when one uses the true distance to infer its X-ray luminosity, its value is brought much closer to the nominal distribution for this association.

In order to investigate the behavior of the X-ray luminosity with spectral type (mass), we divide our candidates into two groups : M0V-M2V (partly convective stars) and M3V-M5V (fully convective stars). Figure 3.8 presents the cumulative distribution of X-ray luminosity, for both groups in βPMG and ABDMG. Table 3.VI summarises the median log L_X along with their dispersion for YMGs and field stars. The X-ray luminosity for M3V-M5V βPMG candidates is slightly lower (with a higher dispersion) compared to the M0V-M2V group, and the same behavior is seen for ABDMG candidate members. More observations are clearly needed to confirm this trend which may provide some insights for understanding the X-ray property and magnetic activity of low-mass stars near the brown dwarf boundary.

3.7 Summary and Conclusion

The study aims at extending the census of low-mass star members of seven young nearby associations. A Bayesian statistical analysis described in Paper I was developed for identifying candidates based on a minimal set of observables (proper motion, photometry, position in the sky) combined with a kinematic model of the association. This method yields a membership probability to a given association as well as the most probable (statistical) distance and the predicted radial velocity. In the present study, radial
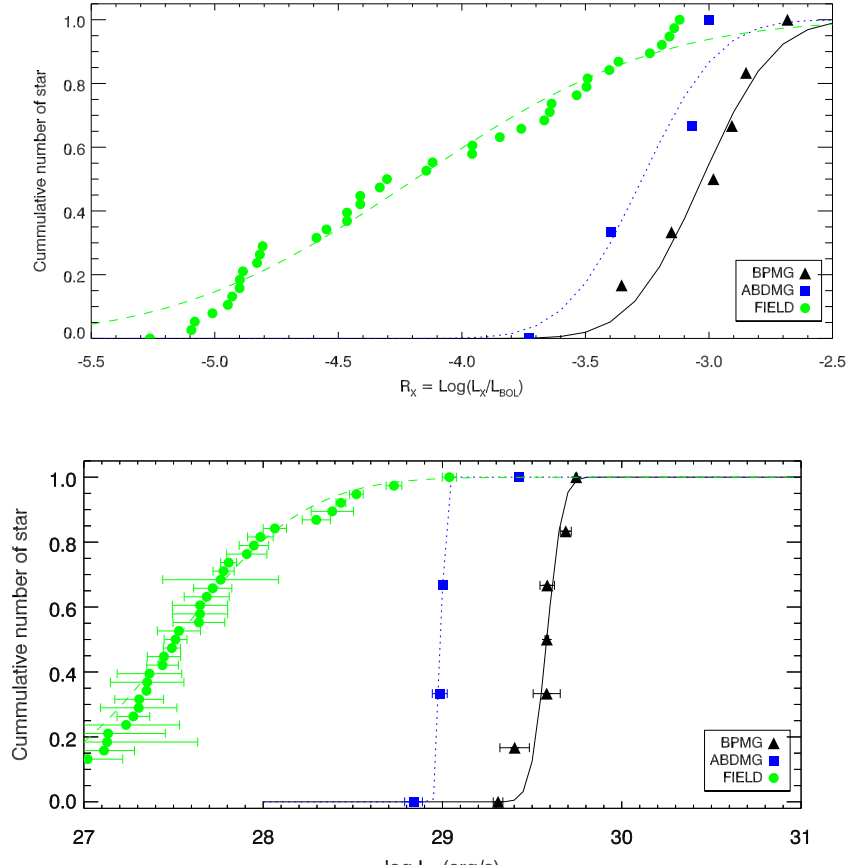
Figure 3.6 Top panel : Cummulative distribution of R_X (log L_X/L_{bol}) for M0V-M5V *bona fide* members, which exclude binaries. Bottom panel : log L_X cummulative distribution for M0V-M5V *bona fide* members of βPMG (black triangles), and ABDMG (blue squares).

velocity measurements were used to better constrain the membership of the candidates.

Starting from a sample of 920 stars, all showing indicators of youth such as Hα and/or X-rays emission, our analysis selected 247 candidates with a membership probability over 90%. To confirm the predicted membership, we have secured radial velocity measurements for 202 candidate members. These measurements were combined with a compilation of 166 measurements from the literature to select a list of 130 young K and M stars with a membership probability to all YMGs exceeding 90% when the radial velocity is included in our Bayesian analysis. A subgroup of 117 candidates are associated with a single YMG distributed as follows : 27 in βPMG, 22 in THA, 25 in COL, 7 in CAR, 18 in ARG and 18 in ABDMG.
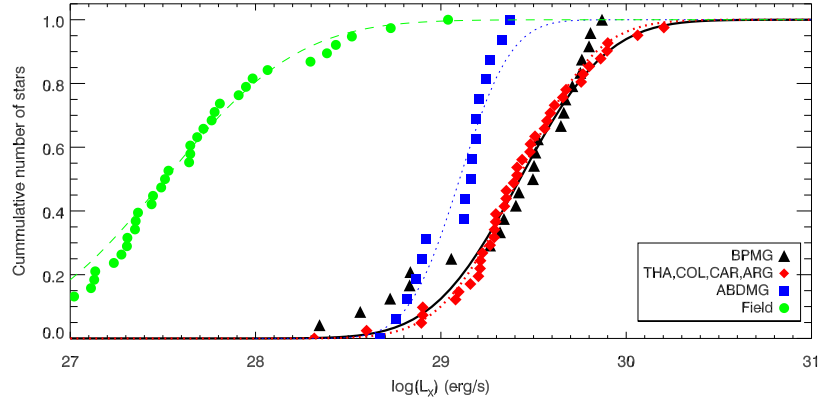
Figure 3.7 Cummulative distribution of log L_X^s for candidate members excluding binary systems compared to old field log L_X distribution.
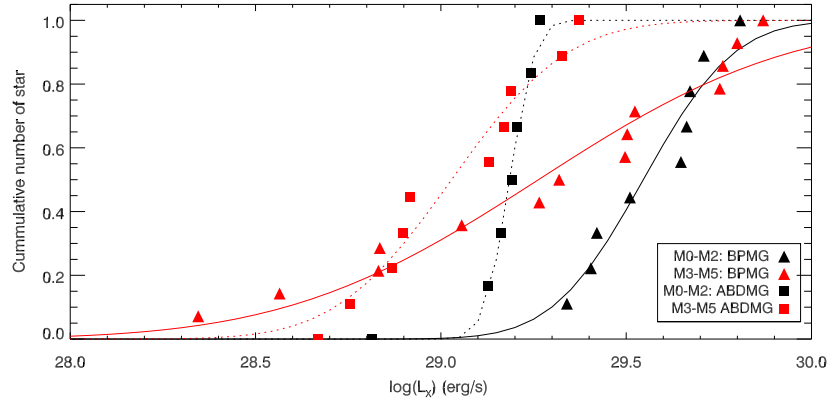
Figure 3.8 Cummulative distribution of log L_X for M0V-M2V and M3V-M5V of βPMG and ABDMG candidate members.

We investigated the rotation-age relation and found that stellar rotation ($v \sin i$) of young M dwarfs is significantly higher compared the their field counterparts. We also find that the X-ray luminosity of $\sim$12-22 Myr-old βPMG members are typically two orders of magnitude more luminous compared to field stars ; this luminosity excess is a factor of $\sim$4 compared to older ($\sim$100 Myr) ABDMG members. Thus, the X-ray luminosity appears to be an excellent age discriminant for M dwarfs.

This work has unveiled a large population of highly probable low-mass members to nearby YMGs. A parallax, and ideally other indications of youth, are mandatory to

firmly establish them as *bona fide* members of their respective association.

Acknowledgments

Table 3.IX. Properties of candidate members of young kinematic groups

Name (2MASS)	I_C[a] (mag)	J (mag)	$\mu_\alpha\cos\delta$[b] (mas yr^{-1})	μ_δ[b] (mas yr^{-1})	Spectral[c] Type	X-ray[d] log(f_x)	Hα[e] (Å)	Li[f] (m Å)	vsini[g] (km s^{-1})	RV$_{meas}$[h] (km s^{-1})	RV$_{pred}$[i] (km s^{-1})	d_π[j] (pc)	d_s[j] (pc)	p[k] (%)	Pv[k] (%)	log $L_X^{x,d}$ (erg s^{-1})	Refs.
β Pictoris moving group																	
J00172353-6645124	9.94±0.05	8.56±0.02	104.3±1.0	-13.5±1.0	M2.5V	-11.77	6.0	...	<7.4[zz]	10.7±0.2[zz]	10.9±1.5	39.0±2.6[vv]	35±3	99.3	99.9	29.41±0.19	18
J00275023-3233060	10.29±0.03[vv]	8.88±0.03	97.8±1.1	-60.9±4.0	M3.5Ve	-11.59	7.8	...	6.2±1.8[zz]	8.8±0.2[zz]	8.3±1.4	32.3±1.8[vv]	33±2	1.8	99.9	29.53±0.15	17
J00275035-3233238	10.48±0.02[vv]	8.97±0.03	117.4±2.8	-29.3±8.1	M3.5Ve	-11.59	5.3	...	<4.2[zz]	8.5±0.2[zz]	8.3±1.4	32.3±1.8[vv]	32±2	97.2	99.9	29.51±0.15	17
J01132817-3821024	9.66±0.07[o]	8.49±0.02	123.0±1.1	-38.3±1.2	M0.0+M1.0	-11.77	2.5	...	<9.1[zz]	14.3±0.5[zz]	11.9±1.4	...	29±2	16.7	99.3	...	18
J01365516-0647379	11.22±0.06	9.71±0.02	175.1±4.4[y]	-98.8±4.4[y]	M4V+>L0	-12.03	6.0	...	...	12.2±0.4[uu]	9.5±1.5	24.0±0.4[uu]	21±1	28.3	99.3	...	18
J01535076-1459503	9.82±0.06	7.94±0.03	105.0±1.4	-45.7±1.4	M3V+M3V	-11.54	6.6	...	<11.2[zz]	10.5±0.4[zz]	12.0±1.5	...	28±2	99.9[l]	99.9[l]	...	18
J03323578+2843554	11.06±0.06[v]	9.36±0.02	40.0±3.0[y]	-60.0±4.0[y]	M4+M4.5	-12.43	5.7	...	24.5±2.2[zz]	9.4±0.4[zz]	8.2±1.9	...	55±4	95.6	96.4	29.33±0.22	11
J04435686+3723033	11.01±0.13[v]	9.71±0.02	27.3±5.1[z]	-64.4±5.1[z]	M3Ve	-12.31	...	...	10.6±1.0[zz]	6.4±0.3[mm]	7.6±2.0	...	59±5	99.9[l]	99.9[l]	28.44±0.37	18
J05082729-2101444	11.61±0.06	9.72±0.02	31.4±2.3	-16.0±2.3	M5V	-12.44	24.9	618[cc]	25.3±4.3[zz]	23.5±1.8[mm]	21.1±1.7	...	25±5	99.9[l]	99.9[l]	...	18
J05241914-1601153	10.59±0.06	8.67±0.03	14.0±5.0[y]	-36.0±2.0[y]	M4.5+M5.0	-11.99	11.7	223[o]	50.0±4.5[zz]	17.5±0.6[zz]	20.9±1.8	...	20±5	99.9[l]	99.9[l]	...	18
J05335981-0221325	9.90±0.06	8.56±0.02	10.0±1.0[y]	-50.0±1.0[y]	M3V	-11.54	6.1	>49[cc]	5.4±1.3[zz]	20.9±0.2[mm]	19.1±1.9	...	42±5	99.9[l]	99.9	29.78±0.17	18
J06131330-2742054	9.55±0.02[vv]	8.00±0.03	-14.9±1.0	-2.1±1.0	M3.5V*	-11.51	5.1	...	<6.7[zz]	22.5±0.2[zz]	21.6±1.6	29.4±0.9[vv]	25±6	99.9[l]	99.9[l]	...	18
J08173943-8243298	9.08±0.06	7.47±0.02	-81.9±0.9	102.6±1.5	M4*	-11.24	7.6	...	32.2±2.6[zz]	15.6±1.5[zz]	12.8±1.5	...	27±2	99.9[l]	99.9[l]	...	18
J08224744-5726530	10.29±0.06	8.63±0.02	-481.4±9.0[y]	159.0±9.0[y]	M4.5+>L0	-11.97	7.3	...	6.4±2.4[zz]	14.7±0.2[zz]	17.2±1.4	...	6±1	17.9	91.9	...	7
J11493184-7851011	10.73±0.00[m]	9.45±0.02	-43.4±2.9	-8.1±1.8	M1V	-12.07	4.7	560[m]	18.0±5.0	13.4±1.3[m]	10.8±1.6	...	68±6	75.2	91.7	29.68±0.17	18
J13545390-7121476	9.80±0.06	8.55±0.02	-165.0±6.5	-132.7±6.8	M2.5V	-12.02	3.3	...	<3.5[zz]	5.7±0.2[zz]	7.3±1.7	...	21±1	8.5	99.1	28.73±0.16	18
J16572029-5343316	9.97±0.07	8.69±0.02	-14.7±6.1	-85.9±2.2	M3V	-12.24	2.5	...	<3.5[zz]	1.4±0.2[zz]	-2.0±2.0	...	51±3	91.1	99.9	29.27±0.27	18
J17150219-3333398	9.32±0.06	7.92±0.02	7.6±5.3	-176.9±1.2	M0V	-11.46	3.0	...	76.3±5.3[zz]	-14.6±3.5[zz]	-9.4±2.1	...	23±1	94.6	99.0	29.35±0.13	18
J17292067-5014529	10.30±0.00[m]	8.87±0.03	-6.3±1.5	-63.5±4.1	M3Ve	-12.13	6.7	50[m]	23.5±1.9[zz]	-0.1±0.9[mm]	-3.5±2.0	...	64±5	99.3[l]	99.9[l]	29.56±0.27	6
J18142207-3246100	10.64±0.00[m]	9.44±0.02	7.3±4.7[y]	-39.9±4.7[y]	M1.5V*	-11.66	3.1	200[m]	3.0±1.5	-5.7±0.8[m]	-9.8±2.1	...	90±8	80.6[l]	99.9[l]	...	6
J18151564-4927472	10.36±0.06	8.92±0.02	8.3±1.6	-71.5±1.6	M3V(sb)	-11.96	7.6	>46[w]	76.7±10.9[zz]	0.3±3.6[mm]	-3.8±2.0	...	61±4	89.4[l]	99.9[l]	...	18
J18202275-1011131	8.67±0.00[p]	7.64±0.02	10.5±5.9[n]	-33.9±4.0[n]	K5Ve+K7Ve	-11.67	9.8	530[m]	...	-13.7±0.0[mm]	-16.4±2.0	...	61±6	1.0[l]	96.4[l]	...	6
J18420694-5554254	10.88±0.06[o]	9.49±0.02	11.2±5.3	-81.4±2.7	M1Ve	-11.79	6.9	...	<8.6[zz]	0.3±0.5[zz]	-1.2±1.9	...	54±4	73.1	99.9	29.76±0.25	18
J18465255-6210366	9.99±0.00[m]	8.75±0.02	14.6±1.4	-81.1±1.3	K7Ve	-12.01	1.9[m]	332[m]	9.9±0.6	2.4±0.1[m]	1.2±1.9	...	54±3	54.1	99.9	29.53±0.28	6
J18504448-3147472	9.44±0.00[m]	8.31±0.02	16.6±1.8	-74.7±0.7	K7Ve	-11.65	1.8[m]	492[m]	49.7±0.6	-6.0±1.0[m]	-9.7±2.0	...	53±3	91.3	99.9	29.89±0.14	6
J18580415-2953045	9.98±0.00[m]	8.86±0.02	11.5±1.4	-49.5±1.4	M0Ve	-11.76	2.8[m]	483[m]	33.8±3.4	-4.9±1.0[m]	-10.1±2.0	...	76±5	97.9[l]	99.9[l]	...	6
J19102820-2319486	10.59±0.06	9.10±0.02	17.6±1.9	-51.6±1.5	M4V	-11.86	8.2	>55[cc]	12.2±1.8[zz]	-7.0±0.3[mm]	-11.9±2.0	...	67±5	99.9[l]	99.9[l]	29.88±0.19	18
J19233820-4606316	10.19±0.05	9.11±0.03	17.9±0.9	-57.9±0.9	M0V	-12.07	2.0	422[w]	15.4±3.0[zz]	-0.0±0.4[mm]	-4.1±2.0	...	70±4	97.8	99.3	29.71±0.23	18
J19243494-3442392	11.29±0.05	9.67±0.02	23.2±1.8	-72.1±1.8	M4V	-12.50	13.9	...	10.9±2.9[zz]	-3.7±0.2[zz]	-8.0±2.0	...	54±3	99.9[l]	99.9[l]	29.06±0.31	18
J19560294-3207186	10.85±0.06	8.96±0.03	32.6±1.9	-61.0±1.2	M4V	-11.76	6.2	...	35.0±4.9[zz]	-3.7±2.2[mm]	-7.8±1.9	...	55±4	98.5[l]	99.5[l]	29.81±0.16	8,12
J19560438-3207376	10.13±0.06	8.71±0.03	30.3±1.5	-66.6±1.0	M0V	-11.76	0.7[ff]	110[ff]	...	-7.2±0.5[mm]	-7.8±1.9	...	55±3	99.9[l]	99.9[l]	29.81±0.16	8,12
J20013718-3313139	10.27±0.05	9.15±0.02	27.1±2.6	-60.9±1.8	M1V	-12.23	2.6	...	<2.6[zz]	-3.7±0.2[mm]	-7.3±1.9	...	61±4	98.1	98.9	29.43±0.25	12
J20100002-2801410	10.20±0.02[vv]	8.65±0.02	40.4±0.9	-62.7±0.9	M2.5+M3.5	-11.84	10.1	...	46.5±4.1[zz]	-5.8±0.6[zz]	-8.5±1.9	48.0±3.1[vv]	52±3	99.9[l]	99.9[l]	...	18
J20333759-2556521	11.57±0.01[vv]	9.71±0.02	51.8±1.7	-76.8±1.4	M4.5V	-12.42	11.4	...	19.8±2.6[zz]	-7.6±0.4[zz]	-8.1±1.9	48.3±3.3[vv]	40±3	99.9[l]	99.9[l]	28.89±0.36	18
J20434114-2433534	10.11±0.05	8.60±0.02	56.2±1.3	-72.0±1.3	M3.7+M4.1	-11.71	6.5	...	26.9±2.7[zz]	-5.8±0.6[mm]	-7.9±1.8	28.1±3.9[uu]	44±3	99.9[l]	99.9[l]	...	18
J20560274-1710538	9.25±0.06	7.85±0.02	59.3±3.0[n]	-63.0±3.2[n]	K7V+M0V	-11.78	1.4	420[m]	15.6±1.2	-6.9±0.8[m]	-9.2±1.8	...	44±3	99.9[l]	99.9[l]	...	5
J21100535-1919573	9.57±0.06	8.11±0.03	88.6±1.2	-92.5±1.2	M2V	-11.44	5.4	>41[w]	9.7±1.2[nn]	-5.7±0.4[mm]	-7.9±1.7	...	32±2	99.9[l]	99.9[l]	29.67±0.14	18
J21103147-2710578	12.02±0.05	10.30±0.02	70.6±1.9	-72.3±2.8	M4.5V	-12.48	9.0	...	15.8±1.3[zz]	-4.3±0.2[zz]	-5.8±1.8	...	41±3	99.9[l]	99.9[l]	28.84±0.27	18

Table 3.IX — continued

Name (2MASS)	I_c^a (mag)	J (mag)	$\mu_\alpha \cos\delta^b$ (mas yr^{-1})	μ_δ^b (mas yr^{-1})	Spectral^c Type	X-ray^d log(f_x)	Hα^e (Å)	Li^f (mÅ)	vsini^g (km s^{-1})	RV$_{meas}^h$ (km s^{-1})	RV$_{pred}^i$ (km s^{-1})	d_π^j (pc)	d_δ^i (pc)	p^k (%)	p$_V^k$ (%)	log L_x^d (erg s^{-1})	Refs.
J21212873-6655063	8.90±0.00^m	7.88±0.03	98.2±1.1	-105.7±1.8	K7V	...	...	15^m	4.5±1.2	3.3±0.8^m	5.6±1.7	30.2±1.3	32±2	54.7	99.9	...	4,9
J22424896-7142211	8.87±0.00^m	7.79±0.02	95.2±0.8	-52.3±0.8	K7Ve+K5V	-11.28	1.9^m	440^m	7.5±1.2	8.6±0.5^m	8.6±1.6	...	37±2	93.1	99.9	...	6
J23233085-1215513	8.56±0.00^m	7.45±0.02	137.9±1.0	-81.0±1.0	M0Ve	-11.32	2.8	185^m	8.8±1.0^m	1.2±0.6^{mm}	0.8±1.4	...	28±1	93.7	99.9	29.67±0.12	6
J23500639+2659519	11.92±0.05^v	10.14±0.02	182.0±2.0^y	-44.0±0.0^y	M3.5V	-12.27	9.8	...	...	-0.7±2.8^{uu}	-5.1±1.4	...	24±2	82.4	96.8	28.57±0.26	18
J23512227+2344207	11.36±0.06^v	9.68±0.02	269.8±4.2^y	-77.3±4.2^y	M4V	-12.37	7.3	...	...	-2.1±0.5^{uu}	-4.5±1.4	...	16±1	81.6	97.8	28.15±0.23	18
TW Hydrae Association																	
J10120908-3124451	10.51±0.03^{vv}	8.85±0.02	-74.8±1.1^v	-9.4±1.0^v	M4Ve*	...	5.7^{vv}	...	17.8±2.7^{zz}	14.6±0.6^{zz}	15.9±1.3	53.9±5.1^{vv}	48±4	99.9^l	99.9^l	...	17
J10182870-3150029	9.94±0.00^m	8.87±0.03	-55.5±3.2	-22.6±3.7	M0Ve*	-11.70	3.8^m	510^m	...	20.7±1.5^m	15.5±1.3	...	55±4	99.9	98.3	...	2
J11102788-3731520	9.29±0.06	7.65±0.02	-107.3±0.9	-18.0±1.1	M4Ve+M4Ve	-11.64	12.7	710^m	11.6±1.0^m	14.5±0.2^{mm}	12.9±1.5	...	43±4	99.9^l	99.9^l	...	1
J11132622-4523427	10.71±0.06	9.41±0.03	-44.1±1.4	-8.1±1.3	M0Ve*	-12.00	17.7	589	...	15.8±2.0^{ee}	13.1±1.5	96.2±11.1^x	63±5	99.9	99.9	...	5
J11211723-3446454	9.66±0.05	8.43±0.04	-67.4±0.0^m	-17.0±0.0^m	M1Ve	-11.47	2.3^m	580^m	12.3±1.2^{mm}	11.3±0.8^m	12.0±1.5	55.6±2.2^x	53±4	99.9	99.9	...	5
J11211745-3446497	9.73±0.05	8.43±0.04	-67.4±0.0^m	-17.0±0.0^m	M1Ve	-11.47	1.5^m	550^m	12.0±1.2^{mm}	11.6±0.8^m	12.0±1.5	59.5±2.5^x	52±4	99.9	99.9	...	5
J11315526-3436272	9.27±0.06	7.67±0.03	-82.6±0.8	-22.6±1.0	M2+M2.5+M9	-11.36	8.7	629^m	53.5±3.5	12.7±3.8^m	11.4±1.6	50.0±1.7^x	47±4	99.9^l	99.9^l	...	1
J11321831-3019518	11.31±0.06	9.64±0.02	-89.6±1.3	-25.8±1.3	M5Ve	-7.29	6.8^{bb}	600^{bb}	...	12.3±1.5^{bb}	10.9±1.6	...	46±3	99.9	99.9	...	10
J12072738-3247002	10.14±0.06	8.62±0.03	-72.7±0.9	-29.3±0.9	M3Ve+M3Ve	-12.04	2.4^{pp}	500^{ee}	...	8.5±1.2^{ee}	8.8±1.8	53.8±1.4^x	48±4	99.9^l	99.9^l	...	5
J12153072-3948426	9.50±0.00^m	8.17±0.03	-74.0±0.8	-27.7±0.8	M1Ve	-11.60	2.6^m	555^m	12.9±1.2	7.5±0.1^m	9.1±1.9	54.1±3.5^x	51±4	99.9^l	99.9^l	...	5
J12313807-4558593	10.72±0.07	9.33±0.03	-64.4±3.1	-28.6±1.0	M3Ve*	-12.40	3.1^{pp}	160^{ii}	...	8.1±4.0^q	8.9±2.0	77.5±3.6^x	56±4	99.9	99.9	...	5
J12345629-4538075	10.24±0.12^y	8.99±0.03	-49.2±1.6	-21.2±0.8	M1.5Ve*	-12.08	4.4	360^{ii}	...	9.0±0.4^{ee}	8.6±2.0	...	59±5	99.9	99.9	...	5
J12350424-4136385	10.49±0.00^m	9.12±0.02	-70.5±1.1	-29.9±1.1	M2Ve	-11.98	7.5	500^m	3.0±3.0	6.6±0.8^m	8.1±2.0	...	54±4	99.9	99.9	...	2
Tucana-Horologium Association																	
J01220441-3337036	9.34±0.06	8.31±0.02	107.2±1.0	-59.0±1.0	K7Ve	-11.65	0.8	0^m	4.9±1.0^{mm}	4.7±0.4^{mm}	4.4±1.4	...	39±2	98.4	99.9	29.62±0.13	11
J01521830-5950168	10.26±0.06	8.94±0.02	107.8±1.8	-27.0±1.8	M2-3V	-7.29	2.3^{ff}	>20^{ff}	...	8.1±1.8^{mm}	9.9±1.5	...	40±2	95.7	99.9	...	12
J02001277-0840516	10.05±0.05	8.77±0.02	108.0±3.0^y	-62.0±2.0^y	M2.5V	-11.84	4.2	...	15.5±1.6^{zz}	4.8±0.2^{zz}	3.0±1.4	...	38±2	11.6	91.3	29.42±0.15	18
J02045317-5346162	12.08±0.06^o	10.44±0.02	95.6±2.9	-30.9±3.1	K5V	-11.84	-1.8	...	6.9±2.2^{zz}	10.9±0.3^{zz}	10.0±1.5	...	42±3	95.7^l	99.9^l	29.50±0.17	18
J02155892-0929121	9.80±0.06	8.43±0.03	92.0±3.0^y	-38.0±5.0^y	M2.5+M5+M8	-11.71	6.9	...	17.6±1.9^{zz}	2.5±0.3^{zz}	4.5±1.4	...	44±3	13.1^l	99.9^l	...	18
J02224418-6022476	10.51±0.05	8.99±0.02	136.9±1.7	-14.4±1.7	M4V	-11.53	8.1	...	25.1±2.9^{zz}	13.1±0.9^{zz}	11.3±1.6	...	32±2	64.8^l	99.9^l	29.57±0.14	18
J02414683-5259523	8.62±0.00^m	7.58±0.02	98.5±1.6	-14.0±1.3	K6Ve	-11.28	1.2^m	298^m	80.4±3.8^{mm}	12.5±1.6^m	11.8±1.5	...	42±2	96.5^l	99.9^l	30.05±0.13	5
J02414730-5259306	9.79±0.00^m	8.48±0.03	92.2±1.1	-4.2±1.5	M2.5V	-11.28	5.5	10^m	10.4±1.9^{mm}	12.7±1.2^m	11.8±1.5	...	44±3	95.9^l	99.5^l	30.09±0.13	5
J02423301-5739367	9.51±0.00^m	8.56±0.02	83.8±0.9	-8.8±1.3	K5Ve	-12.22	0.4^m	120^m	5.6±0.5	12.4±0.1^m	12.0±1.6	...	49±3	91.8	99.9	29.25±0.24	5
J03190864-3507002	9.60±0.06	8.58±0.03	89.7±1.6^y	-19.4±1.6^y	K7Ve	-12.13	1.3	65^m	6.1±1.2	13.5±0.2^m	12.9±1.5	...	44±3	86.7	99.9	29.24±0.27	7
J03244056-3904227	11.53±0.07^v	9.87±0.02	86.5±2.0	-17.1±2.8	M4V	-11.48	12.3	...	62.8±9.1^{zz}	13.0±3.5^{zz}	13.6±1.5	...	43±3	92.1^l	97.7^l	29.87±0.13	18
J03315564-4359135	9.32±0.00^m	8.30±0.02	87.4±1.7^y	-5.6±1.2^y	K6Ve	-11.85	1.9	251^m	10.7±0.2	15.5±0.3^m	14.2±1.5	...	44±2	96.7	99.9	29.53±0.16	7
J03454058-7509121	12.39±0.05	10.82±0.02	64.3±5.6	23.0±2.5	M4V	-12.24	3.1	...	43.6±6.0^{zz}	13.1±3.2^{zz}	13.3±1.6	...	54±4	99.9^l	99.9^l	29.30±0.18	18
J04213904-7233562	11.20±0.05	9.87±0.00^m	62.2±1.3	25.4±1.3	M2.5V	-12.15	3.5	...	<4.2^{zz}	15.0±0.3^{zz}	14.4±1.7	...	54±4	99.9	99.9	29.40±0.17	18
J04365738-1613065	10.53±0.06	9.12±0.03	70.0±5.0^y	-26.0±4.0^y	M3.5V	-11.54	5.1	...	51.5±5.8^{zz}	15.7±0.5^{zz}	16.3±1.6	...	47±4	27.2^l	99.3^l	29.90±0.15	18
J04440099-6624036	10.53±0.05	9.47±0.02	53.0±4.0	30.2±4.0	M0.5V	-12.37	2.6	...	<5.6^{zz}	16.7±0.4^{zz}	15.8±1.7	...	55±4	94.2	99.9	29.20±0.20	18
J04480066-5041255	9.79±0.00^m	8.74±0.03	54.3±1.8	14.1±1.8	K7Ve(vb)	-11.94	1.7	40^m	5.4±1.0^{mm}	19.3±0.1^{mm}	17.7±1.6	...	53±3	94.3	99.9	...	7
J05332558-5117131	10.00±0.00^m	8.99±0.02	44.0±1.8	24.2±1.7	K7V	-12.38	1.6	50^m	18.2±1.0^{mm}	19.6±0.4^{mm}	19.2±1.7	...	55±4	97.2	99.9	29.18±0.20	18
J17080882-6936186	10.51±0.06	9.06±0.02	-55.6±1.7	-80.2±1.7	M3.5V	-12.12	8.1	...	77.1±11.2^{zz}	6.3±3.3^{zz}	4.9±1.6	...	49±3	88.7^l	98.0^l	29.36±0.27	18
J17130733-8552105	9.69±0.06	8.59±0.03	-35.2±0.9	-58.1±0.9	M0V	-11.86	3.9	...	99.2±9.3^{mm}	16.3±3.8^{zz}	9.9±1.7	...	62±4	97.0^l	92.2^l	29.81±0.18	18

Table 3.IX — continued

Name (2MASS)	I_c[a] (mag)	J (mag)	$\mu_\alpha \cos\delta$[b] (mas yr⁻¹)	μ_δ[b] (mas yr⁻¹)	Spectral[c] Type	X-ray[d] log(f_x)	Hα[e] (Å)	Li[f] (m Å)	vsini[g] (km s⁻¹)	RV$_{meas}$[h] (km s⁻¹)	RV$_{pred}$[i] (km s⁻¹)	d_π[j] (pc)	d_x[i] (pc)	p[k] (%)	Pv[k] (%)	log L_x[d] (erg s⁻¹)	Refs.
J19225071-6310581	10.89±0.05	9.45±0.02	-10.7±1.9	-77.4±1.9	M3V	-11.89	8.2	...	29.5±2.2[zz]	6.4±1.5[zz]	0.8±1.6	...	61±4	99.9[l]	99.9[l]	29.77±0.23	18
J21370885-6036054	11.14±0.06[v]	9.64±0.02	41.3±1.8	-91.3±1.8	M3V	-11.89	6.9	...	7.2±2.0[zz]	2.3±0.2[zz]	0.9±1.5	...	48±3	99.9[l]	99.9[l]	29.57±0.19	18
J21490499-6413039	12.18±0.06	10.35±0.03	47.8±1.9	-96.5±2.0	M4.5V	-12.10	11.4	...	76.3±8.8[zz]	3.9±3.2[zz]	2.5±1.5	...	44±2	99.9[l]	99.9[l]	29.28±0.21	18
J22021626-4210329	10.08±0.06	8.93±0.03	51.8±0.9	-93.3±1.0	M1V	-11.90	2.8	...	10.2±2.1[zz]	-2.6±0.5[zz]	-4.9±1.5	...	45±2	98.9	99.9	29.49±0.17	18
J22440873-5413183	10.71±0.06	9.36±0.03	70.9±9.1	-60.1±8.3	M4*	-11.97	6.1	...	27.2±2.8[zz]	1.6±1.6[mm]	0.6±1.5	...	49±4	95.7[l]	99.9[l]	...	18
J23131671-4933154	11.54±0.05[v]	9.76±0.02	77.4±1.6	-90.4±1.6	M4V	-11.96	9.3	...	11.5±3.0[zz]	1.9±0.3[zz]	0.4±1.5	...	39±2	99.9[l]	99.9[l]	29.32±0.22	18
J23204705-6723209	11.34±0.06	9.99±0.04	80.0±1.6	-97.1±9.9	M5V(vb)	-12.08	11.5	...	11.4±2.8[zz]	6.6±0.3[zz]	5.7±1.5	...	41±3	99.9	99.9	...	7
J23261069-7323498	9.91±0.00[m]	8.84±0.03	72.1±1.0	-66.8±1.0	M0V(sb)	-11.80	5.1	123[l]	61.0±0.9[m]	8.0±1.9[mm]	7.3±1.6	...	49±2	99.9	99.9	29.49±0.16	18
J23285763-6802338	10.52±0.06[o]	9.26±0.02	67.9±1.7	-65.6±3.2	M2.5V	-11.98	6.0	...	50.3±5.8[zz]	10.8±3.4[zz]	6.1±1.5	...	49±3	99.9	99.9	29.22±0.19	18
J23452225-7126505	11.78±0.06	10.19±0.02	76.5±1.8	-64.0±1.8	M3.5V	-12.19	11.1	...	12.9±2.9[zz]	8.6±0.3[zz]	7.3±1.6	...	46±3	99.9[l]	99.9[l]	29.22±0.19	18
J23474694-6517249	10.36±0.06	9.10±0.02	80.7±1.2	-66.4±1.2	M1.5V	-12.24	2.5	...	<8.7[zz]	6.2±0.5[zz]	5.9±1.5	...	45±2	99.9	99.9	29.16±0.23	18
Columba Association																	
J01540267-4040440	10.71±0.05[v]	9.78±0.02	50.3±2.0	-14.7±1.2	K7V	-12.18	0.8	...	8.9±3.3[zz]	12.7±0.2[zz]	12.5±1.0	...	84±4	81.1	97.6	29.75±0.18	18
J02303239-4342232	8.88±0.08	8.02±0.03	81.4±0.8	-13.5±1.0	K5Ve	-11.85	0.0[m]	50[m]	7.0±1.2	16.0±1.3[mm]	15.1±1.0	...	51±2	31.9	97.4	29.65±0.14	7
J02335984-1811525	11.51±0.08[v]	10.09±0.03	51.1±2.9	-23.5±1.9	M3.0+M3.5	-12.05	8.5	...	16.4±1.5[zz]	12.4±0.3[zz]	12.7±1.0	...	77±5	99.5[l]	99.9[l]	...	18
J03050976-3725058	10.83±0.09	9.54±0.02	51.6±1.3	-11.5±1.3	M1.5+M3.0	-12.53	5.2	...	15.4±2.2[zz]	14.3±0.6[zz]	17.0±1.0	...	71±4	98.8[l]	96.9[l]	...	18
J03241504-5901125	10.55±0.00[m]	9.55±0.02	37.8±1.2	10.5±1.1	K7V	-12.40	1.6	235[m]	12.3±1.2	17.5±1.3[m]	17.6±1.1	...	90±5	71.1	99.3	29.60±0.23	3
J03494535-6730350	10.85±0.05	9.85±0.02	41.6±1.0	19.5±1.0	K7V	-12.30	1.7	...	<8.6[zz]	16.8±0.2[mm]	17.4±1.1	...	81±4	17.0	93.8	29.60±0.19	18
J04071148-2918342	10.14±0.06	9.06±0.02	41.6±1.1	-6.1±1.0	K7.5+M1.0	-11.98	3.2	...	20.1±1.8[zz]	21.2±0.4[zz]	20.4±1.0	...	71±5	99.5	99.9	...	18
J04091413-4008019	12.04±0.05	10.65±0.02	46.4±1.9	8.1±1.7	M3.5V	-12.40	16.9	...	10.8±2.8[zz]	21.3±0.5[zz]	20.7±1.1	...	63±5	99.0	99.9	29.29±0.29	18
J04240094-5512223	11.16±0.09	9.80±0.02	41.6±2.1	17.2±2.1	M2.5V	-12.39	3.7	...	10.2±2.3[zz]	20.1±0.5[zz]	20.2±1.1	...	68±5	54.2[l]	98.4[l]	29.36±0.27	18
J04515303-4647309	10.95±0.00[m]	9.80±0.02	29.0±3.0[y]	14.5±2.7[y]	M0V	-11.63	1.0[m]	80[m]	...	24.0±0.8[m]	22.0±1.1	...	76±6	99.9	99.9	30.21±0.17	7
J05100427-2340407	10.52±0.06	9.24±0.03	43.4±4.4	-13.0±0.9	M3+M3.5	-11.75	5.4	...	<8.4[zz]	24.3±0.3[zz]	23.0±1.1	...	49±6	95.8	99.9	...	18
J05100488-2340148	10.80±0.06	9.60±0.04	35.6±1.6	-13.1±1.5	M2+M2.5	-11.75	6.6	...	<7.6[zz]	24.4±0.2[zz]	23.0±1.1	...	57±5	98.9	99.9	...	18
J05111098-4903597	12.05±0.06	10.64±0.03	33.0±2.5	20.4±2.1	M3.5V	-11.99	6.8	...	11.1±3.2[zz]	22.1±0.4[zz]	22.4±1.1	...	62±6	97.4	99.9	29.68±0.21	18
J05142736-1514514	12.05±0.05	10.71±0.04	36.0±6.0[y]	-16.0±2.0[y]	M3.5V(vb)	-12.14	9.7	...	7.8±1.6[zz]	21.2±0.2[zz]	22.4±1.1	...	63±8	96.3	99.1	...	18
J05142878-1514546	12.44±0.06	10.95±0.02	34.1±8.1[y]	-14.2±8.0[y]	M3.5V(vb)	-12.14	5.7	...	8.5±1.1[zz]	21.4±0.3[zz]	22.4±1.1	...	58±8	97.6	98.9	...	18
J05164586-5410168	11.80±0.05	10.43±0.02	26.3±1.9	26.6±2.4	M3V	-12.25	2.7	...	<7.2[zz]	21.9±0.4[mm]	21.8±1.1	...	69±6	88.0	99.9	29.51±0.26	18
J05195695-1124440	11.75±0.06	10.37±0.02	24.0±2.0[y]	-18.0±3.0[y]	M3.5V	-12.19	11.8	...	<8.7[zz]	23.4±0.5[zz]	22.1±1.1	...	73±7	98.4[l]	99.9[l]	29.62±0.23	18
J05241317-2104427	11.81±0.06	10.21±0.02	33.1±3.7	-16.0±4.8	M4V	-12.37	8.3	...	<6.5[zz]	24.5±0.3[zz]	23.4±1.1	...	50±6	96.4[l]	99.3[l]	29.12±0.29	18
J05331130-2914199	11.87±0.11[v]	10.22±0.03	28.0±2.0[y]	-2.0±3.0[y]	M4V	-12.34	9.4	...	18.2±3.1[zz]	25.4±0.4[zz]	24.0±1.1	...	55±7	96.0[l]	99.9[l]	29.22±0.27	18
J05395494-1307598	12.17±0.06	10.60±0.02	26.4±8.5	-18.9±8.5	M3V	-12.45	5.6	...	<8.5[zz]	24.9±0.4[zz]	23.0±1.1	...	54±8	96.4[l]	99.4[l]	29.11±0.32	18
J05425587-0718382	11.52±0.05	10.10±0.03	19.1±2.1	-22.2±2.0	M3V	-12.21	7.0	...	82.3±6.1[zz]	29.7±3.9[zz]	22.2±1.1	...	73±7	97.7[l]	98.6[l]	29.60±0.22	18
J05432676-3025129	11.53±0.06	10.41±0.02	11.6±2.6	-0.3±1.2	M0.5V	-12.05	4.5	...	43.6±3.3[zz]	30.8±2.3[zz]	24.3±1.1	...	87±11	99.9	99.5	29.91±0.21	18
J05470650-3210413	11.36±0.06	9.86±0.02	23.9±0.9	6.8±0.9	M2.5V	-12.22	5.6	...	19.0±2.1[zz]	21.9±0.6[zz]	24.4±1.1	...	52±7	99.3[l]	96.6[l]	29.31±0.25	18
J06002304-4401217	11.67±0.06	10.31±0.04	24.4±4.3	15.3±3.6	M4V+M4V	-12.05	12.2	...	35.4±5.7[zz]	22.3±1.6[zz]	24.0±1.2	...	58±9	99.1	99.4	29.31±0.25	18
J07065772-5353463	9.62±0.06	8.54±0.03	-7.8±1.1	40.4±1.3	M0V	-11.77	2.7	...	17.1±1.9[zz]	22.4±0.6[zz]	22.9±1.2	...	53±5	99.4	99.9	29.77±0.17	18
J08083927-3605017	10.91±0.06	9.53±0.02	-7.2±1.6	8.4±1.6	K7V	-11.93	3.3	570[m]	8.0±1.2	25.3±0.8[mm]	24.1±1.2	...	90±13	75.9[l]	96.4[l]	30.06±0.23	18
J09331427-4848331	9.99±0.06	8.94±0.03	-46.5±1.2	23.4±2.6	K7V	-11.93	2.7	0[m]	80.0±8.0	22.0±0.8[m]	20.4±1.2	...	59±4	22.2	98.0	29.70±0.16	18
J22424884+1330532	9.63±0.05[v]	8.63±0.02	73.7±1.8[y]	-41.2±2.0[y]	K5Ve*	-11.76	1.5[oo]	...	...	-14.9±1.5[oo]	-14.4±1.1	...	51±2	37.6	94.4	...	11
J23301341-2023271	9.02±0.06[n]	7.20±0.02	314.5±7.2[y]	-208.1±6.1[y]	M3V	-11.44	3.3	0[m]	3.9±1.2	-5.7±0.8[m]	-2.9±1.0	16.2±0.9	13±1	0.1[l]	91.3[l]	28.90±0.13	18

Table 3.IX — continued

Name (2MASS)	I_c[a] (mag)	J (mag)	$\mu_\alpha \cos\delta$[b] (mas yr^{-1})	μ_δ[b] (mas yr^{-1})	Spectral[c] Type	X-ray[d] log(f_x)	$H\alpha$[e] (Å)	Li[f] (m Å)	vsini[g] (km s^{-1})	RV_{meas}[h] (km s^{-1})	RV_{pred}[i] (km s^{-1})	d_π[j] (pc)	d_x[i] (pc)	P[k] (%)	Pv[k] (%)	log L_x[i,d] (erg s^{-1})	Refs.
Carina Association																	
J04082685-7844471	10.31±0.05	9.28±0.02	55.7±2.3	42.8±1.4	M0V	−12.13	2.7	...	12.8±2.6[zz]	16.4±0.4[zz]	17.0±0.5	...	53±2	70.8	96.3	29.41±0.16	18
J06112997-7213388	11.00±0.05	9.55±0.02	23.4±1.6	60.8±1.6	M4V+M5V	−12.33	9.0	...	36.0±4.0[zz]	18.2±2.0[zz]	19.9±0.5	...	48±2	98.7[l]	99.1[l]	...	18
J06234024-7504327	11.23±0.05	9.88±0.03	13.9±1.8	47.2±1.8	M3.5+M5	−11.94	8.0	...	12.6±2.8[zz]	19.2±0.4[zz]	19.1±0.5	...	61±3	98.9[l]	99.9[l]	...	18
J07523324-6436308	10.70±0.06	9.70±0.03	−5.9±1.5	27.8±1.5	K7V(vb)	−12.49	2.1	...	10.7±3.6[zz]	21.1±0.4[zz]	21.7±0.5	...	88±5	99.4	99.9	...	18
J07540718-6320149	11.66±0.06	10.33±0.03	−10.8±2.4	30.0±2.4	M3V	−12.23	8.5	...	15.1±2.6[zz]	23.1±0.4[zz]	21.9±0.5	...	80±5	99.9[l]	99.9[l]	29.66±0.20	18
J09032434-6348330	10.77±0.06	9.57±0.03	−34.5±1.4	35.4±1.4	M0.5V(vb)	−12.09	2.9	...	10.7±3.5[zz]	20.7±0.4[zz]	20.8±0.6	...	66±3	76.0	93.4	...	18
J10140807-7636327	11.34±0.06	9.75±0.02	−47.2±1.7	30.6±3.6	M4V+M5V	−12.17	11.0	...	27.3±3.5[zz]	14.7±1.5[zz]	17.1±0.6	...	68±3	99.9[l]	99.9[l]	...	18
Argus Association																	
J00503319-2449009	9.42±0.00[s]	7.95±0.02	223.7±2.3[y]	−40.9±2.3[y]	M3.5+M4.5	−11.49	5.8	...	...	6.0±1.1[jj]	4.0±1.5	11.8±0.7	22±1	99.9[l]	99.9[l]	...	18
J03033668-2535329	9.29±0.04[n]	8.00±0.02	213.2±1.9[y]	94.5±1.8[y]	M0.0+M6.0	−12.03	0.4	0[m]	...	20.1±0.8[m]	16.1±0.9	38.6±3.8	18±1	99.9	92.5	...	18
J04464970-6034109	9.82±0.05	8.55±0.02	56.8±1.4	109.5±1.4	M1.5V	−12.00	5.3	...	55.5±7.9[zz]	15.5±3.5[zz]	12.1±1.6	...	37±2	91.2	91.1	29.23±0.17	18
J05090356-4209199	11.01±0.06	9.58±0.02	27.9±1.7	58.8±2.2	M3.5V	−12.16	8.2	...	29.2±2.7[zz]	16.8±1.7[zz]	18.5±1.5	...	51±4	65.8[l]	89.5[l]	29.35±0.19	18
J06134539-2352077	10.16±0.06	8.37±0.03	−28.0±3.9	105.3±1.3	M3.5+M5	−11.39	6.1	...	8.9±3.1[zz]	22.9±0.2[zz]	23.4±1.7	...	16±2	99.9[l]	99.9[l]	...	18
J09423823-6229028	11.82±0.05	10.21±0.03	−150.3±3.2	79.5±5.3	M3.5+M3.5	−12.20	3.7	...	<4.1[zz]	11.7±0.2[zz]	7.4±1.9	...	30±1	98.4	98.9	...	18
J09445422-1220544	10.39±0.00[t]	8.50±0.02	−328.8±4.6[y]	33.3±4.6[y]	M5V	−11.67	15.3	...	36.0±2.8[zz]	13.5±0.4[zz]	14.5±1.7	...	12±1	99.9[l]	99.9[l]	28.63±0.14	18
J10252563-4918389	10.52±0.06	9.12±0.04	−182.1±6.7	54.5±6.4	M4V	−12.05	8.3	...	6.4±2.4[zz]	1.7±0.2[zz]	7.5±1.9	...	27±1	99.9	99.4	28.89±0.19	18
J12092998-7505400	11.29±0.05	9.91±0.02	−65.3±2.5	−0.6±2.5	M3V	−12.41	7.5	...	<8.3[zz]	1.9±0.5[zz]	0.5±1.8	...	77±5	95.9[l]	99.9[l]	29.44±0.26	18
J12170465-5743558	9.69±0.06	8.71±0.02	−92.7±1.3[y]	−12.3±1.3[y]	K7V	−11.63	1.4	160[m]	24.5±2.5	−1.6±0.8[m]	−0.1±1.8	...	54±3	86.5	98.0	29.93±0.13	18
J15553178-3512028	10.66±0.00[f]	8.93±0.02	−226.0±3.0[y]	156.0±2.0[y]	M4+M7	−11.87	8.1	...	...	−15.5±0.7[uu]	−17.6±1.2	...	13±1	99.9	99.9	...	18
J18450097-1409053	10.25±0.06	8.47±0.04	46.0±6.0[y]	−84.0±13.0[y]	M5V(vb)	−11.74	8.8	...	14.4±2.1[zz]	−23.0±0.3[zz]	−24.1±1.4	...	16±2	88.2[l]	99.9[l]	...	18
J19224278-0515536	11.36±0.06	9.92±0.02	30.9±5.2	−15.6±5.2	K5V	−12.10	−1.0	...	9.4±0.9[zz]	−26.3±0.2[zz]	−23.8±1.5	...	45±6	99.0[l]	99.9[l]	29.30±0.26	18
J19312434-2134226	10.04±0.06	8.69±0.02	63.0±1.6	−110.1±1.6	M2.5V	−11.97	8.9	...	30.3±3.1[zz]	−25.6±1.5[nn]	−21.8±1.3	26.0±2.0[uu]	25±2	1.3	96.8	28.91±0.20	18
J20163382-0711456	9.76±0.07	8.59±0.03	84.6±8.1	−0.6±23.6	M0V+M2V	−12.35	1.7	...	5.7±1.2[zz]	−23.0±0.2[zz]	−21.2±1.5	...	33±3	96.0	99.9	...	18
J22332264-0936537	10.08±0.06	8.53±0.02	148.0±1.8	4.9±1.3	M3+M3	−11.61	6.1	...	...	−4.4±1.4[uu]	−9.9±1.1	...	32±1	99.9[l]	94.1[l]	...	18
J23205766-0147373	10.87±0.00[l]	9.35±0.02	171.9±4.3[y]	27.9±4.3[y]	M4+M4	−12.13	6.7	...	...	−7.2±0.4[uu]	−5.1±1.1	41.0±2.7[uu]	29±1	95.1[l]	97.7[l]	...	18
J23532520-7056410	10.34±0.05	8.68±0.02	306.7±8.8[aa]	46.3±8.8[aa]	M3.5V	−12.22	4.8	...	...	0.6±2.4[kk]	0.0±1.3	...	17±1	96.4[l]	99.9[l]	28.32±0.17	18
AB Doradus moving group																	
J00340843-2523498	9.40±0.06[v]	8.48±0.03	83.4±1.6	−98.2±1.4	K7Ve*	−11.90	2.1[oo]	...	11.1±1.2[zz]	−8.9±0.3[mm]	−8.0±1.7	...	49±2	99.4	99.9	...	11
J01034210+4051158	10.50±0.00[u]	9.37±0.04	118.6±4.0[y]	−162.3±4.0[y]	M2.6+M3.8	−11.50	1.9	...	...	−10.9±0.4[uu]	−11.5±1.5	29.9±2.0[uu]	33±1	74.0	97.0	...	14,16
J01123504+1703557	11.65±0.13[v]	10.21±0.02	92.0±1.0[y]	−98.0±1.0[y]	M3V	−12.31	5.7	...	23.7±2.2[zz]	−1.5±0.5[zz]	−1.5±1.8	...	48±2	97.9[l]	99.9[l]	29.13±0.23	18
J01225093-2439505	11.48±0.06	10.08±0.03	120.1±2.6	−121.5±1.7	M3.5V	−12.46	9.7	...	14.2±3.2[zz]	11.2±0.3[mm]	15.6±2.1	...	33±1	99.9	99.9	28.67±0.23	18
J01372322+2657119	9.33±0.09[v]	8.43±0.02	116.7±1.1[y]	−129.2±0.7[y]	K5Ve	−11.70	...	...	...	−5.9±3.0[oo]	−3.6±1.6	...	37±1	99.9	99.9	29.53±0.13	11
J01484087-4830519	10.42±0.06	9.19±0.03	111.2±1.2	−51.0±1.2	M1.5V	−11.96	3.1	...	<4.2[zz]	21.5±0.2[zz]	23.1±2.0	...	36±2	20.7	99.9	29.24±0.17	18
J02070786-1810077	12.58±0.05[v]	10.70±0.02	100.0±2.0[y]	−100.0±2.0[y]	M4V	−12.33	14.3	...	47.2±13.1[zz]	19.1±3.7[zz]	17.0±2.1	...	38±2	99.9[l]	99.9[l]	28.92±0.25	18
J04141730-0906544	11.09±0.05	9.63±0.02	96.0±6.0[y]	−138.0±3.0[y]	M3.5V	−11.80	6.1	78[bb]	...	23.4±0.3[uu]	21.9±1.7	23.8±1.4[uu]	28±2	99.3	99.9	29.20±0.16	16

Table 3.IX — continued

Name (2MASS)	I_c[a] (mag)	J (mag)	$\mu_\alpha \cos\delta$[b] (mas yr^{-1})	μ_δ[b] (mas yr^{-1})	Spectral[c] Type	X-ray[d] log(f_x)	Hα[e] (Å)	Li[f] (m Å)	vsini[g] (km s^{-1})	RV$_{meas}$[h] (km s^{-1})	RV$_{pred}$[i] (km s^{-1})	d_π[j] (pc)	d_s[i] (pc)	P[k] (%)	Pv[k] (%)	log L_x[d] (erg s^{-1})	Refs.
J04363294-7851021	12.53±0.05	10.98±0.02	32.8±2.8	47.4±2.7	M4V	-12.19	14.1	...	16.2±3.0[az]	26.5±0.3[az]	26.5±1.6	...	56±5	81.8[l]	99.9[l]	29.39±0.21	18
J04522441-1649219	9.10±0.00[l]	7.74±0.02	123.4±3.4[y]	-210.6±3.5[y]	M3Ve*	-11.51	6.3	20[ii]	...	26.7±1.5[ov]	25.8±1.6	16.3±0.4[uu]	16±1	99.9[l]	99.9[l]	...	7,11,16
J04554034-1917553	10.91±0.05	9.78±0.02	21.8±1.6	-66.1±1.6	M0.5V	-12.20	4.4	...	77.3±8.6[az]	22.2±3.7[az]	22.5±1.6	...	49±4	98.3	99.3	29.27±0.21	18
J04571728-0621564	10.55±0.05	9.51±0.02	18.0±2.0[y]	-92.0±5.0[y]	M0.5V	-12.33	3.1	...	11.3±1.4[az]	23.4±0.3[az]	22.5±1.6	...	49±3	96.4	99.9	29.13±0.25	18
J05240991-4223054	11.74±0.06	10.58±0.02	4.9±1.9	-13.3±2.5	M0.5V	-12.34	2.8	...	10.8±2.5[az]	33.4±0.6[az]	30.9±1.6	...	52±9	89.0	97.9	29.18±0.30	18
J05254166-0909123	9.91±0.00[l]	8.45±0.03	39.9±4.6[y]	-189.7±4.6[y]	M3.5+M4	-11.82	3.3	...	8.4±2.5[az]	26.3±0.3[nm]	24.1±1.5	20.7±2.2[uu]	21±1	99.9[l]	99.9[l]	...	18,16
J05301858-5358483	9.72±0.06	7.91±0.02	207.5±9.0[y]	387.1±9.0[y]	M3+M6+M4	-11.68	3.9	...	10.2±3.4[az]	31.3±0.2[az]	31.0±1.6	...	3±1	7.0	97.7	...	18
J05531299-4505119	9.67±0.00[m]	8.60±0.03	32.8±1.4[y]	-4.9±1.4[y]	M0.5V	-11.94	1.4	140[m]	8.1±1.2	31.7±0.8[m]	31.3±1.6	...	34±4	98.7	99.9	...	18
J08471906-5717547	11.03±0.05[v]	9.41±0.02	-123.2±1.2	14.9±1.3	M4V	-11.88	10.1	...	10.3±2.8[az]	30.2±0.2[az]	28.4±1.4	...	22±2	93.6[l]	99.9[l]	28.90±0.20	18
J11254754-4410267	11.91±0.05	10.34±0.03	-84.5±2.7	-57.7±7.7	M4+M4.5	-11.74	10.7	>30[xx]	21.4±2.9[az]	20.7±1.0[mm]	19.2±1.4	...	48±3	79.7[l]	99.9[l]	...	13
J12383713-2703348	10.07±0.05	8.73±0.04	-172.0±3.0[y]	-188.0±6.0[y]	M2.5V	-12.06	3.1	...	<3.6[az]	9.9±0.2[az]	8.3±1.7	...	25±1	99.2	99.9	28.81±0.19	18
J15244849-4929473	9.45±0.06	8.16±0.03	-121.1±3.0[y]	-238.9±2.7[y]	M2V(sb1)	-12.49	0.5	...	<3.1[az]	10.3±0.2[az]	7.4±1.3	...	23±1	95.9[l]	99.9[l]	...	18
J16074132-1103073	11.29±0.06	9.82±0.02	-64.0±4.0[y]	-148.0±5.0[y]	M4V	-12.45	7.1	...	24.4±8.0[az]	-8.5±1.2[az]	-13.4±1.6	...	36±2	98.3[l]	97.5[l]	28.76±0.25	18
J20395460+0620118	8.84±0.06[v]	7.92±0.02	90.0±1.1	-97.8±1.7	K7Ve	-12.36	...	...	...	-20.6±1.5[ov]	-19.3±1.5	...	39±2	80.0	97.5	28.91±0.21	11
J20465795-0259320	10.15±0.05	9.12±0.03	59.1±2.4	-108.4±2.4	M0V	-12.22	1.6	...	9.6±1.3[az]	-14.2±0.3[az]	-15.2±1.5	...	46±2	99.3	99.9	29.19±0.24	18
J21130526-1729126	9.22±0.00[m]	8.35±0.03	74.4±0.8	-145.1±0.8	K6Ve	-12.07	0.1[m]	20[m]	7.9±1.2	-7.4±0.8[m]	-7.2±1.7	...	39±1	99.9	99.9	29.21±0.16	7
J21464282-8543046	10.43±0.05	8.84±0.02	184.0±5.0[y]	-212.0±32.0[y]	M3.5V	-11.67	12.7	...	19.4±2.8[az]	23.5±0.7[az]	22.2±1.6	...	18±1	55.6[l]	99.9[l]	28.93±0.16	18
J21471964-4803166	12.29±0.06	10.73±0.02	50.4±3.2	-72.9±2.5	M4V	-12.41	6.4	...	42.1±4.4[az]	10.4±2.9[az]	8.9±1.8	...	67±3	1.4[l]	98.2[l]	29.33±0.23	18
J23320018-3917368	10.28±0.06	8.90±0.03	189.5±4.2	-183.7±7.9	M3V	-11.63	5.7	...	6.0±1.6[az]	11.1±0.2[az]	11.9±2.1	...	23±1	99.9	99.9	29.18±0.18	18
J23513366-3127229	11.22±0.05[v]	9.82±0.02	108.0±1.0[y]	-84.0±1.0[y]	M2V+L0	-12.18	3.2	78[hh]	12.9±1.3[az]	-13.6±0.3[nm]	-13.7±1.6	...	42±2	99.4[l]	99.9[l]	...	15
Ambiguous candidate members																	
J00281434-3227556	11.86±0.06[o]	10.12±0.02	108.0±3.8	-42.6±2.1	M5V(vb)	-12.30	10.6	...	56.5±7.6[az]	4.6±3.4[az]	...	...	...	...	...	...	18
J01351393-0712517	10.53±0.08	8.96±0.02	96.0±3.0[y]	-50.0±4.0[y]	M4V(sb2)	-11.92	15.3	>23[cc]	51.1±4.8[az]	6.8±0.8[nm]	...	37.9±2.4[uu]	...	...	...	...	18
J02175601+1225266	11.61±0.08[v]	9.96±0.02	50.0±6.0[y]	-42.0±4.0[y]	M3.5V	-12.12	7.0	>22[cc]	...	7.0±1.3[cc]	...	...	...	...	...	...	18
J02365171-5203036	9.78±0.00[m]	8.42±0.02	102.6±0.8	0.8±0.8	M2Ve	-11.57	5.8	380[m]	37.1±3.6[pn]	16.0±0.1[mm]	...	...	...	...	...	...	5
J02485260-3404246	10.99±0.09[v]	9.31±0.03	89.0±1.4	-23.8±1.4	M4V(sb1)	-11.96	9.6	...	7.0±2.4[az]	14.6±0.3[az]	...	...	...	...	...	...	18
J02505959-3409050	12.18±0.15[v]	10.48±0.03	85.8±1.8	-21.0±1.8	M4V	-12.40	10.1	...	52.6±5.8[az]	12.0±3.5[az]	...	...	...	...	...	...	18
J02564708-6343027	11.32±0.06	9.86±0.02	67.4±1.7	8.8±3.8	M4V	-12.26	9.4	...	51.5±7.8[az]	18.5±3.4[az]	...	...	...	...	...	...	18
J05392505-4245211	10.72±0.06	9.45±0.02	40.6±1.2	15.9±3.0	M2V	-11.91	3.5	...	<4.2[az]	21.9±0.2[az]	...	...	...	...	...	...	18
J06434532-6424396	10.67±0.09	9.29±0.02	2.3±2.4	54.5±2.4	M4+M3+M5	-11.97	6.3	...	14.1±2.6[az]	20.2±0.4[az]	...	...	...	...	...	...	18
J08412528-5736021	10.94±0.05	9.58±0.03	-20.7±3.7	26.5±2.0	M3V+M3V	-11.95	9.4	...	<5.6[az]	21.4±0.2[az]	...	...	...	...	...	...	18
J09315840-6209258	11.42±0.06	9.95±0.02	-38.4±4.2	18.6±2.8	M3.5V	-11.96	9.1	...	20.4±2.8[az]	18.8±0.8[az]	...	...	...	...	...	...	18
J10252092-4241539	10.64±0.06	9.50±0.03	-46.8±1.2	-2.2±1.2	M1V	-12.08	4.1	490[xx]	11.5±3.2[az]	17.6±0.5[az]	...	...	...	...	...	...	13
J10423011-3340162	9.21±0.00[m]	7.79±0.02	-122.2±2.2[y]	-29.3±2.2[y]	M2Ve	-11.59	6.5	530[m]	4.4±1.2	11.4±0.8[m]	...	...	...	...	...	...	2
J11091606-7352465	11.22±0.06	9.86±0.03	-53.3±1.9	10.3±1.9	M3V	-12.10	6.2	...	45.0±4.7[az]	13.9±2.4[az]	...	...	...	...	...	...	18

Table 3.IX — continued

Name (2MASS)	I_c^a (mag)	J (mag)	$\mu_\alpha \cos \delta^b$ (mas yr^{-1})	μ_δ^b (mas yr^{-1})	Spectral^c Type	X-ray^d log(f_x)	Hα^e (Å)	Li^f (m Å)	vsini^g (km s^{-1})	RV$_{meas}^h$ (km s^{-1})	RV$_{pred}^i$ (km s^{-1})	d_π^j (pc)	d_s^j (pc)	P^k (%)	P$_V^k$ (%)	log L$_x^{sd}$ (erg s^{-1})	Refs.
J13412668-4341522	12.41±0.06	10.75±0.02	−107.0±3.0	−60.8±3.0	M3.5V	−12.31	8.4	...	<13.1^{zz}	3.1±0.2^{zz}	...	...	...	...	...	...	18
J14252913-4113323	10.06±0.11^{ww}	8.55±0.03	−46.8±2.1^v	−49.2±1.7^v	M2.5Ve*	...	7.0^{vv}	...	93.3±6.9^{zz}	−2.0±1.6^{zz}	...	66.9±4.3^{vv}	...	...	...	...	17
J18141047-3247344	9.16±0.07	8.07±0.02	3.3±1.7	−52.0±1.3	K6Ve(sb2)	−11.66	60.0^{gg}	440^{ii}	117.2±4.6^{zz}	−13.3±7.7^{zz}	...	...	...	...	...	...	6
J23314492-0244395	11.24±0.07^o	9.51±0.02	90.0±2.0^v	−60.0±1.0^v	M4.5V	−11.95	19.0	...	<5.4^{zz}	−5.0±0.3^{zz}	...	...	...	...	...	...	18

[a] I_c magnitude from *DENIS* catalog (Epchtein et al., 1997), unless stated otherwise.

[b] Proper motion from *UCAC3* catalog (Zacharias et al., 2009), unless stated otherwise.

[c] Spectral type with asterisk is for the whole unresolved system.

[d] ROSAT X-ray flux calculated from Riaz et al. (see Section 5.4; 2006) in erg s^{-1} cm^{-2}. L_x calculated from http://heasarc.gsfc.nasa.gov/W3Browse/all/rassdssstar.html.

[e] Hα EW from Riaz et al. (2006), unless stated otherwise.

[f] Lithium EW from Mentuch et al. (2008), unless stated otherwise.

[g] Projected rotational velocity from this work, unless stated otherwise.

[h] Radial velocity measurement from Montes et al. (2001), unless stated otherwise.

[i] Radial velocity and statistical distance derived by our analysis (see Malo et al. (2013) Section 4.5).

[j] Trigonometric distance from van Leeuwen (2007), unless stated otherwise.

[k] P : Membership probability without considering the RV or parallax information and P$_V$: Membership probability with considering the RV (see Malo et al. (2013) Section 4.5).

[l] Membership probability for which the binary hypothesis is higher.

References. — (1) Kastner et al., 1997 ; (2) Webb et al., 1999 ; (3) Torres et al., 2000 ; (4) Zuckerman et al., 2001b ; (5) Zuckerman & Song, 2004 ; (6) Torres et al., 2006 ; (7) Torres et al., 2008 ; (8) Lépine & Simon, 2009 ; (9) Ortega et al., 2009 ; (10) Looper et al., 2010 ; (11) Schlieder et al., 2010 ; (12) Kiss et al., 2011 ; (13) Rodriguez et al., 2011 ; (14) Schlieder et al., 2012a ; (15) Bowler et al., 2012 ; (16) Shkolnik et al., 2012 ; (17) Riedel et al., 2014 ; (18) this work.

Note. — (m) Torres et al., 2006 ; (n) van Leeuwen, 2007 ; (o) Malo et al., 2013 ; (p) magnitude without binary correction; Torres et al., 2006 ; (p) Zuckerman et al., 2001c ; (q) Reid & Cruz, 2002 ; (r) Reid et al., 2003 ; (s) Koen et al., 2010 ; (t) Casagrande et al., 2008 ; (u) Reid et al., 2004 ; (v) UCAC4; Zacharias et al., 2013 ; (w) Moór et al., 2013 ; (x) Weinberger et al., 2013 ; (y) NOMAD; Zacharias et al., 2005 ; (z) PPMXL; Roeser et al., 2010 ; (aa) PPMX; Roeser et al., 2008 ; (bb) Looper et al., 2010 ; (cc) Binks & Jeffries, 2013 ; (dd) Zickgraf et al., 2005 ; (ee) Shkolnik et al., 2011 ; (ff) Kiss et al., 2011 ; (gg) Herbig & Bell, 1988 ; (hh) Shkolnik et al., 2009 ; (ii) da Silva et al., 2009 ; (jj) Kharchenko et al., 2007 ; (kk) RAVE; Zwitter et al., 2008 ; (ll) Gizis et al., 2002 ; (mm) See compilation in Table 3.IV ; (mm) See compilation in Table 3.V ; (oo) Schlieder et al., 2010 ; (pp) Jayawardhana et al., 2006 ; (qq) Upgren & Harlow, 1996 ; (rr) Hawley et al., 1996 ; (ss) Schlieder et al., 2012a ; (tt) Bowler et al., 2012 ; (uu) Shkolnik et al., 2012 ; (vv) Riedel et al., 2014 ; (ww) Schlieder et al., 2012b ; (xx) Rodriguez et al., 2011 ; (yy) Wahhaj et al., 2011 ; (zz) this work.

Table 3.X.   Membership probabilities of all candidates[a]

Name	βPMG P	βPMG P_ν	βPMG $P_{\nu+\pi}$	TWA P	TWA P_ν	TWA $P_{\nu+\pi}$	THA P	THA P_ν	THA $P_{\nu+\pi}$	COL P	COL P_ν	COL $P_{\nu+\pi}$	CAR P	CAR P_ν	CAR $P_{\nu+\pi}$	ARG P	ARG P_ν	ARG $P_{\nu+\pi}$	ABDMG P	ABDMG P_ν	ABDMG $P_{\nu+\pi}$	Field P	Field P_ν	Field $P_{\nu+\pi}$
J00172353-6645124	99.3	99.9	99.9	0.0	0.0	0.0	0.0	0.0	0.0	0.0	0.0	0.0	0.0	0.0	0.0	0.0	0.0	0.0	0.1	0.0	0.0	0.0	0.0	0.0
J00275023-3233060	1.8	99.9	99.9	0.0	0.0	0.0	94.6[b]	0.0	0.0	3.6[b]	0.0	0.0	0.0	0.0	0.0	0.0	0.0	0.0	0.1	0.2	0.0	0.0	0.2	0.0
J00275035-3233238	97.2	99.9	99.9	0.0	0.0	0.0	2.2[b]	0.0	0.0	0.3	0.0	0.0	0.0	0.0	0.0	0.0	0.0	0.0	0.0	0.0	0.0	0.1	0.0	0.0
J00281434-3227556	81.1	83.6	...	0.0	0.0	...	16.4[b]	12.0[b]	...	2.4[b]	4.4[b]	...	0.0	0.0	...	0.0	0.0	...	0.0	0.0	...	0.1	0.1	...
J00340843-2523498	0.0	0.0	...	0.0	0.0	...	0.0	0.0	...	0.0	0.0	...	0.0	0.0	...	0.0	0.0	...	99.4	99.9	...	0.6	0.1	...
J00503319-2449009	0.0	0.0	0.0	0.0	0.0	0.0	0.0	0.0	0.0	0.0	0.0	0.0	0.0	0.0	0.0	0.0	99.9[b]	0.0	0.0	0.0	0.0	0.3	0.1	99.9
J01034210+4051158	0.0	0.0	0.0	0.0	0.0	0.0	0.0	0.0	0.0	0.0	0.0	0.0	0.0	0.0	0.0	0.0	0.0	0.0	74.0	97.0	97.8	26.0	3.0	2.2
J01123504+1703557	1.7	0.0	...	0.0	0.0	...	64.1	0.0	...	18.9	0.0	...	0.0	0.0	...	0.0	0.0	...	97.9[b]	99.9[b]	...	0.4	0.0	...
J01132817-3821024	16.7	99.3	...	0.0	0.0	...	98.4	99.9	...	1.0	0.0	...	0.0	0.0	...	0.0	0.0	...	0.5	0.0	...	0.2	0.7	...
J01220441-3337036	0.1	0.0	...	0.0	0.0	...	0.0	0.0	...	0.0	0.0	...	0.0	0.0	...	0.0	0.0	...	99.9	99.9	...	0.1	0.0	...
J01225093-2439505	0.0	0.0	...	0.0	0.0	...	0.0	0.0	...	0.0	0.0	...	0.0	0.0	...	0.0	0.0	...	0.0	0.0	...	0.1	0.3	...
J01351393-0712517	24.3[b]	11.3[b]	75.9[b]	0.0	0.0	0.0	5.7[b]	0.0	0.0	70.0[b]	88.7[b]	24.1[b]	0.0	0.0	0.0	0.0	0.0	0.0	0.0	0.0	0.0	0.0	0.0	0.0
J01365516-0647379	28.3	99.9	99.9	0.0	0.0	0.0	1.3	0.0	0.0	70.3	0.0	0.0	0.0	0.0	0.0	0.0	0.0	0.0	99.9	0.0	0.0	0.1	0.2	0.1
J01372322+2657119	0.1	0.0	...	0.0	0.0	...	0.0	99.9	...	0.0	0.0	...	0.0	0.0	...	0.0	0.0	...	20.7	99.9	...	0.4	0.1	...
J01484087-4830519	0.0	0.0	...	0.0	0.0	...	79.2	0.0	...	0.0	0.0	...	0.0	0.0	...	0.0	0.0	...	4.2[b]	0.0	...	0.0	0.0	...
J01521830-5950168	0.0	0.0	...	0.0	0.0	...	95.7	0.0	...	0.0	0.0	...	0.0	0.0	...	0.0	0.0	...	0.0	0.0	...	0.0	0.0	...
J01535076-1459503	99.9[b]	99.9[b]	...	0.0	0.0	...	0.0	0.0	...	0.0	0.0	...	0.0	0.0	...	0.0	0.0	...	0.0	0.0	...	0.2	0.1	...
J01540267-4040440	0.0	0.0	...	0.0	0.0	...	0.0	0.0	...	81.1	97.6	...	0.0	0.0	...	0.0	0.0	...	0.0	0.0	...	18.9	2.4	...
J02001277-0840516	10.9	0.0	...	0.0	0.0	...	11.6	91.3	...	77.5	8.6	...	0.0	0.0	...	0.0	0.0	...	0.0	0.0	...	0.1	0.1	...
J02045317-5346162	0.0	0.0	...	0.0	0.0	...	95.7[b]	99.9[b]	...	0.0	0.0	...	0.0	0.0	...	0.0	0.0	...	99.9[b]	99.9[b]	...	0.0	0.0	...
J02070786-1810077	0.4	0.2	...	0.0	0.0	...	0.0	0.0	...	0.0	0.0	...	0.0	0.0	...	0.0	0.0	...	0.0	0.0	...	0.0	0.0	...
J02155892-0929121	20.2	0.0	...	0.0	0.0	...	13.1[b]	99.9[b]	...	66.7[b]	0.0	...	0.0	0.0	...	0.0	0.0	...	0.0	0.0	...	0.0	0.1	...
J02175601+1225266	16.2[b]	19.2[b]	...	0.0	0.0	...	0.0	0.0	...	82.6[b]	80.5[b]	...	0.0	0.0	...	0.0	0.0	...	30.8[b]	0.0	...	1.1	0.2	...
J02224418-6022476	0.1	0.1	...	0.0	0.0	...	64.8[b]	99.9[b]	...	0.1	0.1	...	0.1	0.0	...	0.0	0.0	...	0.0	0.0	...	0.0	0.0	...
J02303239-4342232	0.3	1.0	...	0.0	0.0	...	67.7	1.6	...	31.9	97.4	...	0.0	0.0	...	0.0	0.0	...	0.0	0.0	...	0.0	0.0	...
J02335984-1811525	0.2	0.0	...	0.0	0.0	...	0.0	0.0	...	99.5[b]	99.9[b]	...	0.0	0.0	...	0.0	0.0	...	0.2	0.0	...	0.2	0.0	...
J02365171-5203036	7.6	20.6	...	0.0	0.0	...	70.6[b]	2.4[b]	...	21.5[b]	77.0[b]	...	0.0	0.0	...	0.0	0.0	...	3.4[b]	0.0	...	0.0	0.0	...
J02414683-5259523	0.0	0.0	...	0.0	0.0	...	96.5[b]	99.9[b]	...	0.1	0.0	...	0.0	0.0	...	0.0	0.0	...	0.8	0.0	...	0.0	0.0	...
J02414730-5259306	0.2	0.0	...	0.0	0.0	...	95.9[b]	99.5[b]	...	3.1[b]	0.5	...	0.0	0.0	...	0.0	0.0	...	8.2	0.0	...	0.0	0.0	...
J02423301-5739367	0.0	0.0	...	0.0	0.0	...	91.8	99.9	...	0.0	0.0	...	0.0	0.0	...	0.0	0.0	...	0.0	0.0	...	0.0	0.0	...
J02485260-3404246	12.7[b]	15.9[b]	...	0.0	0.0	...	66.3[b]	12.0[b]	...	21.0[b]	72.1[b]	...	0.0	0.0	...	0.0	0.0	...	0.0	0.0	...	0.0	0.0	...
J02505959-3409050	3.5	1.3	...	0.0	0.0	...	63.6[b]	81.3	...	32.9[b]	17.4[b]	...	0.0	0.0	...	0.0	0.0	...	0.0	0.0	...	0.0	0.0	...
J02564708-6343027	0.1	0.4	0.0	0.0	0.0	0.0	85.0[b]	84.2[b]	0.0	2.1[b]	9.4[b]	0.0	0.0	0.0	0.0	99.9	92.5	0.7	12.8[b]	6.0[b]	0.0	0.4	7.5	99.3
J03033668-2535329	0.0	0.0	...	0.0	0.0	...	0.0	0.0	...	0.0	0.0	...	0.0	0.0	...	0.0	0.0	...	0.0	0.0	...	0.2	0.3	...
J03050976-3725058	0.6	0.6	...	0.0	0.0	...	0.5	2.2	...	98.8[b]	96.9[b]	...	0.0	0.0	...	0.0	0.0	...	0.0	0.0	...	0.0	0.0	...
J03190864-3507002	0.1	0.0	...	0.0	0.0	...	86.7	99.9	...	13.2	0.0	...	0.0	0.0	...	0.0	0.0	...	0.0	0.0	...	0.0	0.7	...
J03241504-5901125	0.0	0.0	...	0.0	0.0	...	0.0	0.0	...	71.1	99.3	...	0.0	0.0	...	0.0	0.0	...	25.2	0.0	...	3.8	0.0	...
J03244056-3904227	2.5	0.7	...	0.0	0.0	...	92.1[b]	97.7[b]	...	5.3[b]	1.6	...	0.0	0.0	...	0.0	0.0	...	0.0	0.0	...	0.0	0.0	...
J03315564-4359135	0.0	0.0	...	0.0	0.0	...	96.7	99.9	...	3.2	0.1	...	0.0	0.0	...	0.0	0.0	...	0.0	0.0	...	0.0	0.0	...

Table 3.X — continued

Name	βPMG			TWA			THA			COL			CAR			ARG			ABDMG			Field		
	P	P_ν	$P_{\nu+\pi}$	P	P_ν	$P_{\nu+\pi}$	P	P_ν	$P_{\nu+\pi}$	P	P_ν	$P_{\nu+\pi}$	P	P_ν	$P_{\nu+\pi}$	P	P_ν	$P_{\nu+\pi}$	P	P_ν	$P_{\nu+\pi}$	P	P_ν	$P_{\nu+\pi}$
J03323578+2843554	99.9^b	99.9^b	⋯	0.0	0.0	⋯	0.0	0.0	⋯	0.0	0.0	⋯	0.0	0.0	⋯	0.0	0.0	⋯	0.0	0.0	⋯	0.0	0.0	⋯
J03454058-7509121	0.0	0.0	⋯	0.0	0.0	⋯	99.9^b	99.9	⋯	0.0	0.0	⋯	0.0	0.0	⋯	0.0	0.0	⋯	0.1	0.0	⋯	0.0	0.0	⋯
J03494535-6730350	0.0	0.0	⋯	0.0	0.0	⋯	2.5	3.0	⋯	17.0	93.8	⋯	0.0	0.0	⋯	0.0	0.0	⋯	74.6	0.0	⋯	5.9	3.2	⋯
J04071148-2918342	0.4	0.2	⋯	0.0	0.0	⋯	0.1	0.0	⋯	99.5	99.9	⋯	0.0	0.0	⋯	0.0	0.0	⋯	0.0	0.0	⋯	0.0	0.0	⋯
J04082685-7844471	0.0	0.0	⋯	0.0	0.0	⋯	26.8	3.3	⋯	0.4	0.4	⋯	70.8	96.3	⋯	0.0	0.0	⋯	1.7	0.0	⋯	0.3	0.0	⋯
J04091413-4008019	0.2	0.1	⋯	0.0	0.0	⋯	0.8	0.0	⋯	99.0	99.9	⋯	0.0	0.0	⋯	0.0	0.0	⋯	0.0	0.0	⋯	0.0	0.0	⋯
J04141730-0906544	0.5	0.0	0.0	0.0	0.0	0.0	0.0	0.0	0.0	0.0	0.0	0.0	0.0	0.0	0.0	0.0	0.0	0.0	99.3	99.9	99.9	0.2	0.0	0.1
J04213904-7233562	0.0	0.0	⋯	0.0	0.0	⋯	99.9	99.9	⋯	0.0	0.0	⋯	0.0	0.0	⋯	0.0	0.0	⋯	0.0	0.0	⋯	0.2	0.0	⋯
J04240094-5512223	0.8	0.9	⋯	0.0	0.0	⋯	5.5^b	0.7	⋯	54.2^b	98.4^b	⋯	0.0	0.0	⋯	0.0	0.0	⋯	39.4	0.0	⋯	0.1	0.0	⋯
J04363294-7851021	5.9	0.0	⋯	0.0	0.0	⋯	3.0^b	0.0	⋯	6.4^b	0.0	⋯	2.1^b	0.0	⋯	0.0	0.0	⋯	81.8^b	99.9^b	⋯	0.6	0.0	⋯
J04365738-1613065	3.8	0.7	⋯	0.0	0.0	⋯	27.2^b	99.3^b	⋯	69.0^b	0.0	⋯	0.0	0.0	⋯	0.0	0.0	⋯	0.0	0.0	⋯	0.0	0.0	⋯
J04435686+3723033	95.6	96.4	⋯	0.0	0.0	⋯	0.0	0.0	⋯	1.9	3.4^b	⋯	0.0	0.0	⋯	0.5	0.0	⋯	0.1	0.0	⋯	1.9	0.2	⋯
J04440099-6624036	7.8	8.9	⋯	0.0	0.0	⋯	94.2	99.9	⋯	0.4	0.1	⋯	1.1	0.0	⋯	0.0	0.0	⋯	3.8	0.0	⋯	0.6	0.1	⋯
J04464970-6034109	0.0	0.0	⋯	0.0	0.0	⋯	0.0	0.0	⋯	0.0	0.0	⋯	0.0	0.0	⋯	91.2	91.1	⋯	0.9	0.0	⋯	0.1	0.0	⋯
J04480066-5041255	0.0	0.0	⋯	0.0	0.0	⋯	94.3	99.9	⋯	1.2	0.4	⋯	0.0	0.0	⋯	0.0	0.0	⋯	4.4	0.0	⋯	0.1	0.0	⋯
J04515303-4647309	0.0	0.0	⋯	0.0	0.0	⋯	0.0	0.0	⋯	99.9	99.9	⋯	0.0	0.0	⋯	0.0	0.0	⋯	0.0	0.0	⋯	0.1	0.0	⋯
J04522441-1649219	0.0	0.0	0.0	0.0	0.0	0.0	0.0	0.0	0.0	0.0	0.0	0.0	0.0	0.0	0.0	0.0	0.0	0.0	99.9^b	99.9^b	99.9^b	0.1	0.0	0.0
J04554034-1917553	0.0	0.0	⋯	0.0	0.0	⋯	0.0	0.0	⋯	0.0	0.0	⋯	0.0	0.0	⋯	0.0	0.0	⋯	98.3	99.3	⋯	1.7	0.7	⋯
J04571728-0621564	0.0	0.0	⋯	0.0	0.0	⋯	0.0	0.0	⋯	0.0	0.0	⋯	0.0	0.0	⋯	0.0	0.0	⋯	96.4	99.9	⋯	3.6	0.3	⋯
J05082729-2101444	99.9^b	99.9^b	⋯	0.0	0.0	⋯	0.0	0.0	⋯	0.1	0.2	⋯	0.0	0.0	⋯	0.0	0.0	⋯	0.0	0.0	⋯	0.0	0.0	⋯
J05090356-4209199	34.0	10.4	⋯	0.0	0.0	⋯	0.0	0.0	⋯	0.0	0.0	⋯	0.0	0.0	⋯	65.8^b	89.5^b	⋯	0.0	0.0	⋯	0.2	0.1	⋯
J05100427-2340407	0.3	0.1	⋯	0.0	0.0	⋯	3.9^b	0.0	⋯	95.8	99.9	⋯	0.0	0.0	⋯	0.0	0.0	⋯	0.0	0.0	⋯	0.0	0.0	⋯
J05100488-2340148	0.1	0.0	⋯	0.0	0.0	⋯	1.0	0.0	⋯	98.9	99.9	⋯	0.0	0.0	⋯	0.0	0.0	⋯	0.0	0.0	⋯	0.0	0.0	⋯
J05111098-4903597	0.0	0.0	⋯	0.0	0.0	⋯	1.0	0.1	⋯	97.4	99.9	⋯	0.0	0.0	⋯	0.0	0.0	⋯	1.4	0.0	⋯	0.0	0.0	⋯
J05142736-1514514	0.1	0.2	⋯	0.0	0.0	⋯	3.3	0.8	⋯	96.3	99.1	⋯	0.0	0.0	⋯	0.0	0.0	⋯	0.0	0.0	⋯	0.3	0.0	⋯
J05142878-1514546	0.9	0.8	⋯	0.0	0.0	⋯	1.5	0.2	⋯	97.6	98.9	⋯	0.0	0.0	⋯	0.0	0.0	⋯	0.0	0.0	⋯	0.1	0.0	⋯
J05164586-5410168	0.1	0.0	⋯	0.0	0.0	⋯	0.1	0.0	⋯	88.0	99.9	⋯	0.0	0.0	⋯	0.0	0.0	⋯	11.7	0.0	⋯	0.0	0.0	⋯
J05195695-1124440	1.3	0.4	⋯	0.0	0.0	⋯	0.1	0.0	⋯	98.4^b	99.9^b	⋯	0.0	0.0	⋯	0.0	0.0	⋯	0.0	0.0	⋯	0.2	0.0	⋯
J05240991-4223054	0.0	0.0	⋯	0.0	0.0	⋯	0.0	0.0	⋯	0.0	0.0	⋯	0.0	0.0	⋯	0.0	0.0	⋯	89.0	97.9	⋯	11.0	2.1	⋯
J05241317-2104427	3.2	0.7	⋯	0.0	0.0	⋯	0.3	0.0	⋯	96.4^b	99.3^b	⋯	0.0	0.0	⋯	0.0	0.0	⋯	0.0	0.0	⋯	0.0	0.0	⋯
J05241914-1601153	99.9^b	99.9^b	⋯	0.0	0.0	⋯	0.0	0.0	⋯	0.0	0.0	⋯	0.0	0.0	⋯	0.0	0.0	⋯	0.0	0.0	⋯	0.0	0.0	⋯
J05254166-0909123	0.0	0.0	0.0	0.0	0.0	0.0	0.0	0.0	0.0	0.0	0.0	0.0	0.0	0.0	0.0	0.0	0.0	0.0	99.9^b	99.9^b	99.9^b	0.0	0.0	0.0
J05301858-5358483	69.1	0.0	⋯	0.0	0.0	⋯	0.0	0.0	⋯	20.4	0.0	⋯	0.0	0.0	⋯	0.9	0.0	⋯	7.0	97.7	⋯	2.6	2.3	⋯
J05331130-2914199	3.9	0.4	⋯	0.0	0.0	⋯	0.1	0.0	⋯	96.0^b	99.9^b	⋯	0.0	0.0	⋯	0.0	0.0	⋯	0.0	0.0	⋯	0.9	0.1	⋯
J05332558-5117131	0.0	0.0	⋯	0.0	0.0	⋯	97.2	99.9	⋯	1.3	0.1	⋯	0.0	0.0	⋯	0.0	0.0	⋯	0.7	0.0	⋯	0.0	0.0	⋯
J05335981-0221325	99.9	99.9	⋯	0.0	0.0	⋯	0.0	0.0	⋯	0.0	0.0	⋯	0.0	0.0	⋯	0.0	0.0	⋯	0.0	0.0	⋯	0.1	0.0	⋯
J05392505-4245211	0.0	0.0	⋯	0.0	0.0	⋯	22.4	26.2	⋯	77.3	73.7	⋯	0.0	0.0	⋯	0.0	0.0	⋯	0.2	0.0	⋯	0.0	0.0	⋯
J05395494-1307598	3.5	0.6	⋯	0.0	0.0	⋯	0.1	0.0	⋯	96.4^b	99.4^b	⋯	0.0	0.0	⋯	0.0	0.0	⋯	0.0	0.0	⋯	0.0	0.0	⋯
J05425587-0718382	2.0	0.8	⋯	0.0	0.0	⋯	0.0	0.0	⋯	97.7^b	98.6^b	⋯	0.0	0.0	⋯	0.1	0.4	⋯	0.0	0.0	⋯	0.2	0.2	⋯
J05432676-3025129	0.0	0.0	⋯	0.0	0.0	⋯	0.0	0.0	⋯	99.9	99.5	⋯	0.0	0.0	⋯	0.0	0.0	⋯	0.0	0.0	⋯	0.2	0.5	⋯
J05470650-3210413	0.7	3.3	⋯	0.0	0.0	⋯	0.0	0.1	⋯	99.3^b	96.6^b	⋯	0.0	0.0	⋯	0.0	0.0	⋯	0.0	0.0	⋯	0.0	0.0	⋯

Table 3.X — continued

Name	βPMG P	βPMG P_ν	βPMG $P_{\nu+\pi}$	TWA P	TWA P_ν	TWA $P_{\nu+\pi}$	THA P	THA P_ν	THA $P_{\nu+\pi}$	COL P	COL P_ν	COL $P_{\nu+\pi}$	CAR P	CAR P_ν	CAR $P_{\nu+\pi}$	ARG P	ARG P_ν	ARG $P_{\nu+\pi}$	ABDMG P	ABDMG P_ν	ABDMG $P_{\nu+\pi}$	Field P	Field P_ν	Field $P_{\nu+\pi}$
J05531299-4505119	0.0	0.0	...	0.0	0.0	...	0.1	0.0	...	0.0	0.0	...	0.0	0.0	...	0.0	0.0	...	98.7	99.9	...	1.2	0.1	...
J06002304-4401217	0.0	0.0	...	0.0	0.0	...	0.5	0.5	...	99.1	99.4	...	0.0	0.0	...	0.0	0.0	...	0.3	0.0	...	0.1	0.0	...
J06112997-7213388	0.0	0.0	...	0.0	0.0	...	0.8	0.6	...	0.2	0.3	...	98.7[b]	99.1[b]	...	0.0	0.0	...	0.3	0.0	...	0.0	0.0	...
J06131330-2742054	99.9[b]	99.9[b]	99.9[b]	0.0	0.0	0.0	0.0	0.0	0.0	0.0	0.0	0.0	0.0	0.0	0.0	0.0	99.9[b]	0.0	0.0	0.0	0.0	0.0	0.0	0.0
J06134539-2352077	0.1	0.1	...	0.0	0.0	...	0.5	0.0	...	0.3	0.1	...	98.9[b]	99.9[b]	...	0.0	0.0	...	0.2	0.0	...	0.0	0.0	...
J06234024-7504327	0.0	0.0	...	0.0	0.0	...	0.0	0.0	...	5.0[b]	43.3[b]	...	93.3[b]	56.6[b]	...	0.0	0.0	...	1.6	0.0	...	0.1	0.0	...
J06434532-6424396	0.1	0.1	...	0.0	0.0	...	0.0	0.0	...	99.4	99.9	...	0.1	0.0	...	0.0	0.0	...	0.3	0.0	...	0.1	0.0	...
J07065772-5353463	0.1	0.0	...	0.0	0.0	...	0.0	0.0	...	0.2	0.1	...	99.4	99.9	...	0.0	0.0	...	0.0	0.0	...	0.1	0.0	...
J07523324-6436308	0.0	0.0	...	0.0	0.0	...	0.0	0.0	...	0.0	0.0	...	99.9[b]	99.9[b]	...	0.0	0.0	...	0.0	0.0	...	0.4	0.0	...
J07540718-6320149	0.0	0.0	...	0.0	0.0	...	0.0	0.0	...	75.9[b]	96.4[b]	...	0.0	0.0	...	0.0	0.0	...	0.0	0.0	...	0.0	0.0	...
J08083927-3605017	99.9[b]	99.9[b]	...	0.0	0.0	...	0.0	0.0	...	0.0	0.0	...	0.0	0.0	...	0.1	0.0	...	0.2	0.0	...	24.1	3.6	...
J08173943-8243298	99.9[b]	99.9[b]	...	0.0	0.0	...	0.0	0.0	...	0.0	0.0	...	0.0	0.0	...	0.0	0.0	...	79.3	0.0	...	0.0	0.0	...
J08224744-5726530	17.9	91.9	...	0.0	0.0	...	0.0	0.0	...	0.0	0.0	...	0.0	0.0	...	0.0	0.0	...	0.0	0.0	...	2.8	8.1	...
J08412528-5736021	0.1	0.0	...	0.0	0.0	...	0.0	0.0	...	61.3[b]	65.6[b]	...	37.6[b]	34.3[b]	...	0.0	0.0	...	93.6[b]	99.9[b]	...	1.0	0.1	...
J08471906-5717547	6.4	0.0	...	0.0	0.0	...	0.0	0.0	...	0.0	0.0	...	0.0	0.0	...	0.0	0.0	...	0.0	0.0	...	0.6	0.0	...
J09032434-6348330	0.1	0.0	...	0.0	0.0	...	0.0	0.0	...	18.0	6.5	...	76.0	93.4	...	5.2[b]	0.0	...	0.0	0.0	...	3.1	0.7	...
J09315840-6209258	24.8	2.1	...	0.0	0.0	...	0.0	0.0	...	19.5[b]	48.6[b]	...	51.2[b]	48.6[b]	...	0.5	0.0	...	0.9	0.0	...	3.0	2.0	...
J09331427-4848331	0.0	0.0	...	0.0	0.0	...	0.0	0.0	...	22.2	98.0	...	0.0	0.0	...	74.7[b]	0.0	...	0.0	0.0	...	0.0	0.0	...
J09423823-6229028	0.4	1.0	...	0.0	0.0	...	0.0	0.0	...	1.2	0.0	...	0.0	0.0	...	98.4	98.9	...	0.0	0.0	...	0.0	0.0	...
J09445422-1220544	0.0	0.0	0.0	99.9[b]	99.9[b]	99.9[b]	0.0	0.0	0.0	0.0	0.0	0.0	0.0	0.0	0.0	99.9[b]	99.9[b]	0.0	0.0	0.0	0.0	0.0	0.0	0.0
J10120908-3124451	0.0	0.0	...	0.0	0.0	...	0.0	0.0	...	0.1	0.0	...	99.9[b]	99.9[b]	...	99.9[b]	0.0	...	0.0	0.0	...	0.0	0.0	...
J10140807-7636327	0.1	0.1	...	99.9	99.9	...	0.0	0.0	...	0.0	0.0	...	0.0	0.0	...	0.0	0.0	...	0.0	0.0	...	0.2	0.5	...
J10182870-3150029	0.0	0.0	...	90.0	98.3	...	0.0	0.0	...	6.1	16.6	...	0.0	0.0	...	0.0	0.0	...	0.0	0.0	...	4.0	1.0	...
J10252092-4241539	0.0	0.0	...	0.0	82.4	...	0.0	0.0	...	0.0	0.0	...	0.0	0.0	...	99.9	99.4	...	0.0	0.0	...	0.1	0.6	...
J10252563-4918389	6.0[b]	24.0[b]	...	91.5[b]	76.0[b]	...	0.0	0.0	...	2.4[b]	0.0	...	0.0	0.0	...	45.3[b]	0.1	...	0.0	0.0	...	0.1	0.0	...
J10423011-3340162	9.3	18.1	...	0.0	0.0	...	0.0	0.0	...	0.1	0.3	...	43.1[b]	80.7[b]	...	0.0	0.0	...	0.3	0.0	...	1.9	0.9	...
J11091606-7352465	0.0	0.0	0.0	99.9[b]	99.9[b]	99.9	0.0	0.0	0.0	0.0	0.0	0.1	0.0	0.0	0.0	0.0	0.0	0.0	0.0	0.0	0.0	0.0	0.0	0.0
J11102788-3731520	0.0	0.0	0.0	99.9	99.9	99.9	0.0	0.0	0.0	0.0	0.0	0.0	0.0	0.0	0.0	0.0	0.0	0.0	0.2	0.0	0.0	0.2	0.0	0.0
J11132622-4523427	0.0	0.0	0.0	99.9	99.9	99.9	0.0	0.0	0.0	0.0	0.0	0.0	0.0	0.0	0.0	0.0	0.0	0.0	0.0	0.0	0.0	0.0	0.0	0.0
J11211723-3446454	0.0	0.0	0.0	99.9	99.9	99.9[b]	0.0	0.0	0.0	0.0	0.0	0.0	0.0	0.0	0.0	0.0	0.0	0.0	0.0	0.0	0.0	0.0	0.0	0.0
J11217745-3446497	0.0	0.0	0.0	17.4	0.0	...	0.0	0.0	0.0	0.0	0.0	0.0	0.0	0.0	0.0	0.0	0.0	0.0	0.0	0.0	0.0	0.0	0.0	0.0
J11254754-4410267	0.7	0.0	...	99.9[b]	99.9[b]	99.9[b]	0.0	0.0	0.0	0.0	0.0	0.0	0.0	0.0	0.0	0.0	0.0	0.0	79.7[b]	99.9[b]	...	2.2	0.3	...
J11315526-3436272	0.0	0.0	0.0	99.9	99.9	...	0.0	0.0	0.0	0.0	0.0	0.0	0.0	0.0	0.0	0.0	0.0	0.0	0.0	0.0	0.0	0.0	0.0	0.0
J11321831-3019518	0.0	0.0	...	0.0	0.0	...	0.0	0.0	...	0.0	0.0	...	0.0	0.0	...	0.0	0.0	...	0.0	0.0	...	0.0	0.0	...
J11493184-7851011	75.2	91.7	...	99.9[b]	99.9[b]	99.9[b]	0.0	0.0	0.0	0.0	0.0	0.0	0.0	0.0	0.0	0.0	0.0	0.0	0.1	0.0	0.0	24.7	8.3	...
J12072738-3247002	0.0	0.0	0.0	0.0	0.0	...	0.0	0.0	0.0	0.0	0.0	0.0	0.0	0.0	0.0	0.0	0.0	0.0	0.0	0.0	0.0	0.0	0.0	0.0
J12092998-7505400	0.9	0.0	...	99.9[b]	99.9[b]	99.9[b]	0.0	0.0	0.0	0.0	0.0	0.0	2.9[b]	0.0	0.0	95.9[b]	99.9[b]	0.0	0.0	0.0	0.0	0.2	0.0	...
J12153072-3948426	0.0	0.0	0.0	0.0	0.0	...	0.0	0.0	0.0	0.0	0.0	0.0	0.0	0.0	0.0	0.0	0.0	0.0	0.0	0.0	0.0	0.0	0.0	0.0
J12170465-5743558	0.1	0.0	0.0	99.9	0.0	...	0.0	0.0	...	1.5	0.0	...	0.0	0.0	...	86.5	98.0	0.0	0.0	0.0	...	11.8	2.0	...
J12313807-4558593	0.0	0.0	0.0	99.9	99.9	99.9[b]	0.0	0.0	0.0	0.0	0.0	0.0	0.0	0.0	0.0	0.0	0.0	0.0	0.0	0.0	0.0	0.0	0.0	0.0

Table 3.X — continued

Name	βPMG			TWA			THA			COL			CAR			ARG			ABDMG			Field		
	P	P_ν	$P_{\nu+\pi}$	P	P_ν	$P_{\nu+\pi}$	P	P_ν	$P_{\nu+\pi}$	P	P_ν	$P_{\nu+\pi}$	P	P_ν	$P_{\nu+\pi}$	P	P_ν	$P_{\nu+\pi}$	P	P_ν	$P_{\nu+\pi}$	P	P_ν	$P_{\nu+\pi}$
J12345629-4538075	0.0	0.0	…	99.9	99.9	…	0.0	0.0	…	0.0	0.0	…	0.0	0.0	…	0.0	0.0	…	0.0	0.0	…	0.3	0.0	…
J12350424-4136385	0.0	0.0	…	99.9	99.9	…	0.0	0.0	…	0.0	0.0	…	0.0	0.0	…	0.0	0.0	…	0.0	0.0	…	0.0	0.0	…
J12383713-2703348	0.0	0.0	…	0.0	0.0	…	0.0	0.0	…	0.0	0.0	…	0.0	0.0	…	0.0	0.0	…	99.2	99.9	…	0.8	0.1	…
J13412668-4341522	7.1	8.8	…	71.6	87.5	…	0.0	0.0	…	2.4^b	1.1	…	0.0	0.0	…	6.2	0.0	…	0.0	0.0	…	12.7	2.5	…
J13545390-7121476	8.5	99.1	…	0.0	0.0	…	0.0	0.0	…	0.0	0.0	…	0.0	0.0	…	0.0	0.0	…	90.9	0.0	…	0.5	0.9	…
J14252913-4113323	21.7^b	47.9^b	89.2^b	44.7^b	42.7^b	10.8^b	0.0	0.0	0.0	0.0	0.0	0.0	0.0	0.0	0.0	0.0	0.0	0.0	0.0	0.0	0.0	33.5	9.4	0.0
J15244849-4929473	3.7	0.0	…	0.0	0.0	…	0.0	0.0	…	0.0	0.0	…	0.0	0.0	…	0.0	0.0	…	95.9^b	99.9^b	…	0.4	0.2	…
J15553178-3512028	0.0	0.0	…	0.0	0.0	…	0.0	0.0	…	0.0	0.0	…	0.0	0.0	…	99.9	99.9	…	0.0	0.0	…	0.2	0.1	…
J16074132-1103073	0.4	0.2	…	0.0	0.0	…	0.0	0.0	…	0.0	0.0	…	0.0	0.0	…	0.0	0.0	…	98.3^b	97.5^b	…	1.4	2.3	…
J16572029-5343316	91.1	99.9	…	0.0	0.0	…	0.0	0.0	…	0.0	0.0	…	1.6	6.3^b	…	8.8^b	0.0	…	0.1	0.0	…	0.1	0.0	…
J17080882-6936186	0.0	0.0	…	0.0	0.0	…	88.7^b	98.0^b	…	0.0	0.0	…	0.0	0.0	…	0.0	0.0	…	0.0	0.0	…	11.3	2.0	…
J17130733-8552105	0.0	0.0	…	0.0	0.0	…	97.0^b	92.2^b	…	0.0	0.0	…	0.0	0.0	…	0.0	0.0	…	0.0	0.0	…	1.3	1.4	…
J17150219-3333398	94.6	99.0	…	0.0	0.0	…	0.0	0.0	…	0.0	0.0	…	0.0	0.0	…	0.0	0.0	…	3.6^b	0.2	…	1.8	0.7	…
J17292067-5014529	99.3^b	99.9^b	…	0.0	0.0	…	0.0	0.0	…	0.0	0.0	…	0.0	0.0	…	0.7	33.5^b	…	0.0	0.0	…	0.0	0.0	…
J18141047-3247344	58.0^b	66.4^b	…	0.0	0.0	…	0.0	0.0	…	0.0	0.0	…	0.0	0.0	…	41.9^b	0.0	…	0.0	0.0	…	0.1	0.0	…
J18142207-3246100	80.6^b	99.9^b	…	0.0	0.0	…	0.0	0.0	…	0.0	0.0	…	0.0	0.0	…	18.9	0.0	…	0.0	0.0	…	0.4	0.3	…
J18151564-4927472	89.4^b	99.9^b	…	0.0	0.0	…	0.0	0.0	…	0.0	0.0	…	0.0	0.0	…	10.6^b	0.0	…	0.0	0.0	…	0.0	0.0	…
J18202275-1011131	1.0	96.4^b	…	0.0	0.0	…	0.0	0.0	…	0.0	0.0	…	0.0	0.0	…	98.8	0.0	…	0.0	0.0	…	0.2	3.6	…
J18420694-5554254	73.1	99.9	…	0.0	0.0	…	0.0	0.0	…	0.0	0.0	…	0.0	0.0	…	26.8^b	0.0	…	0.0	0.0	…	0.0	0.0	…
J18450097-1409053	11.8^b	0.0	…	0.0	0.0	…	0.0	0.0	…	0.0	0.0	…	0.0	0.0	…	88.2^b	99.9^b	…	0.0	0.0	…	0.0	0.0	…
J18465255-6210366	54.1	99.9	…	0.0	0.0	…	0.0	0.0	…	0.0	0.0	…	0.0	0.0	…	45.9^b	0.0	…	0.0	0.0	…	0.0	0.0	…
J18504448-3147472	91.3	99.9	…	0.0	0.0	…	0.0	0.0	…	0.0	0.0	…	0.0	0.0	…	8.7	0.0	…	0.0	0.0	…	0.2	0.2	…
J18580415-2953045	97.9^b	99.9^b	…	0.0	0.0	…	0.0	0.0	…	0.0	0.0	…	0.0	0.0	…	2.0	0.0	…	0.0	0.0	…	0.0	0.0	…
J19102820-2319486	99.9^b	99.9^b	…	0.0	0.0	…	0.0	0.0	…	0.0	0.0	…	0.0	0.0	…	0.4	0.0	…	0.0	0.0	…	0.7	0.2	…
J19224278-0515536	0.3	0.0	…	0.0	0.0	…	0.0	0.0	…	0.0	0.0	…	0.0	0.0	…	99.0^b	99.9^b	…	0.0	0.0	…	0.0	0.1	…
J19225071-6310581	0.0	0.0	…	0.0	0.0	…	99.9^b	99.9^b	…	0.0	0.0	…	0.0	0.0	…	0.0	0.0	…	0.0	0.0	…	1.0	0.7	…
J19233820-4606316	97.8	99.3	…	0.0	0.0	…	0.0	0.0	…	0.0	0.0	…	0.0	0.0	…	1.2	0.0	…	0.0	0.0	…	0.0	0.0	…
J19243494-3442392	99.9^b	99.9^b	…	0.0	0.0	…	0.0	0.0	…	0.0	0.0	…	0.0	0.0	…	0.1	0.0	…	0.0	0.0	…	1.5	0.5	…
J19312434-2134226	98.6	0.0	0.0	0.0	0.0	0.0	0.0	0.0	0.0	0.0	0.0	0.0	0.0	0.0	0.0	1.3	96.8	99.0	0.0	0.0	0.0	0.1	3.2	1.0
J19560294-3207186	98.5^b	99.5^b	…	0.0	0.0	…	0.0	0.0	…	0.0	0.0	…	0.0	0.0	…	0.0	0.0	…	0.0	0.0	…	0.0	0.0	…
J19560438-3207376	99.9^b	99.9^b	99.9^b	0.0	0.0	0.0	0.0	0.0	0.0	0.0	0.0	0.0	0.0	0.0	0.0	0.0	0.0	0.0	0.0	0.0	0.0	1.9	1.0	0.0
J20013718-3313139	98.1	98.9	…	0.0	0.0	…	0.0	0.0	…	0.0	0.0	…	0.0	0.0	…	0.0	0.0	…	0.0	0.1	…	0.0	0.0	…
J20010002-2801410	99.9^b	99.9^b	99.9^b	0.0	0.0	0.0	0.0	0.0	0.0	0.0	0.0	0.0	0.0	0.0	0.0	0.0	0.0	0.0	0.0	0.0	0.0	2.6	0.4	0.0
J20163382-0711456	1.4	0.0	…	0.0	0.0	…	0.0	0.0	…	0.0	0.0	…	0.0	0.0	…	96.0	99.9	…	0.0	0.0	…	0.2	0.0	…
J20333759-2556521	99.9^b	99.9^b	99.9^b	0.0	0.0	0.0	0.0	0.0	0.0	0.1	0.2	0.0	0.0	0.0	0.0	0.0	0.0	0.0	0.0	0.0	0.0	10.1	1.7	0.0
J20395460+0620118	9.9	0.6	…	0.0	0.0	…	0.0	0.0	…	0.0	0.0	…	0.0	0.0	…	0.0	0.0	…	80.0	97.5	…	0.0	0.0	…
J20434114-2433534	99.9^b	99.9^b	99.9^b	0.0	0.0	0.0	0.0	0.0	0.0	0.0	0.0	0.0	0.0	0.0	0.0	0.0	0.0	0.0	0.0	0.0	0.0	0.7	0.1	0.0
J20465795-0259320	0.0	0.0	…	0.0	0.0	…	0.0	0.0	…	0.0	0.0	…	0.0	0.0	…	0.0	0.0	…	99.3	99.9	…	0.0	0.1	…
J20560274-1710538	99.9^b	99.9^b	…	0.0	0.0	…	0.0	0.0	…	0.0	0.0	…	0.0	0.0	…	0.0	0.0	…	0.0	0.0	…	0.0	0.0	…
J21100535-1919573	99.9^b	99.9^b	…	0.0	0.0	…	0.0	0.0	…	0.0	0.0	…	0.0	0.0	…	0.0	0.0	…	0.0	0.0	…	0.0	0.0	…

Table 3.X — continued

Name	βPMG P	βPMG P_ν	βPMG $P_{\nu+\pi}$	TWA P	TWA P_ν	TWA $P_{\nu+\pi}$	THA P	THA P_ν	THA $P_{\nu+\pi}$	COL P	COL P_ν	COL $P_{\nu+\pi}$	CAR P	CAR P_ν	CAR $P_{\nu+\pi}$	ARG P	ARG P_ν	ARG $P_{\nu+\pi}$	ABDMG P	ABDMG P_ν	ABDMG $P_{\nu+\pi}$	Field P	Field P_ν	Field $P_{\nu+\pi}$
J21103147-2710578	99.9[b]	99.9[b]	…	0.0	0.0	…	0.0	0.0	…	0.0	0.0	…	0.0	0.0	…	0.0	0.0	…	0.0	0.0	…	0.0	0.0	…
J21130526-1729126	0.0	0.0	…	0.0	0.0	…	0.0	0.0	…	0.0	0.0	…	0.0	0.0	…	0.0	0.0	…	99.9	99.9	…	0.3	0.0	…
J21212873-6655063	54.7	99.9	99.9	0.0	0.0	0.0	0.0	0.0	0.0	0.0	0.0	0.0	0.0	0.0	0.0	30.5	0.0	0.0	14.6[b]	0.0	0.0	0.3	0.1	0.1
J21370885-6036054	0.0	0.0	…	0.0	0.0	…	99.9[b]	99.9[b]	…	0.0	0.0	…	0.0	0.0	…	0.0	0.0	…	0.0	0.0	…	0.0	0.0	…
J21464282-8543046	10.1	0.0	…	0.0	0.0	…	0.0	0.0	…	2.9	0.0	…	0.0	0.0	…	31.3[b]	0.0	…	55.6[b]	99.9[b]	…	0.0	0.0	…
J21471964-4803166	0.2	0.5	…	0.0	0.0	…	98.4[b]	0.5	…	0.0	0.0	…	0.0	0.0	…	0.0	0.0	…	1.4	98.2[b]	…	0.1	0.8	…
J21490499-6413039	0.0	0.0	…	0.0	0.0	…	99.9[b]	99.9[b]	…	0.0	0.0	…	0.0	0.0	…	0.0	0.0	…	0.0	0.0	…	0.0	0.0	…
J22021626-4210329	0.0	0.0	…	0.0	0.0	…	98.9	99.9	…	0.0	0.0	…	0.0	0.0	…	0.0	0.0	…	0.9	0.0	…	0.1	0.0	…
J22332264-0936537	0.0	0.0	…	0.0	0.0	…	0.0	0.0	…	0.0	0.0	…	0.0	0.0	…	99.9[b]	94.1[b]	…	0.0	0.0	…	0.4	5.9	…
J22424884+1330532	46.8	0.4	…	0.0	0.0	…	0.0	0.0	…	37.6	94.4	…	0.0	0.0	…	0.0	0.0	…	0.0	0.0	…	15.7	5.2	…
J22424896-7142211	93.1	99.9	…	0.0	0.0	…	0.0	0.0	…	0.0	0.0	…	0.0	0.0	…	4.5[b]	0.0	…	2.3[b]	0.0	…	0.1	0.0	…
J22440873-5413183	2.0	0.3	…	0.0	0.0	…	95.7[b]	99.9	…	0.0	0.0	…	0.0	0.0	…	0.0	0.0	…	2.2[b]	0.0	…	0.1	0.0	…
J23131671-4933154	0.0	0.0	…	0.0	0.0	…	99.9[b]	99.9[b]	…	0.0	0.0	…	0.0	0.0	…	0.0	0.0	…	0.0	0.0	…	0.0	0.0	…
J23204705-6723209	0.0	0.0	…	0.0	0.0	…	99.9	99.9	…	0.0	0.0	…	0.0	0.0	…	0.0	0.0	…	0.1	0.0	…	0.1	0.0	…
J23205766-0147373	0.0	0.0	0.0	0.0	0.0	0.0	0.0	0.0	0.0	0.0	0.0	0.0	0.0	0.0	0.0	95.1[b]	97.7[b]	99.9[b]	0.0	0.0	0.0	4.9	2.3	0.1
J23261069-7323498	0.0	0.0	…	0.0	0.0	…	99.9	99.9[b]	…	0.0	0.0	…	0.0	0.0	…	0.0	0.0	…	0.0	0.0	…	0.0	0.0	…
J23285763-6802338	0.0	0.0	…	0.0	0.0	…	99.9	99.9[b]	…	0.0	0.0	…	0.0	0.0	…	0.0	0.0	…	0.0	0.0	…	0.0	0.0	…
J23301341-2023271	99.9[b]	6.7[b]	0.4	0.0	0.0	0.0	0.0	0.1	0.0	0.1	91.3[b]	99.9[b]	0.0	0.0	0.0	0.0	0.0	0.0	0.0	0.0	0.0	0.0	1.9	0.0
J23314492-0244395	87.3[b]	43.1[b]	…	0.0	0.0	…	1.1	0.0	…	11.4[b]	56.3[b]	…	0.0	0.0	…	0.0	0.0	…	0.0	0.0	…	0.2	0.5	…
J23320018-3917368	0.0	0.0	…	0.0	0.0	…	0.1	0.0	…	0.0	0.0	…	0.0	0.0	…	0.0	0.0	…	99.9	99.9	…	0.1	0.0	…
J23323085-1215513	93.7	99.9	…	0.0	0.0	…	0.4	0.0	…	5.8	0.0	…	0.1	0.0	…	0.0	0.0	…	0.0	0.0	…	0.1	0.0	…
J23474694-6517249	0.0	0.0	…	0.0	0.0	…	99.9[b]	99.9[b]	…	0.0	0.0	…	0.0	0.0	…	0.0	0.0	…	0.0	0.0	…	0.0	0.0	…
J23500639+2659519	82.4	96.8	…	0.0	0.0	…	99.9	99.9	…	13.4[b]	0.1	…	0.0	0.0	…	0.0	0.0	…	0.0	0.0	…	4.3	3.1	…
J23512227+2344207	81.6	97.8	…	0.0	0.0	…	0.0	0.0	…	13.8	0.0	…	0.0	0.0	…	0.0	0.0	…	0.0	0.0	…	4.6	2.2	…
J23513366-3127229	0.4	0.0	…	0.0	0.0	…	0.0	0.0	…	0.0	0.0	…	0.0	0.0	…	96.4[b]	99.9[b]	…	99.4[b]	99.9[b]	…	0.3	0.0	…
J23532520-7056410	1.6	0.0	…	0.0	0.0	…	0.0	0.0	…	0.0	0.0	…	0.0	0.0	…	0.0	0.0	…	0.0	0.0	…	2.0	0.4	…

[a] Membership probability (P), membership probability including radial velocity information (P_ν), or membership probability including radial velocity and parallax informations ($P_{\nu+\pi}$).

[b] Membership probability (P or P_ν or $P_{\nu+\pi}$) for which the binary hypothesis has a higher probability.

Table 3.XI.   Individual radial and projected rotational velocity measurements

Name of star	Date (DDMMYY)	Instrument	RV (kms^{-1})	vsini (kms^{-1})
J00240899-6211042	081109	*PHOENIX*	5.8 ± 0.7	20.7 ± 2.0
J00172353-6645124	260809	*PHOENIX*	10.8 ± 0.2	6.3 ± 1.8
J00172353-6645124	240910	*PHOENIX*	10.0 ± 0.5	< 8.7
J00171443-7032021	010909	*PHOENIX*	-4.5 ± 0.4	10.1 ± 3.5
J00171443-7032021	170910	*PHOENIX*	-2.5 ± 0.6	12.2 ± 2.6
J00233468+2014282ab	290513	*ESPADONS*	-1.6 ± 0.2	< 4.6
J00233468+2014282ab	310513	*ESPADONS*	-1.7 ± 0.2	< 4.2
J00275023-3233060a	210713	*CRIRES*	8.8 ± 0.2	6.2 ± 1.8
J00275035-3233238b	210713	*CRIRES*	8.5 ± 0.2	< 4.2
J00281434-3227556A	260809	*PHOENIX*	5.9 ± 3.4	53.6 ± 6.6
J00281434-3227556B	260809	*PHOENIX*	3.5 ± 3.3	62.4 ± 9.5
J00340843+2523498aw	300613	*ESPADONS*	-8.8 ± 0.2	11.1 ± 1.2
J01033563-5515561	210713	*CRIRES*	4.0 ± 2.0	35.2 ± 7.0
J01071194-1935359	240910	*PHOENIX*	9.7 ± 0.5	10.8 ± 2.2
J01112542+1526214	150611	*CRIRES*	2.9 ± 0.6	18.4 ± 2.5
J01112542+1526214	020711	*ESPADONS*	1.8 ± 0.2	17.9 ± 1.4
J01123504+1703557	191110	*PHOENIX*	0.4 ± 1.1	25.4 ± 2.3
J01123504+1703557	120711	*CRIRES*	-1.4 ± 0.7	23.1 ± 2.1
J01123504+1703557	060112	*ESPADONS*	-1.6 ± 0.3	22.5 ± 2.2
J01123504+1703557	210713	*CRIRES*	-1.7 ± 0.6	24.1 ± 2.2
J01132958-0738088	181110	*PHOENIX*	106.0 ± 3.3	63.4 ± 9.3
J01132958-0738088	140611	*CRIRES*	41.3 ± 4.1	68.5 ± 8.4
J01132817-3821024B	010909	*PHOENIX*	14.3 ± 0.5	< 9.1
J01225093-2439505	240910	*PHOENIX*	11.4 ± 0.2	14.2 ± 3.2
J01220441-3337036	210811	*ESPADONS*	5.0 ± 0.2	5.0 ± 1.2
J01220441-3337036	230910	*PHOENIX*	5.1 ± 0.3	< 6.1
J01220441-3337036	240910	*PHOENIX*	4.4 ± 0.3	< 6.1
J01220441-3337036	010613	*CRIRES*	3.9 ± 0.5	< 8.3
J01220441-3337036	270510	*PHOENIX*	4.4 ± 0.3	< 6.1
J01351393-0712517	190910	*PHOENIX*	11.8 ± 3.5	50.7 ± 5.9
J01351393-0712517	260710	*PHOENIX*	12.7 ± 3.2	58.6 ± 7.4
J01351393-0712517	210811	*ESPADONS*	6.3 ± 0.5	49.6 ± 3.7
J01351393-0712517	070910	*PHOENIX*	12.4 ± 3.2	50.7 ± 4.9
J01484087-4830519	150909	*PHOENIX*	21.5 ± 0.2	< 4.4
J01484087-4830519	121009	*PHOENIX*	21.6 ± 0.2	< 3.5
J01484087-4830519	170910	*PHOENIX*	21.5 ± 0.2	< 4.4
J01484087-4830519	250910	*PHOENIX*	21.6 ± 0.2	< 4.4
J01535076-1459503A	051209	*PHOENIX*	10.8 ± 0.6	12.2 ± 2.3
J01535076-1459503B	051209	*PHOENIX*	11.2 ± 0.5	< 9.1
J01535076-1459503as	210811	*ESPADONS*	10.3 ± 0.3	11.5 ± 1.1
J01540267-4040440	260809	*PHOENIX*	12.7 ± 0.2	8.9 ± 3.3
J02001277-0840516	120711	*CRIRES*	5.2 ± 0.2	16.1 ± 2.1
J02001277-0840516	130212	*ESPADONS*	4.4 ± 0.2	15.2 ± 1.4
J02045317-5346162	170910	*PHOENIX*	10.9 ± 0.3	7.4 ± 2.3
J02045317-5346162	010909	*PHOENIX*	10.9 ± 0.3	6.5 ± 2.1
J02070786-1810077	201011	*CRIRES*	19.1 ± 3.7	47.2 ± 13.1
J02070176-4406380	250910	*PHOENIX*	-5.2 ± 0.2	5.3 ± 1.7
J02070176-4406380	250810	*PHOENIX*	10.1 ± 0.3	< 4.7
J02070176-4406380	151011	*CRIRES*	-13.6 ± 0.3	< 4.1
J02133021-4654505	260809	*PHOENIX*	14.3 ± 2.0	33.0 ± 2.8
J02155892-0929121	260710	*PHOENIX*	0.5 ± 0.3	18.1 ± 2.3
J02155892-0929121	190910	*PHOENIX*	-0.6 ± 0.3	19.1 ± 2.4
J02155892-0929121	110212	*ESPADONS*	8.3 ± 0.3	16.7 ± 1.5
J02224418-6022476	260710	*PHOENIX*	13.1 ± 0.9	25.1 ± 2.9
J02335984-1811525	280813	*ESPADONS*	12.4 ± 0.3	16.4 ± 1.5
J02365171-5203036	110613	*CRIRES*	16.3 ± 2.3	39.8 ± 5.4
J02365171-5203036	230910	*PHOENIX*	16.8 ± 2.3	36.9 ± 3.0
J02365171-5203036	240613	*CRIRES*	12.0 ± 1.9	39.0 ± 3.5
J02485260-3404246	081109	*PHOENIX*	23.4 ± 0.3	6.5 ± 2.1
J02485260-3404246	151011	*CRIRES*	23.0 ± 0.4	7.2 ± 3.2
J02485260-3404246	170910	*PHOENIX*	0.4 ± 0.3	7.4 ± 2.3
J02505959-3409050	121009	*PHOENIX*	12.0 ± 3.5	52.6 ± 5.8
J02523096-1548357	081109	*PHOENIX*	46.5 ± 0.6	9.6 ± 2.4
J02543316-5108313	010909	*PHOENIX*	1.8 ± 0.2	< 4.4
J02564708-6343027	151011	*CRIRES*	16.2 ± 3.4	48.2 ± 7.2
J02564708-6343027	010909	*PHOENIX*	20.7 ± 3.4	56.5 ± 8.8
J03050976-3725058	170910	*PHOENIX*	15.2 ± 0.6	16.2 ± 2.3
J03050976-3725058	010909	*PHOENIX*	13.4 ± 0.6	14.5 ± 2.2

Table 3.XI — continued

Name of star	Date (DDMMYY)	Instrument	RV (kms^{-1})	vsini (kms^{-1})
J03244056-3904227	130210	PHOENIX	14.6 ± 3.2	70.4 ± 11.2
J03244056-3904227	151011	CRIRES	10.5 ± 4.0	59.0 ± 8.0
J03323578+2843554	210811	ESPADONS	9.2 ± 0.3	21.9 ± 2.0
J03323578+2843554	171110	PHOENIX	13.9 ± 1.5	28.2 ± 2.4
J03454058-7509121	130210	PHOENIX	13.1 ± 3.2	43.6 ± 6.0
J03494535-6730350	170910	PHOENIX	16.3 ± 0.2	8.9 ± 3.2
J03494535-6730350	140210	PHOENIX	17.3 ± 0.2	< 8.3
J04071148-2918342	201009	PHOENIX	20.7 ± 0.7	20.7 ± 1.8
J04071148-2918342	280813	ESPADONS	21.2 ± 0.3	19.6 ± 1.8
J04082685-7844471	281209	PHOENIX	16.4 ± 0.4	13.3 ± 2.2
J04082685-7844471	151011	CRIRES	16.5 ± 0.6	11.6 ± 3.5
J04091413-4008019	131011	CRIRES	21.2 ± 0.4	10.8 ± 3.2
J04091413-4008019	261209	PHOENIX	21.4 ± 0.6	10.8 ± 2.5
J04213904-7233562	261209	PHOENIX	15.2 ± 0.2	5.3 ± 1.7
J04213904-7233562	131011	CRIRES	14.7 ± 0.3	< 3.3
J04240094-5512223	140210	PHOENIX	20.1 ± 0.5	10.2 ± 2.3
J04365738-1613065	150210	PHOENIX	22.1 ± 3.7	54.5 ± 9.4
J04365738-1613065	280813	ESPADONS	15.6 ± 0.5	50.7 ± 4.8
J04363294-7851021	281209	PHOENIX	26.5 ± 0.3	16.2 ± 3.0
J04374183-0527242	141109	PHOENIX	23.2 ± 1.0	21.6 ± 2.3
J04440099-6624036	190910	PHOENIX	16.4 ± 0.5	< 8.7
J04440099-6624036	151011	CRIRES	16.8 ± 0.3	< 2.7
J04464970-6034109	131109	PHOENIX	15.5 ± 3.5	55.5 ± 7.9
J04480066-5041255A	261209	PHOENIX	19.2 ± 0.3	< 5.9
J04554034-1917553	310110	PHOENIX	22.2 ± 3.7	77.3 ± 8.6
J04571728-0621564	310110	PHOENIX	23.0 ± 0.5	12.2 ± 2.6
J04571728-0621564	020313	ESPADONS	23.5 ± 0.3	11.1 ± 1.0
J04571728-0621564	051111	CRIRES	23.0 ± 0.6	12.2 ± 3.4
J05082729-2101444	210412	CRIRES	22.2 ± 1.4	25.3 ± 4.1
J05082729-2101444	200711	CRIRES	25.4 ± 1.7	25.3 ± 4.7
J05090356-4209199	021209	PHOENIX	16.8 ± 1.7	29.2 ± 2.7
J05100427-2340407	190711	CRIRES	23.8 ± 0.6	< 9.1
J05100427-2340407	110212	ESPADONS	24.2 ± 0.2	8.2 ± 0.9
J05100427-2340407a	121009	PHOENIX	24.7 ± 0.5	< 9.1
J05100488-2340148bA	021209	PHOENIX	23.8 ± 0.5	9.6 ± 2.3
J05100488-2340148bA	051209	PHOENIX	23.1 ± 0.2	9.2 ± 2.3
J05100488-2340148bB	051209	PHOENIX	25.5 ± 0.2	< 3.5
J05100488-2340148bB	021209	PHOENIX	26.0 ± 0.3	< 4.7
J05100488-2340148bab	020313	ESPADONS	24.0 ± 0.3	9.5 ± 1.0
J05111098-4903597	151011	CRIRES	22.1 ± 0.4	11.1 ± 3.2
J05130132-7027418a	220413	CRIRES	−3.4 ± 0.6	17.5 ± 2.5
J05130132-7027418b	220413	CRIRES	0.1 ± 0.3	6.4 ± 2.7
J05142878-1514546	301009	PHOENIX	21.7 ± 0.3	7.4 ± 2.2
J05142878-1514546ae	130212	ESPADONS	21.1 ± 0.3	8.7 ± 0.9
J05142736-1514514b	051111	CRIRES	21.4 ± 0.2	6.4 ± 2.5
J05142736-1514514b	130212	ESPADONS	21.5 ± 0.2	7.2 ± 1.1
J05142736-1514514bA	310110	PHOENIX	21.0 ± 0.2	8.2 ± 2.1
J05142736-1514514bB	310110	PHOENIX	21.5 ± 0.6	15.2 ± 3.3
J05164586-5410168	210711	CRIRES	21.8 ± 0.3	6.2 ± 1.8
J05164586-5410168	241009	PHOENIX	22.6 ± 0.7	< 8.7
J05195695-1124440b	301009	PHOENIX	23.4 ± 0.5	< 8.7
J05224571-3917062	130811	CRIRES	1.1 ± 3.1	64.4 ± 5.3
J05241914-1601153	110311	ESPADONS	17.2 ± 0.5	50.5 ± 3.8
J05241914-1601153	261209	PHOENIX	23.0 ± 3.4	48.7 ± 4.6
J05241914-1601153	210910	PHOENIX	21.6 ± 3.5	51.5 ± 7.0
J05241317-2104427	261209	PHOENIX	23.7 ± 0.5	< 9.1
J05241317-2104427	051111	CRIRES	24.3 ± 0.3	5.2 ± 1.6
J05241317-2104427	130212	ESPADONS	24.7 ± 0.2	6.5 ± 1.1
J05240991-4223054	251009	PHOENIX	33.4 ± 0.6	10.8 ± 2.5
J05254166-0909123	150210	PHOENIX	25.7 ± 0.3	8.4 ± 2.5
J05301858-5358483a	220413	CRIRES	31.3 ± 0.2	10.2 ± 3.4
J05335981-0221325	110212	ESPADONS	21.0 ± 0.2	5.4 ± 1.2
J05335981-0221325	240910	PHOENIX	20.9 ± 0.2	5.3 ± 1.6
J05331130-2914199	301009	PHOENIX	25.4 ± 0.4	18.2 ± 3.1
J05332802-4257205	160413	CRIRES	−3.9 ± 0.2	8.9 ± 3.1
J05332558-5117131	151011	CRIRES	19.2 ± 0.4	< 5.9
J05332558-5117131	201209	PHOENIX	19.9 ± 0.4	< 6.5
J05381615-6923321	220413	CRIRES	63.4 ± 0.6	20.4 ± 3.1
J05395494-1307598	281209	PHOENIX	25.3 ± 0.5	< 8.7
J05395494-1307598	091111	CRIRES	24.8 ± 0.3	8.1 ± 2.4

Table 3.XI — continued

Name of star	Date (DDMMYY)	Instrument	RV (kms^{-1})	vsini (kms^{-1})
J05392505-4245211	241209	PHOENIX	22.1 ± 0.2	5.3 ± 1.6
J05392505-4245211	151011	CRIRES	21.6 ± 0.3	< 3.3
J05425587-0718382	060412	CRIRES	29.7 ± 3.9	82.3 ± 6.1
J05432676-3025129	170413	CRIRES	30.8 ± 2.3	43.6 ± 3.3
J05470650-3210413	150210	PHOENIX	22.1 ± 0.7	18.9 ± 2.1
J05470650-3210413	091111	CRIRES	21.8 ± 0.5	19.0 ± 2.2
J05494272-1158500	150210	PHOENIX	27.5 ± 0.3	9.3 ± 2.7
J06002304-4401217a	130811	CRIRES	17.9 ± 2.4	42.0 ± 5.6
J06002304-4401217b	130811	CRIRES	23.7 ± 1.4	28.3 ± 5.8
J06022455-1634494	120811	CRIRES	−9.2 ± 0.6	< 9.1
J06022455-1634494	110212	ESPADONS	−8.2 ± 0.2	9.1 ± 0.9
J06112997-7213388	140711	CRIRES	18.2 ± 2.0	36.0 ± 4.0
J06134539-2352077	200413	CRIRES	22.9 ± 0.2	8.9 ± 3.1
J06131330-2742054	230910	PHOENIX	22.0 ± 0.2	12.1 ± 2.6
J06131330-2742054	201009	PHOENIX	23.9 ± 0.9	21.6 ± 1.9
J06131330-2742054	010113	ESPADONS	22.8 ± 0.2	< 2.4
J06145476-6039206	211209	PHOENIX	26.3 ± 0.2	< 4.4
J06153953-8433115a	150711	CRIRES	1.2 ± 0.6	14.6 ± 2.5
J06153953-8433115b	150711	CRIRES	2.5 ± 0.5	14.6 ± 2.5
J06161032-1320422	010113	ESPADONS	28.4 ± 0.5	28.6 ± 2.5
J06161032-1320422	141009	PHOENIX	28.2 ± 2.7	32.1 ± 8.0
J06234024-7504327	040412	CRIRES	19.4 ± 0.4	13.1 ± 3.0
J06234024-7504327	151109	PHOENIX	18.5 ± 0.6	12.2 ± 2.7
J06373215-2823125	170210	PHOENIX	17.3 ± 0.2	< 3.5
J06434532-6424396	151011	CRIRES	20.1 ± 0.5	14.1 ± 2.8
J06434532-6424396	211209	PHOENIX	20.3 ± 0.4	14.1 ± 2.5
J06475229-2523304	140911	CRIRES	−24.4 ± 0.8	21.3 ± 3.0
J07065772-5353463	210413	CRIRES	22.4 ± 0.6	17.1 ± 1.9
J07105990-5632596a	040412	CRIRES	21.5 ± 3.9	69.0 ± 8.2
J07105990-5632596b	040412	CRIRES	23.2 ± 2.7	42.0 ± 6.2
J07282116+3345127	130212	ESPADONS	10.1 ± 0.5	43.7 ± 3.7
J07420784-6243554	170911	CRIRES	−11.0 ± 0.3	< 5.0
J07523324-6436308	151011	CRIRES	20.9 ± 0.4	9.4 ± 4.0
J07523324-6436308A	141009	PHOENIX	21.3 ± 0.4	11.6 ± 3.3
J07540718-6320149	220413	CRIRES	23.1 ± 0.4	15.1 ± 2.6
J08173943-8243298	150811	CRIRES	14.2 ± 1.5	34.0 ± 3.1
J08173943-8243298	240910	PHOENIX	17.5 ± 1.6	31.1 ± 2.3
J08185942-7239561	120110	PHOENIX	62.8 ± 0.6	< 8.7
J08185942-7239561a	210512	CRIRES	34.6 ± 0.3	< 7.4
J08185942-7239561b	210512	CRIRES	−11.7 ± 0.4	< 4.1
J08224744-5726530a	220413	CRIRES	14.7 ± 0.2	6.4 ± 2.4
J08412528-5736021A	180210	PHOENIX	21.6 ± 0.2	7.2 ± 2.0
J08412528-5736021B	180210	PHOENIX	21.1 ± 0.2	< 4.4
J08422284-8345248	131111	CRIRES	−4.2 ± 5.8	100.3 ± 8.6
J08422284-8345248	170210	PHOENIX	−7.8 ± 3.0	40.7 ± 5.5
J08465879-7246588A	160210	PHOENIX	−31.5 ± 0.2	< 7.4
J08465879-7246588B	160210	PHOENIX	6.7 ± 0.2	< 7.4
J08472263-4959574A	120110	PHOENIX	9.7 ± 0.2	< 2.7
J08472263-4959574B	120110	PHOENIX	7.0 ± 0.6	< 8.7
J08471906-5717547	160210	PHOENIX	30.2 ± 0.2	10.3 ± 2.8
J08475676-7854532	220413	CRIRES	23.4 ± 0.3	6.4 ± 2.5
J09032434-6348330a	220413	CRIRES	20.7 ± 0.4	10.7 ± 3.5
J09315840-6209258	220413	CRIRES	18.8 ± 0.8	20.4 ± 2.8
J09345604-7804193	051209	PHOENIX	17.1 ± 0.3	13.1 ± 2.4
J09345604-7804193	280609	PHOENIX	17.9 ± 0.6	13.7 ± 2.0
J09361593+3731456a	280213	ESPADONS	−44.4 ± 0.2	< 1.9
J09361593+3731456b	280213	ESPADONS	46.5 ± 0.2	< 1.9
J09423823-6229028a	220413	CRIRES	11.9 ± 0.2	< 4.1
J09423823-6229028b	220413	CRIRES	11.4 ± 0.2	< 4.1
J09445422-1220544	010113	ESPADONS	13.5 ± 0.4	36.0 ± 2.8
J10010873-7913074	050412	CRIRES	14.9 ± 0.7	12.9 ± 2.8
J10140807-7636327	040610	PHOENIX	13.5 ± 1.5	27.3 ± 3.0
J10140807-7636327	050412	CRIRES	16.0 ± 1.5	27.3 ± 4.9
J10252092-4241539	220413	CRIRES	17.6 ± 0.5	11.5 ± 3.2
J10252563-4918389	220413	CRIRES	1.7 ± 0.2	6.4 ± 2.4
J11091606-7352465	220413	CRIRES	13.9 ± 2.4	45.0 ± 4.7

Table 3.XI — continued

Name of star	Date (DDMMYY)	Instrument	RV (kms^{-1})	vsini (kms^{-1})
J11102788-3731520Aa	250210	PHOENIX	-9.6 ± 0.5	< 8.3
J11102788-3731520Aa	220210	PHOENIX	33.1 ± 0.5	< 7.4
J11102788-3731520Ab	250210	PHOENIX	33.0 ± 0.3	< 7.4
J11102788-3731520Ab	220210	PHOENIX	-12.8 ± 0.3	< 7.4
J11102788-3731520B	250210	PHOENIX	9.3 ± 0.6	17.1 ± 2.2
J11102788-3731520B	220210	PHOENIX	10.2 ± 0.6	16.2 ± 1.8
J11254754-4410267	050412	CRIRES	20.9 ± 0.8	21.4 ± 2.9
J12025461-7718382	140609	PHOENIX	14.4 ± 0.6	13.7 ± 2.0
J12092998-7505400	190210	PHOENIX	1.9 ± 0.5	< 8.3
J12194808+5246450	190611	ESPADONS	-4.2 ± 0.2	< 3.8
J12202177-7407393	280609	PHOENIX	13.6 ± 3.3	45.6 ± 7.5
J12210499-7116493	230609	PHOENIX	13.5 ± 0.3	< 8.3
J12242443-5339088	210513	CRIRES	-4.2 ± 0.6	17.5 ± 2.5
J12383713-2703348	180611	ESPADONS	9.6 ± 0.2	< 4.4
J12383713-2703348	200210	PHOENIX	10.4 ± 0.2	< 3.5
J12383713-2703348	160711	CRIRES	9.6 ± 0.2	< 2.7
J13193255-4245301	230609	PHOENIX	-38.8 ± 0.5	18.2 ± 3.2
J13215631-1052098	010709	PHOENIX	-4.2 ± 2.2	34.0 ± 2.8
J13390189-2141278	040809	PHOENIX	2.8 ± 1.6	30.1 ± 2.2
J13412668-4341522	270513	ESPADONS	0.4 ± 0.5	37.9 ± 2.9
J13412668-4341522	210513	CRIRES	3.6 ± 0.2	< 4.1
J13545390-7121476	190210	PHOENIX	5.8 ± 0.2	< 2.7
J13545390-7121476	201210	PHOENIX	5.6 ± 0.2	< 3.5
J14142141-1521215A	220210	PHOENIX	-2.8 ± 3.2	102.3 ± 9.1
J14142141-1521215B	220210	PHOENIX	0.0 ± 0.8	24.1 ± 2.7
J14284804-7430205	190609	PHOENIX	11.0 ± 0.6	< 9.1
J14433804-0414354	010709	PHOENIX	-6.7 ± 1.3	27.3 ± 2.1
J15244849-4929473	120910	PHOENIX	13.8 ± 0.2	< 3.5
J15244849-4929473	250210	PHOENIX	6.4 ± 0.2	< 2.7
J15594729+4403595	030313	ESPADONS	-15.8 ± 0.5	54.9 ± 4.6
J16004277-2127380	010709	PHOENIX	-12.8 ± 4.5	92.3 ± 9.2
J16074132-1103073	140210	PHOENIX	-8.5 ± 1.2	24.4 ± 8.0
J16430128-1754274	190609	PHOENIX	-9.8 ± 0.6	9.6 ± 2.0
J16430128-1754274	010909	PHOENIX	-9.7 ± 0.5	< 9.1
J16430128-1754274	100613	CRIRES	-9.3 ± 0.4	7.7 ± 3.0
J16572029-5343316	010810	PHOENIX	1.5 ± 0.2	< 4.4
J16572029-5343316	070910	PHOENIX	1.2 ± 0.2	< 2.7
J16590962+2058160	010709	PHOENIX	8.6 ± 0.3	6.5 ± 2.1
J17080882-6936186	100910	PHOENIX	9.4 ± 3.5	77.4 ± 9.9
J17080882-6936186	190609	PHOENIX	13.6 ± 3.6	75.4 ± 13.0
J17080882-6936186	070910	PHOENIX	-1.7 ± 2.8	75.0 ± 10.2
J17080882-6936186	010909	PHOENIX	8.5 ± 3.5	81.3 ± 13.1
J17104431-5300250A	230510	PHOENIX	-11.4 ± 0.2	12.1 ± 2.6
J17130733-8552105	070610	PHOENIX	17.5 ± 4.6	99.3 ± 9.7
J17130733-8552105	100910	PHOENIX	16.5 ± 4.1	94.3 ± 8.8
J17130733-8552105	070910	PHOENIX	15.6 ± 3.3	105.2 ± 9.7
J17150219-3333398	220511	CRIRES	-14.6 ± 3.5	76.3 ± 5.3
J17165072-3007104a	100613	CRIRES	-4.9 ± 0.5	< 8.7
J17165072-3007104a	010613	CRIRES	-5.4 ± 0.5	< 8.7
J17165072-3007104b	100613	CRIRES	-6.3 ± 2.1	35.2 ± 9.3
J17165072-3007104b	010613	CRIRES	-7.7 ± 3.0	57.0 ± 6.0
J17243644-3152484a	210513	CRIRES	-2.6 ± 3.3	70.4 ± 6.0
J17243644-3152484b	210513	CRIRES	-1.8 ± 0.3	< 7.6
J17261439+1404364	010709	PHOENIX	-54.1 ± 1.8	29.9 ± 5.9
J17261525-0311308	010709	PHOENIX	16.2 ± 0.3	10.3 ± 2.8
J17292067-5014529	270910	PHOENIX	0.3 ± 1.1	23.5 ± 1.9
J17320606-3952257	250510	PHOENIX	-6.1 ± 4.2	91.3 ± 8.8
J17462934-0842362A	250510	PHOENIX	-1.8 ± 0.3	< 2.7
J17462934-0842362B	250510	PHOENIX	-32.7 ± 0.3	< 2.7
J17494867-4005431A	250510	PHOENIX	14.3 ± 3.2	44.8 ± 4.5
J17580616-2222238	010909	PHOENIX	-5.8 ± 0.5	< 9.1
J17580616-2222238	190609	PHOENIX	-5.6 ± 0.5	< 8.7
J18141047-3247344	100713	CRIRES	-13.3 ± 7.7	117.2 ± 4.6
J18151564-4927472	140410	PHOENIX	7.0 ± 3.3	81.3 ± 12.9
J18151564-4927472	010810	PHOENIX	-1.2 ± 2.8	74.0 ± 9.8
J18244689-0620311	250510	PHOENIX	-17.6 ± 0.2	< 3.5

Table 3.XI — continued

Name of star	Date (DDMMYY)	Instrument	RV (kms^{-1})	vsini (kms^{-1})
J18420694-5554254	220810	*PHOENIX*	0.2 ± 0.5	< 8.7
J18420694-5554254	250510	*PHOENIX*	0.3 ± 0.5	< 8.4
J18450097-1409053	060712	*ESPADONS*	−23.5 ± 0.2	13.7 ± 1.3
J18450097-1409053A	140410	*PHOENIX*	−23.1 ± 0.3	14.2 ± 3.2
J18450097-1409053A	250910	*PHOENIX*	−22.2 ± 0.2	14.2 ± 3.3
J18450097-1409053a	041111	*CRIRES*	−24.6 ± 0.8	16.5 ± 2.5
J18450097-1409053a	161011	*CRIRES*	−24.4 ± 0.8	16.5 ± 2.4
J18450097-1409053b	161011	*CRIRES*	−23.2 ± 0.8	13.6 ± 2.6
J18450097-1409053b	041111	*CRIRES*	−23.1 ± 0.6	13.6 ± 2.5
J18495543-0134087	120711	*CRIRES*	75.4 ± 2.4	40.0 ± 4.2
J18495543-0134087	050711	*ESPADONS*	116.6 ± 0.5	34.6 ± 2.6
J18553176-1622495	050712	*ESPADONS*	−43.7 ± 0.2	< 2.5
J18553176-1622495	260611	*CRIRES*	−42.9 ± 0.2	< 2.1
J19102820-2319486	051111	*CRIRES*	−8.0 ± 0.8	16.1 ± 2.7
J19102820-2319486	120410	*PHOENIX*	−6.5 ± 0.3	11.1 ± 2.7
J19102820-2319486	190910	*PHOENIX*	−6.8 ± 0.6	12.9 ± 2.1
J19102820-2319486	050712	*ESPADONS*	−7.2 ± 0.2	11.3 ± 1.3
J19224278-0515536	230513	*ESPADONS*	−26.3 ± 0.2	9.4 ± 0.9
J19225071-6310581	040610	*PHOENIX*	5.6 ± 1.5	28.2 ± 2.2
J19225071-6310581	100910	*PHOENIX*	7.4 ± 1.6	30.1 ± 2.2
J19225071-6310581	020810	*PHOENIX*	6.5 ± 1.6	30.1 ± 2.2
J19233820-4606316	140410	*PHOENIX*	0.2 ± 0.3	14.9 ± 3.0
J19233820-4606316	210810	*PHOENIX*	−0.2 ± 0.3	15.8 ± 3.0
J19243494-3442392	010909	*PHOENIX*	−3.2 ± 0.3	10.3 ± 2.8
J19243494-3442392	250510	*PHOENIX*	−4.1 ± 0.3	11.3 ± 2.9
J19243494-3442392	220810	*PHOENIX*	−3.6 ± 0.2	11.3 ± 2.9
J19312434-2134226	140410	*PHOENIX*	−25.2 ± 1.3	29.1 ± 3.6
J19312434-2134226	051111	*CRIRES*	−25.7 ± 1.4	31.0 ± 2.7
J19420065-2104051	140611	*CRIRES*	−29.2 ± 0.2	< 4.1
J19420065-2104051	140410	*PHOENIX*	−9.1 ± 0.3	< 3.9
J19420065-2104051	050712	*ESPADONS*	−21.9 ± 0.3	< 2.7
J19465260-1915141	310809	*PHOENIX*	−8.1 ± 1.9	32.1 ± 2.7
J19560294-3207186	020810	*PHOENIX*	−2.8 ± 1.8	35.0 ± 4.9
J19594554-5020497	010909	*PHOENIX*	−26.0 ± 0.3	< 5.9
J20013718-3313139	310809	*PHOENIX*	−3.5 ± 0.2	< 2.7
J20013718-3313139	151011	*CRIRES*	−4.0 ± 0.2	< 2.1
J20013718-3313139	250910	*PHOENIX*	−3.5 ± 0.2	< 3.5
J20043077-2342018	250510	*PHOENIX*	−6.5 ± 1.1	27.1 ± 16.8
J20100002-2801410	250910	*PHOENIX*	−2.4 ± 3.2	47.7 ± 4.2
J20100002-2801410	250510	*PHOENIX*	−2.2 ± 3.2	52.6 ± 5.2
J20100002-2801410	310809	*PHOENIX*	−5.7 ± 3.0	44.8 ± 4.2
J20100002-2801410	050712	*ESPADONS*	−5.9 ± 0.4	44.0 ± 3.5
J20144598-2306214	201009	*PHOENIX*	−15.4 ± 0.3	< 3.2
J20144598-2306214	170709	*PHOENIX*	−16.5 ± 0.3	< 3.9
J20163382-0711456	250513	*ESPADONS*	−23.0 ± 0.2	5.7 ± 1.2
J20223306-2927499	190410	*PHOENIX*	3.8 ± 0.7	22.1 ± 8.7
J20333759-2556521	250510	*PHOENIX*	−6.0 ± 0.5	19.2 ± 3.2
J20333759-2556521	151011	*CRIRES*	−5.2 ± 1.0	19.4 ± 2.9
J20333759-2556521	310809	*PHOENIX*	−5.0 ± 0.7	18.2 ± 3.2
J20333759-2556521	040712	*ESPADONS*	−8.8 ± 0.3	20.9 ± 2.0
J20364367-0019545	190410	*PHOENIX*	20.1 ± 0.4	13.2 ± 3.0
J20434114-2433534	190410	*PHOENIX*	−0.3 ± 2.9	41.8 ± 7.4
J20434114-2433534A	240810	*PHOENIX*	−4.1 ± 0.9	22.5 ± 2.4
J20434114-2433534A	170910	*PHOENIX*	−1.5 ± 2.4	37.9 ± 3.3
J20434114-2433534B	170910	*PHOENIX*	−5.4 ± 0.6	22.1 ± 2.5
J20434114-2433534B	240810	*PHOENIX*	−2.0 ± 2.4	35.8 ± 4.6
J20434114-2433534ab	060712	*ESPADONS*	−6.1 ± 0.3	26.0 ± 2.2
J20465795-0259320	240612	*ESPADONS*	−14.1 ± 0.2	9.5 ± 0.9
J20465795-0259320	270609	*PHOENIX*	−14.0 ± 0.5	10.2 ± 2.1
J20465795-0259320	260910	*PHOENIX*	−14.4 ± 0.4	9.1 ± 2.4
J20581836+1541211	010709	*PHOENIX*	−43.1 ± 0.8	18.0 ± 2.5
J21032686+1616569	040809	*PHOENIX*	−4.0 ± 0.6	< 8.3
J21061065-2923466	251009	*PHOENIX*	−35.6 ± 0.3	< 4.7
J21073678-1304581	270609	*PHOENIX*	3.6 ± 3.3	57.6 ± 6.6
J21073678-1304581	040712	*ESPADONS*	−2.3 ± 0.5	52.2 ± 4.4
J21100535-1919573	170709	*PHOENIX*	−6.1 ± 0.5	10.2 ± 2.2
J21100535-1919573	020711	*ESPADONS*	−5.6 ± 0.2	9.4 ± 0.9
J21100535-1919573	260910	*PHOENIX*	−5.5 ± 0.5	10.8 ± 2.3
J21103096-2710513a	210713	*CRIRES*	−3.8 ± 0.4	14.6 ± 2.4
J21103147-2710578b	300513	*ESPADONS*	−4.3 ± 0.2	15.8 ± 1.3
J21252752-8138278	250510	*PHOENIX*	11.9 ± 3.0	44.8 ± 4.2

Table 3.XI — continued

Name of star	Date (DDMMYY)	Instrument	RV (kms^{-1})	vsini (kms^{-1})
J21334415-3453372	040610	*PHOENIX*	4.1 ± 3.7	109.2 ± 10.8
J21334415-3453372	260710	*PHOENIX*	6.3 ± 4.3	93.4 ± 13.1
J21351425-8706336	220810	*PHOENIX*	7.4 ± 3.6	56.5 ± 7.7
J21351425-8706336	040610	*PHOENIX*	16.1 ± 3.5	103.3 ± 10.4
J21374019+0137137	250510	*PHOENIX*	-2.1 ± 3.3	62.4 ± 9.4
J21370885-6036054	030610	*PHOENIX*	2.3 ± 0.2	7.2 ± 2.0
J21464282-8543046	210713	*CRIRES*	23.5 ± 0.7	19.4 ± 2.8
J21471964-4803166	250510	*PHOENIX*	10.6 ± 2.7	40.7 ± 4.2
J21471964-4803166	170709	*PHOENIX*	10.0 ± 3.2	43.8 ± 4.6
J21490499-6413039	020810	*PHOENIX*	3.9 ± 3.2	76.3 ± 8.8
J22021626-4210329	170709	*PHOENIX*	-2.7 ± 0.5	10.2 ± 2.1
J22021626-4210329	240910	*PHOENIX*	-2.5 ± 0.5	10.2 ± 2.2
J22294830-4858285	110613	*CRIRES*	21.7 ± 0.6	13.6 ± 2.5
J22445794-3315015	231010	*PHOENIX*	2.9 ± 0.6	14.5 ± 1.9
J22440873-5413183	181110	*PHOENIX*	2.6 ± 1.2	25.4 ± 2.2
J22440873-5413183	220810	*PHOENIX*	4.6 ± 1.6	29.2 ± 2.5
J22440873-5413183	280610	*PHOENIX*	0.8 ± 1.2	28.1 ± 3.4
J22440873-5413183	200511	*CRIRES*	2.4 ± 1.5	26.3 ± 5.0
J22470872-6920447	170910	*PHOENIX*	38.7 ± 0.2	< 8.3
J22470872-6920447	250510	*PHOENIX*	17.3 ± 0.2	8.9 ± 3.3
J22470872-6920447	060709	*PHOENIX*	39.0 ± 0.2	< 8.3
J22470872-6920447	231010	*PHOENIX*	44.5 ± 0.2	8.9 ± 3.3
J23002791-2618431A	191110	*PHOENIX*	7.3 ± 0.3	< 6.1
J23002791-2618431B	191110	*PHOENIX*	6.6 ± 0.3	< 6.5
J23131671-4933154	030610	*PHOENIX*	2.1 ± 0.3	11.3 ± 2.9
J23131671-4933154	200511	*CRIRES*	1.5 ± 0.4	11.7 ± 3.2
J23172807+1936469	200513	*ESPADONS*	4.4 ± 0.2	6.7 ± 1.0
J23204705-6723209A	220810	*PHOENIX*	6.4 ± 0.3	15.2 ± 3.2
J23204705-6723209B	220810	*PHOENIX*	6.8 ± 0.3	8.4 ± 2.5
J23204705-6723209A	080610	*PHOENIX*	6.6 ± 0.3	15.2 ± 3.2
J23204705-6723209B	080610	*PHOENIX*	6.3 ± 0.3	9.3 ± 2.7
J23221088-0301417	040809	*PHOENIX*	-5.5 ± 0.3	< 6.5
J23221088-0301417	250510	*PHOENIX*	-5.4 ± 0.3	< 6.5
J23261069-7323498	270510	*PHOENIX*	9.6 ± 3.2	65.4 ± 9.5
J23261069-7323498	040809	*PHOENIX*	8.2 ± 3.3	59.5 ± 8.4
J23261069-7323498	220411	*CRIRES*	8.9 ± 3.5	67.5 ± 8.1
J23285763-6802338	170910	*PHOENIX*	10.7 ± 3.4	48.5 ± 6.5
J23285763-6802338	060709	*PHOENIX*	9.9 ± 3.2	50.7 ± 4.9
J23285763-6802338	270510	*PHOENIX*	11.9 ± 3.5	51.5 ± 6.8
J23314492-0244395	210811	*ESPADONS*	-5.3 ± 0.2	< 5.5
J23314492-0244395	190910	*PHOENIX*	-4.8 ± 0.3	< 4.7
J23314492-0244395	181110	*PHOENIX*	-4.7 ± 0.3	5.6 ± 2.0
J23314492-0244395	040809	*PHOENIX*	-4.9 ± 0.3	5.6 ± 2.0
J23323085-1215513	100613	*CRIRES*	1.0 ± 0.5	< 8.7
J23323085-1215513	040809	*PHOENIX*	0.9 ± 0.5	< 9.1
J23320018-3917368	210811	*ESPADONS*	10.9 ± 0.2	5.6 ± 1.2
J23320018-3917368	191110	*PHOENIX*	11.1 ± 0.2	6.3 ± 1.9
J23320018-3917368	240910	*PHOENIX*	11.2 ± 0.2	6.3 ± 1.8
J23320018-3917368	040610	*PHOENIX*	11.1 ± 0.2	6.3 ± 1.8
J23452225-7126505	270510	*PHOENIX*	8.3 ± 0.3	12.3 ± 3.0
J23452225-7126505	060709	*PHOENIX*	8.9 ± 0.2	13.2 ± 2.9
J23452225-7126505	170910	*PHOENIX*	8.4 ± 0.2	13.2 ± 2.9
J23474694-6517249	170910	*PHOENIX*	6.4 ± 0.5	< 8.7
J23474694-6517249	190410	*PHOENIX*	6.1 ± 0.5	< 8.7
J23513366+3127229	210811	*ESPADONS*	-13.6 ± 0.3	12.9 ± 1.3
J04435686+3723033723	210811	*ESPADONS*	6.4 ± 0.2	10.6 ± 1.0
J10120908-312445124a	220413	*CRIRES*	14.7 ± 0.5	15.5 ± 2.6
J10120908-312445124b	220413	*CRIRES*	14.4 ± 0.7	20.4 ± 2.8
J14252913-411332313	210513	*CRIRES*	-9.0 ± 4.0	91.0 ± 7.2
J14252913-411332313	270513	*ESPADONS*	-1.2 ± 1.3	95.3 ± 6.7
J01373940+18353328-1	210811	*ESPADONS*	0.9 ± 0.3	16.6 ± 1.5
J22004158+271513509-	210811	*ESPADONS*	-0.3 ± 0.5	52.9 ± 4.3

BIBLIOGRAPHIE

Anderson, E., & Francis, C. 2012, Astronomy Letters, 38, 331

Barnes, S. A. 2003, ApJ, 586, 464

—. 2007, ApJ, 669, 1167

Barrado Y Navascués, D. 2006, A&A, 459, 511

Barrado y Navascués, D., Stauffer, J. R., & Jayawardhana, R. 2004, ApJ, 614, 386

Bergfors, C., et al. 2010, A&A, 520, A54+

Binks, A. S., & Jeffries, R. D. 2013, ArXiv e-prints

Bobylev, V. V., & Bajkova, A. T. 2007, Astronomy Letters, 33, 571

Bobylev, V. V., Goncharov, G. A., & Bajkova, A. T. 2007, VizieR Online Data Catalog, 908, 30821

Bowler, B. P., Liu, M. C., Shkolnik, E. L., & Dupuy, T. J. 2013, ApJ, 774, 55

Bowler, B. P., Liu, M. C., Shkolnik, E. L., Dupuy, T. J., Cieza, L. A., Kraus, A. L., & Tamura, M. 2012, ArXiv e-prints

Casagrande, L., Flynn, C., & Bessell, M. 2008, MNRAS, 389, 585

Chubak, C., Marcy, G., Fischer, D. A., Howard, A. W., Isaacson, H., Johnson, J. A., & Wright, J. T. 2012, ArXiv e-prints

Cutri, R. M., et al. 2012, Explanatory Supplement to the WISE All-Sky Data Release Products, Tech. rep.

da Silva, L., Torres, C. A. O., de La Reza, R., Quast, G. R., Melo, C. H. F., & Sterzik, M. F. 2009, A&A, 508, 833

Daemgen, S., Siegler, N., Reid, I. N., & Close, L. M. 2007, ApJ, 654, 558

de Bruijne, J. H. J., & Eilers, A.-C. 2012, A&A, 546, A61

de la Reza, R., Torres, C. A. O., Quast, G., Castilho, B. V., & Vieira, G. L. 1989, ApJ, 343, L61

Delfosse, X., et al. 2004, in Astronomical Society of the Pacific Conference Series, Vol. 318, Spectroscopically and Spatially Resolving the Components of the Close Binary Stars, ed. R. W. Hilditch, H. Hensberge, & K. Pavlovski, 166–174

Delfosse, X., Forveille, T., Perrier, C., & Mayor, M. 1998, A&A, 331, 581

Donati, J.-F., Catala, C., Landstreet, J. D., & Petit, P. 2006, in Astronomical Society of the Pacific Conference Series, Vol. 358, Astronomical Society of the Pacific Conference Series, ed. R. Casini & B. W. Lites, 362–+

Donati, J.-F., Semel, M., Carter, B. D., Rees, D. E., & Collier Cameron, A. 1997, MN-RAS, 291, 658

Epchtein, N., et al. 1997, The Messenger, 87, 27

Gagné, J., Lafrenière, D., Doyon, R., Malo, L., Faherty, J., & Artigau, É. 2013, Mem. Soc. Astron. Italiana, 84, 916

Gálvez-Ortiz, M. C., et al. 2010, MNRAS, 409, 552

Gizis, J. E., Reid, I. N., & Hawley, S. L. 2002, AJ, 123, 3356

Glebocki, R., & Gnacinski, P. 2005, VizieR Online Data Catalog, 3244, 0

Gray, D. F. 1992, The observation and analysis of stellar photospheres.

Hawley, S. L., Gizis, J. E., & Reid, I. N. 1996, AJ, 112, 2799

Herbig, G. H., & Bell, K. R. 1988, Third Catalog of Emission-Line Stars of the Orion Population : 3 : 1988

Herrero, E., Ribas, I., Jordi, C., Guinan, E. F., & Engle, S. G. 2012, A&A, 537, A147

Hinkle, K. H., et al. 2003, in Presented at the Society of Photo-Optical Instrumentation Engineers (SPIE) Conference, Vol. 4834, Society of Photo-Optical Instrumentation Engineers (SPIE) Conference Series, ed. P. Guhathakurta, 353–363

Houdebine, E. R. 2012, MNRAS, 421, 3189

Irwin, J., Berta, Z. K., Burke, C. J., Charbonneau, D., Nutzman, P., West, A. A., & Falco, E. E. 2011, ApJ, 727, 56

Janson, M., et al. 2012, ArXiv e-prints

Jayawardhana, R., Coffey, J., Scholz, A., Brandeker, A., & van Kerkwijk, M. H. 2006, ApJ, 648, 1206

Jenkins, J. S., Ramsey, L. W., Jones, H. R. A., Pavlenko, Y., Gallardo, J., Barnes, J. R., & Pinfield, D. J. 2009, ApJ, 704, 975

Kaeufl, H.-U., et al. 2004, in Society of Photo-Optical Instrumentation Engineers (SPIE) Conference Series, Vol. 5492, Society of Photo-Optical Instrumentation Engineers (SPIE) Conference Series, ed. A. F. M. Moorwood & M. Iye, 1218–1227

Kastner, J. H., Zuckerman, B., Weintraub, D. A., & Forveille, T. 1997, Science, 277, 67

Kharchenko, N. V., Scholz, R., Piskunov, A. E., Roeser, S., & Schilbach, E. 2007, VizieR Online Data Catalog, 3254, 0

Kiss, L. L., et al. 2011, MNRAS, 411, 117

Koen, C., Kilkenny, D., van Wyk, F., & Marang, F. 2010, MNRAS, 403, 1949

Landolt, A. U. 2009, AJ, 137, 4186

Leinert, C., Henry, T., Glindemann, A., & McCarthy, Jr., D. W. 1997, A&A, 325, 159

Lépine, S., & Gaidos, E. 2011, AJ, 142, 138

Lépine, S., Hilton, E. J., Mann, A. W., Wilde, M., Rojas-Ayala, B., Cruz, K. L., & Gaidos, E. 2013, AJ, 145, 102

Lepine, S., & Shara, M. M. 2005, VizieR Online Data Catalog, 1298, 0

Lépine, S., & Simon, M. 2009, AJ, 137, 3632

Liu, M. C., Dupuy, T. J., & Allers, K. N. 2013, Astronomische Nachrichten, 334, 85

Looper, D. L., Bochanski, J. J., Burgasser, A. J., Mohanty, S., Mamajek, E. E., Faherty, J. K., West, A. A., & Pitts, M. A. 2010, AJ, 140, 1486

López-Santiago, J., Micela, G., & Montes, D. 2009, A&A, 499, 129

López-Santiago, J., Montes, D., Crespo-Chacón, I., & Fernández-Figueroa, M. J. 2006, ApJ, 643, 1160

López-Santiago, J., Montes, D., Gálvez-Ortiz, M. C., Crespo-Chacón, I., Martínez-Arnáiz, R. M., Fernández-Figueroa, M. J., de Castro, E., & Cornide, M. 2010, A&A, 514, A97+

Luhman, K. L., Stauffer, J. R., & Mamajek, E. E. 2005, ApJ, 628, L69

Lyo, A.-R., Lawson, W. A., & Bessell, M. S. 2004, MNRAS, 355, 363

Makarov, V. V. 2007, ApJS, 169, 105

Makarov, V. V., & Urban, S. 2000, MNRAS, 317, 289

Malo, L., Doyon, R., Lafrenière, D., Artigau, É., Gagné, J., Baron, F., & Riedel, A. 2013, ApJ, 762, 88

Mamajek, E. E., & Hillenbrand, L. A. 2008, ApJ, 687, 1264

Mazeh, T., Prato, L., Simon, M., Goldberg, E., Norman, D., & Zucker, S. 2002, ApJ, 564, 1007

Mentuch, E., Brandeker, A., van Kerkwijk, M. H., Jayawardhana, R., & Hauschildt, P. H. 2008, ApJ, 689, 1127

Messina, S., Desidera, S., Turatto, M., Lanzafame, A. C., & Guinan, E. F. 2010, A&A, 520, A15+

Montes, D., López-Santiago, J., Gálvez, M. C., Fernández-Figueroa, M. J., De Castro, E., & Cornide, M. 2001, MNRAS, 328, 45

Moór, A., Szabó, G. M., Kiss, L. L., Kiss, C., Ábrahám, P., Szulágyi, J., Kóspál, Á., & Szalai, T. 2013, MNRAS, 435, 1376

Nidever, D. L., Marcy, G. W., Butler, R. P., Fischer, D. A., & Vogt, S. S. 2002, ApJS, 141, 503

Ochsenbein, F., Bauer, P., & Marcout, J. 2000, A&AS, 143, 23

Ortega, V. G., Jilinski, E., de la Reza, R., & Bazzanella, B. 2009, AJ, 137, 3922

Pecaut, M. J., & Mamajek, E. E. 2013, ArXiv e-prints

Preibisch, T., & Feigelson, E. D. 2005, ApJS, 160, 390

Reid, I. N., & Cruz, K. L. 2002, AJ, 123, 2806

Reid, I. N., et al. 2003, AJ, 126, 3007

—. 2004, AJ, 128, 463

Reiners, A., & Basri, G. 2008, ApJ, 684, 1390

Reiners, A., Joshi, N., & Goldman, B. 2012, AJ, 143, 93

Reiners, A., & Mohanty, S. 2012, ApJ, 746, 43

Riaz, B., Gizis, J. E., & Harvin, J. 2006, AJ, 132, 866

Riedel, A. R., et al. 2014, ArXiv e-prints

Riedel, A. R., Murphy, S. J., Henry, T. J., Melis, C., Jao, W.-C., & Subasavage, J. P. 2011, AJ, 142, 104

Riedel, A. R., et al. 2010, AJ, 140, 897

Rodriguez, D. R., Bessell, M. S., Zuckerman, B., & Kastner, J. H. 2011, ApJ, 727, 62

Rodriguez, D. R., Zuckerman, B., Kastner, J. H., Bessel, M. S., Faherty, J. K., & Murphy, S. J. 2013, ArXiv e-prints

Roeser, S., Demleitner, M., & Schilbach, E. 2010, AJ, 139, 2440

Roeser, S., Schilbach, E., Schwan, H., Kharchenko, N. V., Piskunov, A. E., & Scholz, R. 2008, VizieR Online Data Catalog, 1312, 0

Rousselot, P., Lidman, C., Cuby, J.-G., Moreels, G., & Monnet, G. 2000, A&A, 354, 1134

Schlieder, J. E., Lépine, S., & Simon, M. 2010, AJ, 140, 119

—. 2012a, ArXiv e-prints

Schlieder, J. E., Lepine, S., & Simon, M. 2012b, ArXiv e-prints

Scholz, A., Coffey, J., Brandeker, A., & Jayawardhana, R. 2007, ApJ, 662, 1254

Shkolnik, E., Liu, M. C., & Reid, I. N. 2009, ApJ, 699, 649

Shkolnik, E. L., Anglada-Escude, G., Liu, M. C., Bowler, B. P., Weinberger, A. J., Boss, A. P., Reid, I. N., & Tamura, M. 2012, ArXiv e-prints

Shkolnik, E. L., Hebb, L., Liu, M. C., Reid, I. N., & Cameron, A. C. 2010, ApJ, 716, 1522

Shkolnik, E. L., Liu, M. C., Reid, I. N., Dupuy, T., & Weinberger, A. J. 2011, ApJ, 727, 6

Skiff, B. A. 2010, VizieR Online Data Catalog, 1, 2023

Skumanich, A. 1972, ApJ, 171, 565

Slesnick, C. L., Carpenter, J. M., & Hillenbrand, L. A. 2006, AJ, 131, 3016

Soderblom, D. R. 2010, ARA&A, 48, 581

Song, I., Zuckerman, B., & Bessell, M. 2012, ArXiv e-prints

Song, I., Zuckerman, B., & Bessell, M. S. 2003, ApJ, 599, 342

Soubiran, C., Jasniewicz, G., Chemin, L., Crifo, F., Udry, S., Hestroffer, D., & Katz, D. 2013, A&A, 552, A64

Steinmetz, M., et al. 2006, AJ, 132, 1645

Torres, C. A. O., da Silva, L., Quast, G. R., de la Reza, R., & Jilinski, E. 2000, AJ, 120, 1410

Torres, C. A. O., Quast, G. R., da Silva, L., de La Reza, R., Melo, C. H. F., & Sterzik, M. 2006, A&A, 460, 695

Torres, C. A. O., Quast, G. R., de La Reza, R., da Silva, L., & Melo, C. H. F. 2001, in Astronomical Society of the Pacific Conference Series, Vol. 244, Young Stars Near Earth : Progress and Prospects, ed. R. Jayawardhana & T. Greene, 43–+

Torres, C. A. O., Quast, G. R., Melo, C. H. F., & Sterzik, M. F. 2008, Young Nearby Loose Associations, ed. B. Reipurth, 757–+

Upgren, A. R., & Harlow, J. J. B. 1996, PASP, 108, 64

van Leeuwen, F., ed. 2007, Astrophysics and Space Science Library, Vol. 350, Hipparcos, the New Reduction of the Raw Data

Wahhaj, Z., et al. 2011, ApJ, 729, 139

Webb, R. A., Zuckerman, B., Platais, I., Patience, J., White, R. J., Schwartz, M. J., & McCarthy, C. 1999, ApJ, 512, L63

Weinberger, A. J., Anglada-Escudé, G., & Boss, A. P. 2013, ApJ, 762, 118

Weise, P., Launhardt, R., Setiawan, J., & Henning, T. 2010, A&A, 517, A88

Yee, J. C., & Jensen, E. L. N. 2010, ApJ, 711, 303

York, D. G., et al. 2000, AJ, 120, 1579

Zacharias, N., et al. 2009, VizieR Online Data Catalog, 1315, 0

Zacharias, N., Finch, C. T., Girard, T. M., Henden, A., Bartlett, J. L., Monet, D. G., & Zacharias, M. I. 2013, AJ, 145, 44

Zacharias, N., Monet, D. G., Levine, S. E., Urban, S. E., Gaume, R., & Wycoff, G. L. 2005, VizieR Online Data Catalog, 1297, 0

Zickgraf, F.-J., Krautter, J., Reffert, S., Alcalá, J. M., Mujica, R., Covino, E., & Sterzik, M. F. 2005, A&A, 433, 151

Zuckerman, B., & Song, I. 2004, ARA&A, 42, 685

Zuckerman, B., Song, I., Bessell, M. S., & Webb, R. A. 2001a, ApJ, 562, L87

Zuckerman, B., Song, I., & Webb, R. A. 2001b, ApJ, 559, 388

Zuckerman, B., & Webb, R. A. 2000, ApJ, 535, 959

Zuckerman, B., Webb, R. A., Schwartz, M., & Becklin, E. E. 2001c, ApJ, 549, L233

Zwitter, T., et al. 2008, AJ, 136, 421

CHAPITRE 4

CARACTÉRISATION DES PARAMÈTRES FUNDAMENTAUX DES ÉTOILES DE FAIBLE MASSE CANDIDATES DANS LES ASSOCIATIONS CINÉMATIQUES JEUNES ET PROCHES - DÉTERMINATION DE L'ÂGE ISOCHRONAL À L'AIDE DES MODÈLES MAGNÉTIQUES D'ÉVOLUTION

BANYAN. IV. FUNDAMENTAL PARAMETERS OF LOW-MASS STAR CANDIDATES IN NEARBY YOUNG STELLAR KINEMATIC GROUPS - ISOCHRONAL AGE DETERMINATION USING MAGNETIC EVOLUTIONARY MODELS

Lison Malo[1,2], René Doyon[2], Gregory A. Feiden[3], Loïc Albert[2], David Lafrenière[2], Étienne Artigau[2], Jonathan Gagné[2], and Adric Riedel[4]

Abstract

Based on high resolution optical spectra obtained with ESPaDOnS at CFHT, we determine fundamental parameters ($T_{\rm eff}$, R, $L_{\rm bol}$, log g and metallicity) for 59 candidate members of nearby young kinematic groups. The candidates were identified through the BANYAN Bayesian inference method of Malo et al. (2013), which takes into account the position, proper motion, magnitude, color, radial velocity and parallax (when available) to establish a membership probability. The derived parameters are compared to Dartmouth Magnetic evolutionary models and to field stars with the goal to constrain the age of our candidates. We find that, in general, low-mass stars in our sample are more luminous and have inflated radii compared to older stars, a trend expected for pre-main sequence stars. The Dartmouth Magnetic evolutionary models show a good fit to

---

[1]Based on observations obtained at the Canada-France-Hawaii Telescope (CFHT) which is operated by the National Research Council of Canada, the Institut National des Sciences de l'Univers of the Centre National de la Recherche Scientique of France, and the University of Hawaii.

[2]Département de physique and Observatoire du Mont-Mégantic, Université de Montréal, Montréal, QC H3C 3J7, Canada

[3]Department of Physics and Astronomy, Uppsala University, Box 516, SE-751 20 Uppsala, Sweden

[4]Department of Astrophysics, American Museum of Natural History, Central Park West at 79th Street, New York, NY 10024, USA

observations of field K and M stars assuming a magnetic field strength of a few kG, as typically observed for cool stars. Using the low-mass members of β Pictoris moving group, we have re-examined the age inconsistency problem between Lithium Depletion age and isochronal age (Hertzspring-Russell diagram). We find that the inclusion of the magnetic field in evolutionary models increase the isochronal age estimates for the K5V-M5V stars. Using these models and field strengths, we derive an average isochronal age between 15 and 28 Myr and we confirm a clear Lithium Depletion Boundary from which an age of 26±3 Myr is derived, consistent with previous age estimates based on this method.

4.1 Introduction

In general, the determination of fundamental parameters, T_{eff}, R, L_{bol}, log g and metallicity, for a single star requires measurements of a trigonometric distance and an interferometric stellar diameter, as well as accurate photometric and spectroscopic observations. Fundamental parameters have been derived for several old (field) low-mass stars as demonstrated by recent works (Boyajian et al., 2012, Casagrande et al., 2008, 2011, Mann et al., 2013, Rajpurohit et al., 2013). However, little is known for the young population as there are relatively few young low-mass stars that have been unambiguously identified in the solar neighborhood, although the number of candidates is rapidly increasing (e.g. Kraus et al., 2014, Malo et al., 2013, Riedel et al., 2014, Rodriguez et al., 2011, 2013, Shkolnik et al., 2012, Torres et al., 2008, Zuckerman & Song, 2004), and none have had their radii measured directly using interferometry.

Of all fundamental parameters, the age is probably the most difficult to constrain because its determination inevitably relies either on model-dependent methods (e.g., isochrone fitting, gyrochronology, the Li depletion boundary ; LDB) or on kinematic traceback techniques for stars that are members of young co-moving groups (Soderblom, 2010, Soderblom et al., 2013, and references therein). In principle, age estimates from all these methods should be consistent but many studies have unveiled some inconsistencies. For example, LDB age is systematically greater than the isochronal age, a tend

that is independent of the evolutionary model used. This discrepancy perhaps suggests that other physical factors (e.g. metallicity, magnetic field strength, accretion history) are needed to fully account for the observational properties of young stars. Investigating the fundamental properties of young low-mass stars is strongly motivated by the fact that a significant (Barnes et al., 2014) fraction of nearby K and M dwarfs host exoplanets (Casagrande et al., 2008, Udry et al., 2007). The derived properties of those exoplanets rely on a good knowledge of the fundamental parameters of their host stars, namely their mass, effective temperature, radius, metallicity and, not least, their age.

This paper is part of a large program aimed at finding and characterizing low-mass stars in Young Moving Groups (YMG). In Malo et al. (2013, hereafter Paper I), we identified more than 150 highly probable members of young co-moving groups. We presented a Bayesian analysis, coined BANYAN, using kinematic and photometric information to infer the membership probability for a sample of low-mass stars showing strong Hα and X-ray emissions. This analysis tool also provides a prediction for the most likely distance and the radial velocity of the candidates assuming that they are true members.

In Malo et al. (accepted; hereafter Paper II), follow-up radial velocity (RV) observations were secured to show that a large fraction of the candidates have measured RVs matching the predictions, strenghtening the case that these are indeed genuine co-moving members. Several of them have now been confirmed as bona fide members based on recent parallax measurements (Riedel et al., 2014, Shkolnik et al., 2012). In paper II, we also showed that these young star candidates have unusually high X-ray luminosities and high rotational ($v \sin i$) velocities compared to field counterparts. Thus, while a parallax will ultimately be needed to confirm their membership, those strong candidates already deserved further investigations.

This paper is focused on the physical characterization of these stars with a strong emphasis to investigate how the magnetic fields affect the physical properties of low-mass stars. We use new high-resolution optical spectroscopy along with atmosphere models and various data from the literature to constrain the fundamental parameters of our young star candidates. The inferred physical properties are compared with Pre-Main Sequence

(PMS) Dartmouth Magnetic evolutionary models[1] from Feiden & Chaboyer (2012) and Feiden & Chaboyer (2013) with the goal of constraining the age and strengthening the case that those candidates are genuine members of their respective moving group. Our data are used to construct an Hertzsprung-Russell (HR) diagram of the βPMG extending further at the low-mass end, enabling an estimate of an isochronal age. New Li measurements are also used to derive an Lithium Depletion Boundary (LDB) age estimate. We show that the age inconsistency problem can be partly solved, if the βPMG members have magnetic field strengths of 2.5 kGauss.

4.2   Sample and Observation

A detailed description of our initial search sample was presented in Papers I and II. In summary, the sample includes low-mass stars (K5V-M5V) showing chromospheric X-ray and Hα emissions, all with reliable I_c photometry and proper motion measurements (< 0.2 mag and $> 4\ \sigma$). The sample comprises 920 stars, of which 75 were previously identified as young in the literature. All candidates were considered for membership in the seven closest (< 100 pc) and youngest (< 100 Myr) comoving groups : TW Hydrae Association (TWA; de la Reza et al., 1989), β Pictoris Moving Group (βPMG; Zuckerman et al., 2001), Tucana-Horologium Association (THA; Torres et al., 2000, Zuckerman & Webb, 2000), Columba Association (COL; Torres et al., 2008), Carina Association (CAR; Torres et al., 2008), Argus Association (ARG; Torres et al., 2008) and AB Doradus Moving Group (ABDMG; Zuckerman & Song, 2004).

Applying our Bayesian analysis to this sample, 247 candidate members were found with a membership probability (P) over 90%, amongh which 50 were already proposed as candidate members in the literature. In Paper II, the membership of 130 candidates was strengthened through radial and projected rotational velocity measurements obtained via infrared and/or optical high-resolution spectroscopy.

---

[1]http ://stellar.dartmouth.edu/models

4.2.1 Definition of a bona fide member

As defined in this paper, a bona fide member is one that has all *XYZUVW* parameters known from parallax, radial velocity and proper motion mesurements consistent with a high membership probability to a given YMG, as determined by various tools such as Bayesian inference (Gagné et al., 2014, Malo et al., 2013) and the convergent point analysis (Rodriguez et al., 2014, 2013). A bona fide member is also required to display youth indicators. The most common indicator is the presence of Li, but this diagnostic is restricted to early M dwarfs younger than a few 10^7 yr since Li is rapidly depleted, especially in fully convective stars (Randich et al., 2001). For older early M dwarfs, the location in the color-magnitude diagram is the only way to constrain their age. In paper II, we showed that bona fide low-mass members of YMGs show unusually high X-ray luminosities and rotational velocities which can be used as an independent youth indicator in the age range ∼10-100 Myr. Spectroscopic evidence of low-gravity (e.g. NaI, KI; Gorlova et al., 2003, Riedel et al., 2014) is another useful youth indicator for mid-late M dwarfs.

In summary, the youth of low-mass stars can be assessed through the following indicators : unusually high luminosity (bolometric, X-ray, and UV when available) compared to old stars of the same temperature (spectral type), unusually high rotational velocity, Li detection (depending on spectral type and age) and the gravity-sensitive NaI and KI lines. Because the interpretation of the observed luminosity is different in the case of an unresolved multiple system, RV monitoring and high-contrast imaging should be persued to identify binary systems within the proposed bona fide members.

4.2.2 New bona fide members

The RV measurements of Paper II combined with recent parallax measurements enable the identification of three new bona fide members. The proposed three new bona fide members are all in the βPMG : J2033-2556 (M4.5V), J2010-2801 (M2.5+M3.5) and J2043-2433 (M3.7+M4.1). They all have a membership probability ($P_{v+\pi}$) greater than 90%, high X-ray luminosity typical of βPMG members and they also show signs of

low gravity (Riedel et al., 2014). J2033-2556 has multi-epoch RV measurements ruling out a binary system with good confidence.

4.2.3 Ambiguous and Uncertain Members

We highlight six other candidates with known parallax whose membership is either ambiguous or uncertain for various reasons. Because of these raisons, we take the conservative approach of excluding these targets from the results presented in this paper.

2MASSJ01351393-0712517 is a spectroscopic binary (M4.5V) identified in Paper II as a strong candidate member of Columba, but a recent parallax measurement (Shkolnik et al., 2012) yields a higher, but still ambiguous, membership probability ($P_{v+\pi}$) of 76% in favor of βPMG. While this star remains a good young star candidate, its membership is not firm enough to declare it a bona fide member of βPMG.

2MASSJ01365516-0647379 (M4V+L0V) is a visual binary that satisfies all criteria to be a bona fide member of βPMG. However, the atmosphere models fitting analysis presented in Section 4.3.1 yields an effective temperature of $\sim$3500 K that appears to be too high for an M4V ($\sim$3100 K) even though its bolometric luminosity (log $L_{\rm bol}$=-2.2 $L_\odot$) is consistent with a βPMG membership. At such a luminosity and temperature, this star should show some Li but it does not.

2MASSJ14252913-4113323 is a M2.5V spectroscopic binary with a strong membership probability in βPMG. This binary was first proposed to be a potential member of TWA (with a marginal kinematic fit) by Riedel et al. (2014) using the EW Lithium absorption and the NaI 8200 index. However, as discussed in Paper II, this object is relatively distant (67 pc) and youth indicators (NaI, Li) are consistent with a membership to an association significantly younger than βPMG, perhaps the Scorpius-Centaurus complex (de Zeeuw et al., 1999). While this star is certainly young, its membership is doubtful enough to not declare it a bona fide member of βPMG.

HIP 11152 is a M3Ve with a high membership probability to βPMG. However, the derived $T_{\rm eff} = 3906\pm20$ K (Pecaut & Mamajek, 2013) is too hot for a star of this spectral type; Pecaut & Mamajek (2013) derived a spectral type of M1V for this star. At this temperature, the star appears under-luminous for a membership in βPMG. Furthermore,

no Li is detected in this star which is incompatible with all other βPMG members of similar T_{eff} that show some Li. If this star is a M3Ve, it most likely has a T_{eff} of $\sim$3100 K close to the Li boundary transition.

2MASSJ00233468+2014282 and 2MASSJ23314492-0244395 are candidate members (K7V(sb2), M4.5V) with a membership probability (P_ν) under 90%. These stars are good young star candidates, but their membership remains to low to consider them into this analysis.

4.2.4 Observations and Data Reduction

Since 2010, 54 young star candidates were observed with ESPaDOnS, a visible-light echelle spectrograph at CFHT[2]. Observations were done using the "star+sky" mode combined with the "slow" and "normal" CCD readout mode. The spectra have a resolving power R $\sim$ 68,000 and covers the 3700 to 10500 Å spectral domain over 40 orders. The observations were obtained with individual exposures of 60 to 1800 seconds depending on the target brightness, yielding typical signal-to-noise ratios (S/N) of $\sim$ 80-120 per pixel (2.6 km s^{-1}).

All observations were processed by CFHT using UPENA 1.0, an in-house software that calls the Libre-ESpRIT pipeline (Donati et al., 1997). We used the processed spectra with the unnormalized continuum and the automatic wavelength solution inferred from telluric lines.

Since no telluric standards were observed within the same night as the science targets, telluric correction was achieved using 40 A0V spectroscopic standards secured from other ESPaDOnS programs available through the CFHT data archive. The telluric correction involves the following steps. First, we find the spectroscopic standard obtained through atmospheric conditions as close as possible to that of the target star. This choice is done by performing a linear combination of several telluric standards minimizing the ratio of absorption depth for several prominent telluric lines. Second, hydrogen absorption lines are removed from the telluric standard spectrum by fitting and dividing

---

[2]CFHT program : 11AC13, 11BC08, 11BC99, 12AC23, 12BC24, 13AC23, 13BC33

out a Voigt profile to each line. Finally, the target spectrum is divided by the corrected telluric standard spectrum, followed by the division of a blackbody curve with the effective temperature of the chosen spectroscopic standard.

In order to compare ESPaDOnS spectra with atmosphere models, the spectra were flux-calibrated by integrating target spectra with appropriate spectral response curves and scaling the results to match the apparent fluxes of the target star through various photometric bands. The apparent magnitudes came from various sources : SDSS-DR9 (Adelman-McCarthy & et al., 2011), UCAC4-APASS (Zacharias et al., 2013), Tycho (Høg et al., 2000), DENIS (Epchtein et al., 1997), Riedel et al. (2014) or Koen et al. (2002, 2010). The relative spectral response curves, effective wavelengths and zero points were taken from the Filter Profile Service[3], and APASS filter transmission curves were kindly provided by Dr. Helmar Adler.

4.3 Spectral analysis

4.3.1 Fundamental Parameters Determination

Fundamental stellar parameters, namely the effective temperature (T_{eff}), surface gravity (log g), metalliticy ([M/H]) and stellar radius (R), were determined by fitting atmosphere models to our spectra. The derivation of the stellar radius requires a distance estimate which, when a parallax is not available, is taken to be the statistical distance (d_s) inferred from the method explains in Paper I.

We adopted the same spectral fitting analysis presented in Mohanty et al. (2004a) and Mentuch et al. (2008) which consists of restricting the analysis to spectral regions strongly sensitive to surface gravity and effective temperature, namely the NaI and KI lines (see Table 4.I).

As stated in Reylé et al. (2011) and Mann et al. (2013), the TiO opacity database is not complete for the BT-Settl models used here, hence TiO bands were not included in our analysis. Moreover, the NaI line at 589 nm is strongly affected by chromospheric emission lines, which may lead to a biased estimate of the effective temperature.

---

[3]SVO : http ://svo2.cab.inta-csic.es/theory/fps

Table 4.I.   Main properties of spectral region fitted

Line element	λ (Å)	$\Delta\lambda$ (Å)	Temperature (K)	Sensitivity	Refs.
Na I	8183,8195	8150-8230	2500-3000	logg, T	1
K I	7665,7699	7660-7770	2500-3000	logg, T	2

References. — (1) Mentuch et al., 2008 ; (2) Mohanty et al., 2004a

4.3.2   Atmosphere Models and Fitting Method

The candidate spectra were fitted with the BT-Settl atmosphere models (Allard et al., 2012) using solar abundances from Asplund et al. (2009). These models are available for temperatures between 400 and 70,000 K, log g between -0.5 to 5.5 and metallicity between -4.0 to +0.5. For the purpose of our analysis, the atmosphere models considered were restricted to T_{eff} between 2700 and 5000 K, log g between 4.0 and 5.5 and [M/H] between -0.5 and +0.3, in steps of 100 K, 0.5 dex, 0.3 dex, respectively.

We have linearly interpolated atmosphere models separated by 100 K to construct a model grid with 50 K resolution in T_{eff} ; analogous averaging of models separated by 0.5 dex yields a grid with 0.25 dex resolution in log g. The metallicity was interpolated at a value of -0.25 dex using the -0.5 and +0.0 atmosphere models. This procedure was done to improve the numerical precision of the fitting procedure, as shown in Mohanty et al. (2004b)

Prior to the fitting procedure, all target spectra were corrected for their heliocentric radial velocity as measured in Paper II and the model spectra were convolved with a Gaussian kernel to match the resolving power and with a rotational broadening profile to match the measured $v \sin i$ (see Paper II, and Table 4.III) of the targets.

The best model fit was determined by minimizing the goodness-of-fit parameter G_k defined by Cushing et al. (2008) as :

$$G_k = \sum_{i=1}^{n} W_i \left(\frac{F_{obs,i} - C_k F_{k,i}}{\sigma_{obs,i}} \right)^2 \qquad (4.1)$$

where $F_{\text{obs,i}}$ is the observed flux at wavelength i, $\sigma_{obs,i}$ is the associated uncertainty, $F_{k,i}$ is the synthetic model flux for the same wavelength, and W_i is the weight applied at each wavelength.

The parameter C_k is set to minimize G_k and corresponds to the value of $(R/d)^2$ where R is the stellar radius and d the distance to the given star. The subscript k refers to a model with a given set of T_{eff}, log g and [M/H].

Uncertainties on the derived fundamental parameters were determined as in Casagrande et al. (2008, 2006) through Monte Carlo simulations ; by repeating the above fitting procedure 51 times, each time with a different random realization of the observed spectrum within the measurement errors (distance, flux calibration, gaussian noise on each spectral pixel). Typical uncertainties are 40 K, 0.15 dex, 0.05 $R_\odot$ for T_{eff}, log g and R, respectively.

The bolometric flux (F_{bol}) was estimated by integrating the best atmosphere model, which depends on T_{eff}, log g and metallicity, at the best radius found. The bolometric luminosity given by $L_{bol} = 4\ \pi\ d^2\ F_{bol}$ was derived from the statistical distance when parallax measurement was not available. The inferred parameters for all candidate stars are given in Table 4.III. Figure 4.1 presents a comparison between observations and the best-fitting atmosphere model for the βPMG candidate member GJ 2006 B.

4.3.3 Comparison to Stars of Known Parameters

For the purpose of validating our analysis, the same method was applied to five stars (GJ 880, GJ 205, HIP 67155 (GJ 526), GJ 687, GJ 411) with known parallax and fundamental parameters determined independently by Boyajian et al. (2012), Mann et al. (2013) and Pecaut & Mamajek (2013). The spectrum of HIP 67155 is from the CADC, but it was also obtained with ESPaDOnS and we applied the same analysis procedure described above. As before, since no telluric standards were observed with the target
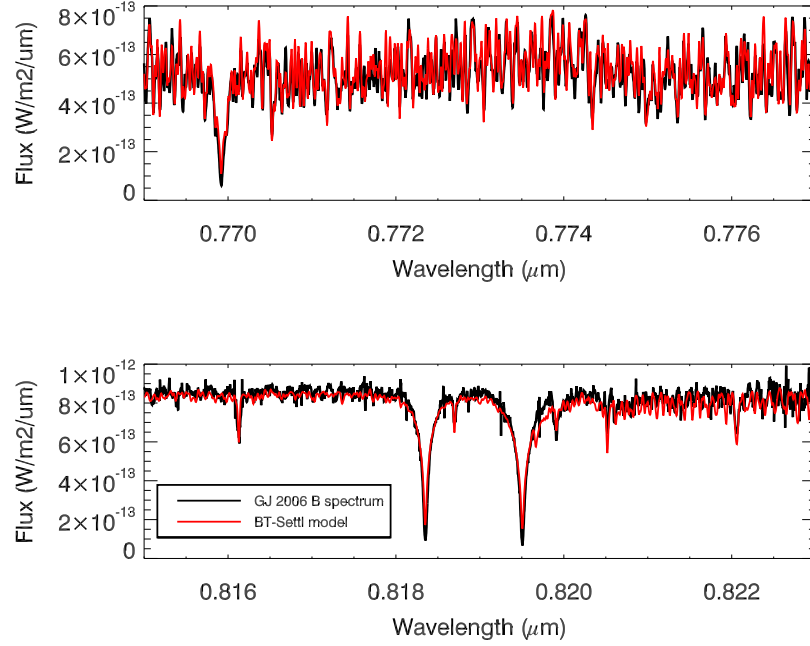
Figure 4.1 Example of fitting results for GJ 2006 B (2MASS J00275035-3233238).

observations, the same procedure described in section 4.2.1 was used to find the best telluric standard. As the ESPaDOnS CCD was replaced between semesters 2010B and 2011A, we selected telluric standards observed with the same CCD as the observations.

Figure 4.2 presents our estimated effective temperatures and radii compared to the literature measurements. There is a good correlation between all estimates with a standard deviation of 3% and 5% for T_{eff} and R, respectively.

4.3.4   Lithium Equivalent Width

Our spectroscopic data includes the Li resonance line at 6707.8 Å, a very important age indicator in young stars. The lithium equivalent width (EW) was measured using the following procedure. All spectra were first corrected for their respective heliocentric velocity.

Then the Li absorption feature was fitted between 6990 and 6710 Å with a two-parameter function : the two parameters are the slope of the local continuum and the
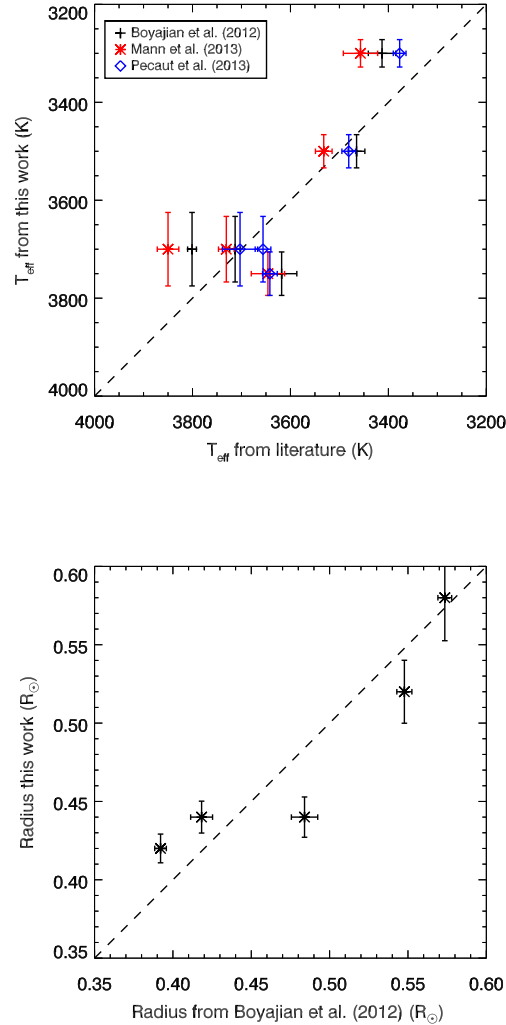
Figure 4.2 Top : Effective temperatures from this work as a function of T_{eff} from the literature. Bottom : Estimated radii from this work as function of radii from the literature.

depth of the assumed Gaussian absorption feature. The width of the assumed Gaussian absorption feature was set to the rotational velocity of the star (measured in paper II) after convolution with the instrumental profile determined by fitting a Gaussian to a slow rotator featuring a high lithium EW. Uncertainties were determined through a Monte Carlo analysis, i.e., by adding random Gaussian noise to the data and repeating the fitting procedure above. Figure 4.3 presents examples of Li absorption lines spanning a

wide range of rotational velocities and EW strengths. The resulting Li EW are given in Table 4.III. The reported uncertainties are statistical only and do not take into account possible systematic uncertainties associated with the location of the local continuum that may be biased by the faint ∼20 mÅ Fe line at 6707.4 Å located ∼4 spectral resolution elements away from the lithium line. For this reason, we adopt a conservative 5σ criterion for reporting upper limits.

4.4   Magnetic Evolutionary Models

We use the fundamental parameters inferred for our candidates and compare them with predictions from evolutionary models with the goal of confirming their youth and constraining their age. Comparisons are performed in the theoretical L_{bol}–T_{eff} plane rather than a color-magnitude diagram in order to avoid uncertainties related to color–T_{eff} transformations (Boyajian et al., 2012). Since low-mass stars generally show strong chromospheric and coronal emission associated with magnetic activity (c.f., Paper II), including effects due to magnetic fields in the stellar models may be relevant. We therefore use the Dartmouth magnetic stellar evolution models (Feiden & Chaboyer, 2012, 2013), which are based on the models by Dotter et al. (2008). The Dartmouth magnetic stellar evolution code allows for the computation of both non-magnetic (i.e., standard) and magnetic stellar models, permitting comparisons.

Standard and magnetic models all have solar calibrated abundances, $Z = 0.0188$, $Y = 0.276$, and a solar calibrated mixing length parameter, $\alpha_{MLT} = 1.884$. The solar calibration differs slightly from that presented by Feiden & Chaboyer (2013) because surface boundary conditions are now matched at an optical depth of $\tau = 10$ for all masses. Magnetic perturbations are introduced using two formulations, one coined a rotational dynamo ($\alpha - \Omega$) approach and the other a turbulent dynamo (α^2) approach (Feiden & Chaboyer, 2013). These two formulations do not refer specifically to actual solutions of the equations of magnetohydrodynamics, but were instead developed to capture relevant physical effects thought to be associated with each dynamo process. In particular, the rotational dynamo formulation considers the stabilizing influence a magnetic field may
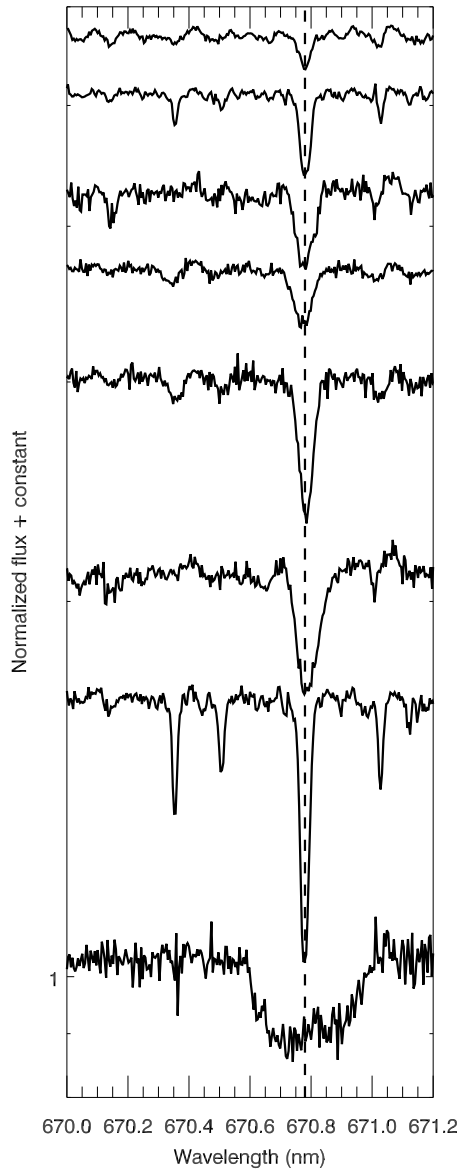
Figure 4.3 Example of Lithium line measurements for SCR1425-4113, HIP 11437, J2033-2556, J1923-4606, J0407-2918, J2110-2710, J0023+2014 and PMI04439+3723W (from bottom to top).

have on thermal convection (modified Schwarschild criterion; Chandrasekhar, 1961), while the turbulent dynamo probes the influence of a reduced convective efficiency by removing energy from convective flows (Chabrier & Küker, 2006).

For investigations of main sequence eclipsing binaries, the effects of stabilization of

convection and reductions of convective efficiency were separated and associated with a rotational and turbulent dynamo, respectively, due to the magnitude of the magnetic field required to impart changes on the structure of a star. Stabilizing convection requires interior magnetic fields of several hundred kilo-Gauss for early-M stars up to several mega-Gauss for mid-M stars at or below the fully convective boundary (Feiden & Chaboyer, 2013, Feiden & Chabrier, submitted). Magnetic field strengths of this magnitude cannot be generated purely by the conversion of kinetic energy from convection into magnetic energy. An input of energy from rotation would be required. However, removing kinetic energy from convection without explicitly modifying the Schwarzschild criterion can impart the same structural changes as stabilizing convection, but with effects that correspond to magnetic field strengths in the range of several tens of kilo-Gauss (Browning, 2008, Chabrier & Küker, 2006). Therefore, it was reasonable to separate the two effects and attribute them to separate "dynamo mechanisms" (Feiden & Chaboyer, 2013).

The two effects on stellar structure, however, need not be strictly independent. For example, if a turbulent dynamo produces a magnetic field of a given magnitude drawn from kinetic energy in convection, that magnetic field can have a stabilizing effect on the convective flows. This is especially true for pre-main-sequence stars that may generate their magnetic field via a turbulent dynamo, but have physical conditions that make stabilizing convection just as relevant of a process when the magnetic field has a strength of only several tens of kilo-Gauss.

Given this, we use magnetic models calculated with both a turbulent dynamo formulation and the rotational dynamo formulation. Turbulent dynamo models have the radial magnetic field strength profile defined as a fraction, Λ, of the equipartition magnetic field strength at the given grid point within the model (for details, see Feiden & Chaboyer, 2013, Feiden & Chaboyer 2014). Four values of Λ were tested : $\Lambda = 0.5$, 0.75, 0.90, and 0.99, but only the last case will be discussed here. At the masses considered in this study, equipartition of magnetic energy with kinetic energy in convection ($\Lambda = 1.0$) corresponds to a surface magnetic field strength of approximately 3.0 kG with interior fields around 50.0 kG. Rotational dynamo models were constructed with a dipole radial profile with a peak magnetic field occurring at a depth $R = 0.5\,R_\odot$ for fully

convective stars and at the model tachocline, for stars with radiative cores. Three values of the surface magnetic field were used, $B_{\text{surf}} = 1.0$, 2.0, and 2.5 kG, the latter being consistent with equipartition between magnetic and thermal pressures. Peak magnetic field strengths were on the order of 50 kG, and thus could be plausibly generated by a turbulent dynamo (Browning, 2008). The magnetic field strengths are representative of the values (typically between 1 and 4 kG) measured in K & M dwarfs (Reiners, 2012).

All three models are compared in the HR diagram of Figure 4.4. Non-magnetic, magnetic α^2, and magnetic $\alpha - \Omega$ with 1 kG show modest differences. On the other hand, the magnetic $\alpha - \Omega$ model with a field strength of 2.5 kG shows a significant luminosity enhancement of $\sim$0.3 dex (at T_{eff} below 3400 K) compared to the non-magnetic case and/or other models.

Recent theoretical studies (Browning, 2008, Gastine et al., 2012) and observational studies (Donati et al., 2006, Morin et al., 2008) have shown that fully convective objects with high stellar rotation should be able to produce large-scale magnetic field. Therefore, the discussion above will maintly focus on comparing fundamental parameters of low-mass star candidates to the magnetic $\alpha - \Omega$ model.

4.5 Results

The analysis below includes the new data presented in this work as well as data from other sources. The properties of all stars are compiled in Table 4.III. The sample includes stars of various status : bona fide members, candidate members with parallax but ambiguous membership (see Section 4.2.2), and candidates without parallax. Of all 59 stars studied spectroscopically through this work (54 candidates + 5 stars from E. Shkolnik observing program), 7 turned out to be field contaminants. The properties of those stars are given in Table 4.IV. They will serve, along with other data from the literature, as an old sample for comparison.
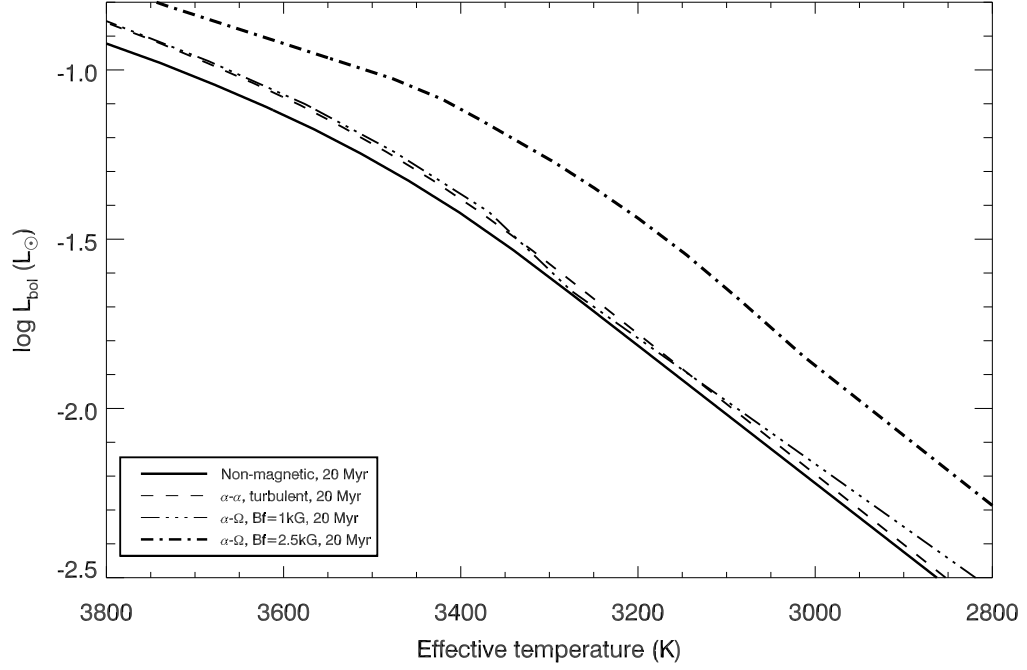
Figure 4.4 Bolometric luminosity difference between Rotational and Turbulent dynamos at an age of 20 Myr. The non-Magnetic Dartmouth model, turbulent dynamo, rotational dynamo with field strength of 1 and 2.5 kG are represented by the thick solid line, dashed line, long dashed line and dash dotted line, respectively.

4.5.1 Hertzsprung-Russell Diagram

Figure 4.5 presents the Hertzsprung-Russell (HR) diagram for our sample of bona fide members (top panel) as well as young bona fide members from the literature whose fundamental parameters were estimated by Pecaut & Mamajek (2013). Only stars with parameters accurate to better than 5σ are considered. The bottom panel is the same diagram but for the candidate members only. Several of our candidates are multiple systems, including several visual binaries, the majority of them uncovered through our radial velocity survey (Paper II). The bolometric luminosities of theses systems, given in Table 4.III, include all components. For the purpose of comparing them with single stars, we made the simplified assumption that they are equal-luminosity systems, hence their luminosity was reduced by a factor of two in Figure 4.5. This approximation is reasonable since the median flux ratio of the visual binaries uncovered in Paper II is 0.72.

Figure 4.5 also includes a sample of old M dwarfs whose fundamental parameters were determined interferometrically by Boyajian et al. (2012). The sample is complemented by two field stars with measured parallax from Shkolnik et al. (2012) and archival ESPaDOnS spectra to which our analysis could be applied for deriving their fundamental parameters. As shown in Figure 4.5, the inferred bolometric luminosities and $T_{\rm eff}$ for the old stars we analyzed agree reasonably well with the old sequence. Thus, we can be confident that our analysis is viable for deriving fundamental parameters of our young star candidates.

Older stars in Figure 4.5 are compared with a 4-Gyr Dartmouth magnetic and non-magnetic evolutionary models. For the non-magnetic case, one can note a discrepancy of about 0.1 dex in log $L_{\rm bol}$ between observations and evolutionary models for $T_{\rm eff} >$ than 3500 K. The disagreement is somewhat larger for lower $T_{\rm eff}$ and has been noted before by Boyajian et al. (2012) using other models (e.g. Baraffe et al., 1998). Interestingly, a magnetic $\alpha - \Omega$ model with a field strength between 1 and 2 kG (as typically observed; Reiners, 2012) provides a very good fit to observations. *One of main results of this work is that the inclusion of magnetic field in evolutionary models provides a better fit to observations for K5V to M5V stars.*

The young star data of Figure 4.5 are also compared with young isochrones of 5, 10 and 20 Myr for magnetic models of 2.5 kG. Note that the 100 Myr isochrone is very close (∼0.1 dex above at $T_{\rm eff}$ = 3400 K) to the 4 Gyr isochrone. In general, there is a trend in Figure 4.5 (top panel) where young bona fide members show higher luminosities compared to older (field) stars. The trend is also as expected within moving groups in the sense that, at a given $T_{\rm eff}$, candidate members of βPMG (10-20 Myr), are more luminous (∼0.5 dex) compared to older ABDMG members (∼70-120 Myr). Moving groups of intermediate ages (THA, COL ; ∼20-40 Myr) are also over luminous compared to ABDMG but they share similar luminosities with βPMG members.

We also note that, qualitatively, a single isochrone does not provide a good fit for all $T_{\rm eff}$. This is particularly obvious for βPMG for which a ∼20 Myr-old isochrone appears to fit the data reasonably well for $T_{\rm eff}$ greater than ∼3500 K whereas an isochrone younger than 5 Myr appears to better fit the data at lower $T_{\rm eff}$. We shall come back to this
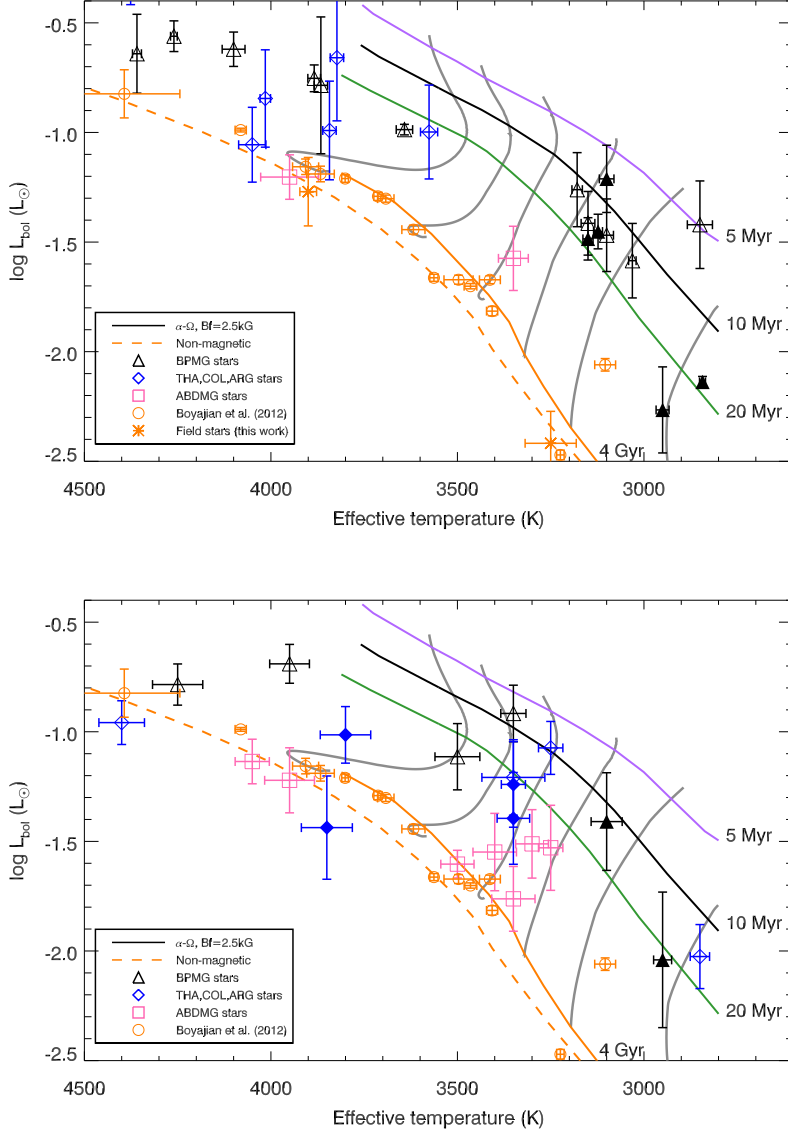
Figure 4.5 Top panel : Bolometric luminosity as a function of effective temperature for young bona fide members. Binary stars are shown with filled symbols and their luminosity was reduced by a factor of two in this figure (see text). The non-magnetic and magnetic $\alpha - \Omega$ Dartmouth model with field strength 2.5 kG are represented by dashed and solid lines, respectively. The magnetic Dartmouth isochrones of 5 Myr, 10 Myr, 20 Myr and 4 Gyr are represented by purple, black, green and orange color lines, respectively. From right to left, grey mass tracks are represented for stars with masses between 0.1 and 0.6 $M_\odot$. Bottom panel : Same figure for candidate members only.

point in section 4.6.1. The same trend is also seen for late-type members of ABDMG that appear over-luminous for their expected age, and for the candidate members sample

(bottom panel).

4.5.2   Radius-Effective Temperature Relation

To complete this analysis, we present in Figure 4.6 the T_{eff} - Radius diagram for the same samples used to construct the HR diagram. All young star candidates show inflated radii compared to Main Sequence (MS) stars, which is not surprising since the radius is effectively derived from the luminosity. The same trend observed in the HR diagram is also seen here, in that βPMG members have radii that are not consistent with a single isochrone. Late-type ($T_{\text{eff}} < 3500$ K) stars have radii typically a factor of $\sim$2 larger than early-type members, which is consistent with the over luminosity factor of $\sim$4 (0.6 dex) observed in the HR diagram (see Figure 4.5).

The main results of this analysis are the following : (1) as expected, bona fide members with known parallax show over luminosity, hence apparent inflated radii, compared to MS stars, and (2) no single theoretical isochrone can fit the observed fundamental parameters for low-mass members of βPMG.

4.6   Discussion

4.6.1   The Age of the βPictoris Moving Group

βPMG is one of the youngest, nearest and best studied co-moving group in the solar neighborhood. The age of this group remains somewhat uncertain, although it is likely to be between 8 and 40 Myr. Soderblom et al. (2013) presents a recent review of the various age estimates for βPMG along with the pros and cons of the various methods used so far. In summary, four different methods have been used : isochronal age, kinematic age, the Lithium Depletion Boundary (LDB) method, and the Li abundance.

Using the HR diagram method, Barrado y Navascués et al. (1999) and Zuckerman et al. (2001) determined an isochronal age of 20$\pm$10 Myr and 12^{+8}_{-4} Myr, respectively. The kinematic age method consists of tracing back the orbits of all members in time and finding when the volume of the group was smallest (i.e. when pairs of stars appeared to be closest to one another or to the group). Traceback ages of 11-12 Myr have been
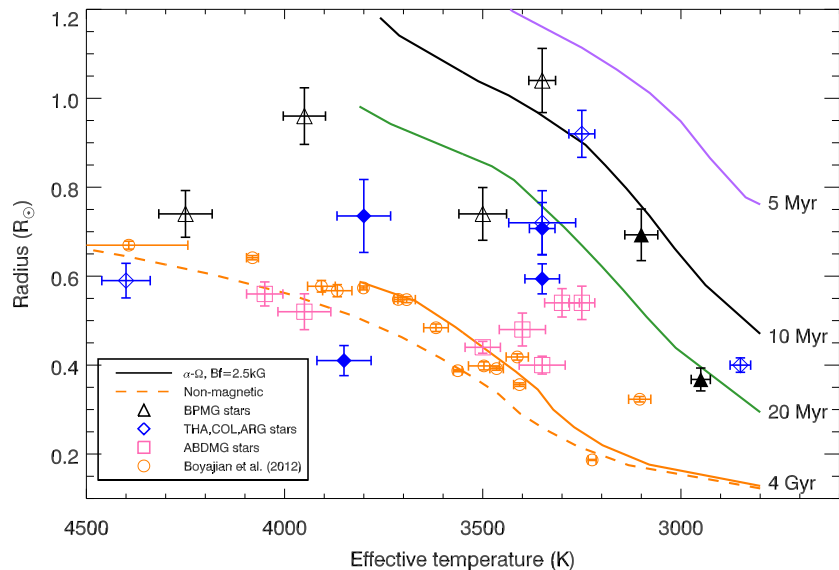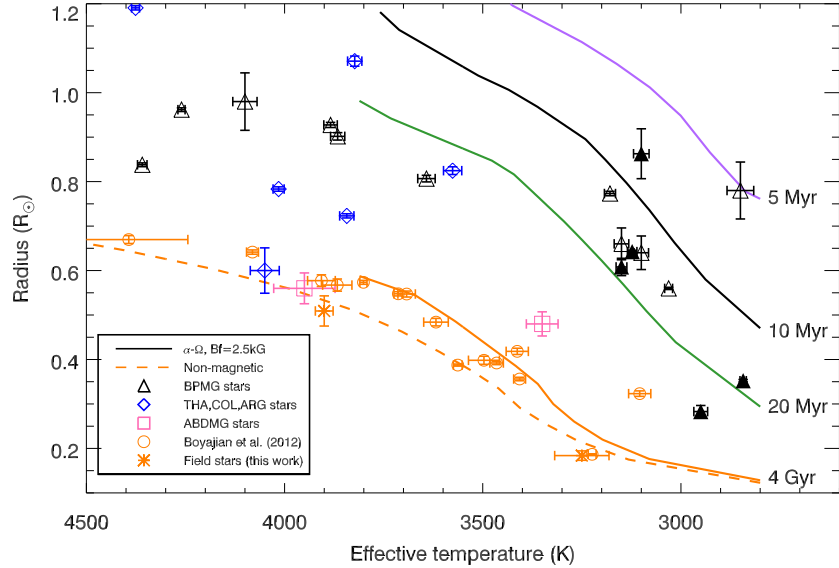
Figure 4.6 Top panel : Estimated radius as a function of effective temperature for young bona fide members. Binary stars are shown with filled symbols. The legend is the same as Figure 4.5. Bottom panel : Same figure for candidate members only.

calculated by Ortega et al. (2002) and Song et al. (2003) while Makarov (2007) found a wider age range of 22 ± 12 Myr using the flyby technique. Kinematic age methods have the distinct advantage of being independent of stellar models. On the other hand, they

rely on the crucial - and not necessarily correct - assumption that all members are coeval, and that the group formed within a relatively small volume at birth. This method cannot be used reliably for groups (older than 50 Myr) as uncertainties in space velocities translate into large positional extent at birth. Furthermore, kinematic age methods suffer somewhat from some subjectivity in that the method does work only for some selected members. The third method, LDB, makes use of the fact that Li is rapidly depleted in low-mass stars and massive BDs, which in turn translates into a very sharp luminosity boundary between stars with and without Li. The LDB method (Bildsten et al., 1997, Jeffries, 2006) is probably one of the most reliable methods for aging clusters as it relies on relatively simple physics and it is weakly dependent on the evolutionary models used (Soderblom et al., 2013). The first LDB age estimate of 20 Myr for βPMG was reported by Song et al. (2002), based on the observation of the binary system HIP 112312 (M4V + M4.5V) whose primary shows a strong Li EW while the companion does not. Song et al. (2002) argued that theoretical pre-MS evolutionary models were not able to simultaneously match the observed luminosity and the Li depletion pattern for both components and concluded that LDB ages are systematically overestimated. Recently, Binks & Jeffries (2013) determined an LDB age of 21$\pm$4 Myr based on several Li EW measurements. Finally, the Li abundance can also be used to derive the age through comparison with evolutionary and atmosphere models. Macdonald & Mullan (2010) used this method to infer an age of $\sim$40 Myr for βPMG.

The results presented in this work give us the opportunity to derive both an iso-

Table 4.II. βPMG age from several indicators

Method	Derived sample age (Myr)	
	with π	all
Isochrone T $>$ 3500 (no B field)	15$\pm$1	21$\pm$3
Isochrone T $<$ 3500 (no B field)	5$\pm$1	5$\pm$1
Isochrone T $>$ 3500 (1 kG)	24$\pm$4	27$\pm$3
Isochrone T $<$ 3500 (1 kG)	6$\pm$1	6$\pm$1
Isochrone T $<$ 3500 (2.5 kG)	14$\pm$1	16$\pm$2
LDB with binary	30$\pm$2	...
LDB without binary	26$\pm$3	...

chronal age from low-mass stars and a new estimate of the LDB age thanks to new Li measurements. Morever, our high resolution spectroscopic observations provide useful constraints for identifying multiple systems that could affect the interpretation of the results.

4.6.1.1 Isochronal Age from Low-Mass Stars

Here we use the Darmouth evolutionary models to estimate the age of all stars with good fundamental parameters, i.e. the same sample of bona fide members used for constructing the HR diagram in Figure 4.5. Figure 4.7 shows the estimated age for all stars as a function of T_{eff}, for non-magnetic and magnetic $\alpha - \Omega$ models (1 and 2.5 kG).

Figure 4.7 provides a different way to illustrate that a single isochrone cannot match all of the observations. It also shows that the isochronal age depends on the magnetic field strength assumed. Table 4.II gives a summary of various average age estimates for stars with effective temperature higher than or below 3500 K. First, we focus on the results using non-magnetic models. All stars with T_{eff} higher than $\sim$3500 K show a similar and average age of 15±1 Myr while those with $T_{\text{eff}} < 3500$ K are best fitted with an age of 4.5±0.5 Myr; those values were obtained by excluding all 5σ outliers. Using the larger sample including candidates without parallax yields ages of 21±3 Myr for T_{eff}>3500 and 5±1 Myr for T_{eff}< 3500 K. This discrepancy in age was also noted by Binks & Jeffries (2013) using Siess (Siess et al., 2000) evolutionary models (see their Figure 2) and Yee & Jensen (2010) showed the same results using three different models (see their Figure 3).

Figure 4.7 shows that the age estimate does not vary monotonically with T_{eff} and instead shows an abrupt transition around $\sim$3500 K. This systematic age difference with T_{eff} (or mass) is probably not inherent to an age spread within the βPMG. While such an age dispersion is certainly possible, if not expected (Soderblom et al., 2013, see also 6.1.2), there is no good reason to expect very low-mass stars to be systematically younger than most massive ones. One can exclude ages as young as 4 Myr since all M dwarfs would be Li-rich at that age, which is not the case.
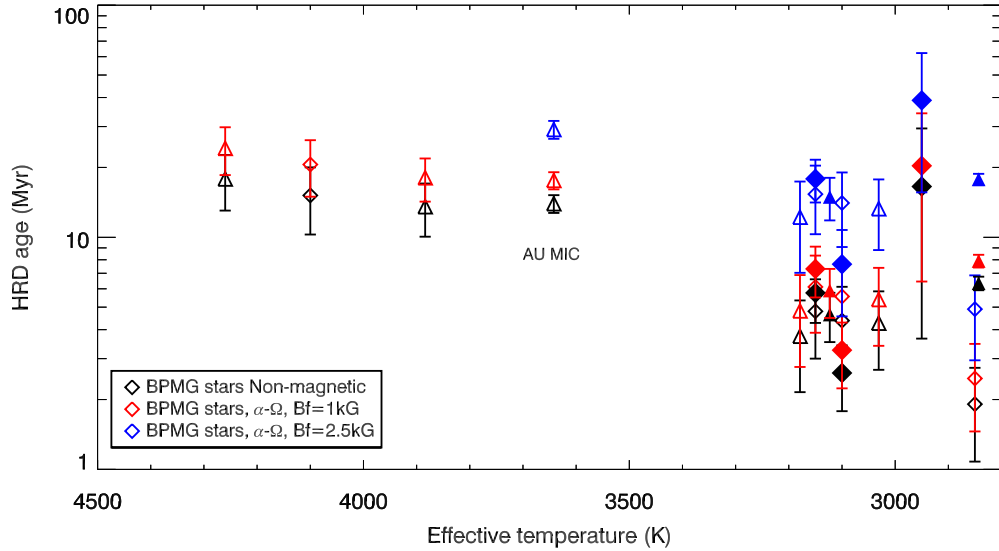
Figure 4.7 HR diagram age as a function of effective temperature for βPMG bona fide members. Binary stars are shown with filled symbols. Literature data from Pecaut & Mamajek (2013) is represented by triangle. The star identified, AU MIC, has a measured magnetic field strength ($B\,f$) of 2.3 kG ; see text.

If the age is not responsible for the observed excess luminosity in very low-mass stars, what could be the cause ? One possibility is that those stars could be equal-luminosity unresolved binary systems that would be very difficult to detect spectroscopically. This binary hypothesis is far from satisfactory since it can account for only half of the observed luminosity excess and would imply that the binary frequency is higher at lower masses. It is unlikely that it could be the case.

A more attractive alternative is to invoke the effect of magnetic field on evolutionary models, in particular the $\alpha - \Omega$ dynamo model for which the bolometric luminosity appears quite sensitive to magnetic field strength. As shown in Table 4.II and Figure 4.7, magnetic models tend to increase the inferred age. For stars with $T_{\text{eff}} < 3500$ K, the age is increased from $\sim$5 to $\sim$15 Myr. This latter age is certainly much more probable than the former for βPMG. The apparent age difference between stars below and higher T_{eff} $\sim$3500 K could thus be explained if early-type stars have magnetic field strengths systematically lower compared to late-type ones. Using the compilation of magnetic field

measurements of Reiners (2012)[4], one finds that old K0V-K5V stars have an average magnetic field of 0.20±0.1 kG compared to 2.6±0.9 kG for M0V-M5V. Thus, there is a very significant trend for the magnetic strength to increase between K and M stars. However, this trend seems to disappear for young stars. Instead, using the same compilation, this time for PMS, one finds average magnetic field strengths of 2.2±0.7 kG and 2.4±0.8 kG for young K and M stars, respectively.

The main conclusion from this discussion is that ignoring magnetic field systematically underestimates the ages derived from isochrones. The data presented here compared to the Darmouth magnetic evolutionary models suggests an isochronal age for βPMG likely between 15 and 28 Myr (Bf =1 kG for T>3500 K).

4.6.1.2   An Age Gradient in βPMG ?

The age derived above is an average value for the whole association and does not allow for a likely age spread. As discussed in Soderblom et al. (2013), the characteristic timescale τ_{SF} for the duration of a star formation event over a region of length scale l should be :

$$\tau_{SF} \sim l_{pc}^{1/2} \, \text{Myr}$$

Taking the current membership of βPMG and fitting an ellipsoid to the Galactic positions XYZ of all members, one can estimate a characteristic radius of the group defined as $R_c \sim (abc)^{1/3}$, where a, b and c are the fitted semi-major axes of the ellipsoid. One finds $R_c \sim 14$ pc or $\tau_{SF} \sim$5 Myr. Thus, from a theoretical point of view, βPMG members are expected to show an age spread of the order of $\sim$5 Myr.

There are two βPMG bona fide members for which magnetic field strengths are available ; these measurements can be used for estimating the isochronal age of these individual stars based on magnetic evolutionary models. Those two stars are HIP 102409 (AU MIC), with a magnetic field strength Bf of 2.3 kG (Saar, 1994), and HIP 23200 (Gl 182), with Bf=2.5 kG (Reiners & Basri, 2009). Only AU MIC is labeled in Fi-

---

[4]http ://solarphysics.livingreviews.org/Articles/lrsp-2012-1/

gure 4.7, since Gl 182 has a measured bolometric luminosity under our 5σ criterion. The magnetic $\alpha - \Omega$ model (Bf=2.5 kG) predicts an age of $\sim 29\pm3$ Myr for AU MIC and $\sim 26 \pm 10$ for GJ 182 ; the latter estimate requires a small extrapolation since our grid of magnetic $\alpha - \Omega$ models does not extend beyond T_{eff}=3800 K.

Interestingly, both AU MIC and GJ 182 have a similar T_{eff} within $\sim$200 K and yet their Li EW differ by more than a factor of three. Indeed, as shown in Table 4.III, AU MIC (T_{eff}=3642$\pm$22 K) has a relatively low Li EW (80 mÅ) compared to other βPMG members of similar effective temperature, for instance GJ 182 (270 mÅ ; T_{eff}=3866$\pm$18 K) and HIP 23309 (360 mÅ ; T_{eff}=3884$\pm$17 K). An age difference provides a natural explanation for explaining such a large difference in Li EW. This trend for AU MIC to have a relatively low Li-EW compared to other βPMG of similar T_{eff} may be an indication that AU MIC is somewhat older than a typical member of the βPMG.

4.6.1.3   The Lithium Depletion Boundary Age

Li is rapidly depleted in young low- and very low-mass stars, which in turn translates into a very sharp luminosity boundary between stars without and with lithium measurements. Using a K-band color-magnitude diagram and Li EW measurements both from the literature and new observations, Binks & Jeffries (2013) determined an LDB age of 21$\pm$4 Myr for βPMG. Here, we repeat this analysis using a slightly different methodology. As before, we work in the L_{bol} - T_{eff} plane and we use a maximum likelihood method for determining the LDB luminosity and its uncertainty. Figure 4.8 presents the HR diagram of all stars considered for the LDB analysis ; this figure is similar to Figure 4.5, except that stars are color coded to discriminate those with (blue symbols) and without lithium (red symbols). As usual, we treat two samples separately : one with measured parallaxes, and the other complemented with strong candidate members lacking parallaxes. All stars considered for the LDB analysis are identified in Table 4.III. The sample includes all data available from the literature including new observations presented here. Figure 4.8 shows three kinds of objects : (1) K5V-K7V dwarfs with radiative core and convective envelope which still have high EW Li, (2) early-M dwarfs which may have radiative core or be fully convective object without lithium and (3) late-type

fully convective M dwarfs with lithium detection.

The bolometric luminosity L_0 at which the LDB occurs was determined using a maximum likelihood function. Let L_i^a be the measured bolometric luminosity of the ith target in the sample of n stars with Li and L_i^b be the measured bolometric luminosity for the ith stars in the sample of m stars without Li. The true bolometric luminosity of each star is characterized by a probability density function $f(l)$:

$$f(l) = \frac{1}{\sigma_i\sqrt{2\pi}}e^{-\frac{1}{2}\left(\frac{l-l_i}{\sigma_i}\right)^2}$$

where σ_i is the luminosity measurement uncertainty. Let P^a be the probability that all stars with lithium have a true luminosity above L_0, P^b the corresponding probability that stars without lithium have a true luminosity below L_0, and $\mathscr{L}(L_0)$ the probability density function for L_0, the LDB luminosity. We have,

$$\mathscr{L}(L_0) = P^a P^b$$

with

$$P^a(L > L_0) = \prod_i^n \int_{L_0}^{\infty} f(l_i^a)\,dl$$
$$P^b(L < L_0) = \prod_i^m \int_{-\infty}^{L_0} f(l_i^b)\,dl$$

$$(4.2)$$

Applying this methodology yields the most probable value and uncertainty for L_0, which can then be compared with theoretical predictions from the Darmouth models (see Figure 4.9) to derive the corresponding LDB age. Here we adopt the same definition as Binks & Jeffries (2013) for L_0, the luminosity at which 99% of the initial Li abundance is depleted. Using the whole sample with parallax (11 stars) yields L_0=-1.59$\pm$0.06 $L_\odot$ for a
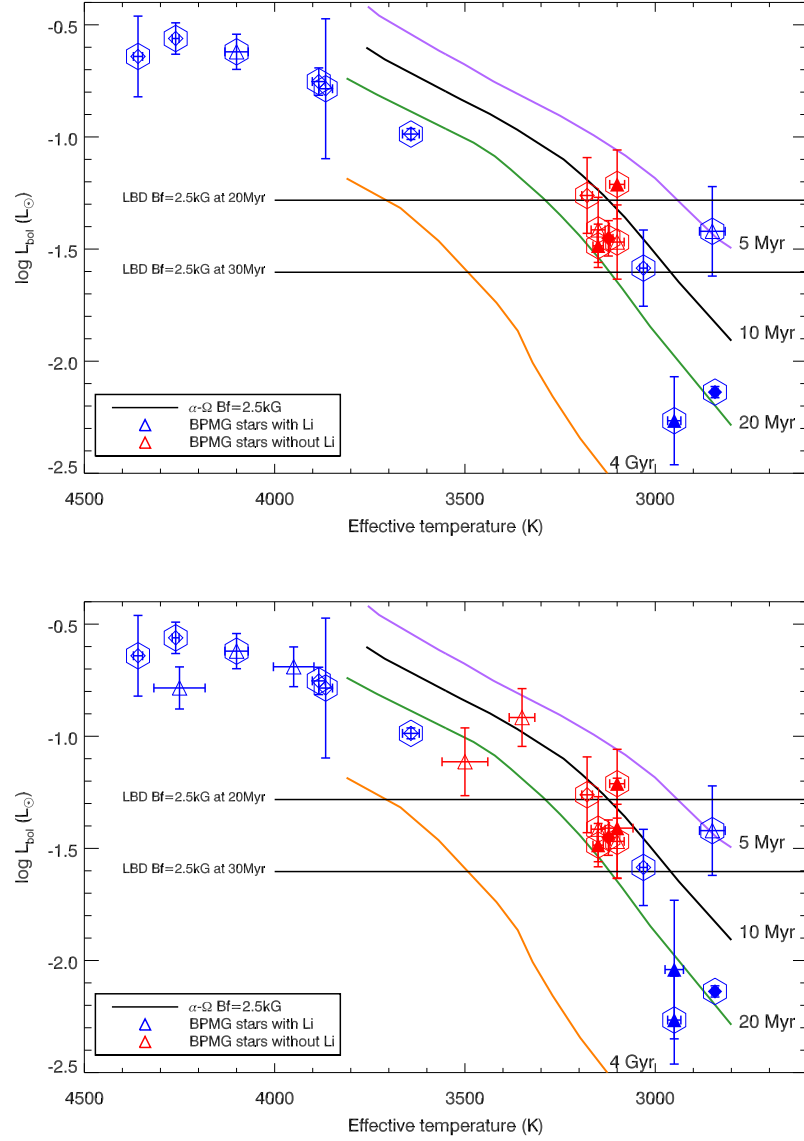
Figure 4.8 Top : Location of the Lithium Depletion Boundary (LDB) using luminosity as function of effective temperature for βPMG stars with known parallax measurements. Binary stars are identified with filled symbols. Bona fide members are marked by hexagonal symbols. Literature data from Pecaut & Mamajek (2013) is represented by diamonds. Stars with and without lithium detection are represented by blue and red symbols, respectively. The magnetic Dartmouth isochrones are as defined in Figure 4.5. Bottom : Same figure, but complemented with other strong βPMG candidates lacking parallax measurements.

corresponding age of 30$\pm$2 Myr. The LDB age is potentially sensitive to the luminosity correction applied to binary systems, especially those that happen to be close to L_0.

Excluding binary systems from the sample (5 stars left) yields L_0=-1.49±0.08 $L_\odot$ for an age of 26±3 Myr. We adopt this value as the best LDB estimate since it is less likely affected by uncertainties associated with binarity.

Our LDB age of 26±3 Myr is consistent with the value of 21±4 Myr derived by Binks & Jeffries (2013) using a different methodology and different evolutionary models. This is another illustration that the LDB age is relatively insensitive to the choice of evolutionary models, magnetic or not. It is encouraging that LDB age estimates for βPMG are in good agreement with the isochronal age range between 15 and 28 Myr.

One should caution that the LDB age is not without systematic uncertainties associated with ill-understood Li depletion processes like rotation (Bouvier, 2008, da Silva et al., 2009), magnetic field (Chabrier et al., 2007) and early accretion history (Baraffe et al., 2009). It has been suggested that strong differential rotation at the base of the convective envelope may be responsible for enhanced Li depletion in solar-type slow rotators (Bouvier, 2008). Finally, accretion activity could potentially enhance lithium depletion rate during the first few Myr of star formation, in which case the LDB age should be regarded as an upper limit. Both the LDB method and magnetic evolutionary models yield a consistent age for βPMG of 26±3 Myr.

4.6.2 The Age of Columba and THA

We can apply the same analysis to other groups (Columba, THA and Argus) albeit with less accuracy, since there are fewer candidates with the required measurements than in βPMG (see Table 4.III). Since the data is sparse, we combined all three groups together assuming that they have approximately the same age, which is probably not inaccurate given they all share age estimates between 20 and 40 Myr. The sample comprises 12 stars, of which 6 have parallaxe measurements. As for βPMG, we divide the sample between early (T > 3500 K) and late-type (T < 3500 K) stars. The best isochrone fits yield 21±4 Myr for (T > 3500 K) and 10±3 Myr for (T < 3500 K). Again, the same trend is observed for late-type stars having relatively young ages. The age inferred from early-type stars is consistent with age estimates of these groups in the literature.

Since no late-type members with Li was found for these groups, only lower limits
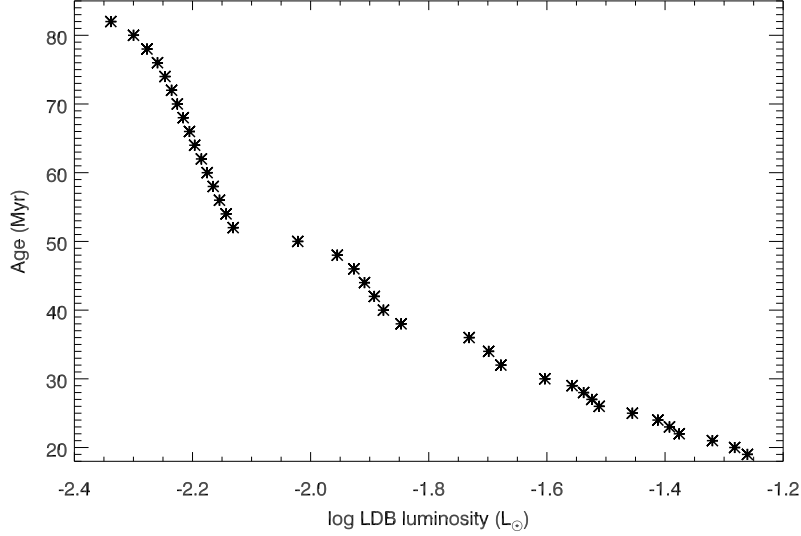
Figure 4.9 Age as function of the LDB Luminosity from Dartmouth Magnetic model (Bf = 2.5 kG) predictions. The LDB luminosity is defined as the luminosity for which 99% of the initial lithium has been depleted at that age.

can be set for the average LDB age. Figure 4.10 shows the HR diagrams of the group. The significant number of late-type stars with undetected lithium spanning a wide range of luminosity provides a useful lower limit for L_0. Using the same maximum likelihood method described above, one can define a 3σ lower limit for L_0 at which there is a probability of finding 99.7% of stars above L_0. This limit is $L_0 <$-2.29 $L_\odot$ corresponding to an age lower limit of ~ 79 Myr.

If we take into account only candidates of THA and COL, excluding the ARG member, the 3σ lower limit for L_0 is -2.04 $L_\odot$ corresponding to an lower limit age of $\sim$ 50 Myr. These lower limits are consistent with the fact that βPMG is very likely younger than those associations.

4.7   Summary & Concluding Remarks

We used multi-band optical photometry, high-resolution optical spectroscopy combined with atmosphere model fitting to determine the fundamental parameters ($T_{\rm eff}$, R, $L_{\rm bol}$, log g and metallicity) of 59 candidates and bona fide members, to nearby young
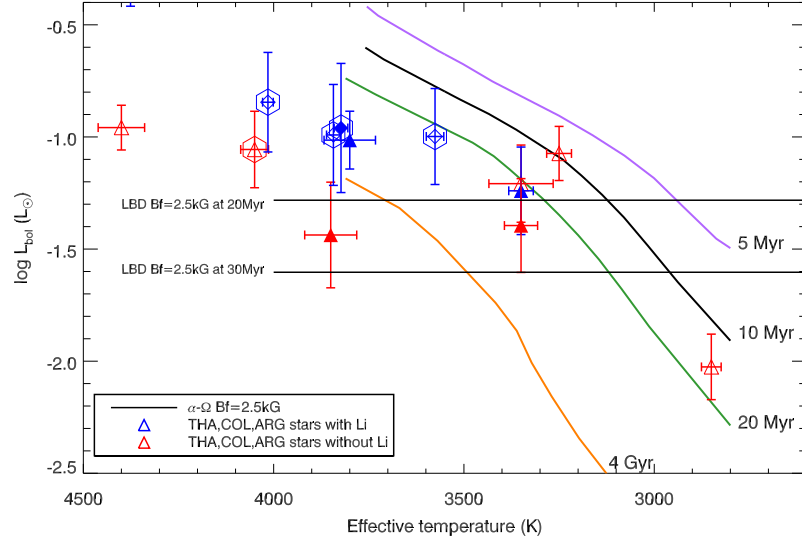
Figure 4.10 Locating the Lithium Depletion Boundary using Luminosity as function of effective temperature for THA, COL, ARG stars with known parallax measurements and candidates lacking parallaxes. Binary stars are identified with filled symbols. Bona fide members are marked by hexagonal symbols. Literature data from Pecaut & Mamajek (2013) is represented by diamonds. The magnetic Dartmouth isochrones are as defined in Figure 4.5.

moving groups. In general, the candidates have higher bolometric luminosities and inflated radii compared to field old dwarfs.

We have explored the effects of the magnetic field on the age determination using the isochrone fitting method and the LDB method. Using Dartmouth magnetic evolutionary models, we have shown that there is a good agreement between the models and the fundamental properties of old field stars by assuming a magnetic field strength of 2 kG, as typically observed or an old low-mass stars. For βPMG members, isochronal ages inferred from magnetic models are systematically higher than those inferred from models that ignore the effects of magnetic field. We infer an isochronal age between 15 and 28 Myr using the magnetic models. This age pertains to the average age of the group. This relatively large age interval may reflects a dispersion in the magnetic properties of the stars and/or a possible age spread within the association. The LDB method yields an age of 26±3 Myr, consistent with previous estimates and in agreement with the isochronal age derived in this work.

The sample of young low-mass stars discussed in this work represents a relatively small fraction of all candidate members to nearby moving groups identified through Bayesian inference. Many other candidates have yet to be characterized and the vast majority remains to be identified. Bayesian inference has proven to be very efficient at identifying young low-mass stars and opens the exciting prospect of probing the substellar and planetary mass regime of these groups.

A paradigm shift for the study of young co-moving groups is expected when GAIA releases accurate astrometry (proper motion, parallax) and radial velocities for nearly all young low-mass stars in the solar neighborhood, enabling detailed characterization of these groups. While GAIA promises to revolutionize our understanding of nearby co-coming groups, other key measurements are needed to provide better observational constraints to evolutionary models, notably : interferometric radius measurements, high-resolution optical spectroscopy for atmospheric characterization, better radial velocity measurements (0.1 km s^{-1}) and magnetic field measurements through high-resolution infrared spectro-polarimetry, which will be possible with the SPIRou instrument under development (Delfosse et al., 2013).

Table 4.III.   Fundamental properties of YMG *bona fide* and candidates

Name[a] (2MASS)	Other Name	Spectral[b] Type	vsini[c] (km s^{-1})	RV[c] (km s^{-1})	P_v^d (%)	d_s^e (pc)	d_π^f (pc)	$P_{v+\pi}^d$ (%)	Temperature (K)	Radius ($R_\odot$)	$\log L_{bol}$ (erg s^{-1})	$\log g$ (dex)	[M/H] (dex)	EW Li (Å)	$\log L_X^g$ (erg s^{-1})	Parameters Refs.
							BPMG bona fide									
J00275035-3233238[a]	GJ 2006 A	M3.5Ve	4.0	8.80±0.19	99.9	32±2	32.3±1.8[j]	99.9	3100±18	0.64±0.04	−1.47±0.17	4.50±0.00	−0.50±0.10	>28.70	29.50±0.12	1
J00275023-3233060[a]	GJ 2006 B	M3.5Ve	6.0	8.50±0.21	99.9	33±2	32.3±1.8[j]	99.9	3150±18	0.66±0.04	−1.41±0.15	4.50±0.00	−0.50±0.10	>25.55	29.50±0.12	1
J01112542+1526214[a]	GJ 3076	M5V+M6V	17.9	1.80±0.20	99.9	21±2	21.8±1.0[j]	99.9	2950±17	0.40±0.02	−1.96±0.17	4.50±0.08	−0.00±0.22	592.74±3.12	28.62±0.18	1
J02232663+2244069	HIP 11152	M3Ve	6.0[l]	10.40±2.00[l]	99.9	...	28.7±2.3	99.9	...	0.59±0.05	−1.13±0.16	...	...	>21.45	29.58±0.22	2
J02272924+3058246	HIP 11437 A	K8	5.0[m]	6.74±0.03[m]	99.9	...	40.0±3.6	99.9	4300±114	0.82±0.11	−0.72±0.15	4.50±0.25	−0.00±0.09	243.88±1.62	29.90±0.14	1
...	...				...	...			4359±12	0.84±0.08	−0.64±0.18	...	...	220.00[u]	...	2
J02412589+0559181[a]	hip12545 AB	K6Ve(sb1)	20.0[j]	10.00[j]		...	42.0±2.7		4100±30	0.98±0.06	−0.62±0.08	4.50±0.16	0.30±0.00	445.73±3.67	29.93±0.14	1
...	...					...			4044±14	0.96±0.06	−0.66±0.13	...	...	450.00[i]	...	2
J04593483+0147007	HIP 23200	M0Ve	14.0[i]	19.82±0.04[n]	99.9	...	25.9±1.7	99.9	3866±18	0.90±0.07	−0.79±0.31	...	...	270.00[i]	...	2
J05004714-5715255[a]	HIP 23309	M0.5 kee	5.8[i]	19.40±0.30[i]	99.9	...	26.8±0.8	99.9	3884±17	0.93±0.03	−0.75±0.06	...	...	360.00[i]	...	2
J06131330-2742054[a]	...	M3.5V*	2.4	22.80±0.20	99.9	25±6	29.4±0.9	99.9	3150±13	0.86±0.03	−1.18±0.08	4.50±0.00	−0.50±0.07	>28.30	29.50±0.07	1
J06182824-7202416	HIP 29964	K4Ve	16.4[i]	16.20±1.00[o]	99.9	...	38.6±1.3	99.9	4260±9	0.96±0.04	−0.56±0.07	...	...	420.00[i]	...	2
J10172689-5354265	TWA 22AB	M6Ve+M6Ve	...	13.57±0.26[p]	99.9	...	17.5±0.2	99.9	2843±8	0.50±0.01	−1.84±0.03	...	...	510.00[q]	...	2
J20100002-2801410	...	M2.5+M3.5	44.0	−5.90±0.40	99.9	52±3	48.0±3.1[j]	99.9	3100±19	1.22±0.08	−0.91±0.12	4.50±0.05	−0.00±0.14	>45.70	29.60±0.17	1
J20333759-2556521[a]	...	M4.5V	21.0	−8.80±0.30	99.9	40±3	48.3±3.3[j]	99.9	2850±33	0.78±0.06	−1.42±0.20	4.25±0.15	−0.25±0.28	504.21±4.70	29.03±0.35	1
J20434114-2433534[a]	...	M3.7+M4.1	26.0	−6.10±0.30	99.9	44±3	28.1±3.9[k]	99.9	3200±42	0.64±0.10	−1.42±0.47	4.50±0.05	−0.50±0.24	>28.25	29.27±0.25	1
J20415111-3226073	HIP 102141 B	M4Ve	15.8[i]	−5.13±0.05[n]	99.9	...	10.7±0.4	99.9	3123±12	0.91±0.04	−1.15±0.08	...	...	0.00[i]	...	2
J20450949-3120266[a]	HIP 102409	M1Ve	9.3[i]	−4.13±0.03[n]	99.9	...	9.9±0.1	99.9	3642±22	0.81±0.02	−0.99±0.02	...	...	80.00[i]	...	2
J22450004-3315258[a]	HIP 112312 B	M5IVe	16.8[i]	2.03±0.04[n]	99.9	...	23.3±2.0	99.9	3031±10	0.56±0.05	−1.59±0.17	...	...	450.00[i]	...	2
J22445794-3315015[a]	HIP 112312	M4IVe	12.1[i]	3.09±0.04[n]	99.9	...	23.3±2.0	99.9	3179±14	0.77±0.07	−1.26±0.17	...	...	0.00[i]	...	2
							BPMG candidate									
J00233468+2014282	...	K7.5V(sb2)	4.6	−1.60±0.20	65.1	53±4	...	...	3900±23	1.18±0.10	−0.56±0.09	4.50±0.16	−0.00±0.00	338.65±1.89	29.66±0.19[h]	1
J01351393-0712517	...	M4V(sb2)	49.6	6.30±0.50	88.7	47±2	37.9±2.4[k]	75.9	3100±42	0.78±0.06	−1.32±0.18	4.50±0.13	−0.00±0.29	>46.70	29.32±0.15	1
J01365516-0647379	G271-110	M4V+>L0	10.0	12.20±0.40	99.9	21±1	24.0±0.4[k]	99.9	3500±75	0.20±0.01	−2.29±0.17	5.50±0.00	−0.25±0.22	>22.85	28.81±0.12	1
J03323578+2843554[a]	...	M4+M4.5	21.9	9.20±0.30	99.9	55±4	...	...	3100±41	0.98±0.08	−1.11±0.18	4.50±0.12	−0.00±0.30	>31.35	29.14±0.24[h]	1
J04435686+3723033	PMI04439+3723W	M3Ve	10.6	6.40±0.20	96.4	59±5	...	...	3700±243	0.54±0.13	−1.34±0.44	5.00±0.22	0.30±0.20	194.12±4.04	29.33±0.22[h]	1
J05082729-2101444	...	M5V	27.6	26.60±0.43	99.9	25±5	...	...	2900±108	0.36±0.09	−2.06±0.99	4.50±0.24	−0.00±0.30	481.82±10.11	28.44±0.37[h]	1
J05241914-1601153	...	M4.5+M5.0	50.5	17.20±0.50	99.9	20±5	...	...	2950±52	0.46±0.11	−1.82±0.98	4.25±0.12	−0.25±0.25	464.25±23.30	28.70±0.33[h]	1
J05335981-0221325	...	M3V	5.4	21.00±0.20	99.9	42±5	...	...	3250±30	1.10±0.13	−0.94±0.22	4.50±0.05	−0.50±0.15	>23.85	29.78±0.17[h]	1
J14252913-4113323	SCR1425-4113	M2.5Ve*	95.3	−1.20±1.30	47.9	60±4	66.9±4.3	89.2	3200±43	1.52±0.12	−0.67±0.11	4.50±0.07	−0.25±0.24	684.64±15.15	...	1
J18580415-2953045[a]	TYC6872-1011-1	M0Ve	33.8[i]	−4.90±[i]	99.9	76±5	...	...	3950±53	0.96±0.06	−0.69±0.09	5.25±0.13	0.30±0.06	466.26±5.23	30.09±0.16[h]	1
J19102820-2319486[a]	...	M4V	11.3	−7.20±0.20	99.9	67±5	...	...	3350±33	1.04±0.07	−0.92±0.13	4.75±0.05	−0.00±0.17	>23.30	29.88±0.19[h]	1
J19233820-4606316[a]	...	M0V	13.6	0.30±0.26	99.3	70±4	...	...	4250±67	0.74±0.05	−0.78±0.09	5.25±0.14	0.30±0.15	425.92±3.02	29.71±0.23[h]	1
J21100535-1919573[a]	...	M2V	9.4	−5.60±0.20	99.9	32±2	...	...	3500±60	0.74±0.06	−1.11±0.15	4.75±0.16	−0.00±0.13	>21.20	29.67±0.14[h]	1
J21103147-2710578[a]	...	M4.5V	9.4	−5.60±0.20	99.9	41±3	...	...	2950±24	0.52±0.04	−1.74±0.26	4.50±0.12	−0.00±0.32	501.48±9.30	28.84±0.27[h]	1

216

Table 4.III — continued

Name[a] (2MASS)	Other Name	Spectral[b] Type	vsini[c] (km s⁻¹)	RV[c] (km s⁻¹)	P_v[d] (%)	d_s[e] (pc)	d_π[f] (pc)	$P_{v+\pi}$[d] (%)	Temperature (K)	Radius ($R_\odot$)	$\log L_{bol}$ (erg s⁻¹)	$\log g$ (dex)	[M/H] (dex)	EW Li (Å)	$\log L_X$[g] (erg s⁻¹)	Parameters Refs.
								THA bona-fide								
J00240899-6211042	HIP 1910 AB	M0Ve*	20.9[i]	6.60±0.60[i]	99.0	...	53.0±7.6	99.9	3823±18	1.07±0.17	-0.66±0.29	...	...	194.00[i]	...	2
J00251465-6130483	HIP 1993	M0Ve	7.3[i]	6.40±0.10[i]	99.0	...	45.8±5.1	99.9	4015±14	0.78±0.10	-0.85±0.22	...	...	40.00[i]	...	2
J00345120-6154583	HIP 2729	K5Ve	122.8[i]	-1.00±2.00[q]	99.0	...	43.9±1.9	99.9	4376±10	1.19±0.06	-0.33±0.09	...	...	360.00[i]	...	2
J00452814-5137339	HIP 3556	M3V	5.0[f]	-1.60±19.99[s]	11.0	...	40.4±4.3	90.0	3576±23	0.82±0.10	-1.00±0.21	...	...	55.00[l]	...	2
J21443012-6058389	HIP 107345	M1V	8.2[i]	2.30±0.50[i]	99.0	...	43.6±4.9	99.9	3843±18	0.72±0.09	-0.99±0.22	...	...	55.00	...	2
								THA candidate								
J01220441-3337036[a]	...	K7Ve	5.0	5.00±0.20	99.9	39±2	...	...	4400±61	0.59±0.04	-0.96±0.10	5.25±0.13	-0.00±0.00	>19.50	29.62±0.13[h]	1
J02001277-0840516[a]	...	M2.5V	15.0	4.80±0.20	91.3	38±2	...	...	3250±32	0.92±0.05	-1.07±0.12	4.50±0.12	-0.25±0.16	>25.05	29.42±0.15[h]	1
J02155892-0929121[a]	...	M2.5+M5+M8	16.7	8.30±0.30	99.9	44±3	...	...	3350±32	1.00±0.08	-0.94±0.15	5.00±0.00	-0.25±0.18	24.40±4.85	29.67±0.14[h]	1
J04365738-1613065[a]	...	M3.5V	50.7	15.60±0.50	99.3	47±4	...	...	3350±84	0.72±0.07	-1.21±0.17	5.00±0.18	-0.00±0.27	>48.20	29.90±0.15[h]	1
								COL bona-fide								
J03413724+5513068[a]	HIP 17248	M0.5V	5.0	-3.20	99.9	...	35.2±2.7	99.9	4050±36	0.60±0.05	-1.06±0.17	5.25±0.23	0.30±0.00	>19.35	...	1
								COL candidate								
J01373940+1835332	TYC 1208-468-1	K3V+K5V	16.6	0.90±0.30	95.8	63±3	...	...	4350±193	1.50±0.23	-0.15±0.05	5.00±0.54	-0.00±0.15	440.80±3.74	...	1
J02335984-1811525[a]	...	M3.0+M3.5	16.4	12.40±0.30	99.9	77±5	...	...	3350±43	0.84±0.07	-1.09±0.16	5.00±0.07	-0.00±0.21	>27.55	29.80±0.19[h]	1
J04071148-2918342[a]	...	K7.5+M1.0	19.6	21.20±0.70	99.9	71±5	...	...	3800±67	1.04±0.08	-0.71±0.09	5.00±0.11	0.30±0.15	286.83±4.22	29.82±0.16[h]	1
J05100427-2340407	...	M3+M3.5	8.2	24.20±0.30	99.9	49±6	...	...	3300±33	0.88±0.11	-1.11±0.26	4.75±0.08	-0.00±0.24	>22.95	29.72±0.19[h]	1
J05142878-1514546	...	M3.5V(vb)	7.2	21.50±0.20	98.9	58±8	...	...	3100±13	0.48±0.08	-1.72±0.54	4.50±0.00	-0.25±0.14	>23.25	29.48±0.27[h]	1
J05241317-2104427	...	M4V	6.5	24.70±0.20	99.3	50±6	...	...	3150±27	0.54±0.06	-1.59±0.35	4.50±0.00	-0.50±0.16	>23.55	29.12±0.29[h]	1
J23314492-0244395	...	M4.5V	5.5	-5.30±0.20	56.3	45±2	...	...	2900±19	0.82±0.04	-1.37±0.13	4.25±0.10	-0.50±0.17	>28.00	29.46±0.15[h]	1
								ARG candidate								
J09445422-1220544[a]	NLTT 22503	M5V	36.0	13.50±0.40	99.9	12±1	13.9±0.3[k]	99.9	2850±25	0.40±0.02	-2.03±0.15	4.50±0.18	-0.00±0.31	>41.25	28.63±0.11[h]	1
J18450097-1409053	...	M5V(vb)	13.7	-23.50±0.20	99.9	16±2	...	...	3000±23	0.46±0.06	-1.84±0.48	4.50±0.05	-0.25±0.20	>26.30	28.78±0.24[h]	1
J19224278-0515536	...	K5V	9.4	-26.30±0.20	99.9	45±6	...	...	3200±35	0.56±0.07	-1.53±0.37	4.75±0.11	-0.50±0.22	>23.65	29.30±0.26[h]	1
J20163382-0711456[a]	...	M0V+M2V	5.7	-23.00±0.20	99.9	33±3	...	...	3850±68	0.58±0.06	-1.14±0.19	5.25±0.20	-0.00±0.16	>21.15	28.78±0.25[h]	1
								ABDMG bona-fide								
J03472333-0158195	HIP 17695	M2.5V kee	18.0	16.00	99.9	...	16.1±0.7	99.9	3350±40	0.48±0.03	-1.57±0.15	5.00±0.00	-0.25±0.21	23.10±1.69	...	1
J22232904+3227334	HIP 110526 AB	M3V*	16.0	-20.60	68.0	...	15.5±1.6	99.9	3350±43	0.68±0.07	-1.28±0.26	5.00±0.04	-0.00±0.24	24.95±4.50	...	1
J23060482+6355339	HIP 114066	M1V	8.0	-23.70	99.9	...	24.5±1.0	99.9	3950±77	0.56±0.03	-1.20±0.10	5.25±0.14	0.30±0.14	33.10±2.18	...	1
								ABDMG candidate								
J01123504+1703557[a]	GuPsc	M3V	22.5	-1.60±0.30	99.9	48±2	...	...	3250±32	0.54±0.04	-1.53±0.19	4.75±0.07	-0.25±0.19	>30.10	29.13±0.23[h]	1
J04571728-0621564[a]	...	M0.5V	11.1	23.50±0.30	99.9	49±3	...	...	3950±66	0.52±0.04	-1.22±0.15	5.25±0.16	0.30±0.12	>19.05	29.13±0.25[h]	1
J10285555+0050275[a]	HIP 51317	M2V	1.1	8.30±0.30	99.9	...	7.06±0.02	99.9	3500±44	0.44±0.01	-1.60±0.06	5.00±0.13	-0.25±0.18	>24.25	...	1
J12383713-2703348[a]	...	M2.5V	4.4	9.60±0.20	99.9	25±1	...	...	3400±58	0.48±0.04	-1.55±0.18	5.00±0.14	-0.25±0.22	>23.55	28.81±0.19[h]	1

Table 4.III — continued

Name[a] (2MASS)	Other Name	Spectral Type[b]	vsini[c] (km s^{-1})	RV[c] (km s^{-1})	P_t^d (%)	d_s^e (pc)	d_π^f (pc)	$P_{v+\pi}^d$ (%)	Temperature (K)	Radius ($R_\odot$)	log L_{bol} (erg s^{-1})	log g (dex)	[M/H] (dex)	EW Li (Å)	log L_X^g (erg s^{-1})	Parameters Refs.
J20465795-0259320[a]	...	M0V	9.5	−14.10±0.40	99.9	46±2	...	...	4050±45	0.56±0.03	−1.14±0.10	5.25±0.20	0.30±0.00	26.22±3.75	29.19±0.24[h]	1
J23320018-3917368[a]	...	M3V	5.6	10.90±0.20	99.9	23±1	...	...	3350±57	0.40±0.02	−1.76±0.15	5.00±0.08	−0.00±0.23	> 23.75	29.18±0.18[h]	1
J23513366+3127229[a]	...	M2V+L0	12.9	−13.60±0.30	99.9	42±2	...	...	3300±43	0.54±0.03	−1.51±0.16	4.25±0.12	−0.25±0.18	> 22.10	29.15±0.19[h]	1

[a] Stars used for further analysis.

[b] Spectral type with asterisk is for the whole unresolved system.

[c] Measured vsini and Radial velocity (RV) using ESPaDOnS spectrum (see paper II), unless stated otherwise.

[d] Membership probability including radial velocity information (P_t), or membership probability including radial velocity and parallax information ($P_{v+\pi}$).

[e] Statistical distance derived by our analysis (see Section 5 of paper I).

[f] Parallax measurement from van Leeuwen (2007), unless stated otherwise.

[g] X-ray luminosity using the parallax measurement, unless stated otherwise.

[h] X-ray luminosity using the statistical distance.

Note. — (i) Torres et al. (2006); (j) Riedel et al. (2014); (k) Shkolnik et al. (2012); (l) Schlieder et al. (2010); (m) Song et al. (2003); (n) Bailey et al. (2012); (o) Montes et al. (2001); (p) Shkolnik et al. (2011); (q) Fernández et al. (2008); (r) Bobylev et al. (2007); (s) Scholz et al. (2007); (t) Mennuch et al. (2008); (u) da Silva et al. (2009).

References. — (1) This work; (2) Pecaut & Mamajek (2013).

Table 4.IV. Fundamental properties of Field stars

Name[a] (2MASS)	Other Name	Spectral Type	$v\sin i$[b] (km s^{-1})	RV[b] (km s^{-1})	P_{i}[c] (%)	d_{s}[d] (pc)	d_{π}[e] (pc)	$P_{v+\pi}$[c] (%)	Temperature (K)	Radius ($R_{\odot}$)	$\log L_{bol}$ (erg s^{-1})	$\log g$ (dex)	[M/H] (dex)	EW Li (Å)	$\log L_{X}$[f] (erg s^{-1})	Parameters Refs.
								Field-bona-fide								
J00182256+4401222	GJ 15A	M1.5 V	2.90[i]	11.81±0.10[n]	...	...	3.57±0.01[k]	...	3563±11	0.39±0.00	−1.66±−0.02	...	−0.36	...	...	2
J05312734-0340356	GJ 205	M1.5 V	1.00[i]	8.66±0.10[n]	...	...	5.66±0.04[l]	...	3801±9	0.57±0.00	−1.21±−0.02	...	0.35	...	...	2
...	...	...	...	...	...	...	...	...	3700±75	0.58±0.03	−1.23±0.04	5.50±0.12	−0.00±0.21	>22.95	...	1
J09142298+5241125	GJ 338A	M0.0 V	2.90[i]	11.14±0.10[n]	...	...	5.81±0.21	...	3907±35	0.58±0.01	−1.16±−0.04	...	−0.18	...	...	2
J09142485+5241118	GJ 338B	K7.0 V	2.80[i]	12.49±0.10[n]	...	...	5.81±0.21	...	3867±37	0.57±0.01	−1.19±−0.04	...	−0.15	...	...	2
J10112218+4927153	GJ 380	K7.0 V	2.70[i]	−25.73±0.10[n]	...	...	4.87±0.01[l]	...	4081±15	0.64±0.00	−0.99±−0.01	...	−0.16	...	...	2
J11032023+3558117	GJ 411	M2.0 V	2.90[i]	−84.69±0.10[n]	...	...	2.55±0.00[l]	...	3465±17	0.39±0.00	−1.70±−0.01	...	−0.41	...	...	2
...	...	...	...	...	...	...	...	...	3500±33	0.42±0.01	−1.63±0.03	5.00±0.08	−0.50±0.16	>24.15	...	1
J11052903+4331357	GJ 412A	M1.0 V	3.00[i]	68.89±0.10[n]	...	...	4.85±0.02[m]	...	3497±39	0.40±0.01	−1.67±−0.02	...	−0.40	...	...	2
J13454354+1453317	GJ 526	M1.5 V	1.40[i]	15.81±0.10[n]	...	...	5.39±0.03[m]	...	3618±31	0.48±0.01	−1.44±−0.02	...	−0.30	...	...	2
...	...	...	2.00	...	...	...	...	...	3750±44	0.44±0.01	−1.49±0.04	5.00±0.19	−0.00±0.16	>24.25	...	1
J17362594+6820220	GJ 687	M3.0 V	2.80[i]	−28.78±0.10[n]	...	...	4.53±0.02[m]	...	3413±28	0.42±0.01	−1.67±−0.02	...	−0.09	...	...	2
...	...	...	...	...	...	...	...	...	3300±28	0.44±0.01	−1.69±0.04	4.75±0.10	−0.25±0.13	>27.90	...	1
J17574849+0441405	GJ 699	M4.0 V	2.80[i]	−110.51±0.10[n]	...	...	1.82±0.01[m]	...	3224±10	0.19±0.00	−2.47±−0.02	...	−0.39	...	...	2
J18052735+0229585	GJ 702B	K5 Ve	2.70[i]	−7.70±0.20[o]	...	...	5.08±0.02[l]	...	4393±149	0.67±0.01	−0.82±−0.11	...	0.03	...	...	2
J18424666+5937499	GJ 725A	M3.0 V	5.00[i]	−0.83±0.10[n]	...	...	3.57±0.03	...	3407±15	0.36±0.00	−1.82±−0.02	...	−0.49	...	...	2
J18424888+5937374	GJ 725B	M3.5 V	7.00[i]	1.10±0.10[n]	...	...	3.57±0.03	...	3104±28	0.32±0.01	−2.06±−0.03	...	−0.36	...	...	2
J20531977+6209156	GJ 809	M0.5	2.80[i]	−17.16±0.10[n]	...	...	7.05±0.03	...	3692±22	0.55±0.01	−1.30±−0.02	...	−0.21	...	...	2
J22563497+1633130	GJ 880	M1.5 V	2.80[i]	−27.32±0.10[n]	...	...	6.85±0.05	...	3713±11	0.55±0.00	−1.29±−0.02	...	0.06	...	...	2
...	...	...	...	...	...	...	...	...	3700±66	0.52±0.02	−1.35±0.03	5.25±0.12	−0.00±0.15	>21.05	...	1
								Field-candidate								
J06022455-1634494	...	M0V	9.10	−8.20±0.20	99.90	41±9	...	...	3600±37	0.70±0.18	−1.13±0.55	5.00±0.13	−0.00±0.12	27.93±3.89	29.21±0.31[g]	1
J09361593+3731456	HIP 47133	M2+M2	1.90	0.00±0.50	98.59	30±6	...	...	3900±22	0.72±0.05	−0.97±0.12	5.25±0.17	−0.50±0.00	>19.25	28.88±0.23	1
J12194808+5246450	HIP 60121	K7V	3.80	−4.20±0.20	99.90	32±6	...	...	3950±170	0.60±0.12	−1.11±0.34	5.00±0.35	−0.00±0.18	>18.70	28.61±0.25	1
J15594729+4403595	...	M1V	54.90	−15.80±0.50	99.90	20±5	...	...	3600±86	0.42±0.11	−1.60±0.81	5.00±0.14	−0.00±0.32	>47.10	28.85±0.34[g]	1
J18495543-0134087	...	M2.5V(sb1)	34.60	116.60±0.50	99.90	23±6	...	...	3400±74	0.32±0.10	−1.94±1.19	5.25±0.14	−0.25±0.21	>34.20	28.77±0.37[g]	1
J19420065-2104051	...	M3.5V(sb2)	2.70	−21.90±0.30	99.90	8±1	...	...	3200±59	0.16±0.05	−2.62±1.44	5.00±0.16	−0.00±0.31	>26.00	27.44±0.44[g]	1
J20531465-0221218	NLTT50066	M3+M4	10.00	−39.90±1.19[q]	99.90	25±6	37.9±5.7[q]	99.90	3550±111	0.46±0.09	−1.51±0.49	5.50±0.18	−0.00±0.24	>23.65	28.88±0.30	1
J21073678-1304581	...	M3V	52.20	−2.30±0.50	69.30	17±4	...	...	3350±60	0.34±0.10	−1.88±1.05	5.00±0.12	−0.25±0.27	>49.75	28.68±0.33[g]	1
J23172807+1936469	GJ 4326	M3.5+M4.5	6.70	4.40±0.20	99.90	7±1	9.1±0.2[p]	...	3250±68	0.26±0.01	−2.12±0.13	4.75±0.18	−0.25±0.27	>26.65	28.13±0.30[g]	1

[a] Stars used for further analysis.

[b] Measured $v\sin i$ and Radial velocity (RV) using ESPaDOnS spectrum (see paper II), unless stated otherwise.

[c] Membership probability including radial velocity information (P_{v}), or membership probability including radial velocity and parallax information ($P_{v+\pi}$).

[d] Statistical distance derived by our analysis (see Section 5 of paper I).

[e] Parallax measurement from van Leeuwen (2007), unless stated otherwise.

[f] X-ray luminosity using the parallax measurement, unless stated otherwise.

[g] X-ray luminosity using the statistical distance.

Note. — (i) Jenkins et al. (2009) ; (j) Glebocki & Gnacinski (2005) ; (k) Montes et al. (2001) ; (l) Casagrande et al. (2011) ; (m) de Bruijne & Eilers (2012) ; (m) Nidever et al. (2002) ; (o) Gontcharov (2006) ; (p) Dittmann et al. (2013) ; (q) Shkolnik et al. (2012).

References. — (1) This work ; (2) Boyajian et al. (2012).

BIBLIOGRAPHIE

Adelman-McCarthy, J. K., & et al. 2011, VizieR Online Data Catalog, 2306, 0

Allard, F., Homeier, D., & Freytag, B. 2012, Royal Society of London Philosophical Transactions Series A, 370, 2765

Asplund, M., Grevesse, N., Sauval, A. J., & Scott, P. 2009, ARA&A, 47, 481

Bailey, III, J. I., White, R. J., Blake, C. H., Charbonneau, D., Barman, T. S., Tanner, A. M., & Torres, G. 2012, ApJ, 749, 16

Baraffe, I., Chabrier, G., Allard, F., & Hauschildt, P. H. 1998, A&A, 337, 403

Baraffe, I., Chabrier, G., & Gallardo, J. 2009, ApJ, 702, L27

Barnes, J. R., et al. 2014, MNRAS

Barrado y Navascués, D., Stauffer, J. R., Song, I., & Caillault, J. 1999, ApJ, 520, L123

Bildsten, L., Brown, E. F., Matzner, C. D., & Ushomirsky, G. 1997, ApJ, 482, 442

Binks, A. S., & Jeffries, R. D. 2013, MNRAS

Bobylev, V. V., Goncharov, G. A., & Bajkova, A. T. 2007, VizieR Online Data Catalog, 908, 30821

Bouvier, J. 2008, A&A, 489, L53

Boyajian, T. S., et al. 2012, ApJ, 757, 112

Browning, M. K. 2008, ApJ, 676, 1262

Casagrande, L., Flynn, C., & Bessell, M. 2008, MNRAS, 389, 585

Casagrande, L., Portinari, L., & Flynn, C. 2006, MNRAS, 373, 13

Casagrande, L., Schönrich, R., Asplund, M., Cassisi, S., Ramírez, I., Meléndez, J., Bensby, T., & Feltzing, S. 2011, A&A, 530, A138

Chabrier, G., Gallardo, J., & Baraffe, I. 2007, A&A, 472, L17

Chabrier, G., & Küker, M. 2006, A&A, 446, 1027

Chandrasekhar, S. 1961, ApJ, 134, 662

Cushing, M. C., et al. 2008, ApJ, 678, 1372

da Silva, L., Torres, C. A. O., de La Reza, R., Quast, G. R., Melo, C. H. F., & Sterzik, M. F. 2009, A&A, 508, 833

de Bruijne, J. H. J., & Eilers, A.-C. 2012, A&A, 546, A61

de la Reza, R., Torres, C. A. O., Quast, G., Castilho, B. V., & Vieira, G. L. 1989, ApJ, 343, L61

de Zeeuw, P. T., Hoogerwerf, R., de Bruijne, J. H. J., Brown, A. G. A., & Blaauw, A. 1999, AJ, 117, 354

Delfosse, X., et al. 2013, in SF2A-2013 : Proceedings of the Annual meeting of the French Society of Astronomy and Astrophysics, ed. L. Cambresy, F. Martins, E. Nuss, & A. Palacios, 497–508

Dittmann, J. A., Irwin, J. M., Charbonneau, D., & Berta-Thompson, Z. K. 2013, ArXiv e-prints

Donati, J.-F., Catala, C., Landstreet, J. D., & Petit, P. 2006, in Astronomical Society of the Pacific Conference Series, Vol. 358, Astronomical Society of the Pacific Conference Series, ed. R. Casini & B. W. Lites, 362–+

Donati, J.-F., Semel, M., Carter, B. D., Rees, D. E., & Collier Cameron, A. 1997, MN-RAS, 291, 658

Dotter, A., Chaboyer, B., Jevremović, D., Kostov, V., Baron, E., & Ferguson, J. W. 2008, ApJS, 178, 89

Epchtein, N., et al. 1997, The Messenger, 87, 27

Feiden, G. A., & Chaboyer, B. 2012, ApJ, 761, 30

—. 2013, ApJ, 779, 183

Fernández, D., Figueras, F., & Torra, J. 2008, A&A, 480, 735

Gagné, J., Lafrenière, D., Doyon, R., Malo, L., & Artigau, É. 2014, ApJ, 783, 121

Gastine, T., Duarte, L., & Wicht, J. 2012, A&A, 546, A19

Glebocki, R., & Gnacinski, P. 2005, VizieR Online Data Catalog, 3244, 0

Gontcharov, G. A. 2006, Astronomy Letters, 32, 759

Gorlova, N. I., Meyer, M. R., Rieke, G. H., & Liebert, J. 2003, ApJ, 593, 1074

Høg, E., et al. 2000, A&A, 355, L27

Jeffries, R. D. 2006, Pre-Main-Sequence Lithium Depletion, ed. S. Randich & L. Pasquini, 163

Jenkins, J. S., Ramsey, L. W., Jones, H. R. A., Pavlenko, Y., Gallardo, J., Barnes, J. R., & Pinfield, D. J. 2009, ApJ, 704, 975

Koen, C., Kilkenny, D., van Wyk, F., Cooper, D., & Marang, F. 2002, MNRAS, 334, 20

Koen, C., Kilkenny, D., van Wyk, F., & Marang, F. 2010, MNRAS, 403, 1949

Kraus, A. L., Shkolnik, E. L., Allers, K. N., & Liu, M. C. 2014, AJ, 147, 146

Macdonald, J., & Mullan, D. J. 2010, ApJ, 723, 1599

Makarov, V. V. 2007, ApJS, 169, 105

Malo, L., Doyon, R., Lafrenière, D., Artigau, É., Gagné, J., Baron, F., & Riedel, A. 2013, ApJ, 762, 88

Mann, A. W., Gaidos, E., & Ansdell, M. 2013, ArXiv e-prints

Mentuch, E., Brandeker, A., van Kerkwijk, M. H., Jayawardhana, R., & Hauschildt, P. H. 2008, ApJ, 689, 1127

Mohanty, S., Basri, G., Jayawardhana, R., Allard, F., Hauschildt, P., & Ardila, D. 2004a, ApJ, 609, 854

Mohanty, S., Jayawardhana, R., & Basri, G. 2004b, ApJ, 609, 885

Montes, D., López-Santiago, J., Gálvez, M. C., Fernández-Figueroa, M. J., De Castro, E., & Cornide, M. 2001, MNRAS, 328, 45

Morin, J., et al. 2008, MNRAS, 390, 567

Nidever, D. L., Marcy, G. W., Butler, R. P., Fischer, D. A., & Vogt, S. S. 2002, ApJS, 141, 503

Ochsenbein, F., Bauer, P., & Marcout, J. 2000, A&AS, 143, 23

Ortega, V. G., de la Reza, R., Jilinski, E., & Bazzanella, B. 2002, ApJ, 575, L75

Pecaut, M. J., & Mamajek, E. E. 2013, ApJS, 208, 9

Rajpurohit, A. S., Reylé, C., Allard, F., Homeier, D., Schultheis, M., Bessell, M. S., & Robin, A. C. 2013, A&A, 556, A15

Randich, S., Pallavicini, R., Meola, G., Stauffer, J. R., & Balachandran, S. C. 2001, A&A, 372, 862

Reiners, A. 2012, Living Reviews in Solar Physics, 9, 1

Reiners, A., & Basri, G. 2009, A&A, 496, 787

Reylé, C., Rajpurohit, A. S., Schultheis, M., & Allard, F. 2011, in Astronomical Society of the Pacific Conference Series, Vol. 448, 16th Cambridge Workshop on Cool Stars, Stellar Systems, and the Sun, ed. C. Johns-Krull, M. K. Browning, & A. A. West, 929

Riedel, A. R., et al. 2014, AJ, 147, 85

Rodriguez, D., Zuckerman, B. M., Kastner, J. H., Vican, L., Bessell, M. S., Faherty, J. K., & Murphy, S. 2014, in American Astronomical Society Meeting Abstracts, Vol. 223, American Astronomical Society Meeting Abstracts, 334.06

Rodriguez, D. R., Bessell, M. S., Zuckerman, B., & Kastner, J. H. 2011, ApJ, 727, 62

Rodriguez, D. R., Zuckerman, B., Kastner, J. H., Bessel, M. S., Faherty, J. K., & Murphy, S. J. 2013, ArXiv e-prints

Saar, S. H. 1994, in IAU Symposium, Vol. 154, Infrared Solar Physics, ed. D. M. Rabin, J. T. Jefferies, & C. Lindsey, 493

Schlieder, J. E., Lépine, S., & Simon, M. 2010, AJ, 140, 119

Scholz, A., Coffey, J., Brandeker, A., & Jayawardhana, R. 2007, ApJ, 662, 1254

Shkolnik, E. L., Anglada-Escude, G., Liu, M. C., Bowler, B. P., Weinberger, A. J., Boss, A. P., Reid, I. N., & Tamura, M. 2012, ArXiv e-prints

Shkolnik, E. L., Liu, M. C., Reid, I. N., Dupuy, T., & Weinberger, A. J. 2011, ApJ, 727, 6

Siess, L., Dufour, E., & Forestini, M. 2000, A&A, 358, 593

Soderblom, D. R. 2010, ARA&A, 48, 581

Soderblom, D. R., Hillenbrand, L. A., Jeffries, R. D., Mamajek, E. E., & Naylor, T. 2013, ArXiv e-prints

Song, I., Bessell, M. S., & Zuckerman, B. 2002, ApJ, 581, L43

Song, I., Zuckerman, B., & Bessell, M. S. 2003, ApJ, 599, 342

Torres, C. A. O., da Silva, L., Quast, G. R., de la Reza, R., & Jilinski, E. 2000, AJ, 120, 1410

Torres, C. A. O., Quast, G. R., da Silva, L., de La Reza, R., Melo, C. H. F., & Sterzik, M. 2006, A&A, 460, 695

Torres, C. A. O., Quast, G. R., Melo, C. H. F., & Sterzik, M. F. 2008, Young Nearby Loose Associations, ed. B. Reipurth, 757–+

Udry, S., et al. 2007, A&A, 469, L43

van Leeuwen, F., ed. 2007, Astrophysics and Space Science Library, Vol. 350, Hipparcos, the New Reduction of the Raw Data

Yee, J. C., & Jensen, E. L. N. 2010, ApJ, 711, 303

Zacharias, N., Finch, C. T., Girard, T. M., Henden, A., Bartlett, J. L., Monet, D. G., & Zacharias, M. I. 2013, AJ, 145, 44

Zuckerman, B., & Song, I. 2004, ARA&A, 42, 685

Zuckerman, B., Song, I., Bessell, M. S., & Webb, R. A. 2001, ApJ, 562, L87

Zuckerman, B., & Webb, R. A. 2000, ApJ, 535, 959

CHAPITRE 5

CONCLUSION

L'objectif principal du travail présenté dans cette thèse est la recherche et la caractérisation des étoiles jeunes de faible masse. Jusqu'à la fin des années 1990, nos connaissances sur l'évolution des étoiles de faible masse étaient restreintes, en raison d'une barrière technologique imposée par leur faible brillance intrinsèque. Depuis ce temps, les connaissances sur les étoiles jeunes relativement plus massives ont augmenté à un rythme effréné, grâce aux données du télescope spatial Hipparcos ainsi que de celles du télescope ROSAT. Cela a permis de montrer l'existence d'associations cinématiques d'étoiles jeunes dans le voisinage solaire, dont les membres partagent une vitesse spatiale et une position Galactique similaires. Sachant que la distribution de luminosité du voisinage solaire était incomplète, plusieurs études ont tenté d'identifier les étoiles de faible masse manquantes dans ces associations, en utilisant le fait que ces dernières ont une luminosité plus grande en raison de leur jeune âge, ou encore en comparant le mouvement Galactique de ces dernières avec celui des membres plus massifs pour ainsi révéler une origine commune. Ces méthodes d'identification, utilisées séparément, sont cependant limitées et ont mené à plusieurs identifications erronées. Il fallait donc mieux structurer la méthodologie menant à la confirmation d'étoiles jeunes membres des associations cinématiques du voisinage solaire.

Pour aider à cet effort collectif, les travaux présentés ici avaient pour but de définir plus précisément les critères identifiant une étoile membre d'un groupe et d'estimer, pour une candidate, une probabilité d'association, ainsi que deux de ses caractéristiques principales, soit la distance et la vitesse radiale, qui peuvent par la suite être mesurées pour confirmer l'appartenance. Cette approche a permis de définir une population plus homogène, et de préciser les caractéristiques propres aux étoiles d'une masse donnée dans les associations de différents âges du voisinage solaire. Le formalisme de cette méthode est basé sur l'inférence bayésienne, où nos connaissances à posteriori sont utilisées pour contraindre les hypothèses de départ. L'outil développé porte le nom de « Bayesian

Analysis for Nearby Young AssociatioNs (BANYAN) ». Les caractéristiques propres à chaque groupe jeune considéré dans cette analyse (TW Hydrae, β Pictoris, Tucana-Horologium, Columa, Carina, Argus et ABDor) ont été déterminées en étudiant les propriétés (vitesse spatiale et position Galactique, et magnitude absolue) des 177 étoiles jeunes connues dans la littérature comme étant membres de ces groupes. Un modèle empirique pour chacun des sept paramètres (U, V, W, X, Y, Z, M_J vs $I - J$), utilisant les huit observables suivant : α, δ, $\mu_\alpha \cos \delta$, μ_δ, v_{rad}, π, I, J, a été dérivé pour en prédire l'amplitude pour un groupe donné. L'analyse est aussi capable de repérer des étoiles qui semblent être des binaires non résolues, car ces dernières présentent une surluminosité par rapport aux étoiles simples de couleur similaire. La nouvelle méthode a été validée en l'appliquant aux 177 membres, ce qui a permis de déterminer que la vitesse radiale et la distance trigonométrique estimées sont en excellent accord avec les valeurs mesurées (à moins de 2 km^{-1} pour la vitesse radiale et de 10% pour la distance trigonométrique). Il a aussi été établi qu'une probabilité minimale de 90% était nécessaire pour identifier une candidate membre.

Par la suite, cette méthode a été appliquée à un échantillon de 758 étoiles de faible masse montrant initialement certains signes de jeunesse (émissions en Hα et en rayons X), ce qui a permis l'identification de 214 nouvelles candidates à l'un des 7 groupes considérés. Une analyse Monte Carlo a permis de déterminer que le taux de contamination par des objets vieux du champ est moins de 14%.

Pour vérifier l'exactitude des prédictions faites par l'analyse (vitesses radiales, distance) et ainsi confirmer l'appartenance aux groupes de ces candidates, un programme d'observation de plus de 150 heures a été entrepris, principalement sur trois observatoires internationaux, le télescope Gemini Sud, le télescope VLT de l'ESO et le télescope Canada-France-Hawaii (TCFH). La caractérisation a débuté par la mesure de la vitesse radiale de 219 candidates. Un spectre optique ou infrarouge, dont la résolution spectrale excédait les 50,000, a été obtenu, ce qui a permis d'extraire une vitesse radiale héliocentrique ayant une précision d'environ 1 km s^{-1}. Entre 2008 et 2012, plus de 401 observations ont été utilisées pour confirmer la la vitesse radiale prédite par l'analyse pour 130 candidates. Ces nombreuses mesures ont aussi permis de vérifier la prédic-

tion faite par l'analyse sur la binarité des étoiles, qui s'est avérée exacte pour 78% des candidates du groupe β Pictoris (β PMG) et AB Doradus (ABDMG). Une caractéristique supplémentaire est obtenue en mesurant l'élargissement des raies ($v \sin i$) sur les mêmes spectres : 20% des candidates ont une grande vitesse de rotation projetée, supérieure à 30 km s^{-1}. De plus, le lien étroit entre la vitesse de rotation et la luminosité en rayon X (force de la dynamo) a permis de comparer la luminosité X des candidates à celle de quelques étoiles de faible masse connues. L'analyse a montré une diminution d'un facteur 4 de la luminosité X à l'intérieur des premiers 120 Mans d'évolution d'une étoile, et une différence de plus de deux ordres de grandeur compativement aux étoiles vieilles de faible masse. La luminosité X est donc un bon indicateur de jeunesse. Une collaboration avec le groupe CTIOPI a aussi permis d'obtenir la distance trigonométrique pour 20 candidates, montrant un excellent accord avec la prédiction dans 90% des cas.

Enfin, les propriétés fondamentales des candidates, soit la luminosité bolométrique, la température et le rayon stellaire ont été déterminées en comparant les spectres optiques de l'instrument ESPaDOnS au CFHT aux modèles d'atmosphère PHOENIX. Qualitativement, les candidates suivies ont des luminosités bolométriques supérieures à celles des étoiles vieilles. Les propriétés fondamentales ont été comparées aux plus récents modèles évolutifs Dartmouth qui incluent le traitement du champ magnétique.

Pour les étoiles de β PMG, en utilisant les modèles dont l'amplitude du champ magnétique est de 1 kGauss, l'âge isochronal dérivé pour les étoiles de $T_{\text{eff}} < 3500$ K n'est pas cohérent avec l'âge déterminé pour celles de $T_{\text{eff}} > 3500$ K (environ 18 Mans de différence). Cependant, si on utilise les modèles magnétique de 2.5 kG pour les étoiles de $T_{\text{eff}} < 3500$ K (ce qui est raisonnable d'après les observations faites pour des étoiles vieilles de type M0V-M4V), cette différence est beaucoup plus faible, et l'âge évalué est aussi plus cohérent avec celui déterminé indépendamment par la méthode dite du « Lithium Depletion Boundary (LDB) ». Cela met en évidence l'importance du traitement du champ magnétique pour estimer l'âge d'une étoile de faible masse.

5.1 Importance des résultats

Les cinq dernières années marquent un tournant dans nos connaissances des étoiles jeunes et les travaux présentés dans le cadre de cette thèse ont grandement participé à l'avancement de celles-ci.

Premièrement, la méthode statistique développée permet une meilleure objectivité sur l'identification d'un membre d'une association, en déterminant quantitativement une probabilité d'association. Cette méthode permet également de considérer facilement une grande quantité d'observables pour comparer différents groupes d'étoiles jeunes aux étoiles vieilles. L'analyse est facilement ajustable à d'autres échantillons de départ, par exemple des étoiles plus massives, des naines brunes ou même des naines blanches. La méthodologie demeure semblable, et consiste toujours à dériver un modèle empirique des caractéristiques propres à la population ciblée pour les comparer à une population différente.

Deuxièmement, l'analyse statistique, complémentée d'observations de suivi a permis d'identifier près de 150 nouvelles étoiles jeunes de faible masse du voisinage solaire, ce qui constitue le triple du nombre de telles étoiles membres connues dans la littérature avant les travaux de cette thèse. La grande quantité d'identifications ainsi que la qualité de la caractérisation permet de faire de ce groupe d'étoiles jeunes une référence pour les études observationnelles et théoriques.

D'un point de vue observationnel, cet échantillon de jeunes étoiles de faible masse situées dans le voisinage solaire est idéal pour la détection et la caractérisation d'exoplanètes, plus particulièrement, par la méthode d'imagerie directe. La connaissance précise de l'âge de ces étoiles a un grand impact : non seulement cela permet d'augmenter l'efficacité d'une méthode de détection en ciblant des étoiles d'un âge précis, mais cela permet aussi d'améliorer grandement la précision des paramètres dérivés pour les exoplanètes détectées. Ce nouvel échantillon d'étoiles jeunes de faible masse permettra aussi de déterminer la fonction de masse initiale des associations jeunes.

D'un point de vue théorique, un grand relevé d'étoiles jeunes et proches, de masses variées et ayant été soumises à des conditions de formation et d'évolution similaires per-

met de contraindre les modèles d'atmosphère et d'évolution, en faisant un moins grand nombre d'hypothèses. Par exemple, ces modèles fixent généralement un taux d'accrétion initial, mais l'étude de cet échantillon pourrait mettre en relief que ce taux varie selon différents facteurs. Grâce à cet échantillon, il a été possible de mesurer l'impact du champ magnétique sur la détermination des paramètres fondamentaux des étoiles jeunes de faible masse. Il a été montré par exemple que l'âge évalué par les modèles d'évolution pour les étoiles de βPMG ayant une $T_{\mathrm{eff}}<$ 3500 K dépend significativement de l'amplitude du champ magnétique considéré par le modèle. Nos résultats montrent que les champs magnétiques doivent être inclus dans les modèles d'évolution étant donné que ces derniers ont une répercussion significative sur la décroissance de leur luminosité en fonction du temps.

5.2 Perspectives d'avenir

Les outils présentés ici pourront être appliqués sur d'autres échantillons d'étoiles afin d'identifier de nouvelles étoiles jeunes de masse variée dans le voisinage solaire. Si une fonction de masse initiale standard s'applique aux populations stellaires des associations jeunes, alors plusieurs étoiles de type K et M seraient encore manquantes. Pour pousser l'identification aux objets encore moins massifs (naines brunes et objets de masse planétaire), il est avantageux d'utiliser l'infrarouge moyen plutôt que le visible. Cette stratégie est d'ailleurs actuellement mise en oeuvre dans les travaux de thèse de Jonathan Gagné.

La distance statistique s'avère être une excellente estimation de la parallaxe pour les étoiles avec des probabilités d'association élevées (avec ou sans vitesse radiale). Cependant, pour confirmer définitivement l'appartenance d'une étoile à un groupe, une mesure trigonométrique de la distance est nécessaire. L'arrivée prochaine (en 2017) des résultats de la mission Gaia, qui mesurera les 6 composantes définissant la cinématique Galactique (U, V, W, X, Y, Z) pour environ 26 millions d'étoiles (V=15), permettra donc d'augmenter considérablement le nombre de membres confirmés. Suivant cette percée majeure, la caractérisation des étoiles dépendra de notre capacité à mesurer les rayons stellaires, qui sera grandement améliorée grâce aux modifications apportées à l'interfé-

romètre CHARA.

Pour mieux contraindre l'évolution de la structure stellaire et l'âge d'une étoile, les données Gaia devront être combinées aux mesures de la topologie du champ magnétique. La caractérisation magnétique des étoiles de faible masse sera possible avec le Spectrographe-Polarimètre infrarouge SPIRou (Delfosse et al. 2013) qui sera déployé au TCFH en 2017.

Finalement, la faible luminosité et la jeunesse de ces étoiles en font des cibles de choix pour la détection d'objets de masse planétaire. Malheureusement, la majorité de ces étoiles sont trop faibles pour les futurs instruments tels que le *Gemini Planet Imager* et SPHERE, tous deux adaptés pour détecter des objets de masse planétaire de quelques fois la masse de Jupiter. Mais ce ne sera que partie remise car, vers la fin des années 2018, le grand télescope spatial James Webb ouvrira ses yeux infrarouges sur le voisinage solaire. D'une sensitivité sans précédent, ce télescope ouvrira de nouvelles recherches et études sur les étoiles de faible masse, naines brunes et exoplanètes.

Annexe I

Articles à titre d'auteur secondaire

La première partie de cette annexe fait état des articles publiés, dont l'estimé d'âge pour les objets étudiés découlent des travaux présentés dans cette thèse. La deuxième partie de l'annexe énumère deux articles, dont mon implication se résume à la prise de mesures, la pré-réduction de celles-ci et la révision du manuscrit.

I.1 Articles découlant directement des travaux de thèse

I.1.1 CFBDSIR2149-0403 : a 4-7 Jupiter-mass free-floating planet in the young moving group AB Doradus ?

Auteurs : Delorme, P. ; Gagné, J. ; Malo, L. ; Reylé, C. ; Artigau, E. ; Albert, L. ; Forveille, T. ; Delfosse, X. ; Allard, F. ; Homeier, D., 2012, A&A, 548, 26.

Contribution : Détermination des probabilités d'association, rédaction d'une partie de la section portant sur l'association. Révision du manuscrit.

I.1.2 Direct-imaging discovery of a 12-14 Jupiter-mass object orbiting a young binary system of very low-mass stars

Auteurs : Delorme, P. ; Gagné, J. ; Girard, J. H. ; Lagrange, A. M. ; Chauvin, G. ; Naud, M.-E. ; Lafrenière, D. ; Doyon, R. ; Riedel, A. ; Bonnefoy, M. ; Malo, L, 2013, A&A, 553, 5.

Contribution : Détermination de l'échantillon observé, détermination des probabilités d'association, révision du manuscrit.

I.1.3 BANYAN. II. Very Low Mass and Substellar Candidate Members to Nearby, Young Kinematic Groups With Previously Known Signs of Youth

Auteurs : Gagné, Jonathan ; Lafrenière, David ; Doyon, René ; Malo, Lison ; Artigau, Étienne, 2014, ApJ, 783, 121.

Contribution : Aide à la rédaction, aux calculs des probabilités, révision du manuscrit.

I.1.4 The Solar Neighborhood. XXXIII. Parallax Results from the CTIOPI 0.9m Program : Trigonometric Parallaxes of Nearby Low-Mass Active and Young Systems

Auteurs : Riedel, Adric R. ; Finch, Charlie T. ; Henry, Todd J. ; Subasavage, John P. ; Jao, Wei-Chun ; Malo, Lison ; Rodriguez, David R. ; White, Russel J. ; Gies, Douglas R. ; Dieterich, Sergio B. ; Winters, Jennifer G. ; Davison, Cassy L. ; Nelan, Edmund P. ; Blunt, Sarah C. ; Cruz, Kelle L. ; Rice, Emily L. ; Ianna, Philip A., 2014, AJ, 147, 85.

Contribution : Rédaction d'une partie de la section sur l'association des membres, calcul des probabilités d'association, prise d'observations exclusivement pour cette publication, révision du manuscrit.

I.1.5 The Coolest Isolated Brown Dwarf Candidate Member of TWA

Auteurs : Gagné, Jonathan ; Faherty, Jacqueline K. ; Cruz, Kelle ; Lafrenière, David ; Doyon, René ; Malo, Lison ; Artigau, Etienne ; 2014, ApJ, 785, 14.

Contribution : Calcul des probabilités d'association, révision du manuscrit.

I.1.6 Discovery of a wide planetary-mass companion to the Young M3 star Gu Psc

Auteurs : Naud, Marie-Eve ; Artigau, Etienne ; Malo, Lison ; Albert, Loïc ; Doyon, René ; Lafrenière, David ; Gagné, Jonathan ; Saumon, Didier ; Morley, Caroline V. ; Allard, France ; Homeier, Deriek ; Beichman, Charles A. ; Gelino, Christopher R. ; Boucher, Anne, 2014, ApJ, 787, 5.

Contribution : Rédaction d'une partie de la section 3 (propriétés de l'étoile hôte Gu Psc), calcul des probabilités d'association, prise de données pour cette publication, révision du manuscrit.

I.2 Articles supplémentaires

I.2.1 The ultracool-field dwarf luminosity-function and space density from the Canada-France Brown Dwarf Survey

Auteurs : Reylé, C. ; Delorme, P. ; Willott, C. J. ; Albert, L. ; Delfosse, X. ; Forveille, T. ; Artigau, E. ; Malo, L. ; Hill, G. J. ; Doyon, R.

Contribution : Acquisition et pré-réduction d'une partie des données. Révision du manuscrit.

I.2.2 Discovery of Two L and T Binaries with Wide Separations and Peculiar Photometric Properties

Auteurs : Artigau, Étienne ; Lafrenière, David ; Doyon, René ; Liu, Michael ; Dupuy, Trent J. ; Albert, Loïc ; Gagné, Jonathan ; Malo, Lison ; Gratadour, Damien

Contribution : Acquisition des données. Révision du manuscrit.

Annexe II

Permissions de l'éditeur

Annexe III

Déclarations des coauteurs des articles